Numéro d'ordre : 41462

THESE DE DOCTORAT

Présentée à

L'UNIVERSITE LILLE 1 SCIENCES ET TECHNOLOGIES
Ecole doctorale Sciences de la Matière, du Rayonnement et de l'Environnement
UFR de Physique

Pour obtenir le titre de

DOCTEUR
Spécialité Sciences des Matériaux

par
Changqing YE

FRAGILISATION DE L'ACIER MARTENSITIQUE T91 PAR L'EUTECTIQUE LIQUIDE PLOMB-BISMUTH

Soutenue à Villeneuve d'Ascq le 17 juillet 2014 devant la commission d'examen :

Guy REUMONT	Professeur, Directeur Polytech'Lille, Université Lille 1	Président
Angéline POULON	Maître de conférences, HDR, Université Bordeaux 1	Rapporteur
Michel VILASI	Professeur, Université de Lorraine	Rapporteur
Grégory NICAISE	Ingénieur-chercheur, IRSN, Fontenay-aux-Roses	Examinateur
Ingrid PRORIOL SERRE	Chargée de recherches CNRS, HDR, UMET	Co-directrice de thèse
Jean-Bernard VOGT	Professeur, ENSCL, UMET	Directeur de thèse

Unité Matériaux Et Transformations UMET
CNRS UMR 8207 – Université Lille 1

Numéro d'ordre : 41462

UNIVERSITE LILLE 1 SCIENCES ET TECHNOLOGIES
Ecole doctorale Sciences de la Matière, du Rayonnement et de l'Environnement
UFR de Physique

PhD Thesis
Materials Science

Changqing YE

EMBRITTLEMENT OF MARTENSITIC STEEL T91 BY LIQUID LEAD-BISMUTH EUTECTIC

Defended on July 17, 2014

Dissertation committee:

Guy REUMONT	Professor, Director Polytech'Lille, Université Lille 1	President of the jury
Angéline POULON	Assistant professor, Université Bordeaux 1	Reviewer
Michel VILASI	Professor, Université de Lorraine	Reviewer
Grégory NICAISE	Researcher, IRSN, Fontenay-aux-Roses	Examiner
Ingrid PRORIOL SERRE	Chargée de recherche CNRS, HDR, UMET	Co-supervisor
Jean-Bernard VOGT	Professeur, ENSCL, UMET	Supervisor

Unité Matériaux Et Transformations UMET
CNRS UMR 8207 – Université Lille 1

CONTENTS

LIST OF ABBREVIATIONS

ADS	Accelerator driven systems
SPT	Small punch tests
LBE	Lead-bismuth eutectic
LME	Liquid metal embrittlement
LMIE	Liquid Metal Induced Embrittlement
LMAD	Liquid metal assisted damage
LMC	Liquid metal corrosion
SEM	Scanning electron microscopy
SIMS	Secondary ion mass spectrometry
HLM	Heavy liquid metal
SNS	Spallation Neutron Source
PSI	Paul Scherrer Institute
ORNL	Oak Ridge National Laboratory
KAERI	Korea Atomic Energy Research Institute
SNU	Seoul National University
JAERI	Japan Atomic Energy Research Institute
TIT	Tokyo Institute of Technology
JAEA	Japan Atomic Energy Agency
SCK-CEN	Belgian Nuclear Research Centre

CEA	Commissariat à l'Energie Atomique et aux Energies Alternatives
ITT	Center of Nano Science and Technology of the Italian Institute of Technology
LFR	Lead faster reactor
LLFP	Long-lived fission products
R&D	Research and development
J-PARC	Japan Proton Accelerator Research Complex
PBWFR	Pb-Bi-cooled Direct Contact Water Fast Reactor
IG	Intergranular
TG	Transgranular
DBTT	Ductile to brittle transition temperature
EDM	Electron discharging machine
CCT	Center Cracked in Tensile
LCF	Low cycle fatigue
R.T./RT	Room temperature
PLD	Pulsed Laser Deposition
LPPS	Low pressure plasma spraying
FM	Ferritic/martensitic
SSRT	Slow strain rate tensile tests
PAG	Prior austenite grain
K	Stress intensity factor
K_{IC}	Linear-elastic fracture toughness, units of Pa$\sqrt{m}$ or psi$\sqrt{in}$

J_{IC}	Elasto-plastic fracture toughness, unit of J/cm^2 or lbf-in/in^2
F_e (N)	Yielding load (SPT)
F_{max} (N)	Maximum load (SPT)
d_{Fe} (mm)	Displacement at yielding load (SPT)
d_{Fmax} (mm)	Displacement at maximum load (SPT)
J_{nf} (J/mm)	Normalized energy to the rupture (SPT)
J_{nFmax} (J/mm)	Normalized energy to maximum load (SPT)
J_f (J/mm)	Fracture energy (SPT)
UE (%)	Uniform elongation
TE (%)	Total elongation
σ_{YS} (MPa)	Yield stress
σ_{UTS} (MPa)	Ultimate tensile strength
e (mm)	Thickness of the SPT specimen
E (GPa)	Young's modulus
γ_e (mJ/m^2)	Surface free energy
YSZ	Yttria Stabilised Zirconia
VHTS	Vickers hardness treatment surface
LNS	Linear notched surface
DCT	Disc-shaped in tension

INTRODUCTION

With the innovation and progress in the global nuclear industry, the development of new types of reactors such as those considered in the Generation IV forum or accelerator driven system (ADS) makes them more and more credible for a sustainable use of nature resources and environment protection and for an efficient treatment of nuclear waste. The success of these projects rests upon deeply conducted research activities in many areas.

Concerning structural materials, the working conditions in which they will be employed are more and more severe and complex. Some of Generation IV reactors and ADS will employ liquid metals such as sodium or heavy liquid metals (lead or lead alloy) for coolant and/or spallation target. Some of their components will be made of T91 martensitic steel or 316L austenitic stainless steel, and both alloys will be in contact with the heavy liquid metal, at high temperature and under stress and under irradiation. Therefore, the compatibility of the structural materials with heavy liquid metals has attracted attention since several years in order to guarantee security. Data on corrosion and on mechanical behaviour, and knowledge on fracture mechanisms in LBE have been acquired especially on T91 and 316L steels. One typical class of fracture modes to be considered is obviously liquid metal embrittlement (LME) and liquid metal assisted damage (LMAD). It has been proved that T91 steel exhibits a certain degree of sensitivity to LME because its microstructure is very dependent on the heat treatment. Besides, the chemistry of LBE, in particular the oxygen content can affect the corrosion resistance and the mechanical behaviour. Nevertheless, the role of all these parameters and their interaction is not fully demonstrated and understood.

The purpose of this thesis is, therefore, to investigate the role of oxygen in LBE and the effect of loading conditions on the sensitivity to LBE embrittlement of T91 martensitic steel in liquid LBE, and to propose a mechanism.

In this thesis, the mechanical behaviour of T91 steel in LBE has been studied by conducting Small Punch Tests (SPT), three-point bending tests and tensile tests in both liquid oxygen saturated LBE and liquid low oxygen LBE. In order to investigate the microstructure effect on the LBE embrittlement, T91 steel has been subjected to the standard heat treatment and the hardening heat treatment. Furthermore, the surface state effects on LME were also systematically studied which include the presence of surface defects and surface coatings. The

investigations were conducted by considering the test temperature and the loading velocity. In addition, in order to obtain more comprehensive information for understanding the mechanical tests results and the mechanisms of LBE embrittlement of T91 steel, the deformation of the sample surface and microstructure analyses were performed by scanning electron microscopy (SEM) and secondary ion mass spectrometry (SIMS).

The overall structure of this thesis is divided into five chapters and a final conclusion part as follows.

Chapter I is dedicated to present the literature review. It has five sub-chapters. The first sub-chapter focuses on the general introduction of the research background of this thesis, including the application of liquid lead-bismuth eutectic (LBE) for the developments of Generation IV nuclear reactors and the accelerator driven system (ADS), as well as the problem of the compatibility of the metallic alloys with liquid metals. The second sub-chapter is devoted to the definition of the liquid metal embrittlement (LME) phenomena and its characteristics. The third sub-chapter presents the existing models which interpret the mechanism of LME failure. The fourth sub-chapter has summarized the research status and results of the behaviour of structural materials T91 steel in contact with liquid LBE. The fifth sub-chapter gives the aim of this thesis.

Chapter II describes the materials (T91 steel and LBE) and the experimental techniques used in this thesis research work, which include the details of mechanical tests preparations (Small Punch Tests, three-point bending tests and tensile tests), as well as the implementation of the related equipment for performing mechanical tests in liquid low oxygen LBE environment.

Chapter III is divided into two sub-chapters. The first sub-chapter introduces the experimental results of the investigation on the LBE embrittlement sensitivity of T91 steel performed by Small Punch Tests and the factors leading to ductile to brittle behaviour transition in liquid LBE. The second sub-chapter is the discussion and the conclusion of the experimental results on the effects of various factors (microstructure, temperature, oxygen content in LBE and displacement velocity) that promotes the transition from ductile to brittle in liquid LBE of T91 steel.

Chapter IV presents in detail the experimental results of surface defects effects on the investigation of the LBE embrittlement sensitivity of T91 steel. These include SPT performed on Vickers micro notched surface specimens, SPT performed on linear notched surface

specimens, tensile tests performed on smooth and V-notched surfaces cylindrical specimens, and three-point bending tests performed on the notched single edge specimens.

Chapter V is divided into two sub-chapters. The first sub-chapter focuses on the interpretation and discussion of the results on the base of a new hypothetical mechanism proposed in this thesis. And the second sub-chapter is an attempt at solution to LBE embrittlement effect on T91 steel by a surface coating technique.

Finally, the general conclusions obtained in this thesis and prospects are presented.

CHAPTER I : LITERATURE REVIEW

Liquid metal embrittlement, corrosion, radiation damage and the compatibility of the metallic alloys with liquid metals are the main materials relevant issues for the successful implementation of the Generation IV nuclear reactors and a spallation target of ADS, which prefer to choose a liquid lead or lead-bismuth eutectic (LBE) as the coolant/target material. In this chapter, liquid metal embrittlement (LME) phenomena and its characteristics, as well as the models for mechanism of LME failure are introduced. In addition, a brief review of recent studies on the behaviour of the structure material T91 steel in contact with LBE is presented. Finally, the objective of this PhD thesis is introduced.

1.1 Research background

In recent years, with the development of Generation IV nuclear reactors, experimental and demonstration fusion reactors and accelerator driven systems for nuclear waste transmutation, the interest in heavy liquid metal (HLM) coolants was revived.

Liquid Lead Bismuth Eutectic (LBE) has excellent thermo-hydraulic properties and has been selected as coolant and spallation neutron source for Multi-purpose Hybrid Research Reactor for High-tech Applications (MYRRHA), an accelerator driven system (ADS) under development in Belgium.

Accelerator driven systems (ADS) are nuclear fission reactors with a subcritical core, i.e. $k_{\text{eff}} < 1$. Therefore, to operate ADS, an external neutron source is needed for a stationary behaviour of the core. A possible external neutron source is provided by a proton accelerator and a spallation target (a heavy liquid metal is often considered). The protons hitting the heavy liquid metal generate neutrons which sustain the chain reaction in the sub-critical core. Fig. 1.1 shows the schematic view of an ADS.

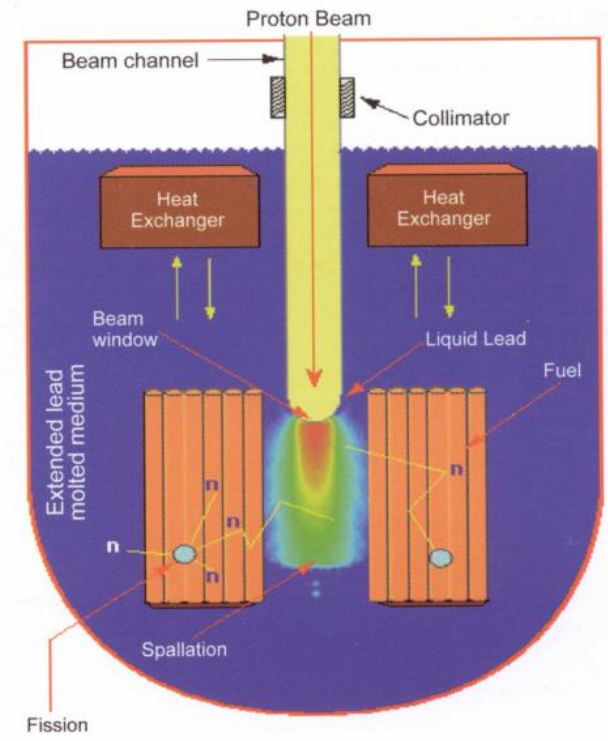

Figure 1.1: Schematic diagram of an accelerator driven system (ADS) [HAN-2007].

Neutron spallation targets are also being developed to provide a neutron source for many applications. For example, the Megawatt Pilot Experiment (MEGAPIE) Spallation Neutron Source (SNS) LBE target (a schematic view of the MEGAPIE target and the model with its main characteristics and main parameters are shown in Fig. 1.2 [DAI-2006-C, FAZ-2008]). It has been designed and constructed in the frame of ADS development and has been tested at the SINQ facility of the Paul Scherrer Institute (PSI) in Switzerland.

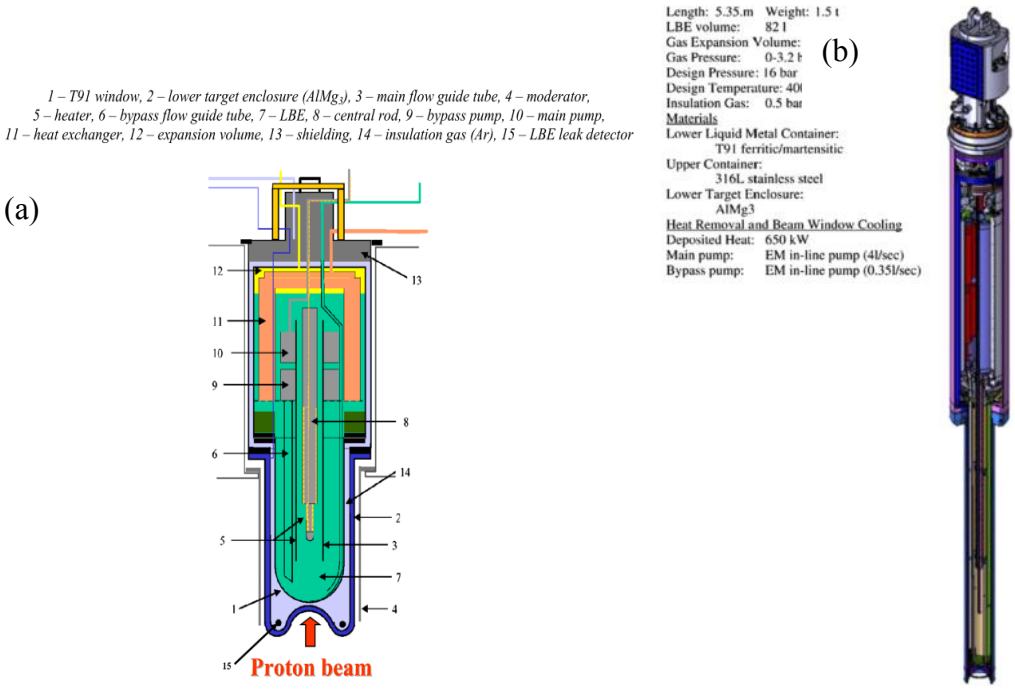

Figure 1.2: The MEGAPIE target: (a) schematic diagram, and (b) model and its main characteristics and main parameters [FAZ-2008].

Other heavy liquid metals can be considered for the neutron spallation targets. SNS mercury target is designed in USA as an accelerator-based neutron source to provide pulsed beams of spallation neutrons by bombarding a mercury target with 1 GeV protons. The main purpose of this SNS mercury target is to produce intense pulsed beams of neutrons for research in materials science and condensed matter physics. This mercury target SNS is located at Oak Ridge National Laboratory (ORNL), and SNS is currently the largest civilian science project in the USA founded by the US government Department of Energy. Fig. 1.3 shows the SNS target system.

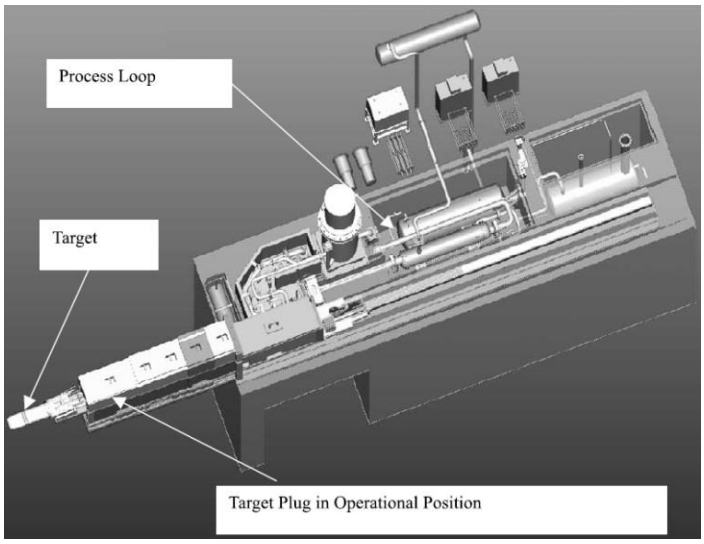

Figure 1.3: The SNS target system, consisting of a stainless steel structure containing mercury, referred to as the target, a process loop, a means for moving the target module between its installed position and a hot cell, and moveable shielding in the target module's path between the hot cell and its installed position [MAN-2001].

Fast neutron reactors or fast reactors are fission reactors where the neutron spectrum in the core is close to the fission neutron spectrum, since the neutrons are not thermalized as in the conventional light-water-cooled reactors. The fast reactor coolant is appropriately chosen in order to provide an effective heat transfer, without a significant thermalisation of the neutron spectrum. In order to achieve this goal, liquid metals (Na or Pb, Pb/Bi) or gas can be (or have been) used. HLM such as lead (Pb) or LBE were proposed and investigated as coolants for fast reactors as early as in the 1950s (e.g. in the USA). Sodium became the preferred choice in the sixties, due to a higher power density achievable with this coolant, which resulted in lower doubling times, an important objective at that time. However, LBE was chosen as the coolant for a number of alpha class submarine reactors in the former Soviet Union, which led to very extensive research and development of the coolant technology and materials, with particular emphasis on the chemistry control of the liquid metal to avoid plugging due to slag formation and to enhance corrosion resistance of the steels specifically developed for such services. More recently, there has been renewed interest in Russia in lead and LBE coolants for civilian fast reactors. The lead-cooled BREST (Russian acronym for Pb-cooled fast reactor) concept developed since the early 1990s is the most widely known, with the LBE-cooled SVBR (Russian acronym for lead-bismuth fast reactor) concept competing for attention. Their features and the associated technologies inspired several projects in the emerging field of ADS, and in particular lead cooling was associated, in the mid-1990s, with the proposal for an energy amplifier project together with LBE as a spallation target coolant and material. Subsequent development of ADS in the USA, Europe, Japan and the Republic of Korea has

adopted a heavy liquid metal (most often LBE) as the coolant for the subcritical core and as coolant and material for the spallation target which provides the external neutron source. At the Korea Atomic Energy Research Institute (KAERI) and Seoul National University (SNU) in the Republic of Korea, both ADS and LFR (lead faster reactor) systems are under the development in order to explore proliferation-resistant and safe transmutation technology. In Japan, both ADS and LFR systems using LBE are under the development. At the Japan Atomic Energy Research Institute (JAERI) an ADS with the thermal power of 800MW has been designed, where 250 kg of minor actinides and some long-lived fission products (LLFP) can be transmuted annually. R&D (research and development) has been conducted on ADS using LBE as a spallation target and a coolant, and research using J-PARC (Japan Proton Accelerator Research Complex) is also planned. The LFR systems using LBE as a coolant have been studied both at Tokyo Institute of Technology (TIT) and the Japan Atomic Energy Agency (JAEA). One of the LFR systems studied at TIT is designated as the Pb-Bi-cooled Direct Contact Water Fast Reactor (PBWFR).

In summary, at present, a number of experimental programs are ongoing world-wide for the transmutation of nuclear waste and the development of HLM cooled fast reactors. These include: The USA Advanced Fuel Cycle Initiative; The European Commission four-year Integrated Project European Research Program for the Transmutation of High Level Nuclear Waste in an Accelerator Driven System, IP-EUROTRANS and GEN IV and Transmutation MATerials (GETMAT). In addition in Europe there are several programs ongoing at national level, as for instance in France the GEDEON, now GEDEPEON (Gestion de Déchets et Production d'Energie par des Options Nouvelles) program, and the MYRRHA project at SCK-CEN (Belgian Nuclear Research Centre) in Belgium. MYRRHA is being developed as a multi-purpose neutron source for R&D applications on the basis of an ADS program; The South Korean programs of HYPER (ADS) and PEACER (reactor); In Japanese program in the framework of ADS development and LFR development; The Russian program for the BREST, and SVBR reactors.

However, one of the problems prevented the successful implementation of the application of HLM engineering projects is the compatibility of the metallic alloys with liquid metals. Essentially the metal corrosion and liquid metal embrittlement (LME) are the most important issues when solid metals are in contact with liquid metals. Due to the LME effect phenomena, the mechanical properties of solid metals can be severely degraded so that structural components can exhibit sudden brittle damage during operation. Therefore, LME plays as a

very important materials research topic for long year to solve engineering problems.

1.2 Liquid metal embrittlement (LME) phenomena and its characteristics

LME is a materials research topic since a long time because it is involved in a very important compatibility issue in industrial applications where solid metals are in contact with liquid metals. The description and analysis in literature have shown that LME does not occur every time a metal or alloy is stressed when in contact with liquid metal, but rather that it depends on a complex combination of factors such as the solid and the liquid metal composition, grain size, strain rate, temperature and surface condition. Nevertheless, the literature shows that both laboratory studies and plant failures can evidence LME under specific liquid metal-solid metal condition. Pure metals and highly alloyed metals such as brasses, bronzes, carbon steels and stainless steels may be embrittled by molten metals over a range of conditions. According to the review of reported LME failures, the failure information of LME is under four headings, namely processing failures (e.g. galvanizing and hot rolling), fabrication failures (e.g. welding, soldering, brazing and machining), operating failures (e. g. nuclear industry and smelters) and secondary failures, i.e. those failures in which LME has occurred as a consequence of some previous failures (e.g. bolts, shafts, bearings and pressure vessels). It should be noted that the incidence of LME in industry is probably greater than that reported since some failures would undoubtedly have been incorrectly identified and many others may not have been reported in the literature.

In this section, the fracture characteristics of materials and the general features of LME are described on the basis of the results obtained in the last few decades.

1.2.1 Fracture in materials

In order to achieve the successful application of the materials in the industrial field, it is very crucial to evaluate its comprehensive performances especially the failure damage of the materials, which relates to the investigation on the final fracture characteristics and the fracture mechanism for the materials. Therefore, the study of the LME damage of alloyed steels cannot be separated with the fracture research. In this section, the general information

of fracture in materials is described, especially the types of fracture in metals and its mechanics.

Fracture is the separation, or fragmentation, of a solid body into two or more parts under the action of stress. The process of fracture can be considered to occur into two steps, crack initiation and crack propagation. Fracture modes can be classified into two general categories, ductile fracture and brittle fracture. A ductile fracture is characterized by appreciable plastic deformation prior to and during the propagation of the crack. An appreciable amount of macroscopic deformation is usually present at the fracture surfaces. Brittle fracture in metals is characterized by a rapid rate of crack propagation, with no macroscopic deformation and very little micro-deformation. It is akin to cleavage in ionic crystals. The tendency for brittle fracture is increased with decreasing temperature, increasing strain rate, and triaxial stress conditions (usually produced by a notch). Brittle fracture is to be avoided at all cost, because it occurs without warning and usually produces disastrous consequences.

1.2.1.1 Types of fracture in metals

Metals can exhibit many different types of fracture, depending on the material, temperature, state of stress and rate of loading. Fig. 1.4 schematically illustrates some of the types of tensile fractures which can occur in metals. A brittle fracture (Fig. 1.4a) is characterized by separation normal to the tensile stress. Outwardly there is no evidence of deformation, although with X-ray diffraction analysis it is possible to detect a thin layer of deformed metal at the fracture surface. Brittle fractures have been observed in bcc and hcp metals, but rarely in fcc metals unless there are facts contributing to grain-boundary embrittlement.

Ductile fracture can take several forms. Single crystals of hcp metals may slip on successive basal planes until finally the crystal separates by shear (Fig. 1.4b). Polycrystalline specimens of very ductile metals, like gold or lead, may actually be drawn down to a point before they rupture (Fig. 1.4c). In the tensile fracture of moderately ductile metals the plastic deformation eventually produces a necked region (Fig. 1.4d). Fracture begins at the centre of the specimen and then extends by a shear separation along the dashed lines in Fig. 1.4d. Fractures are classified with respect to several characteristics, such as strain to fracture, crystallographic mode of fracture, and the appearance of the fracture.

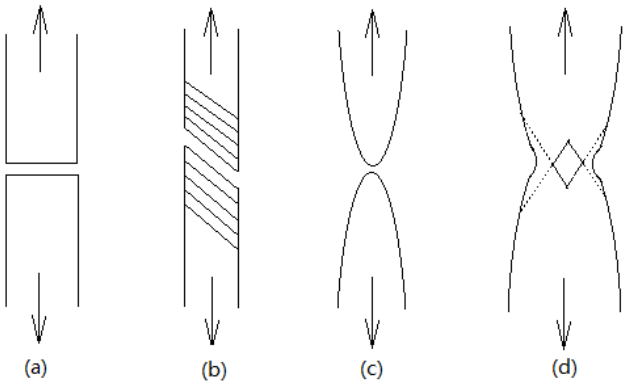

Figure 1.4: Types of fractures observed in metals subjected to uniaxial tension. (a) Brittle fracture of single crystals and polycrystals; (b) shearing fracture in ductile single crystals; (c) completely ductile fracture in polycrystals; (d) ductile fracture in polycrystals [DIE-1976].

A shear fracture occurs as the result of extensive slip on the active slip plane. This type of fracture is promoted by shear stresses. The cleavage mode of fracture is controlled by tensile stresses acting normal to a crystallographic cleavage plane. A fracture surface which is caused by shear appears at low magnification to be gray and fibrous, while a cleavage fracture appears bright or granular, owing to reflection of light from the flat cleavage surfaces. Fracture surfaces frequently consist of a mixture of fibrous and granular fracture, and it is customary to report the percentage of the surface area represented by one of these categories. Based on metallographic examination, fractures in polycrystalline samples are classified as either transgranular (the crack propagates through the grains) or intergranular (the crack propagates along the grain boundaries). A ductile fracture is one which exhibits a considerable degree of deformation. The boundary between a ductile and brittle fracture is arbitrary and depends on the situation being considered. For example, nodular cast iron is ductile when compared with ordinary gray iron; yet it would be considered brittle when compared with mild steel. As a further example, a deeply notched tensile specimen will exhibit little gross deformation; yet the fracture could occur by a shear mode.

1.2.1.1.1 Ductile fracture

Ductile fracture has been studied much less than brittle fracture, probably because it is a much less serious problem. Up to this point ductile fracture has been defined ambiguously as fracture occurring with appreciable gross plastic deformation. Another important characteristic of ductile fracture, which should be apparent from previous consideration of brittle fracture, is that it occurs by a slow tearing of the metal with the expenditure of

considerable energy. Many varieties of ductile fractures can occur during the processing of metals and their use in different types of service. Ductile fracture in tension is usually preceded by a localized reduction in diameter called necking. Very ductile metals may actually draw down to a line or a point before separation produced in uniaxial tension, and which is a kind of failure usually called rupture. Detailed study of the ductile fracture process shows that the central crack forms early and tends to concentrate the deformation at its tip in narrow bands of high shear strain. These shear bands are at angles of 50° to 60° to the transverse direction. Sheets of voids are nucleated in these bands, and the voids grow and coalesce into local fracture of the void sheet. While the average direction of crack growth is radially outward in the direction transverse to the tensile axis, on a finer scale the crack zigzags back and forth across the transverse plane by void-sheet formation. Thus, crack growth in ductile fracture is essentially by a process of void coalescence. Coalescence occurs by elongation of the voids and elongation of the bridges of material between the voids. This leads to the formation of a fracture surface consisting of elongated “dimples,” as if it had formed from numerous holes which were separated by thin walls until it fracture.

1.2.1.1.2 Brittle fracture

The most striking example of brittle fracture in large component is the failure of welded Liberty ships and T-2 tankers during World War II. Some of these ships broken completely in two, while in other instance, the fracture did not completely disable the ship. Most of the failures occurred during the winter months. These calamities focused attention on the fact that normally ductile mild steel can become brittle under certain conditions. Thus, a broad of research program was undertaken to find the causes of these failures and to prescribe the remedies for their future prevention. In a sense, the definition of brittle fracture can be conventionally believed as the fracture of a metal or other material occurring without appreciable prior plastic deformation. In brittle crystalline materials, fracture can occur by cleavage as the result of tensile stress acting normal to crystallographic planes with low indices (cleavage planes). In addition, when fractures occur in polycrystalline iron or steel by transcrystalline cleavage, there is very little energy expended in propagating the fractures, which closely resemble those occur in glass or other brittle isotropic elastic solids.

The first explanation of the discrepancy between the observed fracture strength of crystals and the theoretical cohesive strength was proposed by Griffith. Griffith’s theory in its original form is applicable only to a perfectly brittle material such as glass. However, while it cannot

be applied directly to metals, Griffith's ideas have had great influence on the thinking about the fracture of metals. The Griffith model considers the stability of an existing defect. It is based on a global energy balance: for brittle fracture to occur, the energy stored ahead the crack must be sufficient to overcome the surface energy of the material. Since fracture involves breaking bonds, the stress on the atomic level must be superior to the cohesive stress. This local stress intensification is a pure mechanical local effect of flaws in the material which explains the discrepancy between the actual strength of brittle materials and theoretical estimation. Fracture cannot occur unless the stress at the atomic level exceeds the cohesive strength of the material. A sharp microcrack is one way to provide sufficient local stress concentration. Thus, in addition with the increase of local stress by a flaw, any effect such as chemical effect aiming at weakening the atomic bonds will help the brittle fracture. In addition, the nature state of stress in a metal specimen is an important consideration in the fracture process. Both cleavage-crack nucleation and propagation are favoured by high tensile stresses. On the other hand, slip requires shear stress. When deformation occurs by slip, however, the applied stresses tend to be relieved, which is difficult to achieve large stresses when a metal deforms easily by slip. Therefore, any stress system capable of producing a combination of large tensile stresses and small shear stresses favours cleavage.

In simple uniaxial tension, the stress can be viewed as equivalent to a set of shear stresses oriented at 45° to the tensile stress axis. This relationship is shown in Figs. 1.5a and 1.5b, where the tensile stress in one case is assumed horizontal and in the other vertical. If the two tensile stresses are applied simultaneously to the same specimen, the shear-stress components will oppose each other. So, the shear-stress in the material is reduced under a state of biaxial tensile in the two dimensional case. Also, if a third tensile stress is applied normal to the plane of the above stresses, and all the tensile stresses are assumed equal, a state of hydrostatic tension will occur in which the material experiences no shear stress.

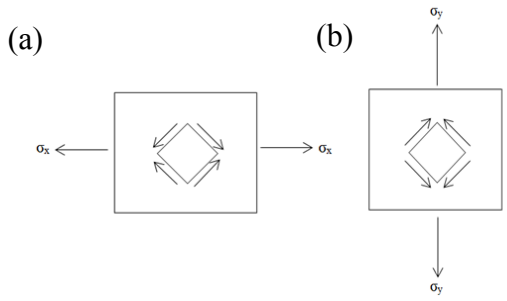

Figure 1.5: Tensile stresses at right angles produce shear stress components which oppose each other [REE-1973].

Whenever a metal specimen is tested under conditions of biaxial or triaxial tension, slip that requires shear stress will tend to be suppressed, and because of this, a high level of tensile stress can be attained and brittle fracture by cleavage can be promoted. An easy way of approximating the state of triaxial tensile involves the placing of a simple V-notch around the gage of a cylindrical tensile-test specimen (Fig. 1.6). Furthermore, the most noticeable effect of a notch is that it can raise the temperature at which fracture can occur by cleavage in a tensile test, or other specimen.

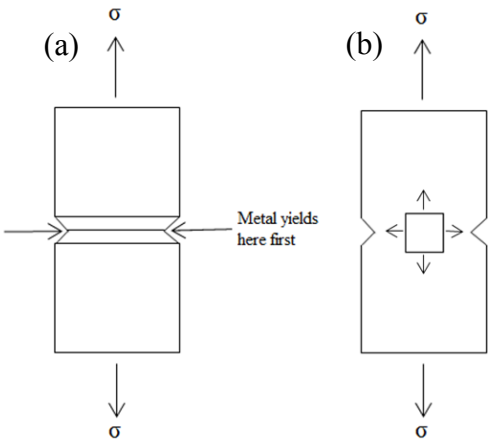

Figure 1.6: A notched tensile specimen yields first at the notch, which develops a state of triaxial tension in the cross-section at the notch; (a) is the three-dimensional view, and (b) is the cross-section showing stress distribution [REE-1973].

Independently of environmental effects, three basic factors contribute to a brittle-cleavage type of fracture. These are (1) a triaxial state of stress, (2) a low temperature, and (3) a high strain rate or rapid rate of loading. All these three factors do not have to be present at the same time to produce brittle fracture.

1.2.1.2 Fracture mechanics

Fracture mechanics is the field of mechanics concerned with the study of the propagation of cracks in materials. It used methods of analytical solid mechanics to calculate the driving force on a crack and those of experimental solid mechanics to characterize the material's resistance to fracture. In modern materials science, fracture mechanics is an important tool in improving the mechanical performance of materials and components. It applies the physics of stress and strain, in particular the theories of elasticity and plasticity, to the microscopic crystallographic defects found in real materials in order to predict the macroscopic

mechanical failure of bodies. Fractography is widely used with fracture mechanics to understand the causes of failures and also verify the theoretical failure predictions with real life failures.

Fig. 1.7 shows the three loading modes for crack extension.

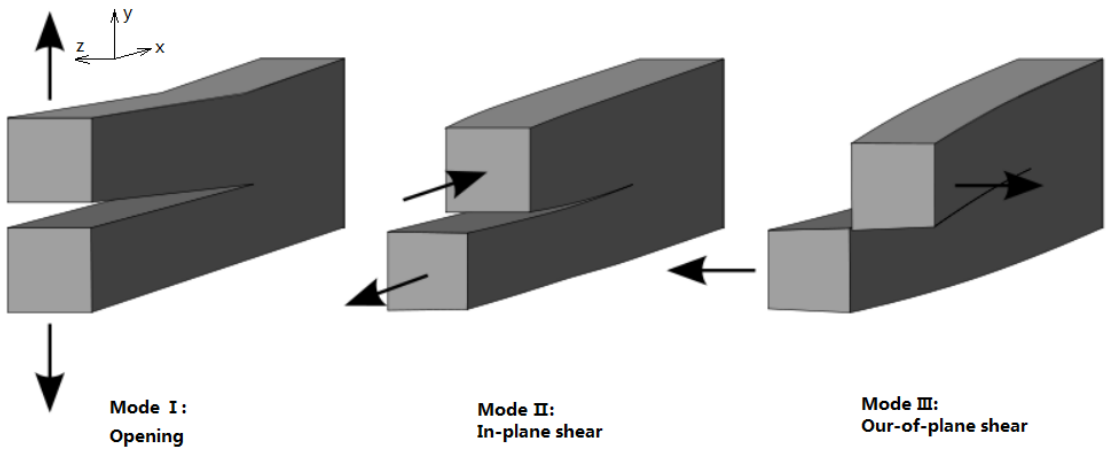

Figure 1.7: Crack-deformation modes.

Mode I, the crack-opening mode, refers to a tensile stress applied in *y* direction normal to the faces of the crack. This is the usual mode for fracture toughness tests and a critical value of stress intensity determined for this mode would be designated K_{IC}. K_{IC} is used to determine linear-elastic fracture toughness for the brittle materials, while for ductile materials the plastic-elastic fracture toughness J_{IC} is employed. Fracture toughness is a quantitative mechanical characteristic of a material, which expresses its resistance to fracture when a crack is present. Normally, brittle fracture materials are characterized by low fracture toughness, while if a material has very much fracture toughness it undergoes ductile fracture. Mode II, the forward shear mode, refers to a shear stress applied normal to the leading edge of the crack but in the plane of the crack. Mode III, the parallel shear mode, is for shearing stresses applied parallel to the leading edge of the crack. Mode I is the most studied situation because it is the most dangerous.

1.2.2 Characteristics of LME

1.2.2.1 Definition and criteria of occurrence of LME

When a solid metal is in contact with a liquid metal, it can be attacked. The following four main forms of attack of solid metals by liquid metals have been identified [FER-1994].

(a) Instantaneous failure of a solid metal under applied or residual stresses when in contact with a liquid metal.
(b) Delayed failure of a solid metal in contact with a liquid metal at a static stress level below the tensile strength of the metal.
(c) Stress independent grain boundary penetration of a solid metal by a liquid metal.
(d) High temperature corrosion of a solid metal by a liquid metal.

Only the first type can be considered as classical liquid metal embrittlement (LME) although delayed failure has often been referred to as LME in the literature. LME (Liquid Metal Embrittlement) or LMIE (Liquid Metal Induced Embrittlement) must be distinguished from LMC (liquid metal corrosion). LMC is a physical or physical-chemical process, involving species dissolution and transport, chemical reaction and new phases. No mechanical action is involved in LMC. LME involves mechanical loading and corrosion process may occur but not such as dissolution.

The following definition of LME is the most often proposed. LME is the reduction in ductility and strength that can occur when normally ductile metals or metallic alloys are stressed while in contact with liquid metals.

LME is considered as a special case of brittle fracture, intergranular (IG) or transgranular (TG) by cleavage, which occurs in absence of an inert environment and not at low temperature. In addition, LME is accompanied by little or no penetration of the embrittling atomic species into the solid metal. In other words, strictly speaking, a time and temperature dependent fracture proves will not be considered as a manifestation of LME.

The loss of ductility arising from LME generally manifests itself as a reduction-in-elongation and reduction-in-area at failure. The true fracture stresses are similarly reduced and in cased of severe embrittlement may be less than the macroscopic yield strength. There are no changes to the bulk properties of the solid metal such as Young's modulus and yield strength,

and the work-hardening behaviour remains unchanged. The stress-strain curve thus remains unaltered up to the point of failure [FER-1994, JOS-1999].

In fact, slight differences between the definitions of LME can be found in the literature but are of minor importance for the understanding of the present PhD thesis. One should return to the review papers on LME Kamdar [KAM-1973], Nicholas [NIC-1979], Gordon [GOR-1982], to the recent models review by P.J.L. Fernandes [FER-1997], B. Joseph [JOS-1999], to the point of view of E.E. Glickman in 2000 [GLI-2000].

1.2.2.2 The pre-requisites of occurrence of LME

Researchers have attempted to define the pre-requisites for LME failure and some have even proposed empirical rules with the aim of predicting the occurrence of embrittlement. But none can fully account for all experimental observations. Nevertheless, two pre-requisites have been determined and are generally agreed upon as follows.

(a) There must be intimate contact or wetting of the solid metal by the liquid metal. Failure to ensure this has led some researchers to erroneously conclude that certain solid metal-liquid metal couples are immune to LME.
(b) The solid metal must be sufficiently stressed to produce plastic deformation. Stress concentrations such as grain boundaries, second phase particles and notches are capable of producing localized plastic deformation sufficient to cause LME cracking, and general plasticity is not essential.

1.2.2.3 Characteristic features of LME failure

There are a number of characteristic features associated with LME failure. These are listed below [FER-1994].

(a) LME failure results in a severe reduction in ductility. This is usually indicated by a small or zero reduction in cross sectional area at failure and significantly reduced fracture toughness. For example, running cracks in plate material will lead to flat fractures with negligible shear lip formation;
(b) Crack initiation occurs at the solid-liquid metal interface;
(c) Crack growth is usually very fast, up to 1 $m \cdot s^{-1}$;

(d) Cracking can be intergranular or transgranular;

(e) Fracture surfaces are covered with a layer of liquid metal which may range from a few atoms to a few millimetres in thickness. Chemical analysis should reveal the presence of liquid metal on the fracture surfaces. Where an abundance of liquid metal is present or where prolonged exposure of the fracture surface to the liquid metal after failure has led to the formation of intermetallic compounds, fractographic features may be concealed;

(f) Typically, final fracture results from a single crack but crack branching or micro-cracking may occur;

(g) The presence of liquid metal at the crack tip is essential for propagating the brittle crack by LME. In cases where the crack runs ahead of the liquid metal, crack growth can only occur by a conventional fracture mechanism such as cleavage, micro-voids coalescence or shear. Depending on the amount of liquid metal available, the conventional fracture surfaces may subsequently become coated with liquid metal. In cases where the liquid metal is depleted during LME crack growth, the crack will arrest if the stress intensity is below the critical stress intensity for the fracture of the material in the absence of LME.

It is important that any failure be assessed critically in the light of the above features and in combination with all other relevant information which may come to light during the investigation. The presence or absence of these features does not prove or preclude that failure occurred due to LME. Finally, it is concluded that LME does not occur every time when a metal or alloy is stressed while in contact with liquid metal, but rather that it depends on a complex combination of factors such as the solid and liquid metal composition, grain size, strain rate, temperature and surface condition.

A tendency to list liquid metal-solid metal couples susceptible to embrittlement appeared motivating. This has been referred to as the specificity of liquid metal embrittlement (LME). These couples have been based on two observations of embrittlement couples, namely the low mutual solubility and the lack of intermetallic compounds between the solid and liquid metals [NIC-1979]. A high mutual solubility may lead to dissolution of the solid metal in the liquid metal, which effectively blunts the crack tip and retards or arrests further crack growth. The tendency for solid and liquid metal to react to form intermetallic compounds has been expressed in several ways. The difference in electronegativity values between solid and liquid metals has been considered, and in many cases the severity of embrittlement increased as the

electronegativity difference decreased. Kelly and Stoloff [KEL-1975] also developed a bond interaction-solubility model, and shown that, in general, couples with low mutual solubility and high interaction energy are more susceptible to embrittlement. Numerous other models also exist [JOS-1999]. However, the reality shows that there is a lot of couples solid material-liquid metal which were expected to feature LME but did not occur, and the reverse also.

Because the modification in a structural parameter (e.g. heat treatment) of a material as well as the numerous working parameters (e.g. strain rate) can lead to LME, it is now admitted that any couple of solid material - liquid metal cannot be simply proclaimed as immune against LME.

1.2.2.4 Liquid metal assisted damage (LMAD)

In some cases, the mechanical properties and the mechanical response are affected by the presence of the liquid metal but there is not a fracture mode transition, such as a ductile to brittle transition. The fracture mode exhibits nearly the same feature with and without the liquid metal but there is acceleration in the damage process. This situation can be observed during low cycle fatigue as pointed out by Vogt et al. for the T91 steel [VOG-2007].

Vogt et al. found a reduction in low cycle fatigue lives and an increased fatigue crack growth rate by liquid LBE. Liquid LBE assists the propagation of the first short cracks so that it prevents nucleation and propagation of other cracks as shown in Fig. 1.8. This liquid metal accelerated damage (LMAD) is expressed through the fatigue resistance curves [VOG-2007, FAZ-2008]. The mechanism for that is a liquid metal assisted plasticity at crack tip.

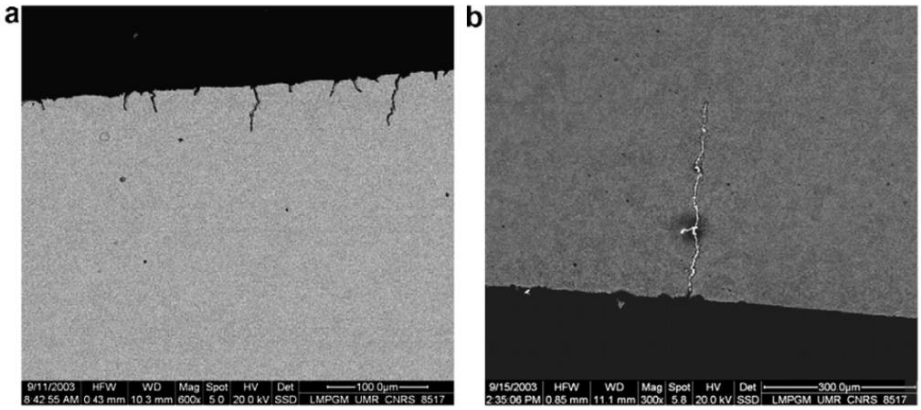

Figure 1.8: Transversal cut of the T91 specimen after fatigue failure at 300°C and $\Delta\varepsilon_t$=2.2% in air (a) and in LBE (b) [VOG-2007].

1.3 Models for mechanism of LME failure take place

Although LME has been discovered for more than a century, it has not been explained clearly. Many scientists tried to give the proper models to describe the mechanisms by which LMIE failure takes place. P. J. L. Fernandes and D. R. H. Jones [FER-1997] had analysed this phenomenon and summarized each of the models in detail and highlighted the advantages and limitations of each model.

1.3.1 Reduction in surface energy model

The reduction in surface energy model is based on the concept that the surface free energy of a solid metal is reduced by the adsorption of a liquid metal, and this idea was first proposed by Rozhanskii and Rebinder. This model indicated that adsorption of surface active substances on the surface of a solid metal can result in a decrease in fracture strength. Furthermore, the surface energy model is in view of the Griffith equation which considers the energy balance between the decrease in potential energy of a stressed body, owing to the release in elastic stored energy and the work done in moving the external surfaces, and the increase in surface energy owning to the cracking.

Based on the Griffith equation, which indicates that the stress required for fracture of a purely elastic material is related to the specific surface energy and the Griffith equation is as follow:

$$\sigma_a = \left(\frac{2E\gamma_e}{\pi a}\right)^{1/2} \qquad 1.1$$

σ_a is the applied stress, E is Young's modulus, γ_e is the specific surface energy, and a is the crack length (half crack length in the case of an elliptical crack). According to Griffith equation, it can get that if the specific surface energy is reduced by the adsorption of a liquid metal species at the crack tip, the applied stress required for fracture is similarly reduced. This theory has been used to explain the effects of hydrogen embrittlement, temper embrittlement and LMIE.

Although the reduction in surface energy model can account for some embrittlement phenomenon, it also received some criticisms, due to this model derived from a purely elastic material and does not considered the effects of crack tip plastic deformation. As a knowledge of that most of solid materials, especially metals, plastic deformation is unavoidable during

crack propagation, this plastic deformation work is usually several orders of magnitude larger than the surface energy of the solid. Orowan modified this original Griffith equation to account for plasticity and Gilman tried to use another different approach to resolve further problems derived and assuming that the material is perfectly plastic. In fact, some experimental results have been successful explained by Gilman's approach. However, due to lack of the surface energy data which prevented this reduction in surface energy model rigorous application. In addition, the limitations and inadequacy of this model are accounted how the effects of various metallurgical and physical variables to affect the susceptibility to LMIE. Furthermore, this model constitutes a thermodynamic approach to the problem of LMIE fracture and does not provide insight into the mechanisms of embrittlement on an atomic scale. Finally, although there are drawbacks of this reduction in surface energy model, to pursue the much more perfect models to explain this complicated phenomenon LMIE, reduction in surface energy original model provides the way of thinking as well as the broader research ideas.

1.3.2 Adsorption induced reduction in cohesion model (SJWK model)

The adsoption induced reduction in cohesion model is an extension of the surface energy model and considers the effect of the liquid metal on the strength of interatomic bonds at the crack tip. This model which is called SJWK model by Joseph et al. [JOS-1999] was proposed independently by different authors.

In this adsorption induced reduction in cohesion model (SJWK model), the presence of a liquid metal atom at the crack tip results in a reduction in the cohesive strengh of the interatomic bonds, which is explained by considering the schematic diagram of the crack tip in Fig. 1.9. Crack growth occurs by breaking successive bonds at the crack tip. When the bond A-A_o is stressed, crack growth may occur by bond breaking along the cleavage planenormal to the applied stress. Alternatively, crack blunting may take place by dislocation glide along the slip plane. The potential energy of the bond A-A_o and the stress acting on it vary with interatomic distance according to the curves $U(x)$ and $\sigma(x)$ respectively (Fig. 1.10). X_o represents the equilibrium atomic separation. σ_m is the maximum stress required to break the bond.

SJWK model proposes that the stress separation curve is approximated by a sine wave and the work required to break the bond is equaled to the surface energy of the newly created

surfaces, which can be shown that σ_m is given by the following equation 1.2:

$$\sigma_m = \left(\frac{E\gamma_e}{x_o}\right)^{1/2} \qquad 1.2$$

Where E is the Young's modulus, γ_e is the surface free energy, x_o is the equilibrium atomic separation.

In SJWK model, if an embrittler atom X (X in Fig. 1.9) is adsorbed at the crack tip, an electronic rearrangement will occur which may result in a reduction in the strengh of the bond A-A_o. From Fig. 1.10, the potential energy of the bond A-A_o is reduced from $U(x)$ to $U(x)_x$ and the stress acting on it from $\sigma(x)$ to $\sigma(x)_x$. Crack growth thus occurs by decohesion of the crack tip bonds at a stress $\sigma_{m\text{-}x}$. The embrittler atom becomes adsorbed on to the newly created surface after fracture and the process repeats itself. In fact, if the decohesion stress is reduced sufficiently then cleavage will be possible even in normally ductile face centred cubic materials.

The adsorption induced reduction in cohesion model is currently widely accepted and although many questions remain unanswered, particularly it is difficult to assess LMIE failure quantitatively using this model. Nevertheless, the adsorption induced reduction in cohesion model is yet to be used successfully to predict the severity of embrittlement under a given set of conditions.

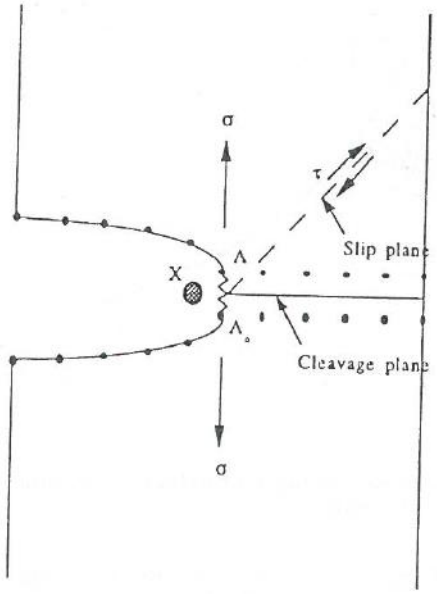

Figure 1.9: Schematic representation of crack in stressed metal exposed to aggressive environment X [FER-1997].

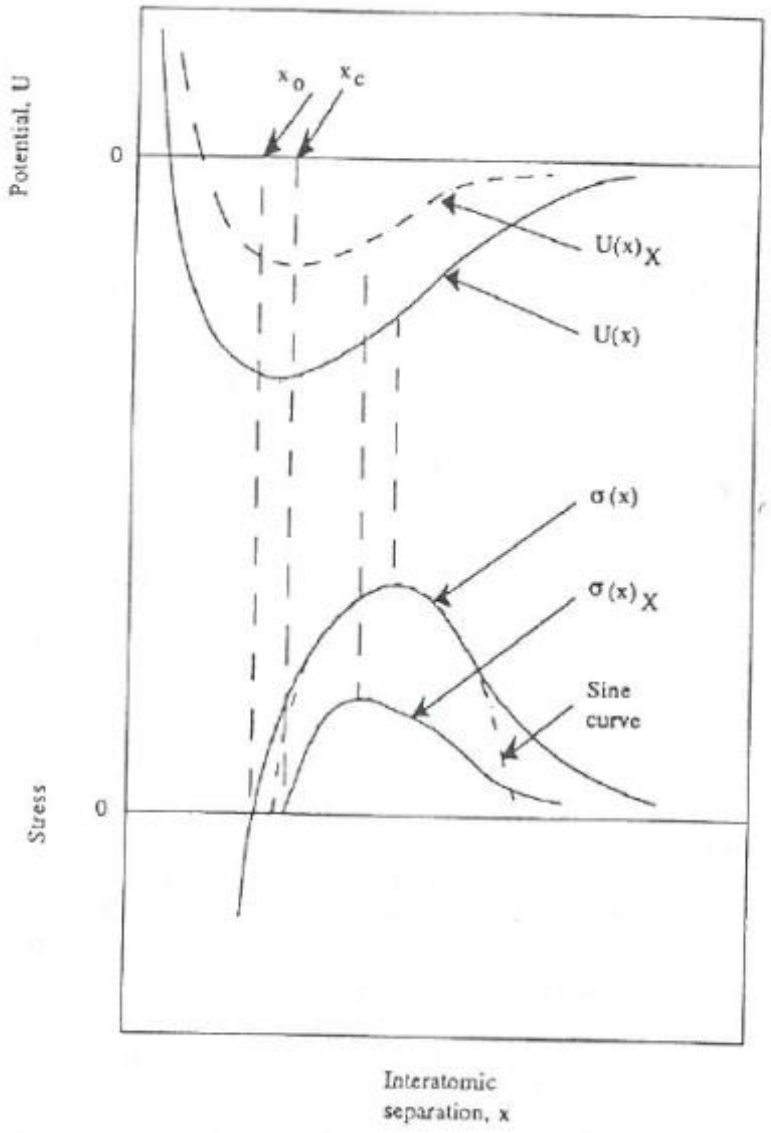

Xo represents equilibrium separation

Figure 1.10: Schematic curves for potential energy *U(x)* and $U(x)_x$, and resulting stress σ(x) and $\sigma(x)_x$, versus interatomic separation for atomic bonds in absence and presence of adsorbed atom X [FER-1997].

1.3.3 Enhanced dislocation emission model

Lynch [LYN-1981] proposed an alternative approach to the adsorption induced bond weakening mechanism, the enhanced dislocation emission model, which assumes that liquid metal at the crack tip adsorption results in a reduction in the shear strength of the bonds that can facilitate dislocation nucleation at the crack tip and leads to failure by extensive localized plasticity and void growth and coalescence immediately ahead of the crack tip, while SJWK model believed that the adsorption of the liquid metal at the crack tip leads to a reduction in

the tensile cohesive strength of the inter atomic bonds.

Fig. 1.11a shows the schematic diagram of a crack tip in an inert environment during ductile failure. At this condition, the presence of oxide films or the existence of lattice distortions on the surface of the crack inhibit dislocation nucleation at the crack tip. Dislocation sources ahead of the crack tip are activated at lower stresses than that required at the crack tip, and extensive plasticity occurs in the region ahead of the crack. Only a proportion of the dislocations which nucleated ahead of the crack egress exactly at the crack tip and therefore contributed to crack growth. Most of the dislocations egress behind the crack front to produce crack blunting, or they contribute to the general strain ahead of the crack tip. In inert environments, crack opening displacement is owing to crack blunting and straining ahead of the crack. Crack growth occurs by the growth and coalescence of these voids with the crack front, which results in the dimpled fracture surface characteristic of ductile failure. In addition, the egress of dislocations at the crack tip is usually random and fracture is therefore not parallel to any crystallographic.

In embrittling environments, the process of the crack growth is significantly altered (shown by Fig. 1.11b), because it is proposed that the embrittler atoms adsorption at the crack tip reduces the shear strength of the interatomic bonds, which facilitates dislocation nucleation and activates the crack tip dislocation sources before extensive dislocation activity ahead of the crack tip occurs. The dislocations nucleated at the crack tip are on suitably inclined slip planes to produce crack growth. In addition, in view of that any imbalance in the amount of slip around the crack tip will produce a back stress acting on previously injected dislocations on the more active slip plane, there is equal amounts of slip occur which on either side of the crack. Furthermore, dislocation egress at the crack tip leads to crack growth rather than blunting, there are smaller strains and plastic zones develop ahead of the crack. Void nucleation sites are therefore not affected until they are just ahead of the crack tip, so relatively little void growth takes place before coalescence with the crack occurs.

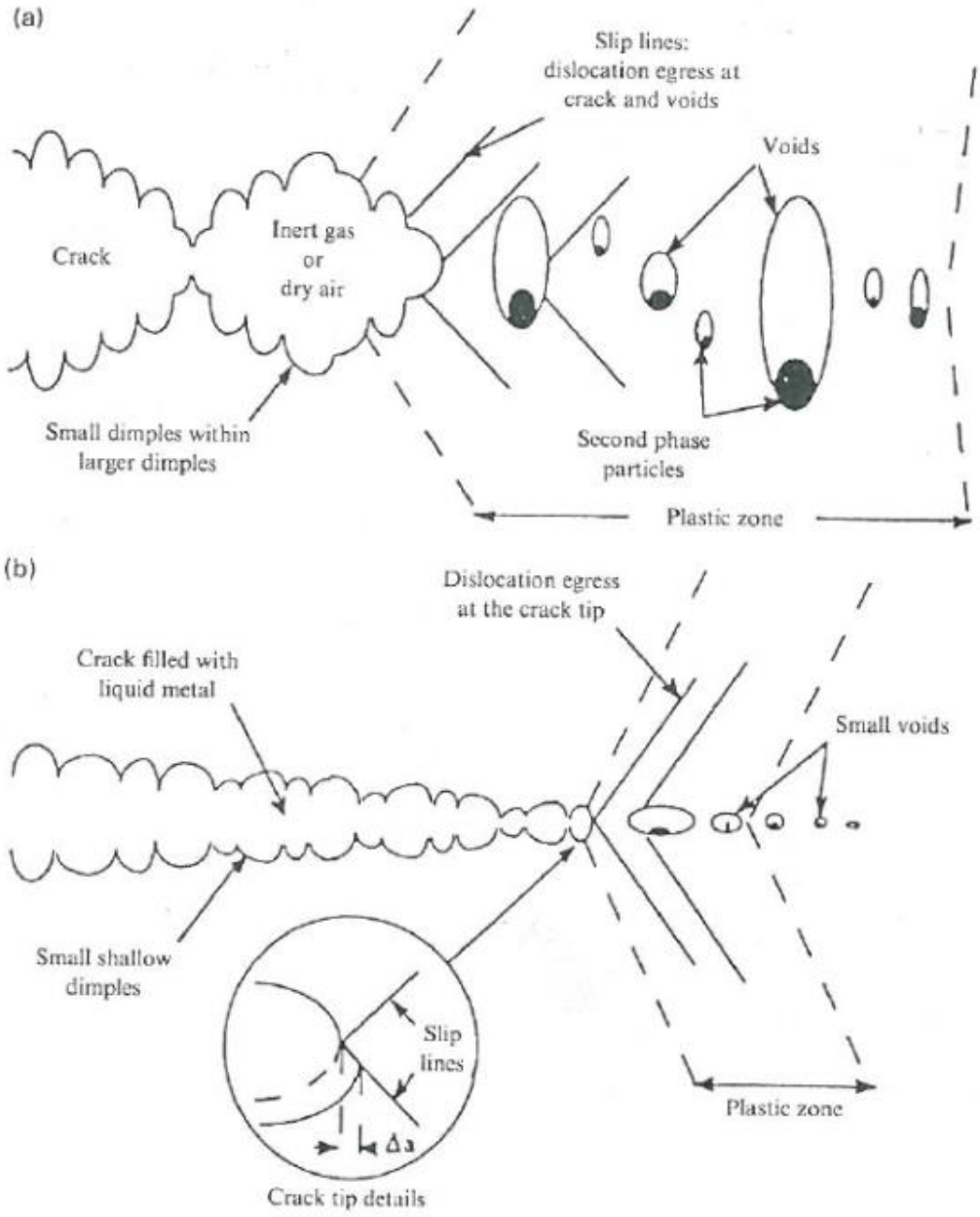

Figure 1.11: Schematic diagram of crack tip in (a) inert environments and (b) liquid metal environments [LYN-1981].

Crack growth occurs by alternate slip and coalescence of the crack with voids ahead of the crack front, which makes smaller and shallower dimples and finer fractographic detail than that observed in inert environments. In fact, a number of studies support enhanced dislocation emission model. Fleischer has shown that dislocation motion is influenced by changes in lattice parameter. In inert environments the atoms at the surface have fewer neighbours than those in bulk of the material and the surface lattice is therefore distorted. These distortions inhibit dislocation nucleation at the surface. In embrittling environments, however, embrittler atoms adsorb on to the surface effectively increasing the number of 'neighbours' and thus reducing the lattice distortions. Therefore, dislocation nucleation is facilitated and increased

dislocation activity is expected ahead of the crack tip. These predictions have been confirmed by computer simulations of the effect of adsorbed surface films on dislocation generation at the crack tip. Furthermore, the most convincing evidence of the enhanced dislocation emission model has been carried out by Lynch and several other researchers, based on the extensive fractographic and metallographic studies.

Finally, although the fractographic analyses described in literature appear to have been carried out thoroughly and are certainly convincing, some limitations to the enhanced dislocation emission model do exist. In LMIE cracking fracture surfaces are usually covered by liquid metal which is often difficult to remove that may conceal important fractographic details. Furthermore, the enhanced dislocation emission model cannot account for the delayed failure observed in some LMIE studies. In torsion tests on notched alpha brass specimens, the crack propagation occurred along the plane of maximum tensile stress which is inconsistent with the enhanced dislocation emission model that predicts that fracture occurs along the plane of maximum shear stress.

1.3.4 Enhanced work hardening model

The enhanced work hardening model is proposed by Dmukhovskaya and Popovich, and this model indicates that enhanced dislocation emission owing to the adsorption of embrittler atoms at the crack tip leads to enhanced work hardening of the material surrounding the crack. In fact, this model is based on the observation that liquid metals adsorption can facilitate dislocation emission and furthermore may also activate Frank-Read dislocation sources immediately ahead of the crack tip.

This model indicates that enhanced dislocation emission results in a reduction in flow stress and an increase in dislocation density in the surface layers of the solid metal where adsorption takes place, which can lead to an increase in the work hardening rate of these layers that therefore become harder than the bulk material. The model also shows that under tensile loading, the plasticity of the surface layer becomes exhausted and microcracks initiate at dislocation pileups and other stress concentration sites, so at this condition, the propagation of cracks proceeds to the depth of the hardened layer, at which stage the work hardening cracking process is repeated.

This model features a repeated work hardening cracking process suggesting that LMIE crack

growth is discontinuous which has been confirmed on the observation of intermittent crack growth. Furthermore, crack initiation occurs at dislocation pileups and other stress concentration sites, thus implying that LMIE is a special case of brittle fracture which allows the effects of temperature, strain rate, solid metal composition and microstructure, and prior cold work to be predicted from the theory of brittle fracture. In addition, since this model is the basic premise that adsorption of a surface active species at the crack tip affects the deformation characteristics of the solid metal, so the model can be used to account for other forms of environmentally assisted cracking.

Actually, there are some similarities between this model and the enhanced dislocation emission model, because both models predict an increase in the dislocation activity around the crack tip. However, the differences between the two models are that the enhanced dislocation emission model shows that the effects of adsorption on dislocation activity are constrained to a few atomic layers around the crack tip, and the deformation characteristics of the lattice away from the crack are not affected. So work hardening is not a requirement for embrittlement. While the enhanced work hardening model proposes that adsorption facilitates the emission, egress, and movement of dislocations, and also suggests that new slip systems are activated, however, which are not supported by fractographic and metallographic studies.

1.3.5 Hancock and lves' model

Model proposes that embrittlement results from the interaction of dislocation pileups and liquid metal atoms diffusion ahead of the crack tip, which is based on the concept that plastic flow occurs around the crack tip during loading resulting in the formation of dislocation pileups at grain boundaries immediately ahead of the crack. If liquid metal atoms are able to penetrate short distances ahead of the crack tip and together with the stresses from the dislocation pileups, this may be sufficient to cause crack growth. In fact, a mathematical analysis for this model has been proposed by Nikolenko which shows that rapid crack growth is possible when the coefficient of diffusion along the grain boundaries is much larger than that for bulk diffusion.

The advantages of this model are that it can predict (at least qualitatively) the effects of temperature, strain rate, solid metal composition and microstructure, and prior cold work on embrittlement. However, some severe limitations of this model exist, for example, the model assumes that failure by LMIE is always intergranular and therefore cannot explain the

embrittlement of single crystals. Furthermore, whether dislocation pileups at subgrain boundaries or slip plane intersection points in single crystals will induce sufficiently high stresses to cause crack initiation is questionable. In addition, it is also uncertain whether diffusion ahead of the crack tip could occur at the very fast crack growth rates often observed in LMIE.

1.3.6 Stress assisted dissolution model

This model is based on the concept that dissolution of the solid metal in the liquid metal occurs at the crack tip under the influence of an applied stress which was first proposed by Robertson and has subsequently been developed by Glikman et al. [GLI-2000]. However, this model has received little support because a number of researchers have pointed out inconsistencies which exist between the model and experimental observations. For example, the model predicts that embrittlement will be more severe in systems showing high mutual solubility, but which is contrary to experimental observations. In addition, the assumption of this model is that solubility will increase under an applied stress is also not entirely justifiable.

1.3.7 Grain boundary penetration model

The grain boundary penetration model originally proposed by Krishtal (quoted in Gordon) [GOR-1982] suggests that crack initiation is preceded by stress assisted diffusion of the embrittling atoms into the base metal along the grain boundaries. The presence of embrittler atoms in the diffusion zone increases the difficulty of slip and reduces the resistance to cracking, and once a critical concentration of embrittling agent is present in the diffusion zone crack initiation occurs. Although a number of experimental observations have been accounted by this model [GOR-1982], some limitations exist. For example, a detailed mathematical analysis of the model has not been carried out, therefore, the feasibility of diffusion occurring to a significant extent, especially at high crack growth rates, has not been confirmed.

1.3.8 Synthesis of the different models

Some of the principal features of these models for LMIE are summarized in Table 1.1 [FER-1997].

Table 1.1: Comparison of principle features of existing models for LMIE [FER-1997].

Model	Principal features	Support	Limitations
Reduction in surface energy	-Thermodynamic approach based on reduction in surface energy for fracture in liquid metal environment -Failure is usually intergranular	-Experimental support -Can account qualitatively for effects of many experimental observations, e.g. temperature, strain rate and grain size	-Lack of surface energy data prevents quantification of embrittlement -Does not consider mechanisms if embrittlement on atomic scale
Adsorption induced reduction in cohesion model	-Adsorption of liquid metal reduces cohesive strength across atomic planes -Failure is by trans granular or intergranular cleavage	-Can account qualitatively for effects of many experimental observations, e.g. temperature, strain rate, and grain size -Fractographic support	-Difficult to quantify -Can not account for many experimental observations
Enhanced dislocation emission	-Adsorption of liquid metal atoms facilitates nucleation and movement of dislocations -Failure is by localized ductile microvoid coalescence	-Experimental support -Strong fractographic support -Many similarities with other environmentally assisted cracking phenomena	-No mathematic analysis -Based on fractographic analyses which are difficult and complicated to carry out -Lack of independent support
Enhanced work hardening	-Adsorption of liquid metal atoms facilitates nucleation and movement of dislocations -Enhanced dislocation activity results in work hardening and exhausts plasticity -Cracking is intermittent	-Experimental support for discontinuous crack growth -Can account qualitatively for effects of many experimental observations, e.g. temperature, strain rate, and grain size	-No mathematical analysis -Lack of experimental support for enhanced work hardening
Hancock and lves	-Liquid metal diffuses along grain boundaries ahead of crack tip and reacts with dislocation pileups to reduce fracture stresses	-Correctly predicts that LMIE fracture is accompanies by extensive plasticity -Mathematical analysis has shown that rapid LMIE cracking is feasible under these conditions -Can account qualitatively for effects of many experimental observations, e.g. temperature, strain rate and grain size	-Can not account for trans granular fracture of fracture of single crystals in LMIE -Lack of experimental support for concept of liquid metal diffusion ahead of crack tip
Stress assisted dissolution	-Crack growth is through stress assisted dissolution of solid metal in liquid metal at crack tip	-limited experimental support	-Lack of experimental support -Predicts wrong dependence of LMIE on liquid metal composition
Grain boundary penetration	-Stress assisted diffusion of liquid metal along grain boundaries ahead of crack tip -Presence of embrittlement ahead of crack tip increased difficulty of slip and reduces resistance to cracking	-Can account qualitatively for effects of many experimental observation, e.g. temperature, strain rate and grain size	-No mathematic analysis -Lack of experimental support for concept of liquid metal diffusion ahead of crack tip -Can not account for trans granular fracture or fracture of single crystals in LMIE

1.4 Behaviour of T91 steel in contact with LBE

Materials research associated with the research and development activities of the MYRRHA and MEGAPIE accelerator driven systems (ADS) projects has been carried out by the mechanical and corrosion groups of several laboratories in Europe with an objective to study the effects of the liquid metal environment (liquid LBE - 45wt% Pb and 55wt% Bi) on the properties of selected structural materials. For these applications, the candidate structural materials are the ferritic-martensitic steel T91 for the parts working at high temperatures under high proton/neutron doses especially for the beam window of the MEGAPIE target, and the austenitic stainless steel 316L for the parts working at lower operating temperature and lower neutron flux components.

The material ferritic-martensitic steel T91 is a modified 9Cr1Mo steel, which was developed to increase the mechanical strength especially at higher temperature by addition of Nb and V that promote the nucleation of a fine distribution of $M_{23}C_6$ carbides (the industrial grade is T91, and called as T91). It has been chosen as the beam window of the MEGAPIE target due to its wide use for the core structure of fission neutron reactors or accelerator irradiation facilities and the extensive in-service properties database available after irradiation in fission reactors. In addition, T91 martensitic steel has low linear thermal expansion, higher thermal conductivity, and better mechanical properties than those of austenitic steels. Furthermore, especially T91 steel has good resistance to irradiation by fission neutron, low irradiation creep, low swelling, and small ductile to brittle transition temperature shift (DBTT).

The role of the T91 steel is very important for construction and implementation of the current nuclear industry. The compatibility of the structural material with the liquid lead-bismuth eutectic (LBE) is known to be one of the critical issues in the development of the ADS, including the good resistance to the corrosion and to LME. Therefore, this section is briefly reviewed the physical properties of LBE, effect of LBE corrosion, mechanical behaviour and fracture properties response of the T91 steel in liquid LBE, the advanced coating method for material protection of T91 steel, the heat treatment effects, as well as the radiation effects.

1.4.1 Lead-bismuth eutectic (LBE)

The normally composition of liquid metal lead-bismuth eutectic (LBE) is 45 at.% Pb and 55 at.% Bi. According to the phase diagram of the Pb-Bi system made by N. A. Gokcen in

1992 (Fig. 1.12), the characteristics of the Pb-Bi system are:

- T_{melt} Bi=271.442°C (544.592K);
- T_{melt} Pb=327.502°C (600.652K);
- The eutectic point at 45.0 at.% Pb and $T_{melt\ LBE}$=125.5°C (398.65K);
- The peritectic point at 71 at.% Pb and 187°C (460.15K);
- The lower limits of the elements solubility in the solid state: 22 at.% Bi in Pb and 0.5 at.% Pb in Bi;
- The intermetallic compound phase (ε-phase region).

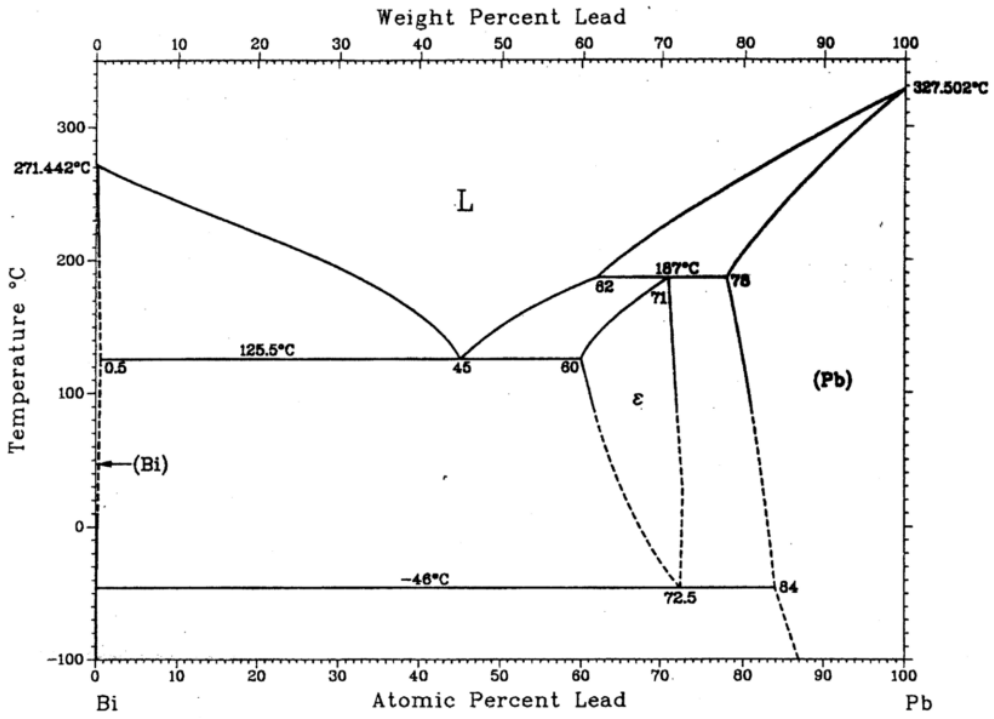

Figure 1.12: Phase diagram of the Pb-Bi system [HAN-2007].

In addition, though LBE is corrosive towards structural steels, this corrosion can be mitigated by controlling the oxygen concentration in the liquid LBE such that a protective oxide coating is formed over them. Therefore, an understanding of the thermochemical behaviour of oxygen in liquid LBE is needed for successful exploitation of the process. Furthermore, the oxide that coexists with LBE saturated with oxygen is not unequivocally known. For the moment, partial phase diagram of the ternary Pb-Bi-O system has been established by phase equilibration studies in the temperature range of 740-840 K (Fig. 1.13) [GAN-2008].

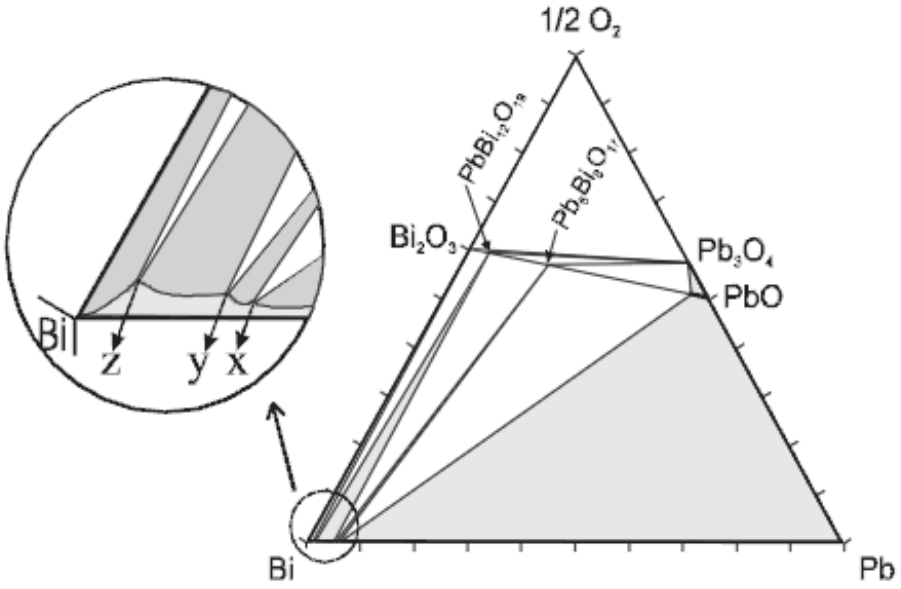

Figure 1.13: Isothermal section of the partial phase diagram of the Pb-Bi-O system at 823 K (where x, y, z are terminal compositions) [GAN-2008]

Considering the excellent performance of LBE, good nuclear properties compared with other liquid metals, LBE is employed in the field of nuclear applications. For example, LBE has a small neutron absorption cross section, good thermal conductivity, and the fact that it does not change its volume upon solidification, as well as lower melting point (125°C) while higher boiling point (1670°C) which is very important for security consideration for engineering design. Table 1.2 shows the basic characteristics of reactor coolants. Table 1.3 shows some relevant properties of possible liquid metal target candidate materials. Table 1.4 shows the volume change of pure lead, bismuth and LBE at melting.

Table 1.2: Basic characteristics of reactor coolants [HAN-2007].

Coolant	Atomic mass (g/mol)	Relative moderating power	Neutron absorption cross-section (1 MeV) (mbarn)	Neutron scattering cross-sections (barn)	Melting point (°C)	Boiling point (°C)	Chemical reactivity (with air and water)
Pb	207	1	6.001	6.4	327	1737	Inert
LBE	208	0.82	1.492	6.9	125	1670	Inert
Na	23	1.80	0.230	3.2	98	883	Highly reactive
H_2O	18	421	0.1056	3.5	0	100	Inert
D_2O	20	49	0.0002115	2.6	0	100	Inert
He	2	0.27	0.007953	3.7	-	-269	Inert

Table 1.3: Some relevant properties of possible liquid metal target candidate materials [HAN-2007].

Coolant	Composition (at.%)	Density at 20°C (g/cm^3)	Density liquid (g/cm^3)	Linear coefficient of thermal expansion 10^{-5}/K (solid)	Linear coefficient of thermal expansion 10^{-5}/K (400°C)	Volume change upon solidification (%)	Specific heat (J/gK)	Thermal neutron absorption (barn)
Pb	Elem.	11.35	10.7	2.91	4	3.32	0.14	0.17
Bi	Elem.	9.75	10.07	1.75	-	-3.35	0.15	0.004
Pb-Mg eutectic	Pb 97.5% Mg 2.5%		10.06	-	-	0	0.15	0.17
Pb-Bi eutectic	Pb 45% Bi 55%	10.05	10.05			0	0.15	0.11
Hg	Elem.		13.55		6.1		0.12	389

Table 1.4: Volume change of pure lead, bismuth and LBE at melting [HAN-2007].

Volume change	Pb	Bi	LBE
$\Delta V_m/V_m$	+3.7	-3.7	~0.0

1.4.2 Corrosion of T91 steel by LBE

When solid metals are contacted with liquid metals, several physical processes, known as liquid metal corrosion (LMC), may take place and impair the mechanical properties (namely strength and ductility) of the exposed materials. LMC is related to several physical processes: dissolution, diffusion, and alloying. Furthermore, if there are impurities they can make the process much more complicate. In the case of LBE, the most important impurity has been found to be oxygen and its concentration is the vital role in the LMC research area that is dissolution and oxidation.

In this section, the corrosion effects of T91 steel by liquid LBE were each reviewed according to the latest research progress.

1.4.2.1. Corrosion by oxidation

Prior to 1980s, most of the studies for reducing the corrosion by liquid LBE focused on the

metallic inhibitors (the corrosion rate by liquid LBE can be significantly reduced through adding especially Zr or Ti into the liquid metal). However, recently, oxygen was recognized to be an effective non-metallic inhibitor for liquid LBE corrosion. That is why recent studies focus on how to control the oxygen concentration and on the behaviour of the protective oxide layer in liquid LBE. Oxygen has been found to react with the major elements of the steel such as Fe, Cr, and Ni to form a protective oxide layer, and it is possible to maintain an iron and chromium based oxide film on the structural material T91 surfaces by carefully controlling the oxygen concentration in liquid LBE. The oxide film formed on the structural material surface can effectively separate the substrate from the liquid metal and the direct dissolution of the structural materials becomes negligible since the diffusion rates of the alloying components are very small in the oxide layer. Therefore, the oxygen control in liquid LBE is an effective method for application of nuclear power systems to reduce the corrosion and enhance the structure life time [ZHA-2009].

All the studies performed on high oxygen concentration LBE concluded that a duplex-layer oxide film formed.

L. Martinelli et al. [MAR-2008-A, MAR-2008-B, MAR-2008-C, MAR-2008-D] has conducted a comprehensive and detailed study of the corrosion in static LBE at 470°C for immersion duration up to 7800 h. They pointed out that the oxide obtained in liquid LBE has a duplex structure. The first inner oxide layer composed of small equiaxed grains in contact with the T91 is constituted of a Fe-Cr spinel which stochiometry, $Fe_{2.4}Cr_{0.6}O_4$, and the second external oxide layer composed of columnar grains contacted with the liquid metal is a magnetite layer (Fe_3O_4) shown by Fig. 1.14. The oxidation mechanism proposed is described as follow:

- The magnetite layer grows at the magnetite/liquid metal interface involving the iron diffusion from the steel to this external interface, and this iron diffusion leads to vacancies formation inside the T91 steel at the T91 steel/oxide interface. Due to the presence of the chromium atoms in the T91 steel, these vacancies can accumulate to form nanometric cavities (nano-cavities);

- The Fe-Cr spinel layer grows at the Fe-Cr spinel/T91 steel interface involving a penetration of oxygen from the liquid metal to the T91 steel/oxide interface, and furthermore the oxygen diffuses across the oxide scale until the Fe-Cr spinel/T91 steel interface via liquid lead nano-channels.

In addition, the growth kinetics simulation results from L. Martinelli et al. indicated that the magnetite layer growth is controlled by iron diffusion inside the Fe-Cr spinel and the magnetite lattice, and the growth rate of Fe-Cr spinel seems to be linked to the magnetite growth rate and consequently also limited by the iron diffusion in the oxide scales lattices. Moreover, even if the iron diffusion occurs in the two oxide lattices, only the Fe-Cr spinel layer seems to be a protective scale for the T91 steel oxidation in liquid LBE according to the investigation of simulation and experiments [MAR-2008-C].

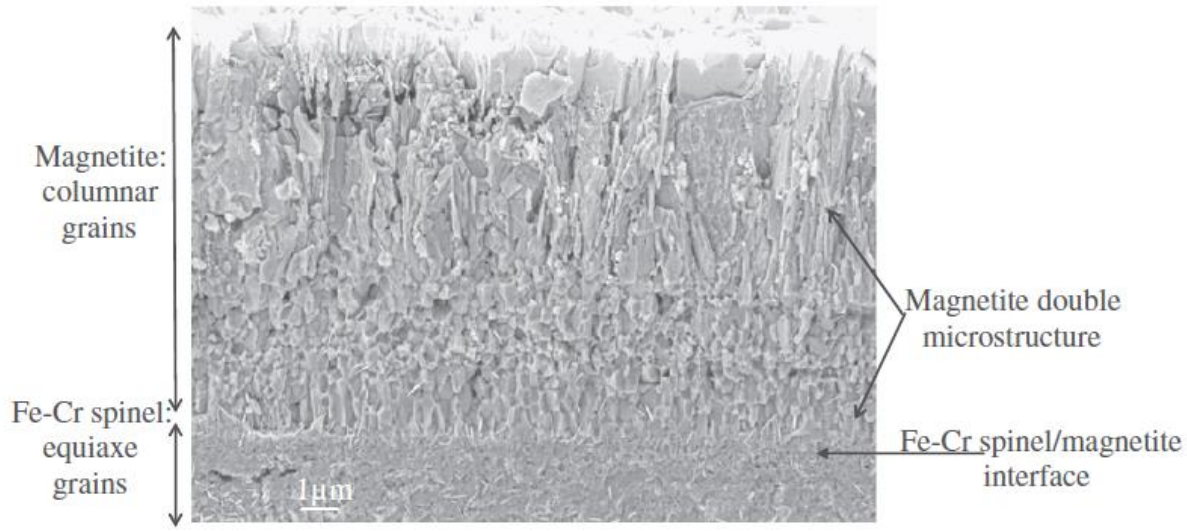

Figure 1.14: SEM-FEG SE picture of fractured cross section of T91 sample immersed 3700 h in oxygen saturated Pb-Bi alloy at 470°C [MAR-2008-B].

Fazio et al. [FAZ-2003] and Aiello et al. [AIE-2004-A] performed experiments in flowing LBE at 400°C. The LBE velocity was 3 m/s and its oxygen content was 10^{-5}-10^{-6} wt%. They found similar oxide layer with Cr enrichment and maxima in Cr concentrations and are accompanied by minima in Fe concentration shown by the concentration profiles Fig. 1.15.

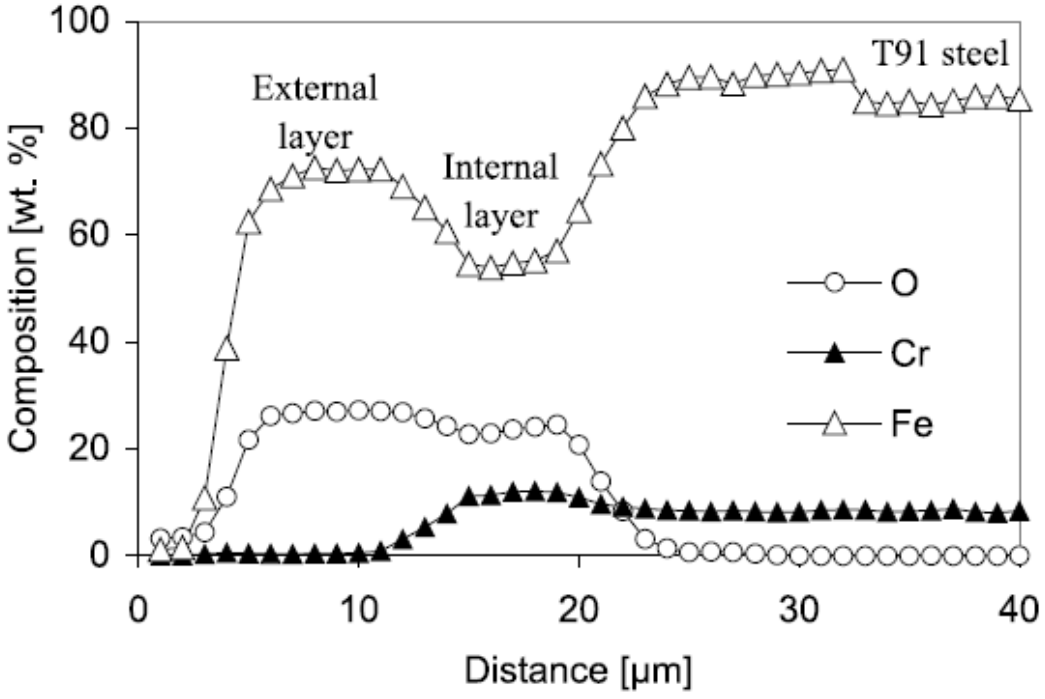

Figure 1.15: Concentration profiles obtained on T91 steel tested at 743 K for 3000 h [BAR-2001].

O. Yeliseyeva et al. [YEL-2008] researched the influence of temperature on the interaction mode of T91 steel with Pb-Bi melt saturated by oxygen and they had established a kinetic model of the evolution of duplex scale on the surface of steel during the corrosion experiments. The model contains three stages of interaction, namely, nucleation, growth and degradation of duplex scale and with the increasing of the temperature, time and concentration of oxygen in the liquid metal, the evolution of duplex scal is accelerated. Furthermore, about the corrosion kinetics of T91 steel in flowing oxygen-containing LBE, Schroer et al. [SCH-2012] have obtained the quantitative data for the thickness of these essentially bi-layer as a function of exposure time, implying dissolution of Fe (or erosion of magnetite) by the flowing LBE at the scale surface and transformation of spinel into magnetite at the magnetite/spinel interface, and the latter is corroborated by an apparent movement of the magnetite/spinel interface from the original position of the T91 steel surface in the direction of the steel. Calculating the metal recession for the magnetite and spinel formation however overestimates the metal recession, possibly because the rate of the solid-state transformation at the magnetite/spinel interface decreases with time. Estimating the amount of metals (Fe) dissolved from the scale also depends on the kinetics assumed for the spinel-into-magnetite transformation, and additionally the actual density (porosity) of the two oxide layers. However, irrespective of a more precise consideration of the transformation of spinel into magnetite, the quantitative data obtained allows for estimating the wall-thinning

and thickness of surface oxides expected for plant components made of T91 steel, and which is meaningful.

1.4.2.2 Corrosion by dissolution

Fazio et al. [FAZ-2003] and Aiello et al. [AIE-2004-A] studied the corrosion behaviour of martensitic steel T91 at 400°C in flowing LBE at low oxygen concentration condition ($C_{[O2]}$=10^{-8}-10^{-10}wt%).

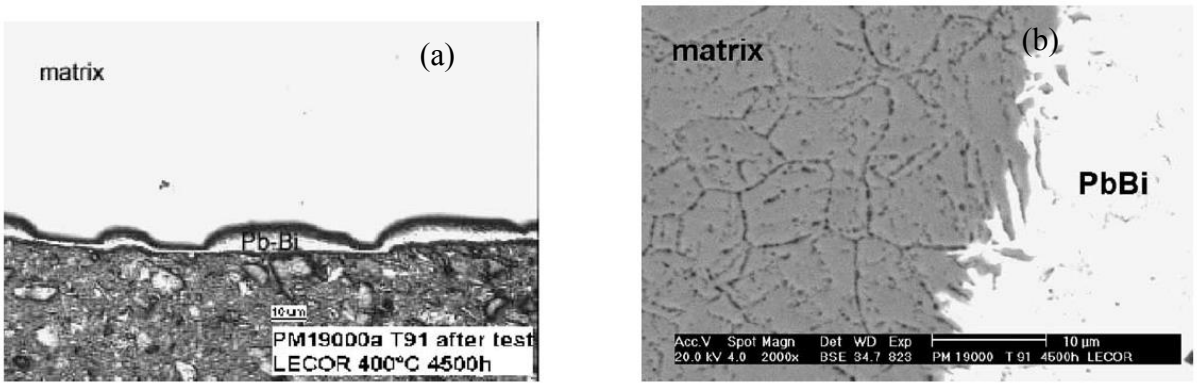

Figure 1.16: (a) Optical micrograph, and (b) SEM cross-section photo of T91 exposed in LECOR loop after 4500 h ($C_{[O2]}$=10^{-8}-10^{-10}wt%, T=400°C) [AIE-2004-A].

They found that the steel was affected by dissolution as shown by Fig. 1.16 (liquid LBE penetrated into the matrix of T91 steel).

Similar long-term corrosion studies on T91 steel in flowing LBE enviroment at temperatures between 575 K and 725 K during 2000 h and 5000 h and 10000 h have been conducted in LINC loop (the operating oxygen concentration range was 10^{-8}-10^{-10} wt% in LBE) at CIEMAT in Spain, and the maximum flow velocity in the region of specimens is approximated 1 $m \cdot s^{-1}$ [MAR-2011-B]. F. J. Martín-Muñoz et al. [MAR-2011-B] show that the material T91 did not exhibit a weight loss after exposure to the flowing LBE at 575 K after 10000 h (metallographic examinations shown an 'unaffected' surfaces or surfaces with a very thin oxide layer) except specimens located in the bottom part of hot test sections (725 K) exposed for 5000 h. There is important weight loss and severe dissolution up to 300 µm depth on surfaces of T91 specimens shown by Fig. 1.17.

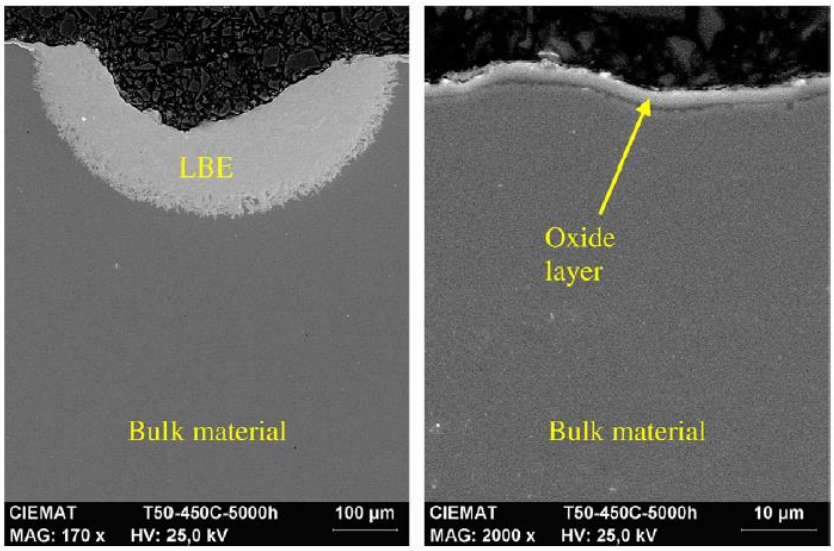

Figure 1.17: Cross-section of T91 after 5000 h at 725 K in flowing LBE. Areas with severe dissolution (left) and thin oxide layer on the rest of surface (right) [MAR-2011-B].

D. Sapundjiev et al. from SCK-CEN [SAP-2006-B] had researched the corrosion resistance of T91 in stagnant liquid lead-bismuth eutectic (LBE), exposed for 175, 500, 1250, 2300 and 3000 h at temperature from 425°C to 600°C under Ar+5%H_2 cover gas atmosphere with dissolved oxygen concentration ~10^{-11} wt% (experimental SEM photos of T91 specimens shown in Fig. 1.18 below 500°C, and Figs. 1.19, 1.20, 1.21, 1.22 above 500°C). The results indicated that material T91 retained oxides formation until the test termination, and these oxides were uniform at the beginning of the experiment while with a time a double layer oxide scale formed comprising of inner columnar and outer laminar structure consisting predominantly of chromium oxide shown by Fig. 1.18. Within the oxides formation, liquid LBE penetration was measured without exception from 1 to 2 µm in the beginning of the tests up to 5-6 µm at the end (Fig. 1.18). D. Sapundjiev et al. also discovered that severe corrosion occurred at temperatures above 500°C where three corrosion modes were distinguished: stable oxide film mode (Fig. 1.19), transition mode (Fig. 1.20), and final dissolution mode (Figs. 1.21, 1.22) featuring Cr and Ni leaching and material loss. The uniform dissolution is confirmed by the light microscopy shown by Fig. 1.20. The main corrosion mechanisms were uniform penetration and dissolution of the penetrated volumes. T91 steel had better corrosion resistance (corrosion rate ~≤137µm/year) at high temperature (＞500°C).

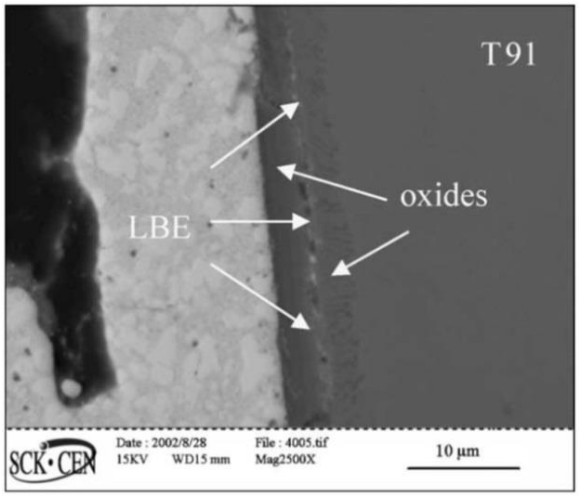

Figure 1.18: Double oxide layer on T91 sample. The outer laminar and the inner columnar parts are separated by subsurface Pb-Bi layer (<500°C) [SAP-2006-B].

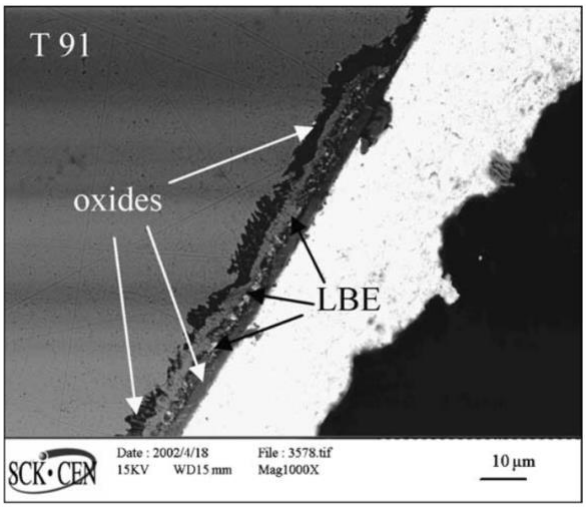

Figure 1.19: Stable oxide corrosion mode on T91. Specimen tested at 605°C for 175h [SAP-2006-B].

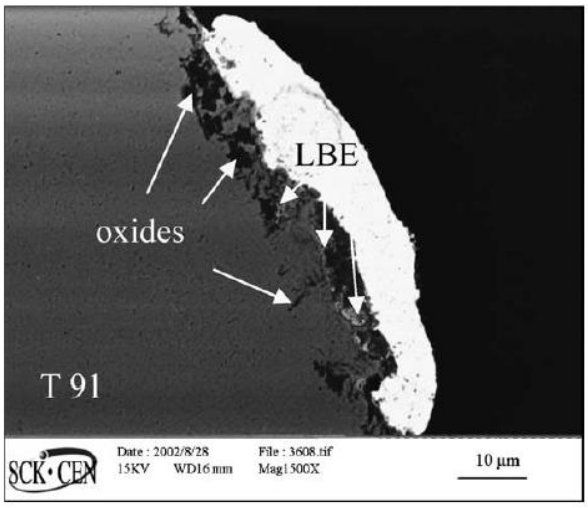

Figure 1.20: T91-initiation of the transition corrosion mode. Specimen tested at 575°C for 500h [SAP-2006-B].

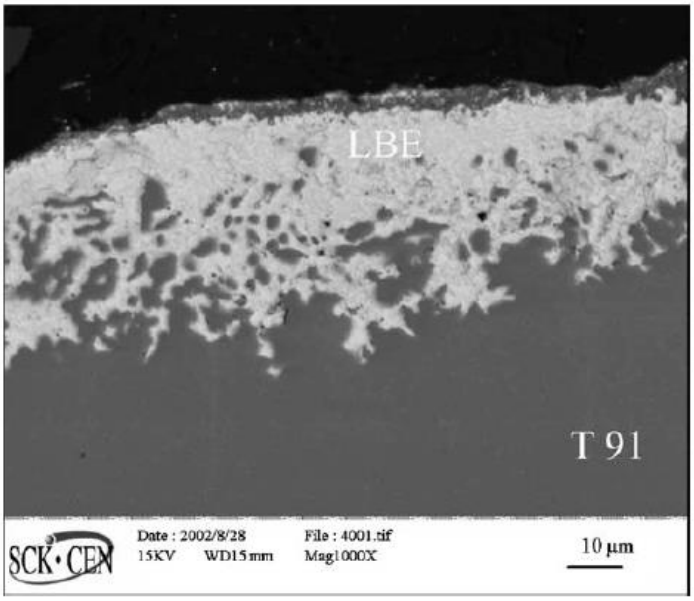

Figure 1.21: T91-dissolution corrosion mode. Specimen tested at 575°C for 2300h [SAP-2006-B].

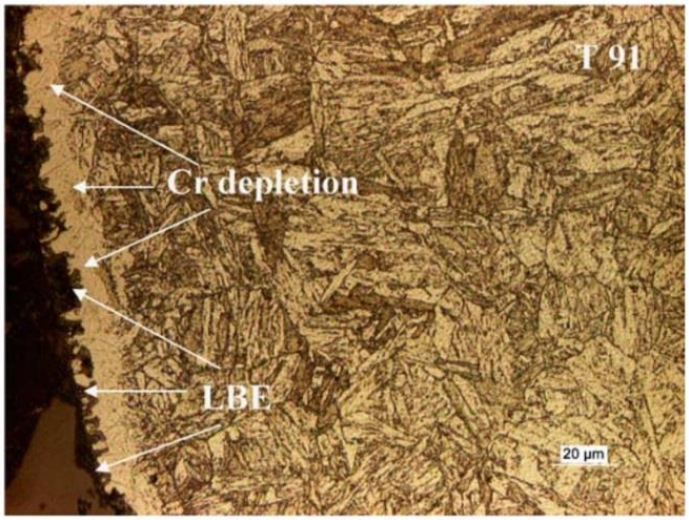

Figure 1.22: Light microscope micrograph of T91 sample from the dissolution corrosion mode. The depleted in Cr surface has undergone structural transformation [SAP-2006-B].

In order to estimate the corrosion rate of steels in the liquid metal, two methods were used, one was using microprobe analyses and the other one was by analyzing the impurity content of the crucibles after the experiment. In generally, the processes of the observed corrosion included dissolusion and diffusion and both of them occur simultaneously but it can be determined which of them dominates at a given condition. Using the secondary and backscattered electron images and the energy dispersive X-ray mappings, the corrosion rate was estimated as a function of the exposure temperature and time. The corrosion rate (i. e. penetration rate) CR_T^i at time t_i and temperature T was estimated using the measureed

penetration: $CR_T^i = l_i/t_i$ (μm/year) [SAP-2006-B], l_i (i=1, …, N) is the penetration at temperature T and exposure time t_i. At a given temperaute CR_T^i have been calculated and their average is taken as the average corrosion rate at this temperature:

$$\overline{CR_T} = \frac{\sum_{i=1}^{N} CR_T^i}{N} \qquad 1.3$$

where N is the number of the exposure time intervals.

D. Sapundjiev et al. [SAP-2006-B] got the conclusions that the corrosion rate of T91 is about 49 μm/year. The corrosion way for martensitic steel which has been degraded uniformly [TAS-1988, FAZ-2003].

1.4.2.3 Effect of surface finishing

J. Martín-Muñoz et al. [MAR-2011-A] had also studied the influence of the specimens' surface finishing states (as-received, grinded, grinded and polished, and electronlitically polished) in the oxidation/corrosion behaviour of T91 steel in liquid LBE. Oxidation tests were carried out at 775 and 825 K from 100 to 2000 h for two different oxygen concentrations atmospheres (10^{-6} wt% O and 10^{-8} wt% O) and for H_2/H_2O molar ratios of 3 and 0.03. They got the general conclusion that the effect of surface finishing on the corrosion/protection processes is not significant under the tested conditions (Figs. 1.23, 1.24). At the same time, they also got the general results in agreement with the literature previously reported [BAR-2001, FAZ-2003, SOL-2004, MAR-2004, SAP-2006-B], such as T91 tested at 775 K and 825 K under an oxidant atmosphere (10^{-6} wt% O). They showed compact and uniform oxide scales with thickness of approximately 30 μm and 50 μm (Fig. 1.23) respectively. However, the same steel tested under reductive atmosphere (10^{-7}~10^{-8} wt% O) present a surface with dissolution, especially after 2000 h exposure in liquid LBE shown by Fig. 1.24.

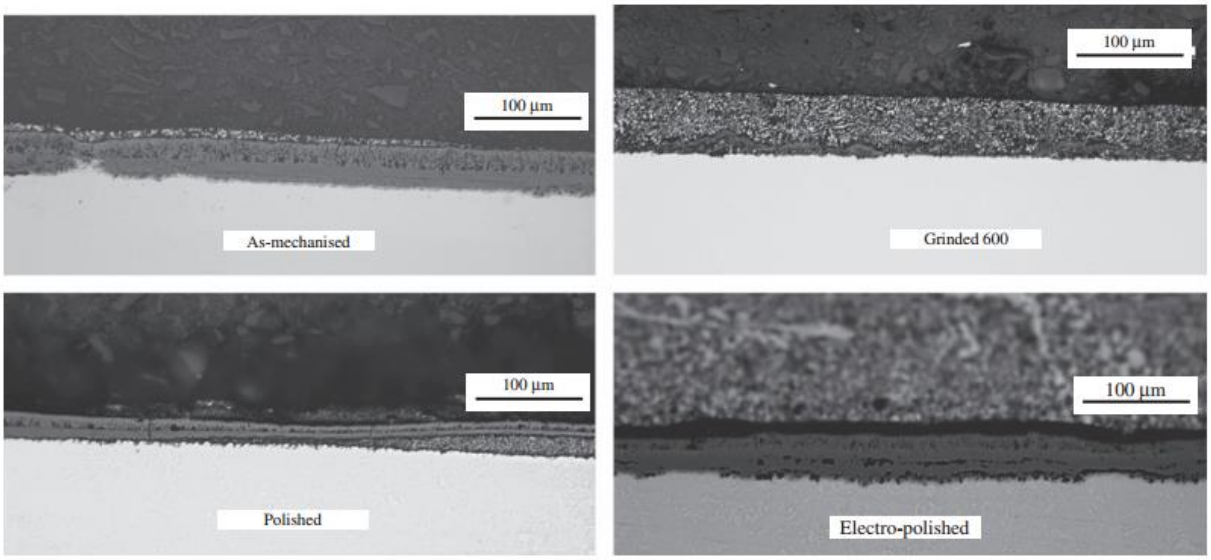

Figure 1.23: Optical micrographs of the cross-sections of T91 exposed in LBE at 825 K during 2000 h. Oxygen conditions: H_2/H_2O=0.03 ([O]=1.4 ×10^{-6} wt%) [MAR-2011-A].

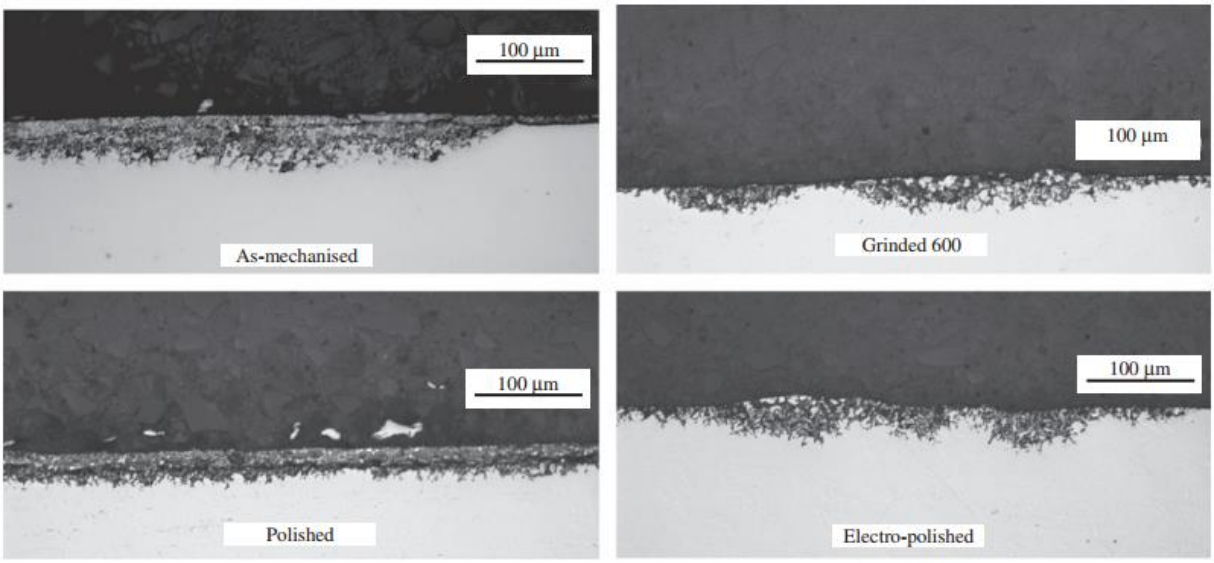

Figure 1.24: Optical micrographs of the cross-sections of T91 exposed in LBE at 825 K during 2000 h. Oxygen conditions: H_2/H_2O=3 ([O]=1.4 ×10^{-7} wt%) [MAR-2011-A].

1.4.3 Effect of LBE on mechanical properties

The effect of liquid LBE on mechanical properties of the T91 steel is summarized in this section, including monotonic properties (tensile, creep), fracture toughness and fatigue behaviour.

1.4.3.1 Monotonic properties

1.4.3.1.1 Tensile behaviour of T91 steel in its standard heat treatment in lead and in LBE

The standard heat treatment of T91 consists in an austenization at 1040 - 1050 °C followed by water quench or air cooling and then in a tempering at 750 - 770 °C, followed by air cooling. With this condition, electro-polished specimens of T91 steel failed in a ductile mode after tensile test at 260°C in oxygen-saturated LBE at an average strain rate of 10^{-4} s^{-1} [NIC-2001-A, NIC-2001-B]. Similar results were obtained later on [BOS-2006, GAB-2008, LON-2008-B, BOS-2008], in which the effect of strain rate, the effect of purity of LBE and the effect of temperature were additionally investigated. It is sometimes mentioned that after test at 300°C lateral cracks around the fracture surface had a cleavage like aspect but the main feature of the surface remains ductile.

In low oxygen content LBE (less than 1 wppm), a ductility trough in the temperature range 300°C-400°C has been pointed out, Fig. 1.25 [LON-2008-B].

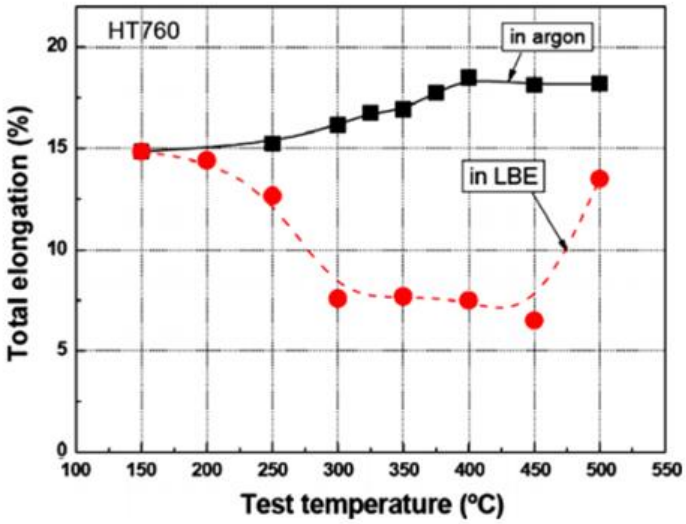

Figure 1.25: Total elongation versus test temperature for 760°C tempered T91 tested in Ar and in LBE (O < 1wppm) at a strain rate of 1×10^{-5} s^{-1} [LON-2008-B].

The tensile curves of the specimens tested in this temperature range show fast failure of the specimens after necking started. In this temperature range, the specimens tested in Ar broke in a typical ductile fracture mode, while the specimens tested in LBE ruptured in a brittle cleavage fracture mode.

So, the main information is that LBE can modify the behaviour of T91 but mainly after large deformation, where cracks form at the surface, suggesting that LBE promoted crack propagation.

Dai et al. [DAI-2006-A] noticed that a deleterious effect over a wide temperature range extending from 300°C to 425°C, in LBE (≤1 ppm oxygen) under argon (Fig. 1.26). In addition, some scattering in the results (particularly the elongation to rupture) was pointed out. This was latter on explained by an uncontrolled distribution of micro-cracks due to EDM (electron discharging machine) cutting.

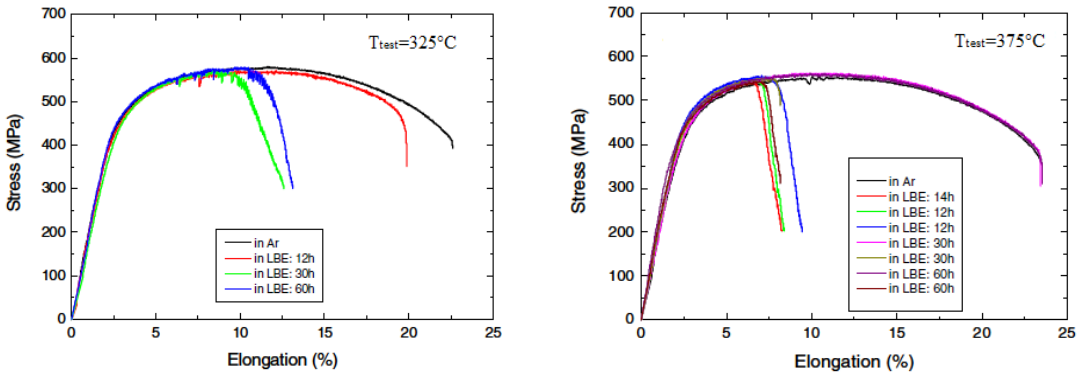

Figure 1.26: Tensile test results of mechanically polished EDM-cut specimens obtained at 325°C (*left*) and at 375°C (*right*) in LBE under argon [DAI-2006-A].

H. Glasbrenner et al. performed tensile tests during the commissioning phase of the LiSoR loop, using flat specimens of MANET II, at a strain rate of 10^{-4} mm s^{-1} [GLA-2003]. Ductile behaviour was observed under argon over the whole temperature range tested (T_{room} to 250°C), whereas some embrittling effect is apparently observed in flowing (1 ms^{-1}) oxygen-saturated or at least 'close to saturation' LBE, once reached 250°C and 300°C. Under the LiSoR loop condition, a mixed fracture surface was obtained with both flat and ductile areas. The final surface preparation of the tensile specimen was not specified. However, the presence of small cracks initially present onto the specimen surface, propagating under the influence of liquid LME, and more specifically bismuth as indicated by the authors, is a plausible hypothesis, possibly more plausible than the suggestion that the specimens of MANET II could be wetted by LBE under these conditions at 250°C or 300°C after two hours pre-exposure to oxidizing LBE before tensile testing. Note that ductile failure was always obtained for MANET II in LBE at the low temperatures tested of 180°C and 200°C.

Another parameter which was found to modify the mechanical response of T91 in LBE is the

pre-exposure of T91 in LBE.

In the framework of the TECLA and MEGAPIE-TEST programmes, C. Fazio et al. studied the T91-LBE couple using the following experimental procedure: long-term exposure of T91 to flowing and reducing LBE at 400°C in the LECOR loop (1500-4500 h) followed by tensile test under argon at the same temperature [FAZ-2003, AIE-2004-B]. The oxygen level in the melt, ranging from 3×10^{-10} to 1×10^{-7} wt. ppm was lowered by addition of Mg and bubbling under pure H_2. The results are: i) a net reduction of the elongation to rupture, ii) a decrease of the ultimate tensile strength, iii) with mixed ductile (at the centre) and brittle (at the periphery) fracture surfaces (Fig. 1.27).

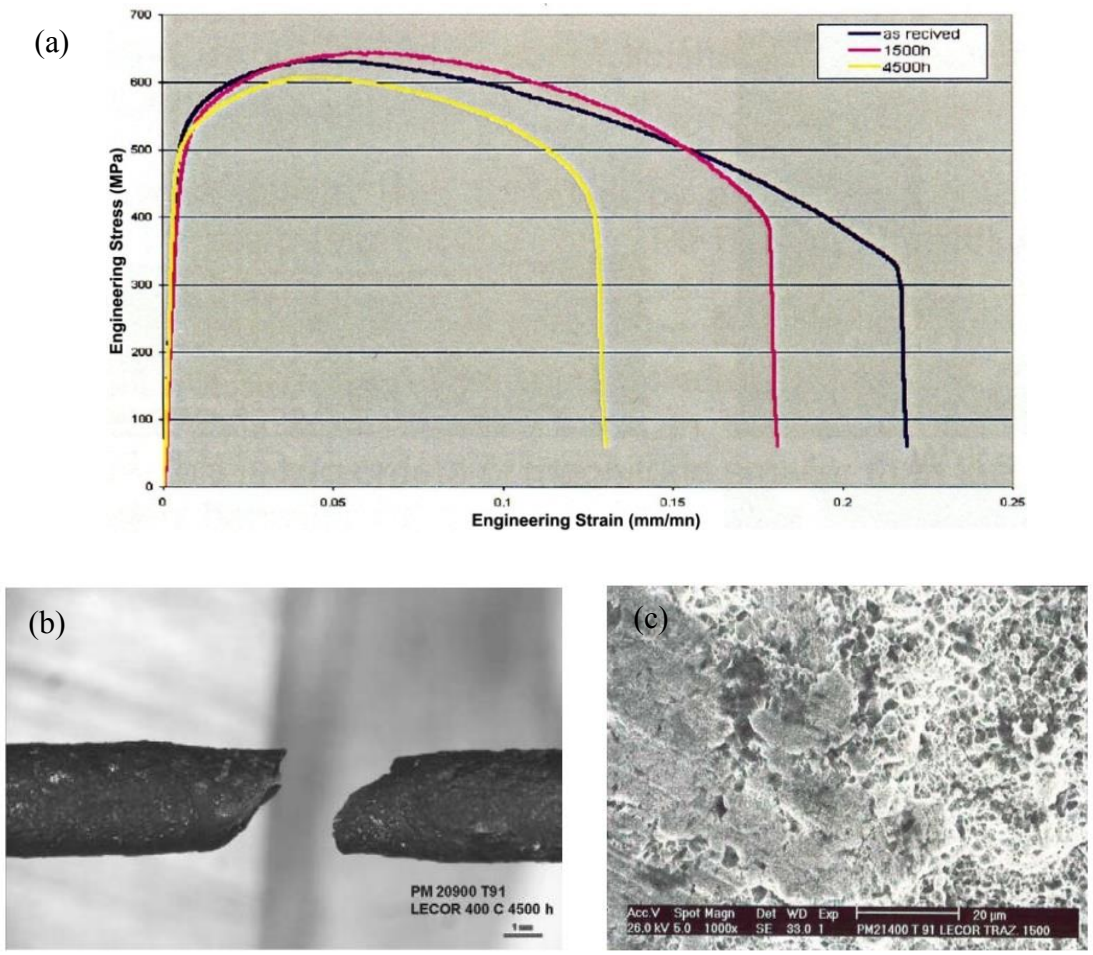

Figure 1.27: a) Stress-train curves obtained at 400°C in argon at strain rate of 3×10^{-3} s^{-1} after long term exposure of T91 to LBE at 400°C in LECOR loop; b) Morphology of T91 specimens after 4500 h in LECOR loop at 400°C followed by tensile testing in argon at 400°C; c) SEM micrograph showing a zone at the periphery of the fracture surface of the T91 tensile specimen [FAZ-2003, AIE-2004-B].

A detrimental effect of long-term exposure to LBE on the tensile properties of T91 was also observed by D. Sapundjiev et al. [SAP-2006-B]. This work also shows an effect of the ageing

temperature, clear at 450°C but undetectable at 300°C.

1.4.3.1.2 Creep

The creep research on ferritic/martensitic steels under air is still very rare and concerning the creep behaviour in liquid lead or LBE environment it was quasi inexistent in the literature at the beginning of the FP6 EUROTRANS-DEMETRA program [GOR-2011].

In Germany, in the framework of the collaboration between KIT and the Prometey Institute (St Petersburg), Jianu et al. [JIA-2009] studied the uniaxial creep-to-rupture behaviour of T91 steel in flowing LBE containing oxygen 10^{-6} wt% at 550°C compared with the tests in air. The results showed that the specimens tested in liquid LBE exhibited strain and strain rate increase up to a factor of about 50 (strain rate), time-to-rupture decrease, and rapid transition into the third creep stage at high stress (above 180 MPa) shown in Fig. 1.28. In addition, analysis of specimen after creep test also revealed that several important surface phenomena lead to different behaviours of the specimens tested in liquid LBE compared to those tested in air. Jianu et al. believed that the propagation process of the crack is mostly controlled by the reduction of the surface energy due to Pb and Bi adsorption on the steel surface under high stress and high strain condition, while under low stress (140 MPa and 160 MPa) and low strain condition this process is delayed due to the competing mechanism of healing the oxide scale cracks.

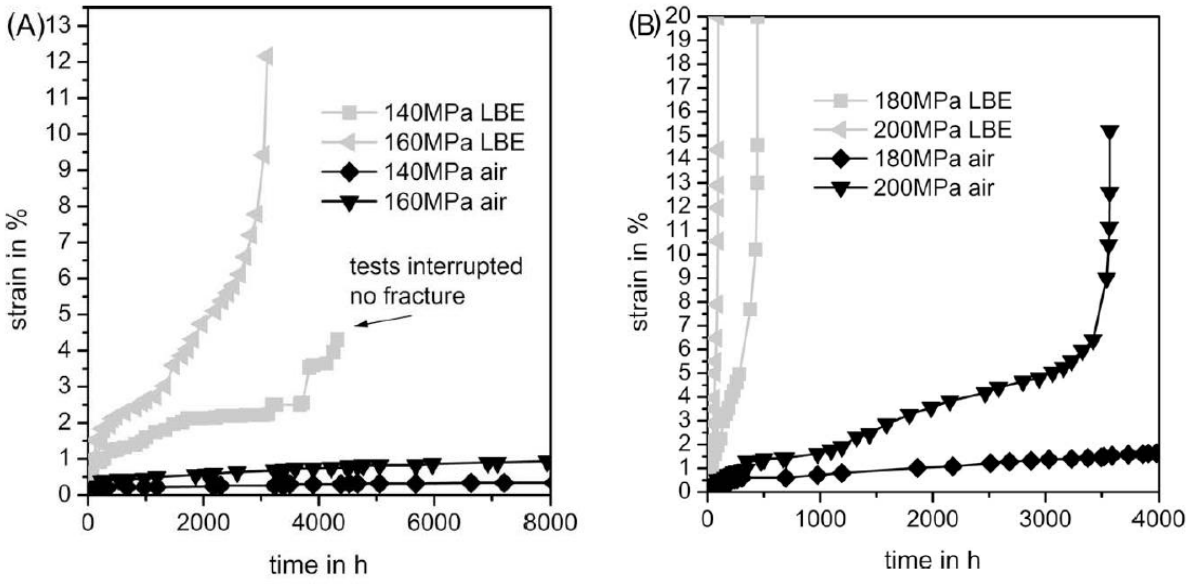

Figure 1.28: Comparision of creep to rupture diagrams of T91 in LBE and in air at 550°C, (a) 140 and 160 MPa, (b) 180 and 200 MPa [JIA-2009].

Yurechko et al. [YUR-2011] had studied the uniaxial creep behaviour of T91 steel in air and in stagnant liquid oxygen-controlled Pb (around 10^{-6} mass%) with static loads ranging from 100 to 200 MPa at 650°C. The analysis results showed almost no difference in creep performance in liquid oxygen-controlled Pb and in air at 650°C. Furthermore there was no dissolution attack and no discovery about lead penetrated on the steel.

1.4.3.2 Toughness

Fracture mechanics experiments on the T91 martensitic steel in contact with liquid LBE have been performed in plane stress [HAM-2008, AUG-2008-B, AUG-2011], and plane strain. Hamouche et al. [HAM-2008, BOS-2009], employed CCT (Center Cracked in Tensile) specimen. In plane stress, at 300°C, the facture toughness reduction due to LBE is of the order of 20-30% compared with air. In plane stress, the fracture mode is cleavage at initiation followed by separated fracture (Fig. 1.29).

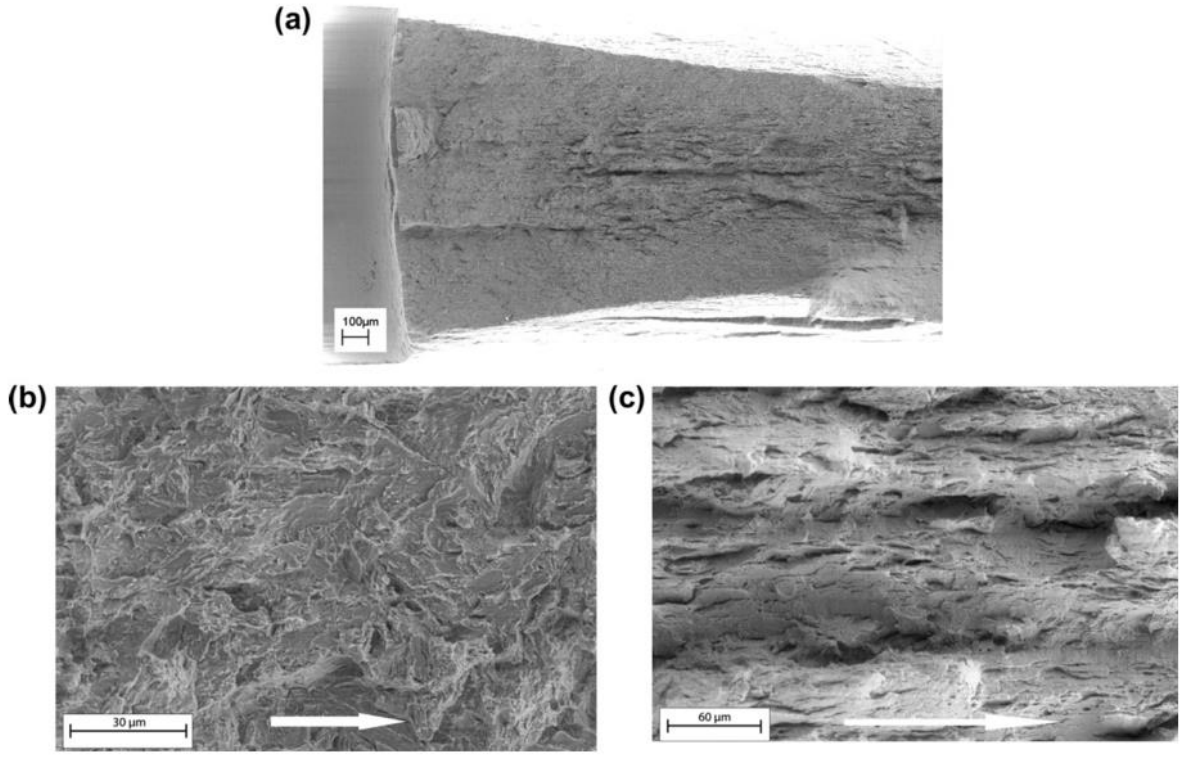

Figure 1.29: (a) Top view of the fracture surface of T91 in the centre cracked in tension (CCT) geometry tested at 300 °C with LBE; (b) view of crack initiation site; (c) view of a shear fracture area (crack propagation proceeds as indicated by the white arrow) [AUG-2011].

G. Coen et al. [COE-2010] discussed the effect of LBE on the plane strain fracture toughness

of T91 steel at 200°C and 300°C for tests performed at a displacement rate of 0.25 $mm \cdot min^{-1}$, in both air and oxygen saturated LBE environment. The average toughness J_Q value at 200°C is 223 $kJ \cdot m^{-2}$ for the test in air and 174 $kJ \cdot m^{-2}$ for the test in LBE. A decrease in J_Q due to LBE is still observed at 300°C. In air, the J_Q value of 222 $kJ \cdot m^{-2}$ moved to 185 $kJ \cdot m^{-2}$ in LBE. In air, the specimen fracture due to a ductile fracture mechanism resulting in the dimples fracture surface while in LBE a mixed ductile-brittle fracture was observed.

1.4.3.3 Fatigue

The fatigue behaviour of T91 steel in LBE is very few documented. Essentially, two main papers deal with this topic [KAL-2003, VER-2006].

Kalkhof and Grosse [KAL-2003] had investigated the LCF behaviour of the ferritic-martensitic 10.5Cr-steel Manet-II at 260°C in air and in stagnant LBE. The results indicated that a significant reduction of lifetime by a factor of ≈7 in the worst case in all applied strain amplitudes was noticed in LBE in comparison with air. Furthermore the propagation of crack in LBE was much faster and the formation of a single crack led to failure of the LCF specimen. D. Kalkhof and M. Grosse confirmed that Manet-II has the different fracture mechanisms in air and in LBE by microstructure investigations, the formation of the first small crack in LBE resulted in fast crack propagation up to failure, while there were many small surface cracks in air shown by Fig. 1.30. In addition, the liquid LBE penetrated even into the smallest sub-cracks in material Manet-II specimen confirmed by the SEM secondary electron image shown by Fig. 1.31.

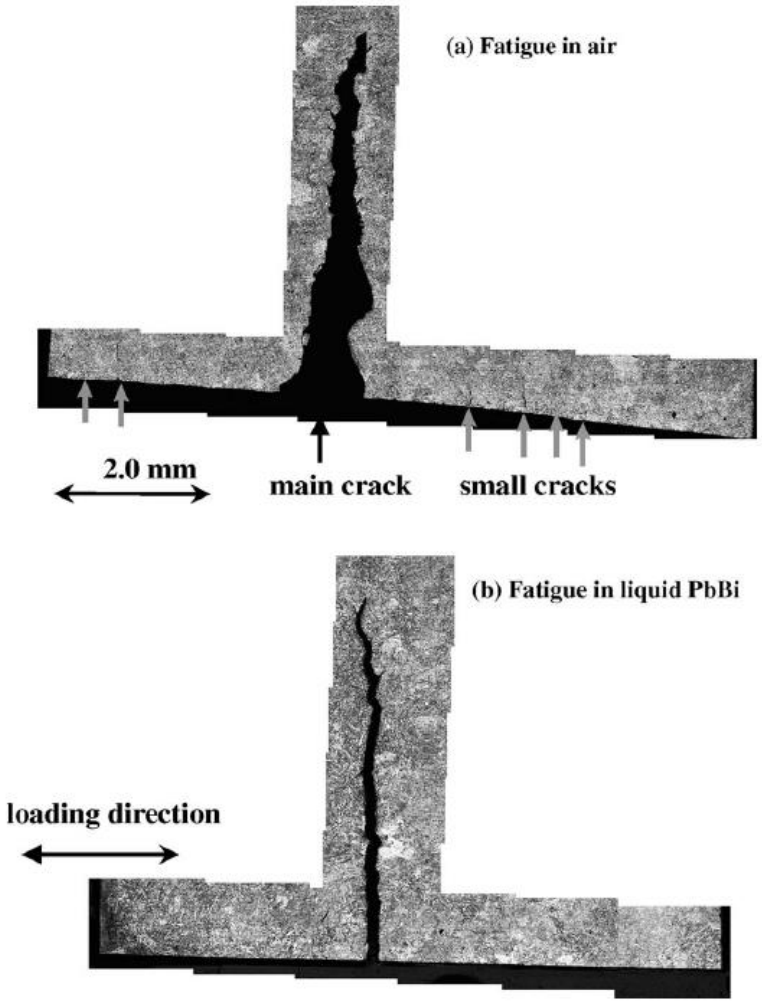

Figure 1.30: Photomicrographs of Manet-II specimens tested in (a) air and (b) in PbBi. Arrows mark the microcrack positions [KAL-2003].

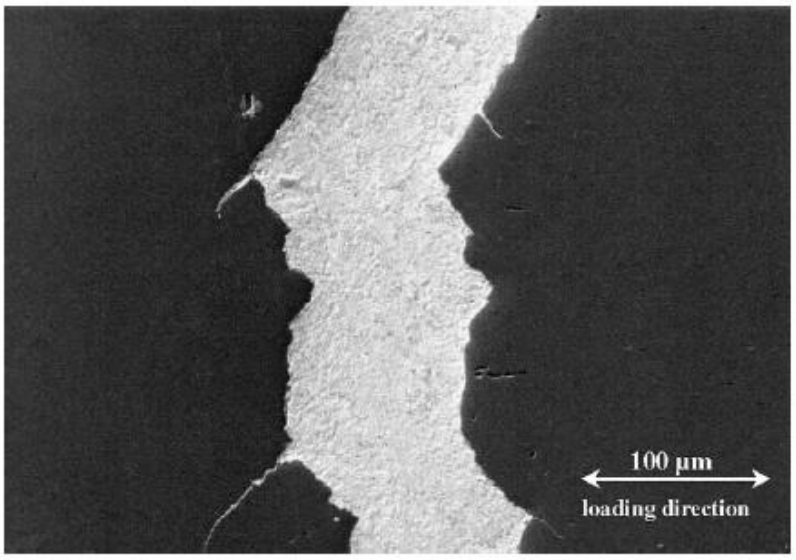

Figure 1.31: Secondary electron image of the main crack and sub-cracks of a Manet-II specimen. LBE penetrated into the smallest sub-cracks [KAL-2003].

A. Verleene et al. [VER-2006] researched the low cycle fatigue (LCF) behaviour of T91 martensitic steel at 300°C in air and in liquid oxygen saturated LBE without particular care to control or measure the oxygen activity in LBE. They got the conclusions that the monotonic and cyclic stress-stain curves do not change with the environment. However, the fatigue life is reduced in the high strain range in LBE compared to air. The metallographic and fractographic investigations suggest that the reduction in the fatigue resistance is due to a liquid metal enhancement of the propagation rate of the short cracks. SEM analysis shows that there is a very high density of cracks observed for tests in air (Fig. 1.32a) whereas only few surface cracks are visible after tests in LBE (Fig. 1.32b). SEM observations indicated that there is LBE presence at each long crack tested in the liquid metal. The cracks initiate on intensive slip bands (Fig. 1.33a), pits or inclusions (Fig. 1.33b) in both air and in LBE environment conditions, while intergranular decohesion is sometimes observed shown by Fig. 1.33c.

The fracture surface contained fatigue striation in both air and LBE environment. But the distance between striations was much higher in LBE than in air suggesting a higher crack growth rate. Here, the presence of LBE resulted in a LMAD.

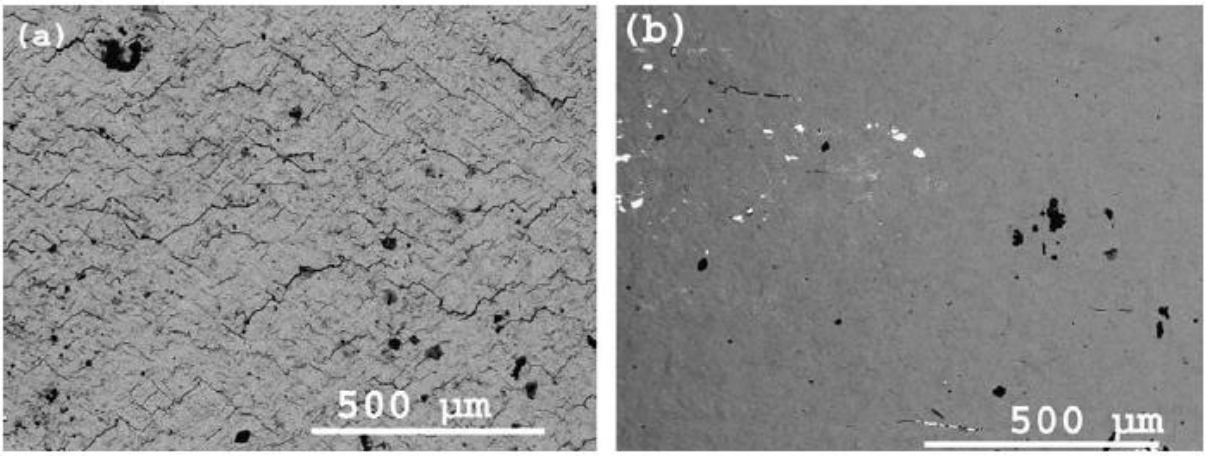

Figure 1.32: SEM observations of sample surface after LCF tests performed ($\Delta\varepsilon_t$=1.6%) in air (a) and in LBE (b) [VER-2006].

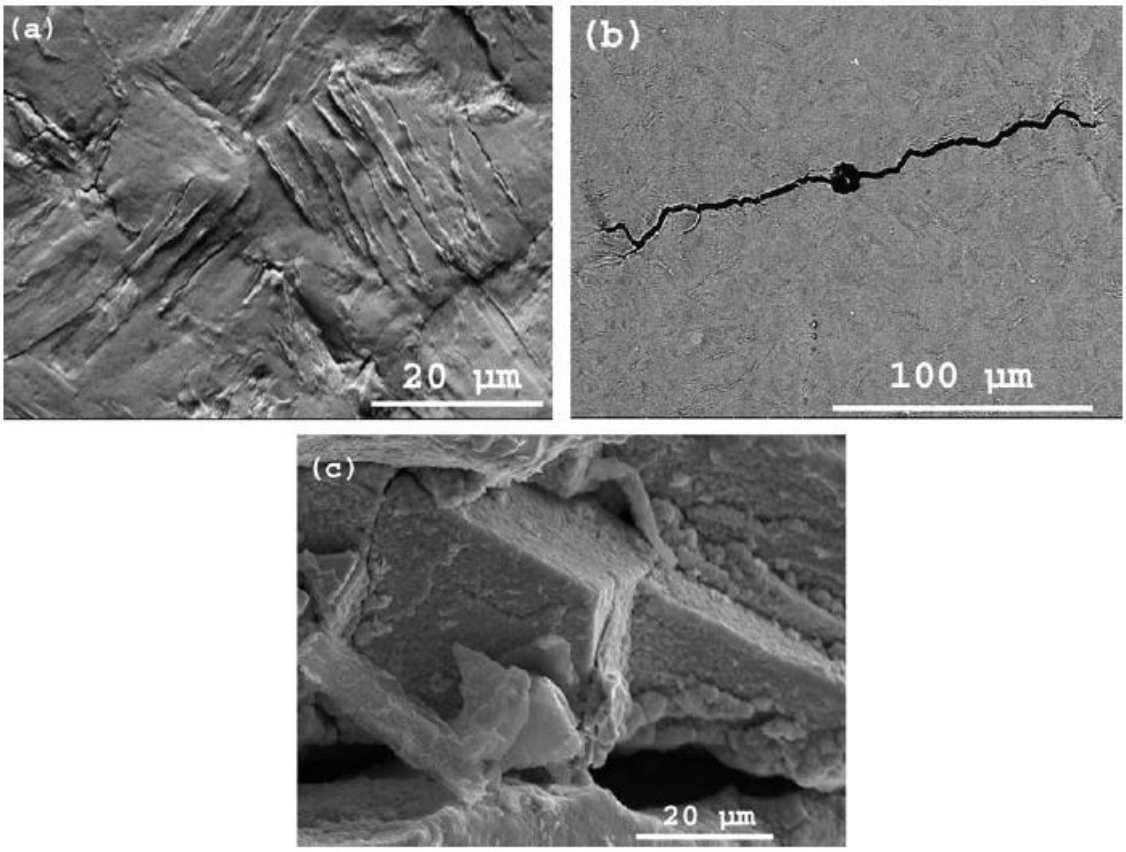

Figure 1.33: Initiation of surface cracks at intrusion extrusion after LCF tests performed in air ($\Delta\varepsilon_t$=1.68%) (a), or pit or inclusions on the surface sample after LCF tests performed in LBE ($\Delta\varepsilon_t$=0.36%) (b), or intergranular decohesions on the surface sample after LCF tests performed in LBE ($\Delta\varepsilon_t$=0.91%) (c) [VER-2006].

The effect of pre corrosion has been investigated [VOG-2007]. Specimens were first immersed at CEA (Commissariat à l'Energie Atomique et aux Energies Alternatives) Saclay because they are able to control the amount of dissolved oxygen in LBE. Then, the specimens were fatigued in liquid oxygen saturated LBE. A clear effect of pre corrosion was observed when dissolution was the mechanism, i.e. when oxygen content in LBE was low. However, when oxidation was the corrosion mechanism, the fatigue life was not affected. It turns out that the chemistry of the liquid metal, especially impurities such as oxygen, is one of the key factors.

1.4.4 The effects of heat treatment on T91

As mentioned previously, high strength materials are more prone to LME. Martensitic steels are used after a specific heat treatment and tempering is an important step in the heat treatment. The standard heat treatment considers a tempering at 750°C-760°C. Research has

been devoted to the role of tempering temperature on LME.

The very first experiments aimed at demonstrating the effect of tempering were performed by Nicaise, Vogt et al. [NIC-2001-A, VOG-2002]. They tempered their T91 at 500°C instead of 750°C which changed the hardness value from 220 HV to 400 HV. The application of this hardening heat treatment to smooth cylindrical specimens of T91 steel was not sufficient to produce an embrittling effect in contact with stagnant saturated oxygen LME at 350°C. However, LME was then observed when notched specimen with a root containing a very hard layer which was susceptible to crack during loading.

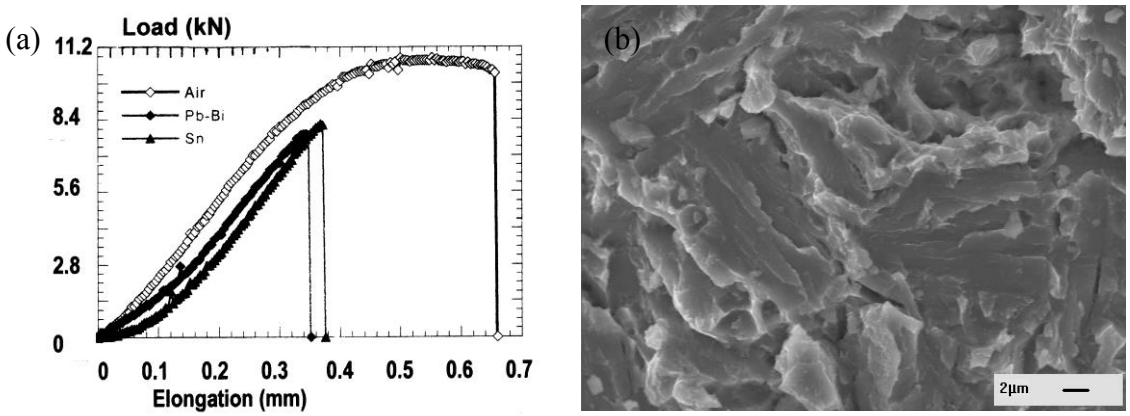

Figure 1.34: (a) Load-displacement curves obtained in air, liquid tin and liquid lead-bismuth eutectic; and (b) trangranular brittle fracture observed after fracture in liquid lead-bismuth eutectic (Fe9Cr1Mo steel tempered at 500°C, all tests at 260°C) [VOG-2002].

Combining the effect of a notch and of a hardening thermal treatment was apparently required to obtain a brittle failure in a variety of liquid metals including LBE at 260°C (Fig. 1.34).

These results were later confirmed by H. Glasbrenner and F. Gröschel [GLA-2004] on U-bent T91 specimens, hardened by means of the same hardening heat treatment applied above Vogt et al. [VOG-2002].

The effect of heat treatment was revisited more recently [LON-2008-B]. The experimental details were a little bit different especially, apparently unnotched specimen (0.75×1.5×5 mm^3), low oxygen LBE (less than 1 wppm) and lower strain rate (1×10^{-5} s^{-1}) were employed. T91 was studied after the following heat treatment conditions: (1) normalized at 1040°C in high vacuum for 60 min and followed by air cooling; and (2) tempered at 760°C, 600°C and 500°C in high vacuum for 2 h and followed by air cooling (HT760, HT600 and HT500 respectively).

With increasing the strength of the steel by lowering the tempering temperature, specimens tempered at 600°C and 500°C (Fig. 1.35) demonstrated more pronounced embrittlement effects, reflected by wider and deeper ductility troughs, indicating clearly that they became more susceptible to the LBE embrittlement. The authors believe that the fracture of the specimens resulted from the propagation of micro-cracks on the transverse surfaces, which were produced during EDM cutting. All specimens tested in Ar environment ruptured in a ductile fracture mode.

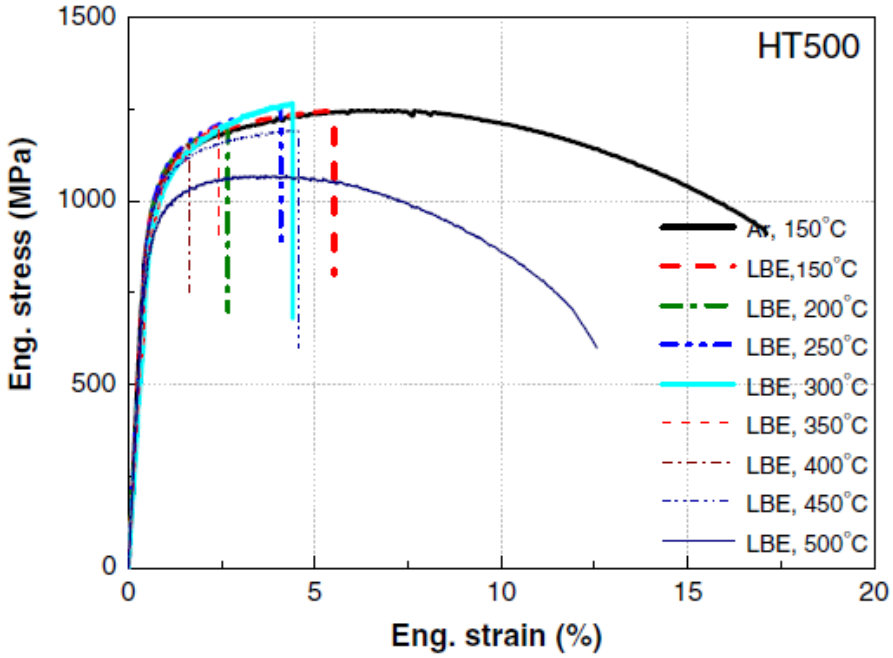

Figure 1.35: Tensile stress-strain curves of T91 steel tempered at 500°C tested in LBE and in Ar [LON-2008-B].

We already know that LME is difficult to be predicted and due to the numerous other parameters such as strain rate, temperature, yield stress, and stress concentration, etc. In generally, researchers prefer to use tensile tests and pre-cracked notched specimens to study the sensitivity of liquid metals on mechanical properties. The tensile tests on smooth cylindrical specimens in different environments are convenient to analyse the standard mechanical properties of materials and are particularly suitable for the study of the crack initiation mechanism in liquid metal. It is better to use pre-cracked notched specimens for studying the variation of crack growth rate with the environment. In addition, from the perspective of the loading state, tensile test is a uniaxial generalized loading before necking and a triaxial localized loading state for the pre-cracked notched specimen test. Besides these two test families, small punch test (SPT) is a mechanical test with a biaxial stress state of the specimen at the beginning of loading when the specimen is punched in the centre by a ball

[SER-2007]. A detailed description of the test is given in chapter II. It appears as an intermediate one between uniaxial and triaxial testing method considered for the study of LME sensitivity of metallic alloys.

I. Serre and J.-B. Vogt [SER-2007, SER-2008] had evidenced the liquid metal embrittlement of T91 martensitic steel by employing the SPT technology, and they also indicated that SPT appears to be more sensitive to evidence LME than the conventional tensile tests. I. Serre, J.-B. Vogt had studied the material T91 with six different tempering conditions (as quenched, tempered at 500°C (TR500), 600°C (TR600), 650°C (TR650), 700°C (TR700) and 750°C (TR750)) corresponding to different values of hardness and tested in air and in liquid LBE at 300°C.

In air, all curves have the same slope but the typical values such as the maximum load and displacement at maximum load were dependent upon the material. This reflected simply the hardening of the materials. Testing in LBE lead to distinguish two groups of materials: 650°C, 700°C and 750°C tempered materials; and R.T. (room temperature, noted as 'T'), 500°C and 600°C tempered materials. The first group exhibits behaviour with large values of displacement. In the second one, LBE promotes a decrease in mechanical properties and a reduction of the ductility (Fig. 1.36).

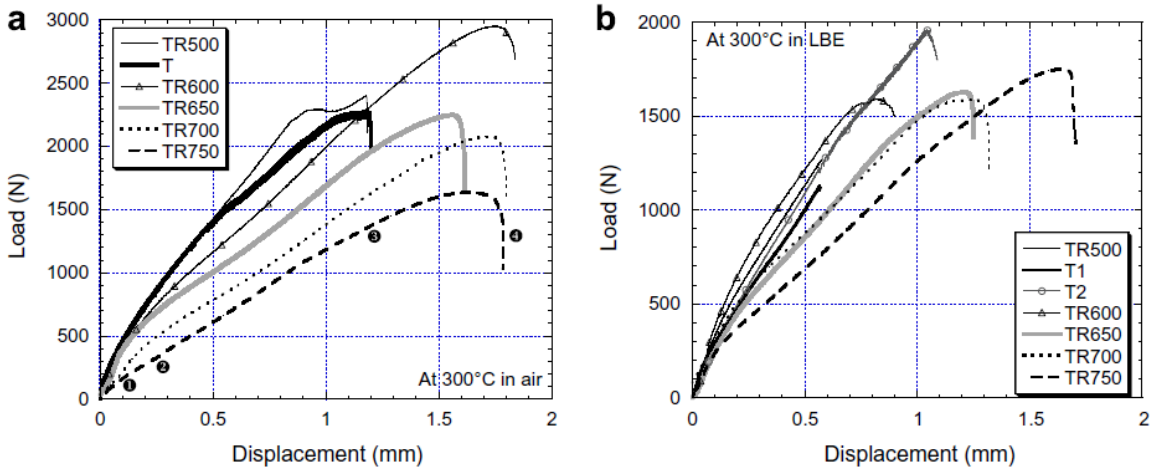

Figure 1.36: Load-displacement SPT curves of the T91 steel according to the heat treatment and tested (a) in air at 300°C and (b) in LBE at 300°C [SER-2008].

Based on the load-displacement SPT curves of the T91 steel, they believed that LBE had assisted a decrease in mechanical properties and a reduction of the ductility of materials with a mixed ductile and brittle fracture, and the load-displacement SPT curves of T91 in air and in LBE at 300°C are shown by Fig. 1.36. In Fig. 1.36a, the tempering heat treatments performed

on the T91 steel affected the mechanical properties of the materials tested in air, while the steel remained ductile regardless of the tempering condition. For the TR600, TR650, TR700 and TR750 materials, cracking is circular, while for the T and TR500 materials, the circular crack is accompanied with radial ones, and furthermore, the radial cracks are more numerous and shorter in the TR500 material than in the T one, and the fracture surface of all the specimens is ductile feature tested in air shown in Fig. 1.37.

However, for tests in LBE, a brittle fracture associated with a peculiar mechanical response was observed for the non-tempered T91 steel or tempered at 500°C and at 600°C, i.e. the hardest materials (Fig. 1.36b). On intermediate high strength material, T91 tempered at 650°C or tempered at 700°C tested in LBE promotes a ductile behaviour but with mixed ductile and brittle fracture and a reduction of mechanical properties measured by SPT (Figs. 1.36b, 1.39). The general tendency for the T, TR500 and TR600 materials fractured in LBE is that cracking initially appears semi-circular and then tend to propagate outwards in a radial direction (Fig. 1.38bcd), while some specimens obtain radial cracks without semi-circular cracking (Fig. 1.38a) as for brittle behaviour. All the fracture surface of the T, TR500, and TR600 materials tested in LBE are always brittle, essentially transgranular (Fig. 1.39b) with some occasional intergranular decohesion (Fig. 1.39a). But the tests carried out on the TR750 material at 300°C in LBE provided a response similar to that in air, the cracking is circular (Fig. 1.38g) and the fracture is ductile.

I. Serre and J.-B. Vogt interpreted the local brittle fracture LBE effect by the formation of very sharp defects in liquid metal during the propagation of ductile cracks or on the surface of samples in contact with LBE, while the limit of this propagation of brittle cracks is maybe due to the material plastic deformation to blunt the crack tip.

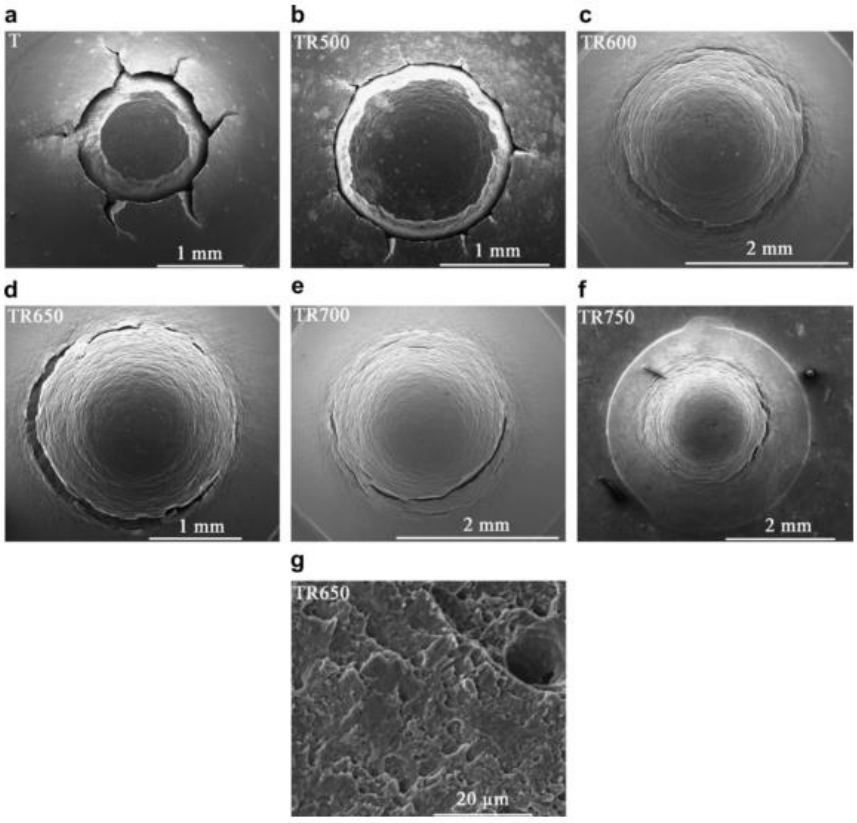

Figure 1.37: SEM micrographs showing cracked surfaces and dutile fracture surface of samples tested in air at 300°C [SER-2008].

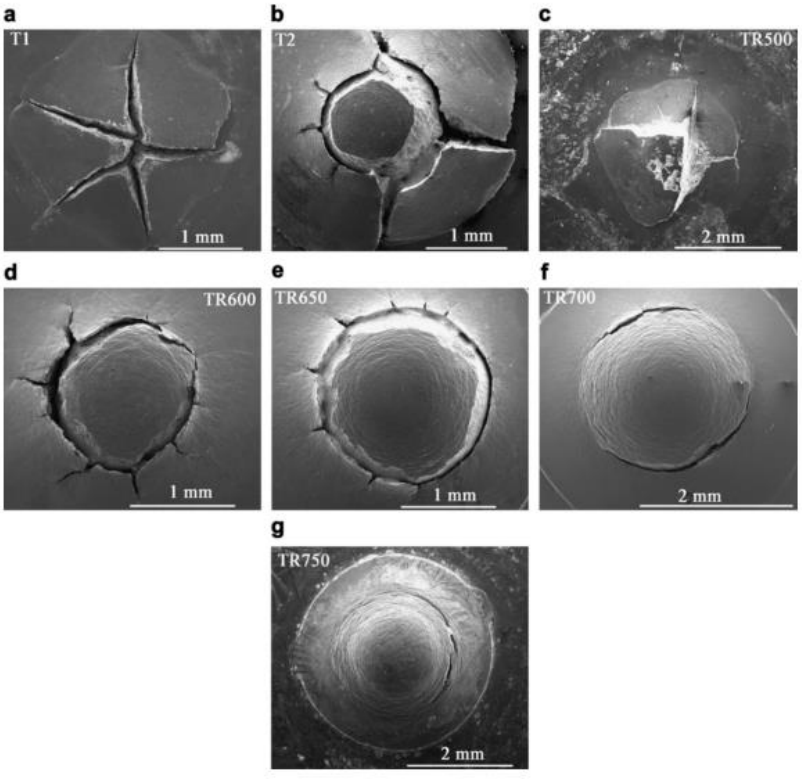

Figure 1.38: SEM micrographs showing cracked surfaces of samples tested in LBE at 300°C [SER-2008].

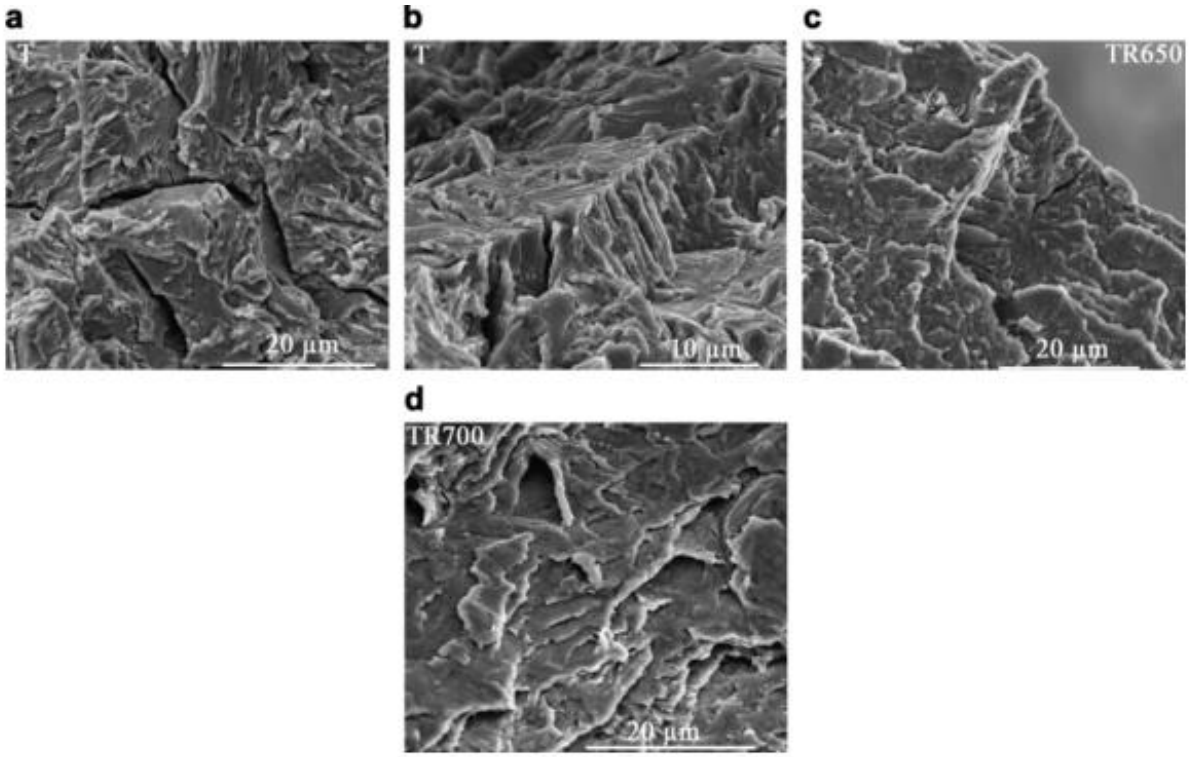

Figure 1.39: SEM fracture surface after tests in LBE at 300°C showing intergranular brittle fracture occasionally observed (a), transgranular brittle fracture mostly observed (b) and mixed fracture near the external part exposed to the LBE (c), in the middle of the fracture surface (d) [SER-2008].

In order to investigate the LBE embrittlement on the fracture properties of T91 steel, Long and Dai [LON-2008-A] used 3-point bending tests at 200°C, 300°C, 400°C and 500°C in LBE and also in argon (Ar) atmosphere. They also researched the relationship between the different heat treatments of specimens of T91 steel on the fracture toughness of T91 steel after exposure in LBE. They found that the fracture toughness was reduced by the presence of LBE and the susceptibility of T91 to LBE embrittlement increased with the hardening of the steel introduced by heat treatments.

The 500°C tempered specimens (HT500) with highest hardening were the most sensitive to LBE embrittlement, which resulted in brittle fracture at lower temperatures and substantial reduction of fracture toughness up to 400°C shown in Fig. 1.40. In addition, HT500 specimen tested in Ar at 300°C was experienced very large bending deformation before rupture, while the other specimens tested in LBE were bent just slightly, particularly for the specimen tested at 300°C shown in Fig. 1.43. This illustrates a significant difference between the fracture behaviours of the specimens tested in Ar and in LBE: ductile fracture mode in Ar but brittle fracture mode in LBE. The 600°C tempered specimens (HT600) with medium hardening appeared quite sensitive to LBE embrittlement as well, and the *J*-values reduced more than

50% in a temperature range of 200-400°C (Fig. 1.41). The specimens of non-hardened normal T91 steel (HT750, 750°C tempered) illustrated also embrittlement effect, and the *J*-values reduced 20-30% in the presence of LBE (Fig. 1.42).

After SEM observation, Long and Dai concluded that almost all of the specimens tested in Ar and some the HT750 specimen tested in LBE ruptured in ductile fracture mode. Most of the specimens with HT600 tested in LBE ruptured in a mixed ductile-brittle fracture mode. Only the HT500 specimens tested at 200°C and 300°C in LBE showed nearly pure cleavage fracture [LON-2008-A].

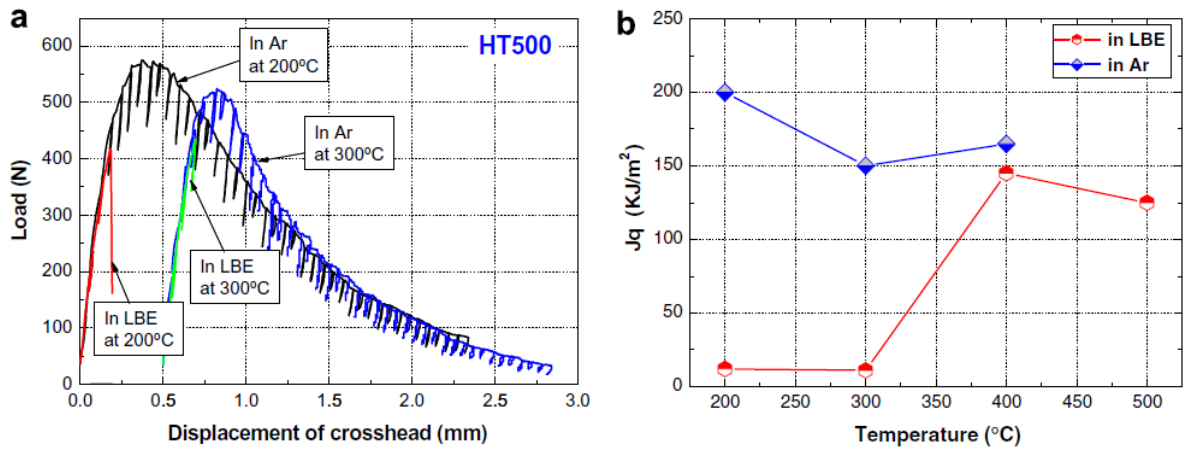

Figure 1.40: (a) load-displacement curves of the HT500 specimens tested in Ar and in LBE at 200°C and 300°C (shifted by 0.5 mm in *X*-axis); (b) *Jq*-values derived from tests at 200-500 °C in Ar (up to 400°C) and LBE [LON-2008-A].

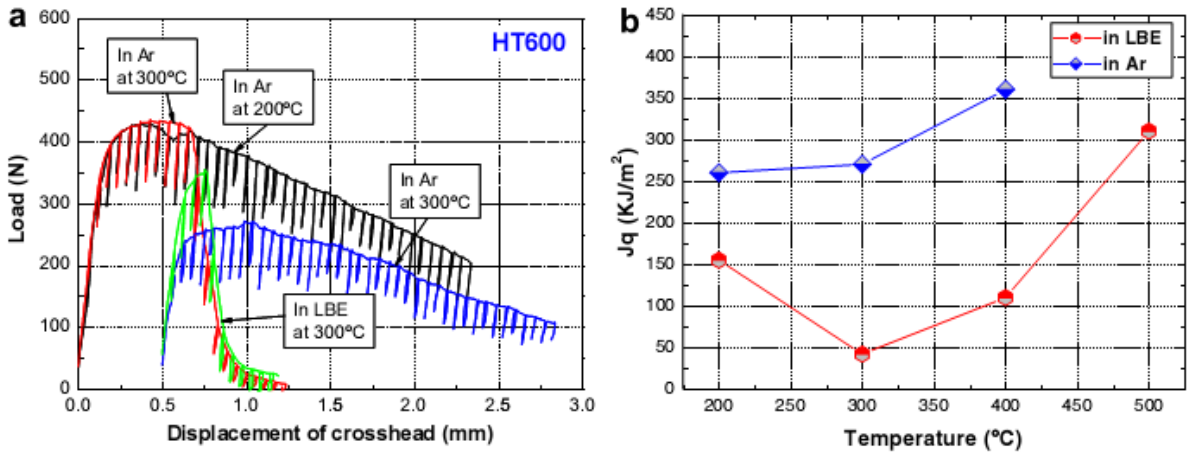

Figure 1.41: (a) Load-displacement curves of the HT 600 specimens tested in Ar and in LBE at 200℃ and 300℃ (shifted by 0.5 mm in X-axis); (b) Jq-values derived from tests at 200-500 ℃ in Ar (up to 400℃) and LBE [LON-2008-A].

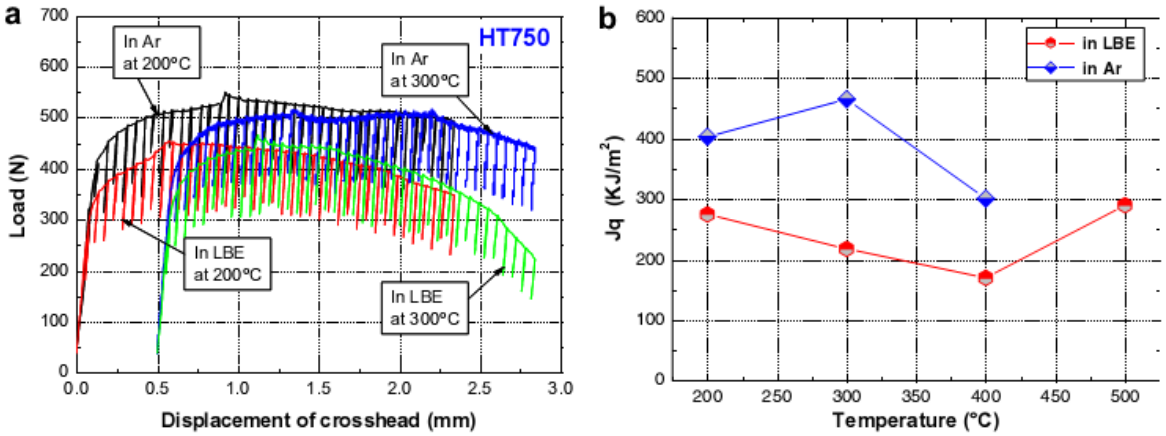

Figure 1.42: (a) Load-displacement curves of the HT750 specimens tested in Ar and in LBE at 200°C and 300°C (shifted by 0.5 mm in X-axis); (b) Jq-values derived from tests at 200-500 °C in Ar (up to 400°C) and LBE [LON-2008-A].

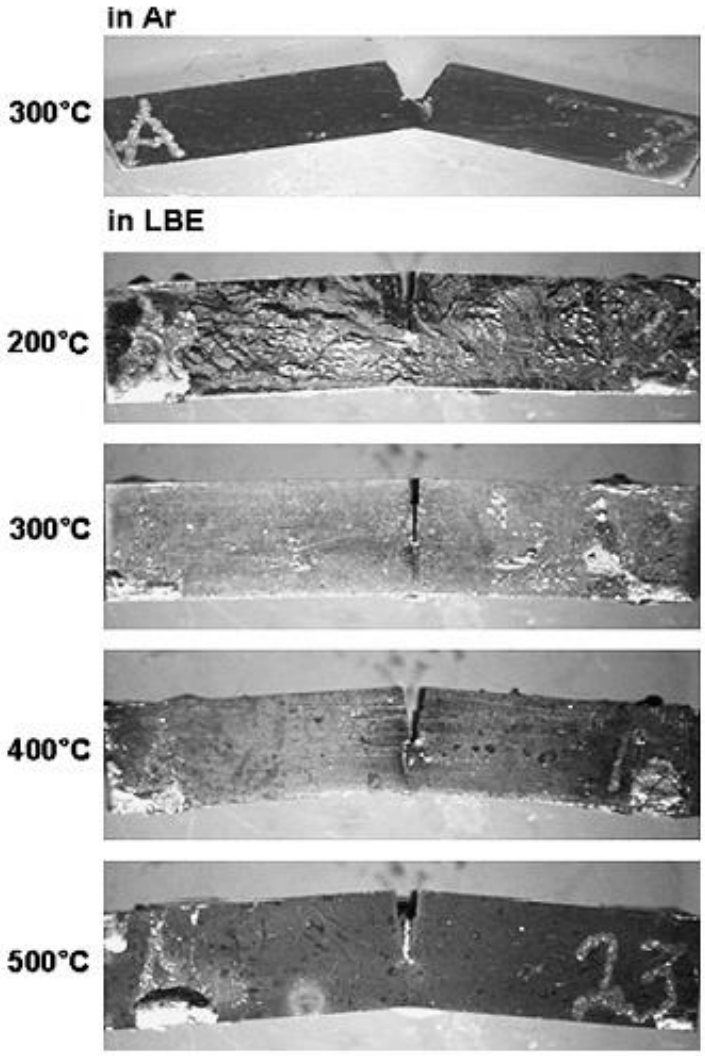

Figure 1.43: Pictures of the HT500 specimens after the bending test in Ar at 300°C and in LBE at different temperatures [LON-2008-A].

1.4.5 Advanced coating method for high temperature operation of steels in LBE

In order to solve corrosion and erosion issues of structural materials by HLM, one of the main approaches is to form a stable and protective layer of iron and chromium oxides on the surface of steels which can be achieved by maintaining the oxygen concentration of the liquid metal in an appropriate range. However, this kind of method is not viable for high temperature (above 500°C) due to the fast kinetics of oxide growth and the considerable reduction of thermal conductivity. Furthermore, below 500°C maintaining oxygen concentration could appear as a method to protect the structure materials but other technical issues, oxide spallation and channel plugging arise [GAR-2013-B].

In this part, the main coatings developped for corrosion resistance will be presented. It must be pointed out that it is a big challenge because the mechanical resistance of the substrate must not be affected by the coating.

A lot of experimental investigations have focused on the development of other approaches of providing corrosion protection, such as aluminizing surface treatments [MUL-2000, DEL-2004], electron beam-treated FeCrAlY coatings [WEI-2008-A, FET-2012], or even new alloys studies, including Fe-12Cr-2Si [SHO-2013].

In order to develop a fully reliable and viable technology to protect the structure steels, the reconsideration of ceramic coatings has been reactivated [RIV-2008, RIV-2010-A, RIV-2010-B, DOU-2011], due to their chemical inertness characteristics. Ceramic coatings have been considered as a taboo in the past, mainly due to the lack of self-healing properties [GAR-2013-B]. In addition, high temperature process can modify the microstructure of the substrate. Here, a low temperature process is presented.

A novel technic using Pulsed Laser Deposition (PLD) for coating T91 by Al_2O_3 has been developed at Center for Nano Science and Technology, Italy. F. García Ferré et al. [GAR-2013-B] studied the corrosion resistance of T91 covered with a nanocrystalline Al_2O_3/amorphous Al_2O_3 composite coatings. The examination of coated steel samples by SEM and EDX after short term exposure to HLMs (500h) at 550°C revealed no sign of corrosion (Fig. 1.44), while the specific conditions of the melt (550°C, saturation of oxygen) led to the formation of a duplex oxide layer (an external magnetite layer and an internal Fe-Cr spinel) ranging from around 15 to around 30 μm on the uncoated surfaces specimens (Fig.

1.45). In a separate study [GAR-2013-A], it was found that these hard, fully dense and compact ceramic barriers attain an unusual ensemble of metal-like mechanical properties, superior plastic behaviour and wear resistance, as well as strong interfacial bonding. The singular combination of all these features makes of PLD-grown Al_2O_3 coatings a suitable and promising candidate for protecting steels from corrosion in HLMs at high temperature [GAR-2013-B].

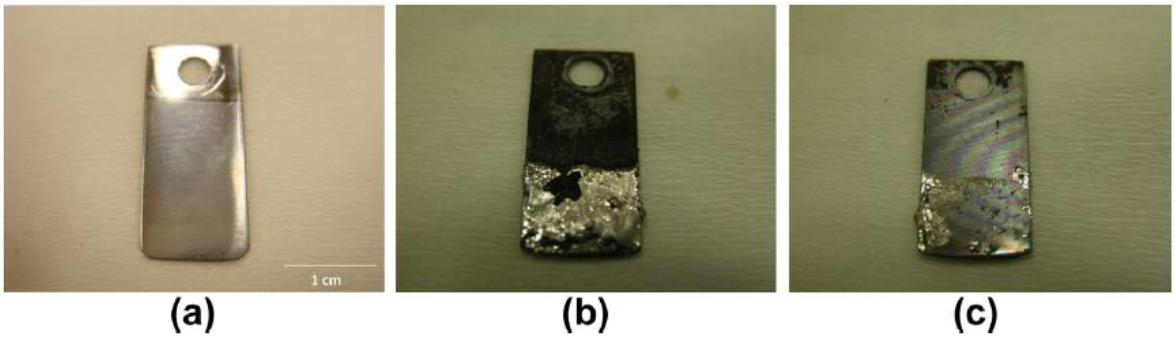

Figure 1.44: As-fabricated coated specimen (a). The uncoated (b) and coated (c) surface of another sample after exposure to molten Pb at 550°C for 500 h in oxidizing conditions. The uncoated face was corroded, while the coated face was protected [GAR-2013-B].

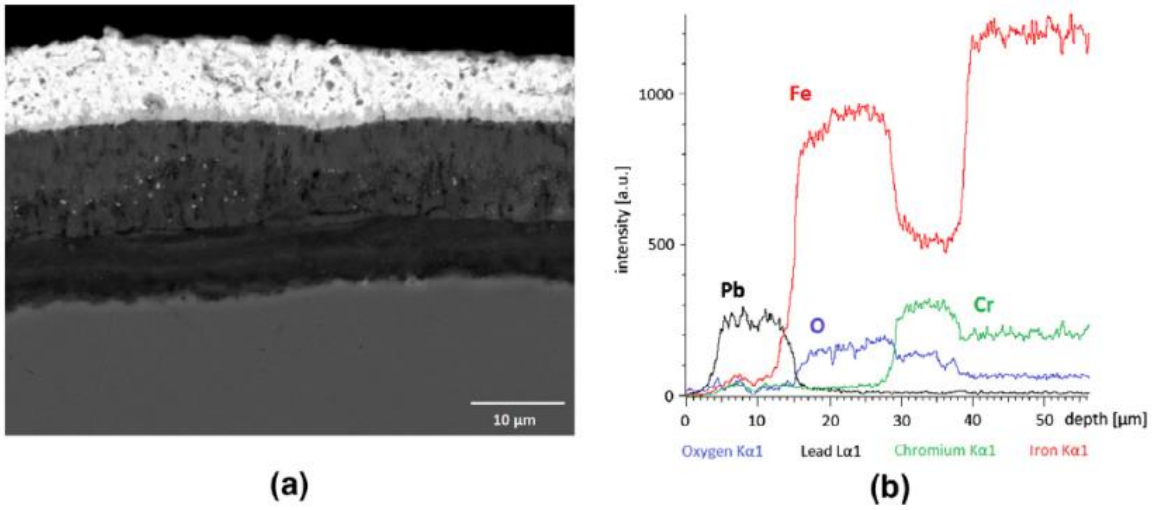

Figure 1.45: Cross-sectional SEM micrograph of the corroded face of a steel sample after exposure to HLMs at 550°C for 500 H (a), and EDX line scan (b). The structure of the oxide consists of an external magnetite layer and an internal iron and chromium oxide spinel [GAR-2013-B].

These materials will be studied by SPT in this thesis.

Coatings (iron aluminide, iron boride and an iron solid solution enriched in chromium and covered by carbide, see Fig. 1.46) deposited by pack cementation was a route developed at Institut Jean Lamour laboratory, Nancy, France for the corrosion protection of T91 steel by

LBE. Proriol Serre et al. [PRO-2011] studied the mechanical behaviour of coated T91 steel in contact with LBE at 300°C by SPT. They found that the coating have little influence on the mechanical behaviour of the coated T91 steel in air, except the iron boride one. The mechanical resistance of the iron-boride coated T91 steel is reduced compared with that of T91 without coating due to the diffusion process, which can induce a modification of T91 substrate during the pack cementation. As for the mechanical behaviour response of T91 in LBE, the fracture of the interface between the steel and the Al-based coating promotes an effect of LBE on the plasticity deformation and on the damage of the T91. While the mechanical damage is not influenced by the LBE in the case of the iron boride coating and the iron-chromium solid solution covered by a $M_{23}C_6$ carbide coating [PRO-2011].

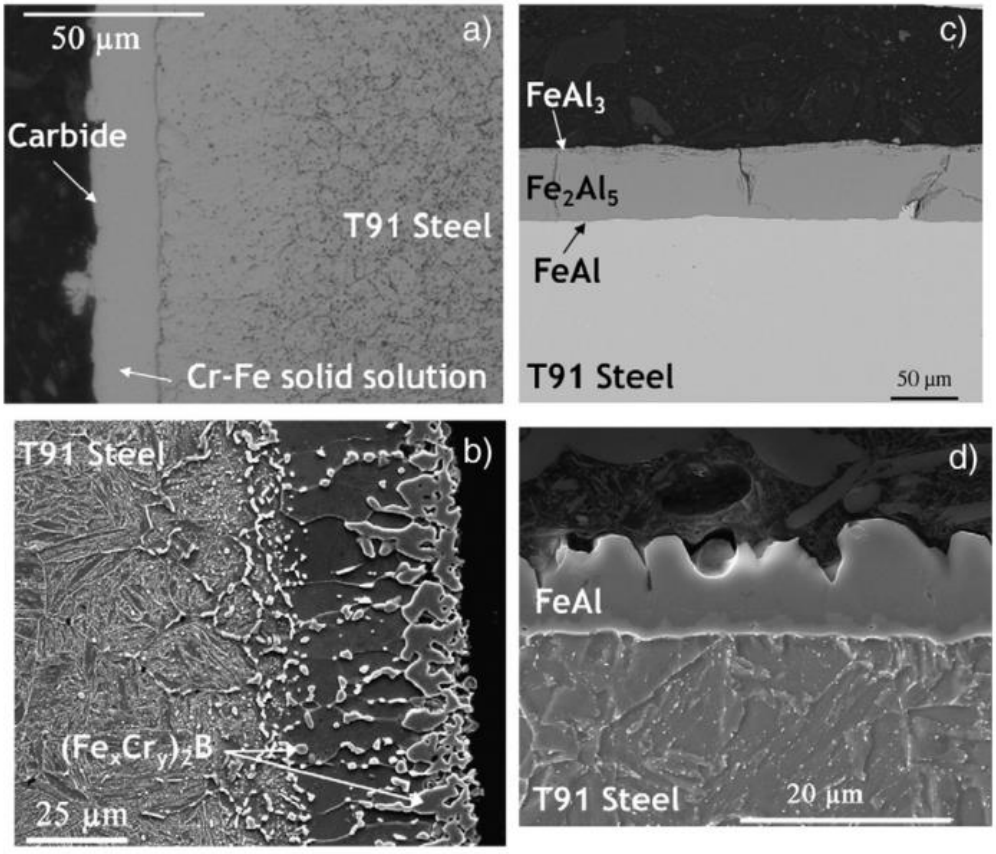

Figure 1.46: SEM micrographs (SE) of cross sections of the T91 steel covered by the different studied coatings [PRO-2011].

However, the coating consisting of a superficial $M_{23}C_6$ (M=Cr+Fe) compound covering a thick layer of $Cr_{1-y}Fe_y$ (0<y<weight%) solid solution exhibits better performance for protecting the T91 steel against liquid LBE accelerated damage indicated by mechanical fatigue tests at 300°C in LBE and in air, i.e. the detrimental effect of LBE on fatigue lives of the T91 steel is reduced (Fig. 1.47) [VOG-2011].

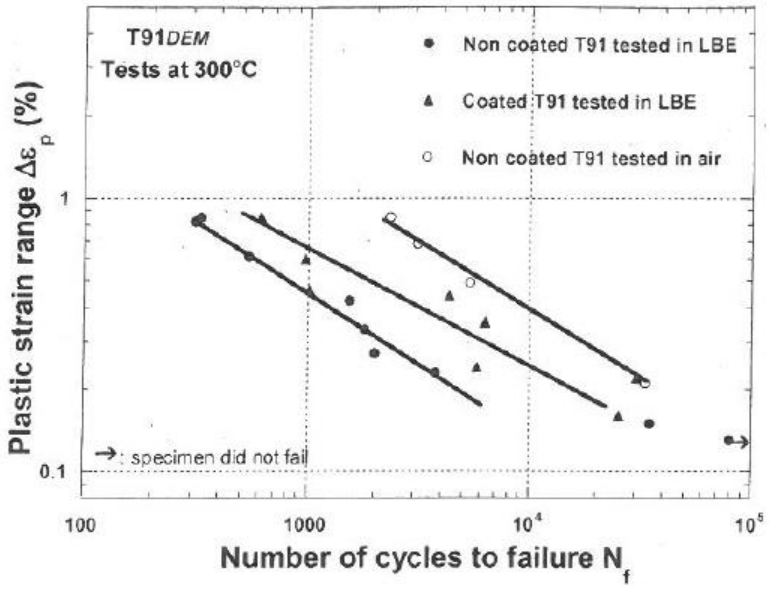

Figure 1.47: Effect of pack cementation coating on the fatigue resistance of the T91$_{DEM}$ steel at 300°C in LBE and comparision with fatigue resistance in air [VOG-2011].

Weisenburger et al. [WEI-2008-B] had studied the influence of modified surface layer of T91 steel on the low cycle fatigue (LCF) behaviour in liquid LBE containing 10^{-6} wt% dissolved oxygen at 550°C. They tried to understand whether LBE or the surface alloying FeCrAlY layer pulsed electron beam treatment (GESA) process has any influence on the LCF behaviour. This layer on the surface of the specimen is coated with FeCrAlY by low pressure plasma spraying (LPPS) and subsequent pulsed electron beam treatment applying the GESA (Gepulste Elektronenstrahlanlage) facility. Fig. 1.48a shows the appearance of the coating after treatment with no gap between coating and substrate, and the turbulent nature of the process is depicted by the swirl structure in the modified surface layer. In addition, there is no visible interface between the modified layer and the substrate after GESA treatment. Weisenburger et al. [WEI-2008-A, WEI-2011] claimed that good behaviour of coated material in LBE with 10^{-6} wt% oxygen up to 650°C and the exposure time up to 10000 h. They pointed out that all the examined data so far do not indicate any significant influence of the GESA modified FeCrAlY layer on top of the T91 proved finally by light optical microscopy (LOM) investigation shown by Fig. 1.48b. Fig. 1.48b shows that there are no alumina particles and no detaching at the interface, and still perfect interface between bulk and surface layer. They also mentioned that the GESA modified layer at the test conditions (550°C) and the test medium (LBE or air) did not change the LCF behaviour of T91 steel, contrary to tests at 300°C, even the duration of the tests and the LBE specimen contact time were comparable.

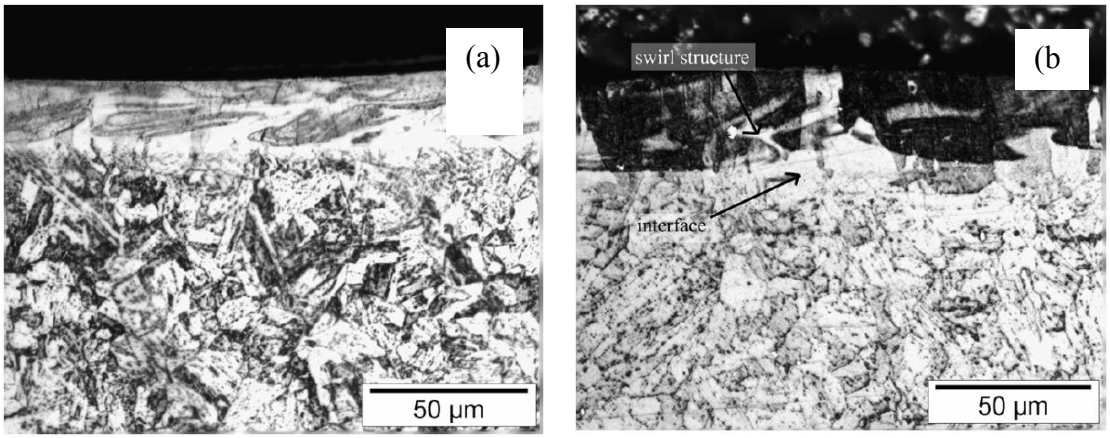

Figure 1.48: LOM of etched cross section of T91 with GESA modified FeCrAlY layer: (a) schowing the perfect bonding of modified coating to substrate and a whirling structure of the modified layer; (b) after LCF test with strain of 2% tested in LBE showing the still perfect bonding of modified coating to substrate and a whirling structure of the modified layer [WEI-2008-B].

Based on the previous research results, Weisenburger et al. [WEI-2012] continued to study the creep properties of T91 steel in liquid LBE having an oxygen concentration of 10^{-6} wt% and a flow velocity of 0.5 m/s [JIA-2009] but with Al-surface-alloyed in order to develop a protective coating to minimize LBE assisted creep effect. They concluded that the surface layers made of FeCrAl alloys on T91 steel have the capability to work as corrosion protection barriers in liquid LBE, the thin oxide layers formed on the surface modified steel samples are less susceptible to crack formation and therefore to liquid LBE enhance creep (Fig. 1.49). In addition, the negative influence of the liquid LBE on the creep behaviour of non-modified T91 is stress dependent and below a threshold stress value of 120 MPa at 550°C, the influence becomes almost negligible as shown in Fig. 1.50. But at 500°C, the stress values of 200 MPa and 220 MPa the creep rates are comparable and lower than creep rates at 180 MPa of original T91 in air at 550°C shown by Fig. 1.51.

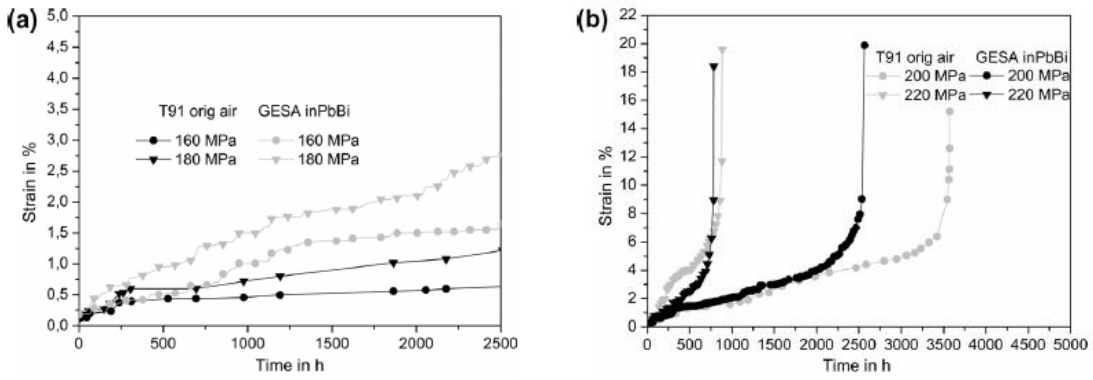

Figure 1.49: Strain versus time at 550°C of original T91 in air and GESA treated (FeCrAl alloys layer) T91 in LBE with stresses of (a) 160, 180 MPa and (b) at 200, 220 MPa [WEI-2012].

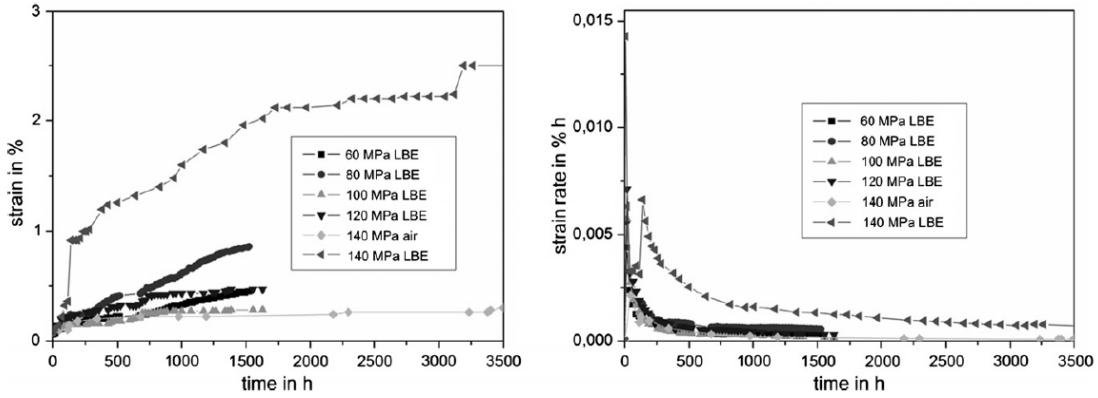

Figure 1.50: Strain and strain rate versus time for low stress level test of original T91 in LBE at 550°C [WEI-2012].

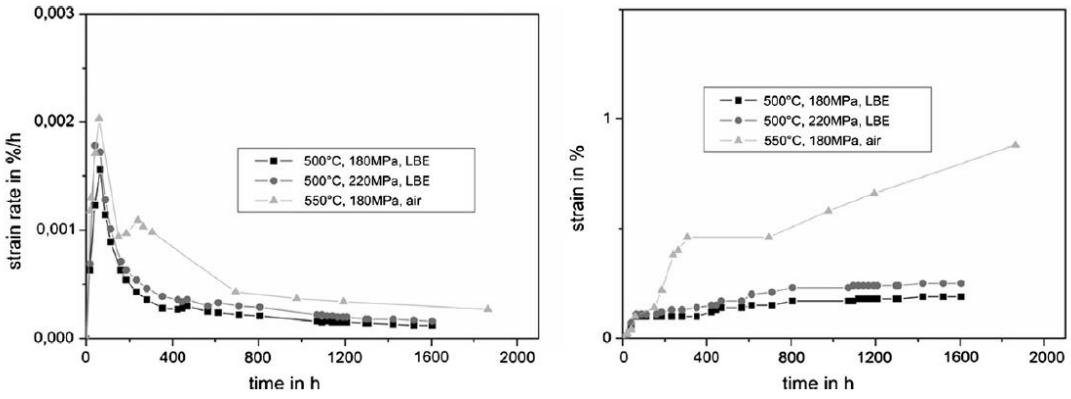

Figure 1.51: Strain and strain rate versus time of original T91 tested in LBE at 500°C for 180 and 220 MPa, and in air at 550°C and 180 MPa load [WEI-2012].

1.4.6 Effects of radiation on structural materials with lead-bismuth eutectic (LBE)

Because T91 is a structural material employed under irradiation, there is a need to document the behaviour of irradiated T91 in LBE.

The analysis of several kinds of experimental tests results indicates that T91 is prone to liquid metal embrittlement (LME)/liquid metal assisted damage (LMAD) if there is plastic deformation and intimate contact with the liquid LBE [NIC-2001-A, AUG-2004, AUG-2005, DAI-2006-A, VOG-2007, AUG-2008-A, HAM-2008, GAB-2008, GOR-2011] or in irradiated condition which can change the microstructure and harden the structure material [MAL-2006, BOS-2008, DAI-2008, DAI-2009]. Dai et al. [DAI-2006-B, DAI-2008] published the tensile properties of ferritic/martensitic (FM) steels (T91, F82H (8Cr2W0.2V), Optimax-A (9Cr1W0.6Mn)) irradiated in particular in an irradiation program conducted at PSI (STIP-I).

The results indicated that an irradiation hardening which increased with dose up to about 10 dpa. Meanwhile, the uniform elongation decreased to less than 1%, while the total elongation remained greater than 5%, except for an F82H specimen of 9.8 dpa tested at room temperature (Fig. 1.52), which failed in elastic deformation region. In Fig. 1.52, the graphs in the left column demonstrate that the fracture mode is a mixed brittle fracture type of intergranular and transgranular cleavage, while the right column shows that the 9.8 dpa specimen tested at 300°C with fracture mode transgranular cleavage although it is not as brittle as the other 9.8 dpa specimen tested at 25°C. In addition, the results also indicated that at higher doses of 11-12 dpa, the ductility of some specimens recovered (Fig. 1.53 demonstrate a transgranular ductile fracture mode with dimples), which could be due to the annealing effect of a short period of high temperature excursion. Furthermore, Fig. 1.54 shows the dose dependence with YS, UTS, STN and TE for different FM steels tested at room temperature. It can be seen that the data fall into a scattering band, so that the different steels show the same trend, especially at doses below 10 dpa, while at higher doses around 11-12 dpa, both hardening and embrittlement effects decrease.

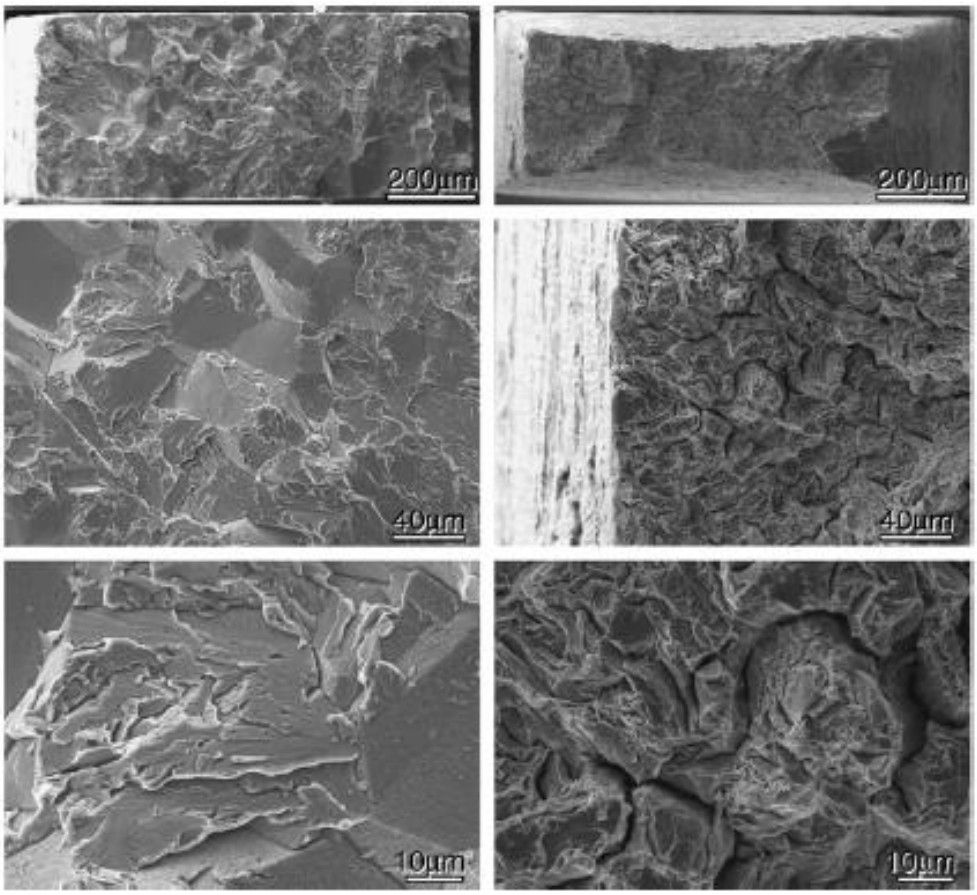

Figure 1.52: SEM micrographs showing fracture surfaces of F82H specimens irradiated to 9.8 dpa and 815 appm He tested at 25°C (left column) and 300°C (right column) [DAI-2008].

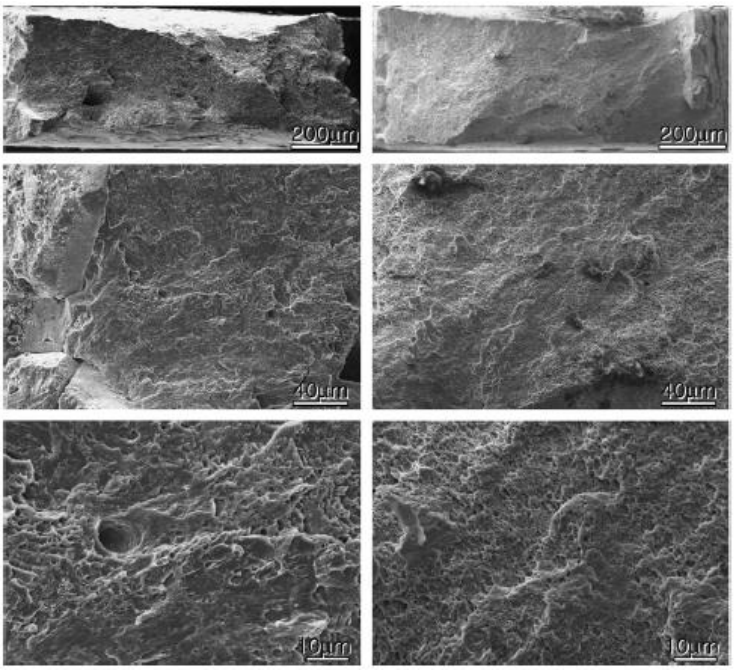

Figure 1.53: SEM micrographs showing fracture surfaces of F82H specimens irradiated to 12 dpa and 1195 appm He tested at 25°C (left column) and 400°C (right column) [DAI-2008].

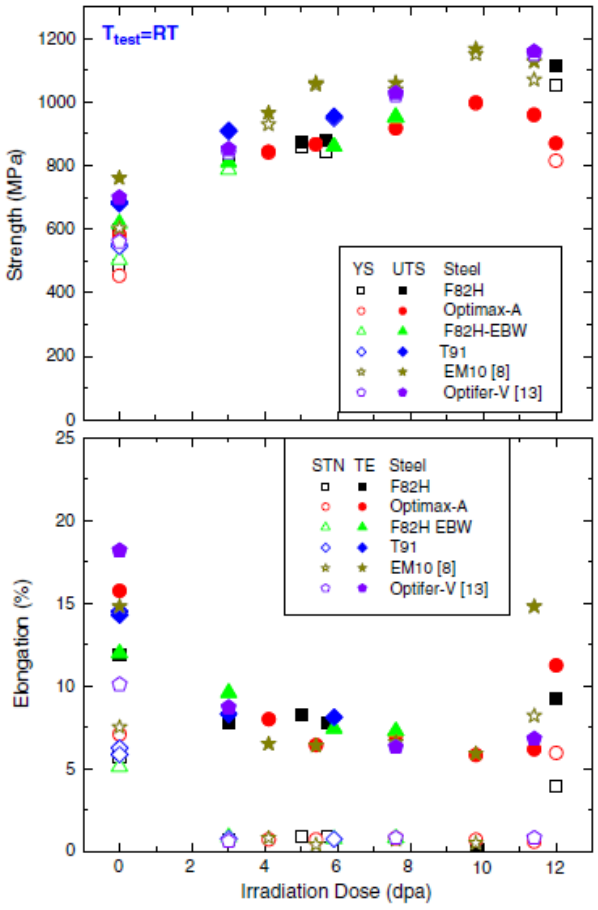

Figure 1.54: Irradiation dose dependence of YS and UTS (upper) and STN and TE (lower) of specimens from different FM steels tested at room temperature [DAI-2008].

About the effects of radiation on structural materials in presence of LBE, Long et al. [LON-2011] conducted slow-strain-rate tensile tests on irradiated ferritic/martensitic (FM) steels. The results indicate that tests in Ar revealed significant irradiation-induced hardening and embrittlement effects (loss of ductility) as compared to the unrradiated ones. Tests in LBE show that additional embrittlement effects induced by LBE are possible depending on test temperature (Fig. 1.55). Furthermore, Fig. 1.56 shows that the fracture surfaces of two irradiated T91 specimens tested in LBE at 250°C and 450°C are in transgranular cleavage fracture mode and the specimens failed without necking, that is to say, irradiated T91 steel can suffer unexpected premature failure in LBE environment. In addition, a combination of the model of adsorption-induced reduction in cohesion of atomic bonds and the kelly-Tyson-Cottrell criterion ($\sigma/\tau \geq \sigma_{max}/\tau_{max}$) for brittle cleavage fracture was used to interpret qualitatively the observation**.**

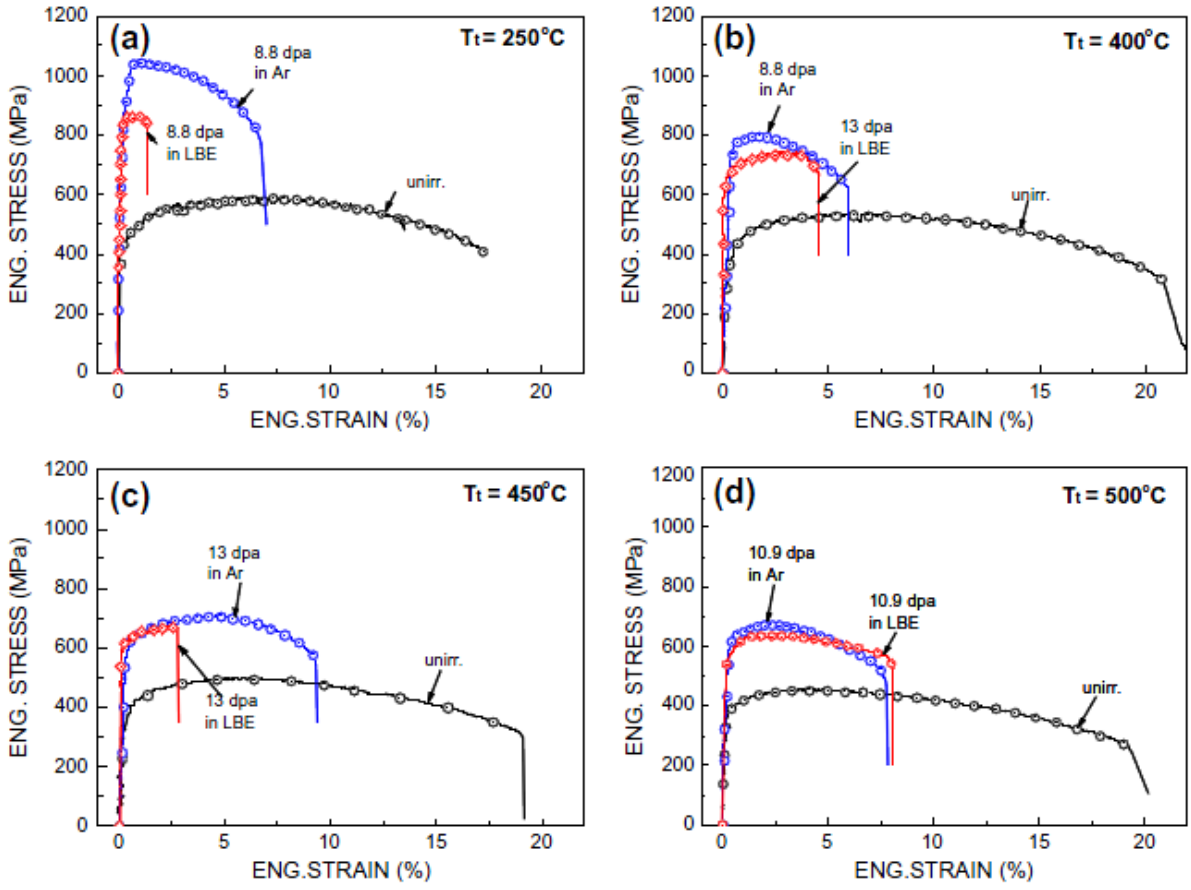

Figure 1.55: Tensile engineering stress-strain curves of the T91 specimens irradiated in STIP-III and tested either in Ar or in LBE at temperatures close to their irradiation temperatures : (a) 250°C; (b) 400°C; (c) 450°C; (d) 500°C. The unirradiated specimesn were tested in Ar [LON-2011].

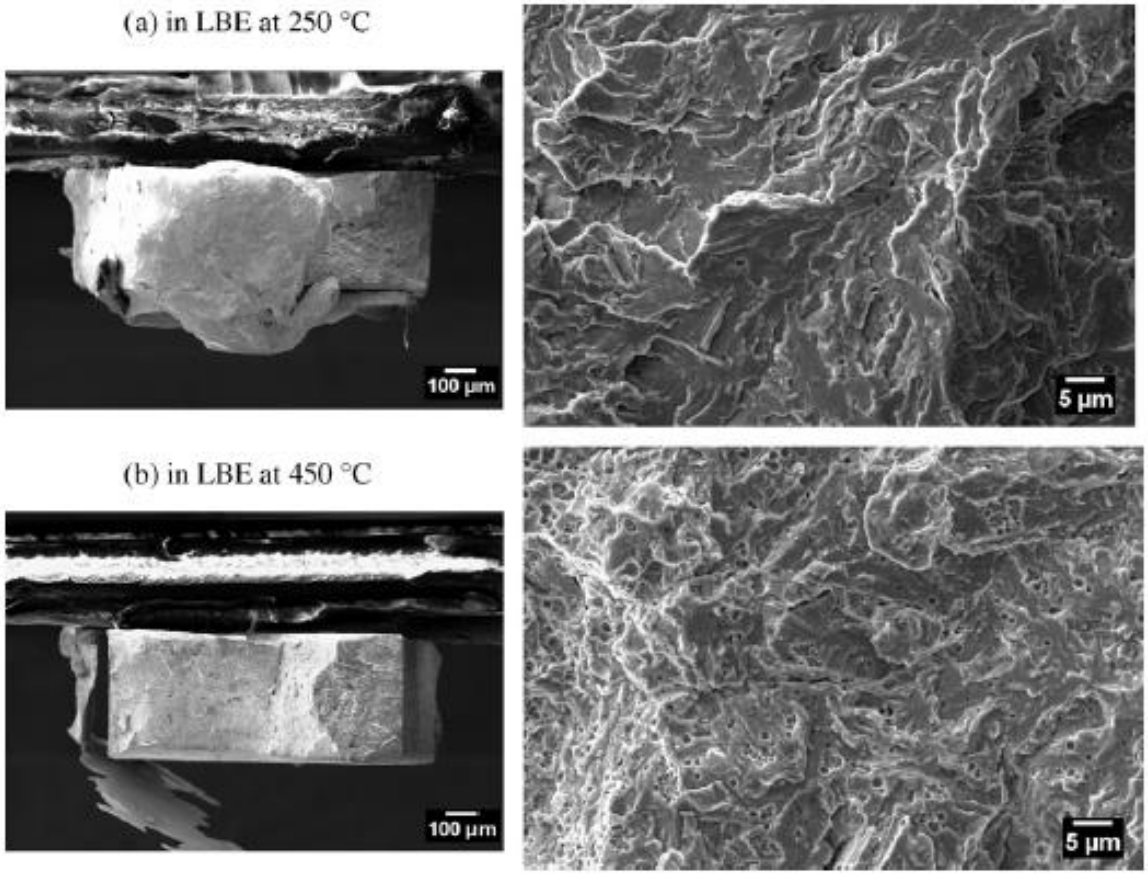

Figure 1.56: Fracute surfaces of the irradiated T91 specimens tested in LBE: (a) specimen 3-ST-B25 irradiated at 253°C to 8.8 dpa/615 appm He and tested at 250°C; and (b) specimen 3-ST-B06 irradiated at 451°C to 13dpa/985 appm He and tested at 450°C [LON-2011].

Both the LME phenomenon and LMC in LBE are currently widely under investigation by numerous laboratories around the globe, while little is known about the possible synergy between irradiation and liquid metal corrosion and embrittlement. Van den Bosch et al. [BOS-2010-B] tried to determine the separate and possibly synergistic effects of the liquid LBE environment and neutron irradiation (TWIN ASTIR irradiation program). The specimens were irradiated in contact with LBE to a dose of about 1.5 dpa at a temperature between 460°C and 490°C and subsequently tested in liquid LBE environment at temperature between 200°C and 450°C, and the obtained tensile results of T91 steel are depicted in Fig. 1.57. For the tensile tests performed at 200°C, there is no difference in yield strength or tensile strength between the reference test performed in Ar-H_2 gas mixture and the test performed in liquid LBE environment after irradiation in liquid LBE. The total elongation is however reduced by about 5% for the test in LBE after irradiation at 460°C-490°C in contact with LBE. At 350°C there is a clear difference between the tensile curves in liquid LBE after irradiation at 460°C-490°C tested at different strain rates. All curves show a decrease in yield strength and tensile strength

but the tensile curves resulting from the tests in LBE at a strain rate of 1×10^{-6} s^{-1} show a strong decrease in total elongation while the curve at a strain rate of 1×10^{-3} s^{-1} does not. At 450°C, the tensile results after irradiation in contact with LBE show a slight decrease in yield strength and total elongation of around 30-50 MPa. The obtained total elongation is similar to that measured on the reference test of non-irradiated T91 tested in LBE. Based on the observed decrease in total elongation at 200°C, 350°C and 400°C, which is similar to this observed in T91 tested in LBE prior to irradiation, there is no synergistic effects seem to be occurring between LME and neutron irradiation while in contact with LBE.

J. Van den Bosch et al. indicated that the softening by 50-100 MPa of the neutron irradiated T91 at 350°C and 450°C was observed and there was no irradiation hardening. But T91 was prone to a certain extent of LME at 200°C, 350°C and 450°C which was not affected by irradiation shown in Fig. 1.57. However, D. Sapundjiev et al. [SAP-2006-A] performed slow strain rate tensile tests (SSRT) in LBE and in air on tensile specimens irradiated in contact with water to about 1.5 dpa at 200°C. Both the tests and the neutron irradiation of the examined T91 steel were performed at 200°C. The SSRT tests were performed using a strain rate of 5×10^{-6} s^{-1}. Sapundjiev et al. pointed out that no effects of the LBE environment were found as compared to the results on the same materials tested in air.

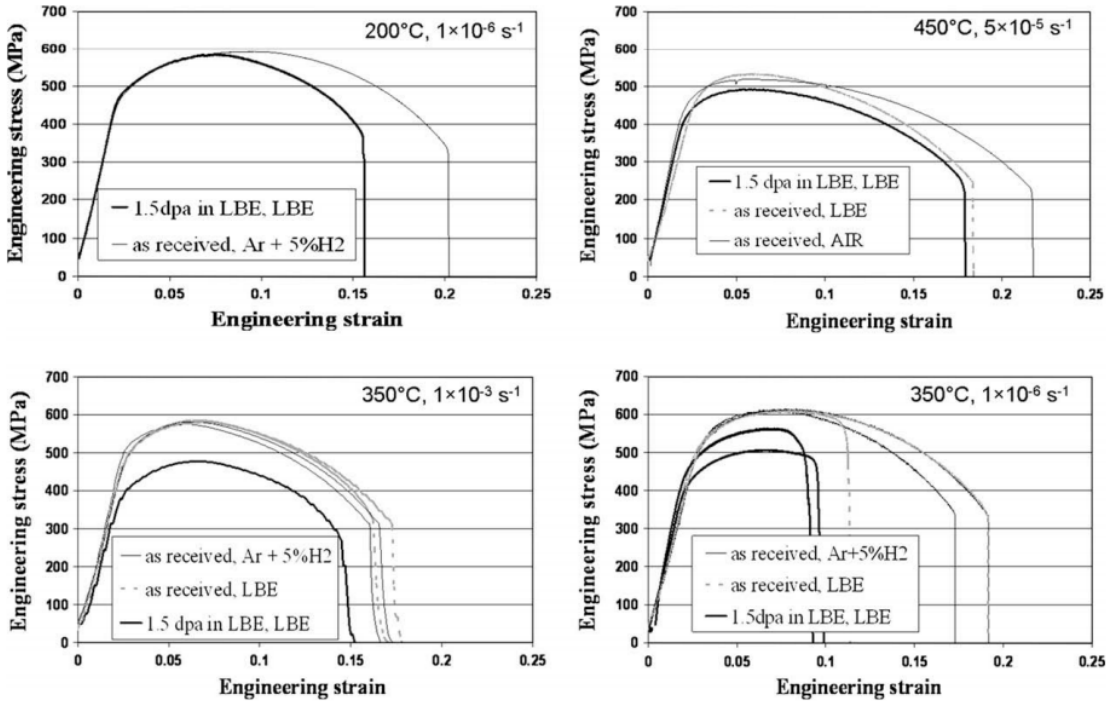

Figure 1.57: Comparison of engineering stress-strain curves of T91 steel irradiated up to 1.5 dpa in contact with liquid LBE and as received T91 steel (normalized and tempered), tested at 200, 350 and 450 °C in liquid LBE environment or gas environment using strain rates between 1×10^{-3} s^{-1} and 1×10^{-6} s^{-1} [BOS-2010-B].

1.5 Aim of the thesis

As previously mentioned, the LME phenomena are very complex since they depend on numerous factors.

The objective of this thesis research consists in understanding the role of the chemistry of liquid LBE on mechanical properties of structural steels, as well as to investigate the factors (velocity, temperature, oxygen content in LBE, heat treatment condition process) promoting the brittle sensitivity of T91 in liquid LBE, and to propose a mechanism.

This thesis work is devoted to understand these issues by doing Small Punch Tests on the material T91 in liquid low oxygen LBE and in liquid oxygen saturated LBE with different displacement velocities and test temperatures.

To reach this proposal, a specific set up has been designed to perform mechanical tests in controlled environment and in controlled oxygen content LBE. Two kinds of different heat treatment condition processes on T91 martensitic steel are employed. In addition, in terms of experimental techniques, three-point bending testing and tensile testing are used to qualitative and quantitative research about the mechanical properties of T91 affected by liquid LBE.

CHAPTER II : MATERIALS & EXPERIMENTAL TECHNIQUES

In this chapter, the materials and the experimental techniques used in this thesis are described, which includes the microstructural analysis of the studied steel, the details of specimens preparation for mechanical tests, the mechanical tests such as Small Punch Tests (SPT), three-point bending tests and tensile tests, the facilities used for performing these mechanical tests in liquid lead-bismuth eutectic (LBE) environment, and the unit for removing oxygen from LBE.

2.1 Materials

The purpose of this section is to present the structural material T91 steel and the heavy metal lead-bismuth eutectic (LBE) used in this work and to confirm that these properties and chemical composition are close to those mentioned in the bibliography.

2.1.1 T91 steel

The target material in this investigation is the T91 martensitic steel supplied in the form of rolled plate. Its chemical composition is given in Table 2.1.

Table 2.1: Chemical composition of T91 steel.

Element	C	Cr	Mo	Si	Mn	P	S	Ni	Nb	V	N	Fe
wt %	0.1025	8.99	0.89	0.22	0.38	0.021	0.0004	0.11	0.06	0.21	0.0442	Bal

The standard heat treatment of T91 steel is a normalizing at 1050°C for one hour followed by air cooling and a subsequent tempering for one hour at 750°C followed by air cooling. It will be labelled as TR750. The Vickers hardness (HV10) of the steel is 278±11 HV.

Another heat treatment has been considered. It consists of a normalizing at 1050°C for one hour followed by air cooling but a subsequent tempering for one hour at 500°C followed by air cooling. It will be labelled as TR500 and HV10=446±22 HV. The difference in hardness value between these two heats treated materials results from the precipitation state [JON-1991, TOT-2006] and the structures of dislocations.

In order to reveal the microstructure of the T91 steel and to measure the mean prior austenitic grain size, optical microscopy was used. The specimens used for this metallographic analysis were mechanically polished with SiC paper up to 1200 grade, and then with suspension liquid solutions: 9 μm diamond product containing exclusively polycrystalline diamonds, water based 3 μm diamond suspension containing a unique mixture of high-performance diamonds, acidic 1 μm alumina suspension. The prepared specimens were etched using Vilella's reagent 1 g picric acid and 5 mL HCl in 100 mL ethanol for 30-50 seconds. Some observations were performed for each sample at different spots in the specimen to evaluate the mean grain size.

Fig. 2.1 gives the optical microscope and scanning electron microscope (SEM) observations of the microstructure of the TR750 and TR500 specimens. The microstructure is tempered martensitic. The prior austenite grain (PAG) size is about 15±5 μm. According to the published results [LON-2008], the carbide precipitates are located mostly on the boundaries of the laths and on PAG especially for the TR750 material, and inside the laths and the boundaries of both the laths and PAG, in the case of the TR500 material.

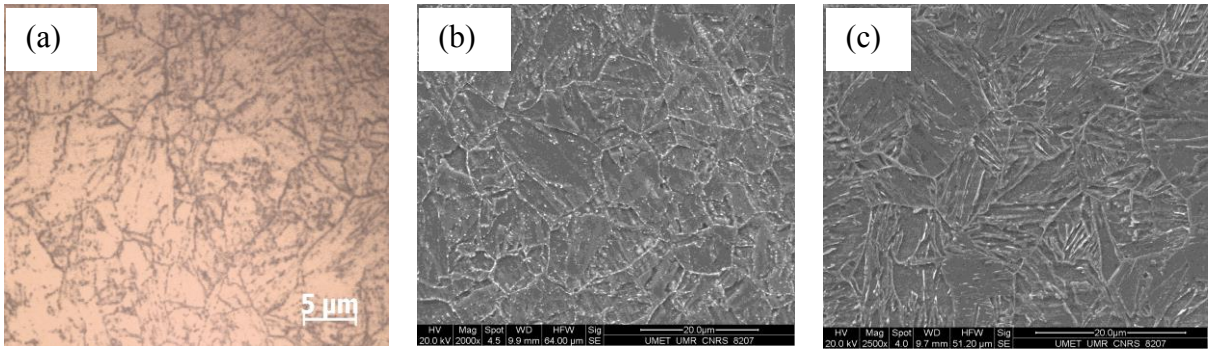

Figure 2.1: Microstructure of T91 steel: (a) optical micrograph of TR750; (b) and (c) SEM micrographs (secondary electrons contrast) of TR750 and TR500 specimens respectively.

2.1.2 Lead-bismuth eutectic (LBE)

The composition of lead-bismuth eutectic (LBE) is 45 wt% Pb and 55 wt% Bi. The LBE ingot (1 kg) comes from company Bertrandias.SA. France. The chemical composition, in particular the presence of some impurities (Fe, Cr, Ni…) corresponds to the specification used in nuclear industry.

2.2 Mechanical tests

In this thesis, mechanical tests were performed in air, in argon/hydrogen gas mixture, in liquid oxygen saturated LBE or in liquid low oxygen LBE to investigate the mechanical properties response and the sensibility of martensitic T91 steel to LBE environment. Three kinds of mechanical tests were employed for studying the sensitivity of materials to LBE embrittlement. The first one is the Small Punch Test (SPT) of square shaped flat specimens. The second one is the three-point bending test of pre-cracked small bending specimen. The third one is the tensile test of cylindrical specimens with smooth or notched surfaces.

Serre and Vogt [SER-2007] who developed the use of SPT for the study of LME, show the sensitivity of this technique to highlight ductile to brittle transition due to liquid metal. Indeed, in comparison with conventional tensile test, the SPT appeared to be more sensitive for the evidence of LME. Furthermore, the size of SPT specimen and the low quantity of employed liquid metal make this test convenient. Therefore, a lot of experiments aiming at pointing out the role of temperature, of loading rate and of oxygen concentration of LBE were performed using SPT.

Three-point bending tests were also performed at different temperatures to investigate the crack propagation mechanism and fracture toughness of T91 steel in air or in LBE.

In addition, the tensile tests were employed to further quantitative analysis of the mechanical properties and of the brittle crack formation mechanism of T91 steel in liquid LBE.

A great part of my PhD work was to design a purification unit to remove the dissolved oxygen in LBE. Then, it was necessary to develop a method for testing the material in a controlled environment.

2.2.1 Small Punch Test (SPT)

The knowledge of the mechanical properties of structural components and their degradation during long-term services are key factors in assessing the structural integrity of any facility and its residual life. As conventional mechanical characterization of materials (with the exception of hardness) is always destructive, the use of tests on miniaturized specimens is considered to be very interesting if suitable samples can be extracted from real components without affecting their operating capacity. One of these tests methods is the small punch test (SPT). When used on large components, this test may be considered quasi-non-destructive [KAM-1986, MIS-1987, BUL-2002, JIA-2003, FIN-2004, KIM-2005, MAT-2007].

In fact, for nuclear application, the use of SPT for mechanical testing is now a worldwide spread interest in order to extract the mechanical and physical properties. There are mainly two reasons that drive the effort to develop this technique: the intrinsic one arises from the limitations imposed by the standard testing, such as the availability of space in the irradiation facilities and the presence of fluence and/or irradiation temperature gradients for large samples, the technical impossibility of machining standard sized geometries out of

commercial structural components like tubes or grids that were irradiated in service. The extrinsic one is especially devoted to reduce as much as possible the personnel dose for post-irradiation testing [WAN-2008]. Thus, this kind of method was widely used in the nuclear engineering design techniques and other pressure and piping techniques to reduce the costs and difficulty associated with machining large standard tensile specimens and to accommodate limited irradiated space [WAN-2008].

In this thesis, as already mentioned, the SPT is used for its very important sensitivity to evidence LME according different experiment parameters.

2.2.1.1 Setup of SPT

A specific setup, which has been designed and validated at Unité Matériaux Et Transformations, Lille1 university, was used to perform SPT in air or in liquid metal (Fig. 2.2). The SPT setup consists of a specimen holder, a pushing rod and a ball. The specimen holder includes a lower die, an upper die which is also used as the tank for the liquid metal and four clamping screws. The load is transferred onto the square specimen (dimension $10\times10\times0.5$ mm^3) by means of the pushing rod and a 2.5 mm diameter tungsten carbide ball in contact with the lower surface of the square specimen. In this way, the puncher being under the specimen, the upper surface of the specimen is in contact with the liquid metal and is submitted to tensile loading.

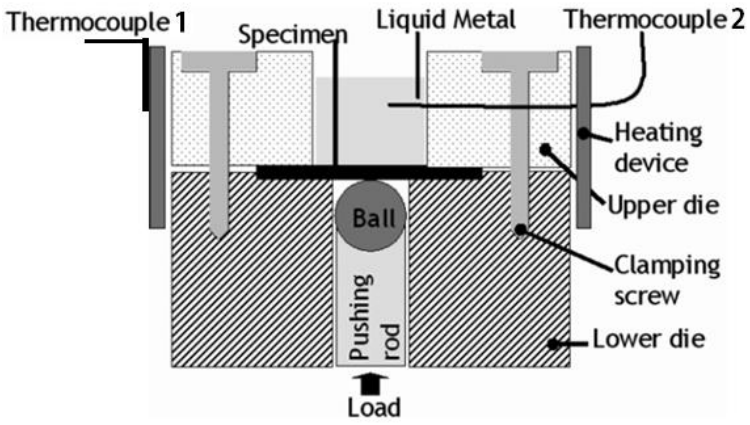

Figure 2.2: Small punch test setup.

The SPT were performed using a tensile electro-mechanical INSTRON machine (Fig. 2.19) with a controlled cross-head speed ranging from 0.0005 to 0.5 mm/min. The temperature was controlled by a heating ring and a thermocouple fixed on the ring (thermocouple 1 - Fig. 2.2).

The exact temperature of the test was controlled with a second thermocouple plunged in the liquid LBE environment or placed 3 mm away from the specimen for test in air. To perform SPT at high temperature, the procedure consisted in heating the specimen and the SPT setup from room temperature to the test temperature at an average heating rate of 8±1 °C/min. When the targeted temperature was reached, the setup with the specimen was maintained for 10 minutes before SPT. After test, the cooling down to room temperature was performed without temperature control. In addition, in order to ensure the experimental data reliability and repeatability, the test was repeated at least three times in the same condition.

2.2.1.2 SPT specimens preparation

SPT square specimens with dimensions of 10×10×0.5 mm^3 were mechanically polished with SiC paper up to 1200 grade, and then polished step by step with suspension liquids to 1 μm as mentioned for the metallographic study (section 2.1.1 of this chapter). The thickness of the specimen was controlled around 500±10 μm.

Besides the smooth surface specimen, another kind of notched surface specimen was prepared to study the effect of the surface defect on the sensitivity to LBE embrittlement of T91 steel. The introduction of a notch has important consequences in the fracture process. For example, the presence of a notch is expected to increase the ductile-brittle transition temperature of steel. The preparation of the notched surface specimen was done according to a new methodology to determine the elasto-plastic fracture toughness, J_{IC}, by means of notched SPT samples described by E. Cárdenas et al [CAR-2012]. Standard SPT specimens were prepared and then a longitudinal notch was machined in the center of one side of the sample, producing a notch depth-to-thickness ration a/t=0.4 shown by Fig. 2.3.

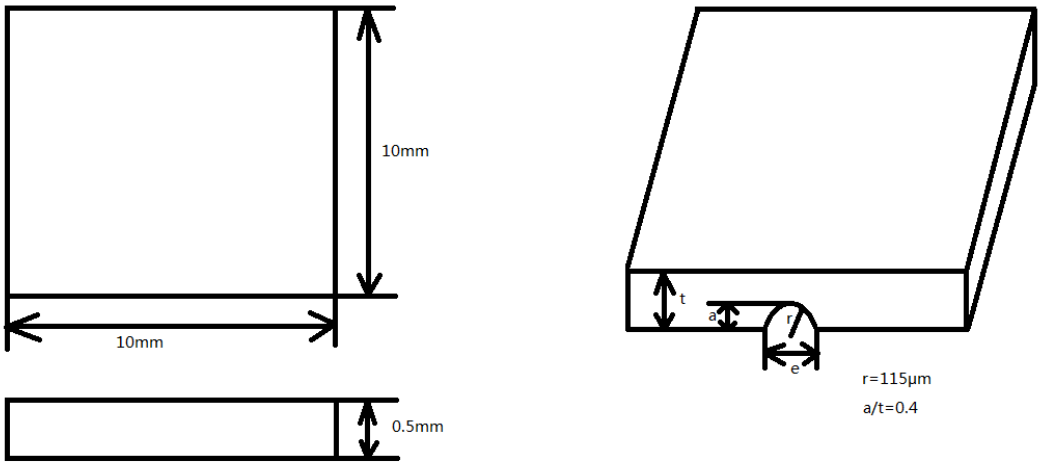

Figure 2.3: Longitudinal notched small punch test (SPT) specimen.

Before the mechanical tests, the notched specimens should be well polished as the smooth ones.

2.2.1.3 SPT load-displacement curves

During the small punch test, the evolution of the load with the displacement was measured. The load-displacement curve gives the data about the deformation and the fracture of the material. Fig. 2.4 gives an example of a load-displacement curve of a ductile material. The curve exhibits four stages.

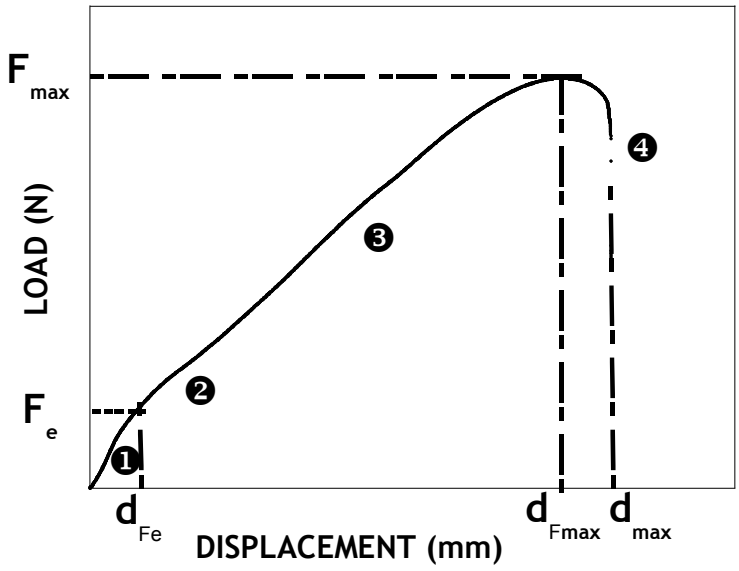

Figure 2.4: Typical load-displacement curve of a ductile material.

The first stage, noted as '❶' on the curve in Fig. 2.4, corresponds to the elastic bending. While the entire specimen undergoes an elastic deformation, the ball-specimen contact area, which is very small in size, is plastically deformed. The second stage (noted as '❷') corresponds to a plastic bending state: the volume of the specimen which is plastically deformed progressively increases spreading from the ball-specimen contact area through the overall thickness and in radial direction. Then a stretching of the membrane occurs in the third stage (noted as '❸'). At this stage, the deformation of the specimen is not caused by bending but by stretching around the contact area between the ball and the specimen. Microcracks are generated during this stage. Finally, during the fourth stage where the load reaches its highest value (noted as '❹'), the main crack forms and propagates. In fact, there is no clear boundary between the different stages according to a physical point of view that one stress state is predominant compared to another one.

The analysis of the load-displacement curve of SPT can provide the following mechanical characteristics of the material:

- The yielding load F_e (N);
- The maximum load F_{max} (N);
- The displacement at yielding load d_{Fe} (mm);
- The displacement at maximum load d_{Fmax} (mm);
- The normalized energy to the rupture J_{nf} (J/mm), which represents the total area under the load-displacement curve, relative to the thickness of the specimen;
- The normalized energy to maximum load J_{nFmax} (J/mm), which represents the area under the load-displacement curve to the maximum load F_{max}, relative to the thickness of the specimen. Furthermore, this normalized energy J_{nFmax} also represents the energy necessary to deform elastically and plastically the specimen and to initiate crack which can lead to macroscopic damage of the specimen. In this thesis, normally, the fracture energy J_f approximately equals to J_{Fmax}. Therefore, in order to analyze the data more conveniently, J_{Fmax} was chosen instead of J_f as the fracture energy, and then which was normalized by the thickness of the specimen (J_{nFmax}).

The yield stress (σ_{YS}) and the ultimate tensile strength (σ_{UTS}) cannot be measured from SPT but several experimental relationships have established between on one hand F_e and σ_{YS}, and on the other hand F_{max} and σ_{UTS}.

Concerning the σ_{YS}, the best agreement is the typical equation 2.1:

$$\sigma_{YS} = \alpha F_e / e^2 \qquad 2.1$$

with e the thickness of the specimen, and α a factor that depends only weakly on the material properties and mainly a function of the test geometry. For the T91 steel, a α factor of 0.33 [SER-2007] has been found to correctly connect F_e with σ_{YS}.

Concerning the σ_{UTS}, the best agreement is given by the equation 2.2 [MIL-2006].

$$\sigma_{UTS} = F_{max} / (5.01e + 1.8e^2) \qquad 2.2$$

When a material becomes brittle, partially or totally, the SPT curve is modified. For a fully brittle material, the plastic domain is strongly reduced and the load-displacement curve is quasi linear right to rupture. It means that there is little plastic bending or zero plastic membrane stretching as shown in Fig. 2.5a [JU-2003]. Sometimes, the curve contains a drop or a pop-in indicating sudden little fracture at some local places in the material (Fig. 2.5b).

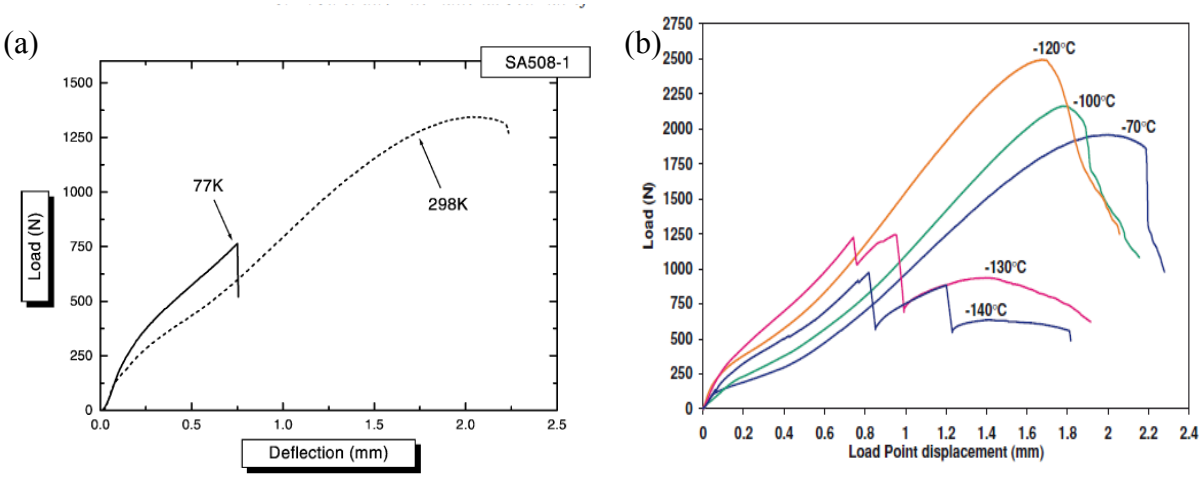

Figure 2.5: Different evolutions of the load-displacement curves in steels with brittleness occurrence: (a) taken from Ju's work [JU-2003], and (b) taken from Contreras's work [CON-2008].

2.2.2 Three-point bending tests

The three-point bending tests aimed at establishing the fracture toughness which describes the ability of a material containing a crack to resist fracture. The three-point bending test has been chosen because the specimen has a flat part which is easy for preparation and further investigation and testing. However, the results of the testing method are sensitive to specimen and loading geometry and strain rate.

The linear-elastic fracture toughness of a material is determined from the stress intensity factor (K) at which a thin crack in the material begins to grow. It is denoted K_{IC} and has the units of Pa$\sqrt{m}$ or psi$\sqrt{in}$. Plastic-elastic fracture toughness is denoted by J_{IC}, with the unit of J/cm^2 or lbf-in/in^2, and is a measurement of the energy required to grow a thin crack.

The subscript IC denotes mode I crack opening under a normal tensile load perpendicular to the crack, since the material can be made deep enough to stand shear (mode II) or tear (mode III), which have been described in chapter I. Fracture toughness is a quantitative way of expressing a material's resistance to brittle fracture when a crack is present. Brittle fracture is very characteristic of materials with weak fracture toughness.

2.2.2.1 Three-point bending test specimen

The three-point bending tests specimens were fabricated from the T91 steel plate with the standard heat treatment (normalizing at 1050°C for 1h followed by air cooling and subsequent tempering at 750°C for 1h followed by air cooling). The dimensions of the three-point bending tests specimens are 55×10×5 mm^3 with a notch of 5 mm in depth (Table 2.2) based on the standard ASTM-E1820 (Fig. 2.6). The outer surfaces of the specimens were polished with SiC paper up to 1200 grade, and then polished step by step with suspension liquids to 1µm as for the SPT specimens, that is the same polish preparation method as small punch tests specimens.

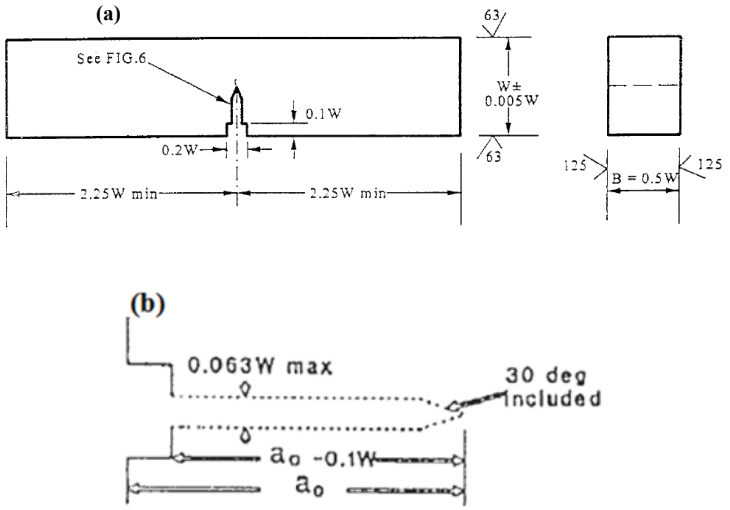

Figure 2.6: Dimensions of the three-point bending test specimen (recommended single edge bend [SE(B)] specimen) based on the standard ASTM-E1820 (a), and the notch dimension corresponds to this specimen (b) [AST-2001].

Table 2.2: Dimensions of three-point bending tests specimens for investigation in this paper based on the standard ASTM-E1820 [AST-2001].

Dimensions of three-point bending tests specimens		E1820 standard criteria
L	length of specimen : 55mm	L>4.5W
W	width of the specimen: 10mm	1≤W/B≤4 S=4W
B	thickness of the specimen : 5mm	
S	distance between the support points : 45mm	
B_N	net thickness : mm	
Dimensions of the notch		
a_0	length of the notch at the beginning of the test : 5mm	r <0.05W
r	radius of curvature of the notch : 100-120 µm	
b_0	the size of non-ruptured ligament	W-a_0

2.2.2.2 Three-point bending test fixture

The three-point bending tests fixture used in this work is illustrated in Fig. 2.7. This fixture was designed according to the standard ASTM-E1820 [AST-2001].

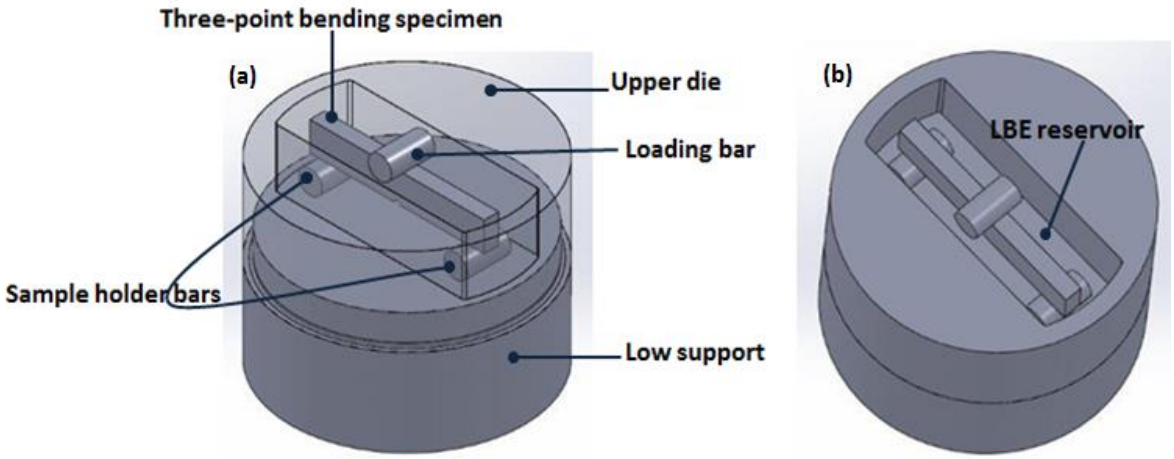

Figure 2.7: Setup for the three-point bending test in liquid LBE environment: (a) perspective view, and (b) top view.

The setup comprises a lower support with the two sample holder bars on which the specimen is put so that the notch is on the inferior part of the specimen. The loading bar is placed on the middle of the specimen. An upper die which acts as a reservoir covers the lower support with the specimen. A heating ring surrounds the setup and the temperature is controlled by a heating cable and a thermocouple. The exact test temperature is measured with another thermocouple plunged in the liquid LBE. The average rate of heating temperature is about 5 °C/min. When the setting temperature was reached, the setup was maintained for 10

minutes, then the three-point bending test started. In addition, a preload of 40 N is applied to the specimen to fix it at the exact position before starting the three-point bending test procedure. Especially, for the three-point bending test in liquid LBE, once the specimen is fixed, the liquid oxygen saturated LBE (prepared in an auxiliary oven outside this setup) is poured into the reservoir until the entire notched portion is immerged. Then the heating of the specimen is proceeded. Once the experiment is finished, the heating is stopped and the specimen is removed from the setup.

The tests were conducted in air (room temperature) or in liquid oxygen saturated LBE (300°C) at a constant cross-head speed (0.5, 0.05, 0.005 mm/min) with the tensile electro-mechanical INSTRON machine (shown by Fig. 2.19). Load - cross-head displacement curves were recorded during the tests.

2.2.2.3 Determination of the *J*-integral for the basic test method

The J-integral represents a method to calculate the strain energy release, or work (energy) per unit fracture surface area in a material, namely,

$$J = -\frac{dU}{Bda} \tag{2.3}$$

where U is the potential (strain) energy, B and a are the thickness and crack length of a given specimen, respectively, according to the standard ASTM1820-01 [AST-2001], and the J-integral can be calculated incrementally using the following equation 2.4:

$$J = J_{el} + J_{pl} \tag{2.4}$$

where J_{el} is the elastic component of J, and J_{pl} is the plastic component. The equations are as follows [AST-2001]:

$$J_{el} = \frac{\mathrm{K_{IC}^2}(1-\nu^2)}{\mathrm{E}} \tag{2.5}$$

$$J_{pl} = \frac{2\mathrm{A_{pl}}}{\mathrm{B_N}\,\mathrm{b_0}} \tag{2.6}$$

where A_{pl} is the area of under the load-displacement curve defining the work needed for the plastic deformation as shown in Fig. 2.8.

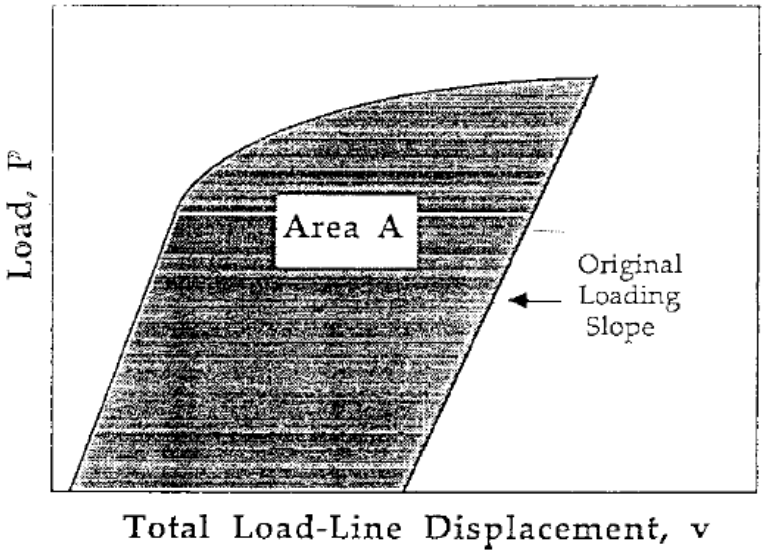

Figure 2.8: Definition of area for *J* calculation using the basic method [AST-2001].

It can be calculated directly using the load-displacement curve, and υ is the Poisson's ratio of the material (for the T91 steel, υ=0.3), *E* is the Young's modulus of the material. *E* changes with testing temperature and a correlation between *E* and *T* has been established by Long et al. [LON-2009]) and represented in Fig. 2.9.

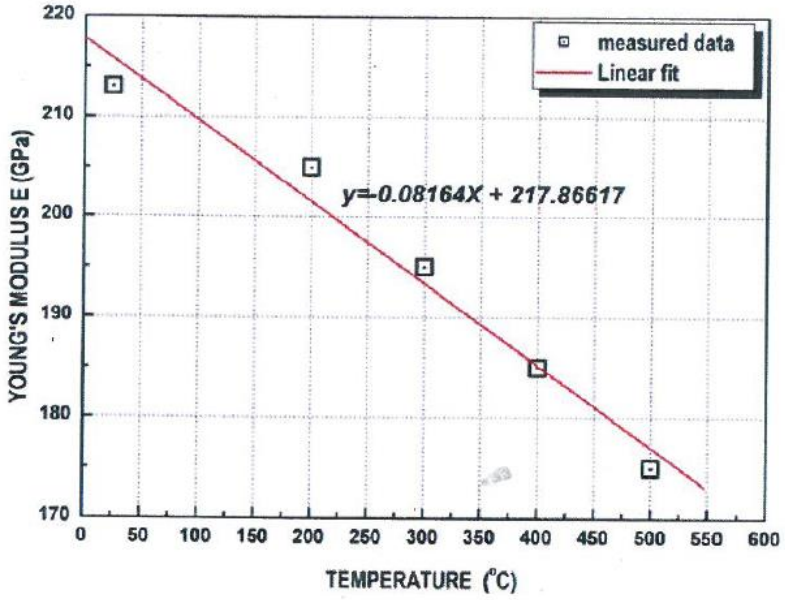

Figure 2.9: Correlation between the Young's modulus and the temperature for the T91 steel [LON-2009].

The different heat treatments performed for T91 steel are expected not to modify the value of E. The Young's modulus *E* used for TR750 has been calculated based on the relation given in Fig. 2.9 and the values are summarized in Table 2.3.

Table 2.3: Young's modulus *E* used for martensitic T91 steel (TR750 material).

Temperature (°C)	25	200	250	300	400	450
Young's modulus *E* (GPa)	216	202	198	193	185	181

K_{IC} is the critical stress intensity factor, which is in Mode I fracture for slow rates of loading and negligible plastic-zone adjustment. It depends on the geometry of the crack, as well as the loading mode. B_N is the net specimen thickness ($B_N = B$ if no side grooves are present), and b_o is W-a_o. K_{IC} is given by equation 2.7, which in turn requires to define the geometric factor correction f(a/W).

$K_{IC} = \left(\frac{P_{max}S}{(BB_N)^{\frac{1}{2}}W^{\frac{3}{2}}}\right) f\left(\frac{a}{W}\right)$	2.7
$f\left(\frac{a}{W}\right) = \frac{3(\frac{a}{w})^{1/2}[1.99 - \left(\frac{a}{w}\right)\left(1-\frac{a}{w}\right)\left(2.15 - 3.93\left(\frac{a}{w}\right) + 2.7\left(\frac{a}{w}\right)^2\right)]}{2(1+\frac{2a}{w})(1-\frac{a}{w})^{3/2}}$	2.8 [AST-2001]

P_{max} is the maximum load that the specimen was able to sustain according to the load-displacement curves (see Fig. 2.10). In fact, there are three different configurations curves shown in Fig. 2.10.

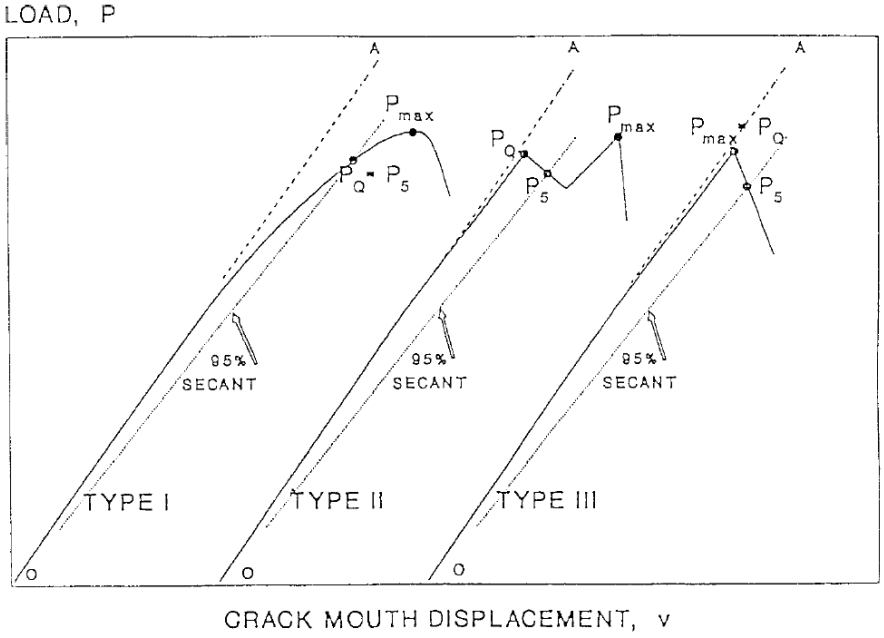

Figure 2.10: The principle types of load-displacement records [AST-2001].

In order to determine K_{IC} in accordance with this test method, it is necessary first to calculate a conditional result, K_Q (stress intensity factor calculated from P_Q), which involves a construction on the test record, and then to determine whether this result is consistent with size and yield strength requirements as equivalent to K_{IC}. The procedure is as follows [AST-2001] (Fig. 2.10):

- Construct a secant line as shown on Fig. 2.10 with a slope $(P/v)_5=0.95(P/v)_o$ where $(P/v)_o$ is the slope of the tangent OA to the initial portion of the data record. If the load at every point on the record that precedes P_5 is lower than P_5, then P_5 is P_Q (Fig. 2.10, Type I). However, if there is a maximum load preceding P_5 that exceeds it, then this maximum load is P_Q (Fig. 2.10, Type II and III). The J-integral from P_Q is called J_Q.
- Calculate the ratio P_{max}/P_Q. If this ratio does not exceed 1.10, the equations 2.7, 2.8 can be used to calculate K_Q corresponds to the load P_Q and to the crack length a_Q. If P_{max}/P_Q does exceed 1.10, then the test is not a size-independent K_{IC} test, because it is then possible that K_Q bears no relation to K_{IC}.
- Calculate $2.5(K_Q/\sigma_{YS})^2$ where σ_{YS} is the 0.2% offset yield strength in tension. If this quantity is less than both the specimen thickness, B, and the length of the initial uncracked ligament, b_o, then K_Q is equal to K_{IC}. Otherwise, the test is not a qualified and size independent K_{IC} test.

2.2.3 Tensile tests

In the light of the simple and commonly practical consideration, the tensile tests were chosen to obtain the quantitative mechanical characteristics of T91 steel in liquid LBE. In addition, tensile testing on the round smooth surface specimen method is the traditional material science test method to get the general mechanical properties of studied materials with quantitative data in particular environment. Tests on sharp notched specimens were also performed. They could be used to measure the slow crack growth resistance of the material tested. Here, they have been simply employed to point out the effect of stress triaxiality. Tensile specimens with threaded extremities were machined from the plates of T91 steel in the standard heat treatment. The cylindrical tensile specimens have a diameter of 4 mm and a gauge length of 20 mm as shown by Fig. 2.11a. In the case of the notched specimen, the depth of the notch is 0.5 mm as shown by Figs. 2.11b, 2.11c. In addition, since the preparation of tensile specimens is just to verify the general mechanical properties behaviour response of

TR750 steel in liquid LBE, the surfaces of all the tensile specimens (smooth/notched) were not polished very good (except only one smooth surface specimen was experienced with electrolytically polished surface for comparing analysis) and the machined tensile specimens were just cleaned with ethanol with the ultrasonic cleaning machine for 5 minutes and then dried.

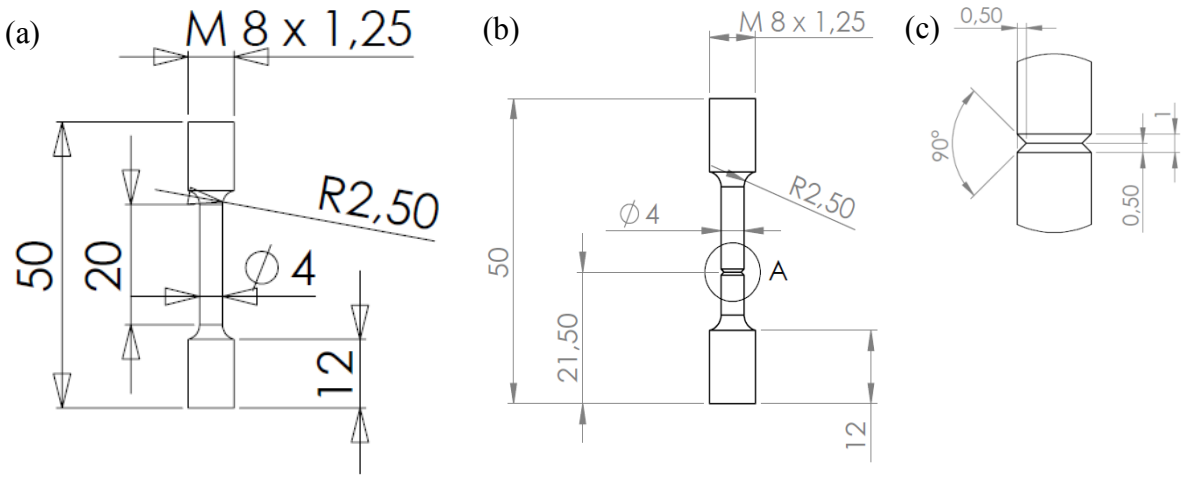

Figure 2.11: Sketches of the tensile test specimens: (a) smooth surface, (b) notched surface and (c) is the detail dimension of the notch.

The tensile tests were conducted on material TR750 steel mainly at 300°C in liquid oxygen saturated LBE bath and in low oxygen LBE bath with the tensile electro-mechanical INSTRON machine at a constant cross-head speed of 0.12, 0.005, 0.0005 mm/min, which corresponds to a normal strain rate of $10^{-4}s^{-1}$, $4\times10^{-6}s^{-1}$, $4\times10^{-7}s^{-1}$ respectively. The choice of this strain rate was based on the LBE embrittlement sensitivity effect of TR750 steel at 300°C confirmed by SPT in this thesis. For smooth specimens, the load - cross-head displacement curves were recorded during the tests, and were converted to engineering stress - engineering strain curves. The tensile properties of T91 steel such as the yield stress (*YS*), the ultimate tensile stress (*UTS*), the uniform elongation (*UE*), and the total elongation (*TE*) were evaluated from the tensile tests curves.

The specimen was screwed in the lower part which serves as the LBE reservoir. The reservoir was filled by LBE (oxygen saturated or low oxygen) so that at least half the length of the specimen was in contact with the liquid metal. We also made sure that the notched part of the specimen was immersed. The upper part of the specimen is screwed to the loading bar (Fig. 2.12). A heating ring surrounding the reservoir allows tests at high temperature controlled by a heating cable and a thermocouple. For tests in liquid LBE, another thermocouple was

employed to measure the liquid metal temperature as the experimental test temperature. The average rate of heating temperature was about 5 °C/min. When the setting temperature was reached, the setup remained for 10 minutes, and then the tensile test started.

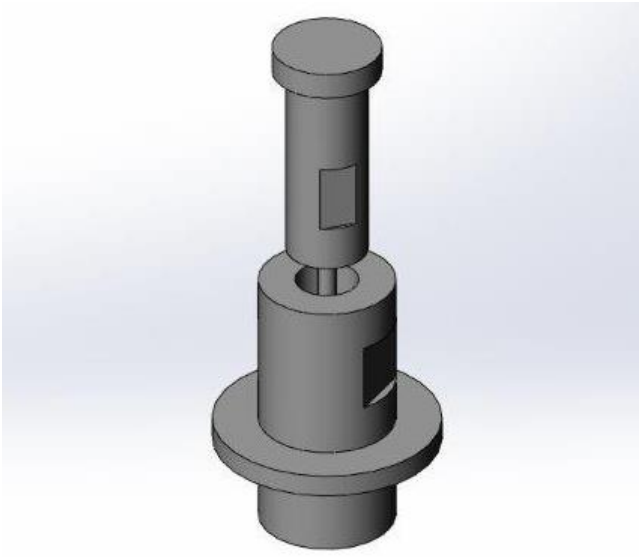

Figure 2.12: Setup of the tensile testing to achieve the tensile tests in liquid LBE environment.

2.3 Tests in controlled oxygen LBE

Let us remember that one of the main purposes of this PhD thesis is to perform mechanical tests in low oxygen LBE. For that, it is necessary to build a purification unit for oxygen removing from LBE.

For the ADS or LFR systems, the main purpose to control oxygen concentration in liquid LBE system is not only to try to form and maintain the protective layers in the surface of the structural materials, but also to prevent lead oxide precipitation. If the dissolved oxygen level reaches above a certain value, it leads to the formation of oxides in the liquid metal LBE, resulting in plugging and degradation of heat transfer. On the other hand, if the oxygen level falls below a certain value, the protective oxide layer on the structure materials dissolves leading to corrosion (dissolution). Hence, the oxygen concentration level should be constantly monitored and kept within a certain range. In a typical operating temperature range of 350-550°C, the upper limit of oxygen concentration in LBE is 5.5×10^{-5} wt%, and the minimum oxygen concentration is 1.0×10^{-8} wt%. When there is sufficient oxygen concentration in LBE, an oxide layer of magnetite begins to form, since the formation free energy of ferrous ferric oxide is lower than those of lead oxide and bismuth oxide (Fig. 2.13). So it is possible to

prevent corrosion of the surface of the structural materials in contact with LBE with the protection of magnetite film (Fe_3O_4). The lowest oxygen limit partial pressure is the dissociation pressure of the oxide Fe_3O_4 in balance with the metal iron. However, when the oxygen partial pressure is too high or even exceeds the saturation oxygen partial pressure then lead oxide (PbO) begins to form and precipitate which will contaminate the coolant alloy and promotes some changes in the properties of the liquid metal serviced in nuclear coolant system [TAN-2009]. During this process the main oxide formed in liquid LBE is lead oxide that is because it is the most stable oxide when compared to other lead oxides and bismuth oxides [HAM-2007].

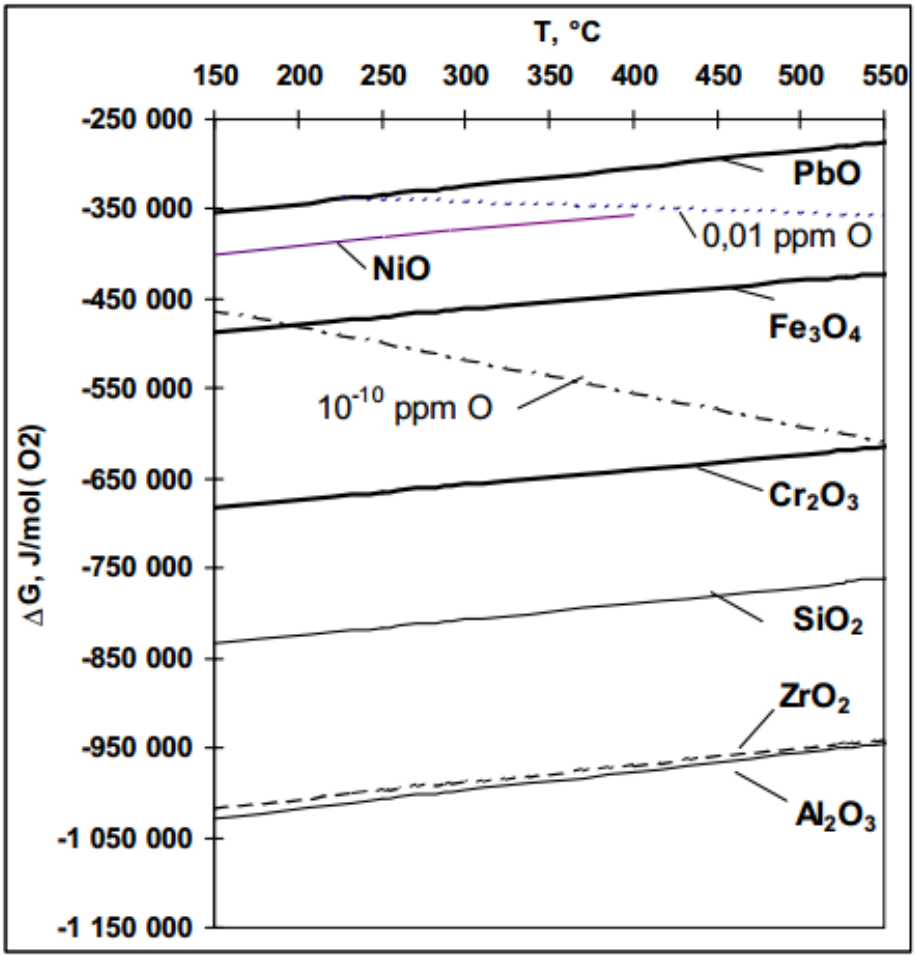

Figure 2.13: Ellingham diagram for lead-bismuth eutectic melt [HAN-2007].

Accurate measurement of the dissolved oxygen concentration in liquid LBE was a critical issue for the active chemistry control in the system. The lower limit of the dissolved oxygen in LBE is defined as the concentration of oxygen required to form Fe_3O_4 protective oxide layer and the upper limit as the saturation level of oxygen at a particular temperature, beyond which the formation of PbO starts. The limits are obtained from the following two reactions,

taking place in liquid LBE.

$$Pb + O \rightleftarrows PbO \quad 2.9$$

$$3Fe + 4O \rightleftarrows Fe_3O_4 \quad 2.10$$

Furthermore, in order to perform mechanical tests (SPT, three-point bending tests, and tensile tests) in liquid low oxygen LBE for the investigation of the mechanical properties and for the study of liquid LBE embrittlement sensitivity of T91 steel, a special equipment had to be designed and validated, which included the liquid LBE purification unit and the controlled atmosphere cell for mechanical tests.

In this section, the setup of LBE purification unit, oxygen measurement in liquid LBE, and the controlled atmosphere cell for mechanical tests system of this PhD thesis are described.

2.3.1 LBE purification unit

2.3.1.1 The setup of LBE purification unit

The setup of LBE purification unit is based on the principle of the chemical reaction between oxygen and hydrogen to produce water at the temperature higher than 500°C (equation 2.11):

$$PbO_{(dissolved)} + H_{2(gas)} \rightleftarrows H_2O + Pb_{(liquid)} \quad 2.11$$

The entire original design drawing of the LBE purification unit is shown in Fig. 2.14a and a photograph in Fig. 2.14b. Basically, the unit comprises:

- a pre-purification tank, tank 1;
- an advanced purification tank 2;
- a connecting pipe between tank 1 and tank 2;
- an oxygen sensor placed in tank 2;
- a connecting pipe between tank 2 and mechanical test cell.

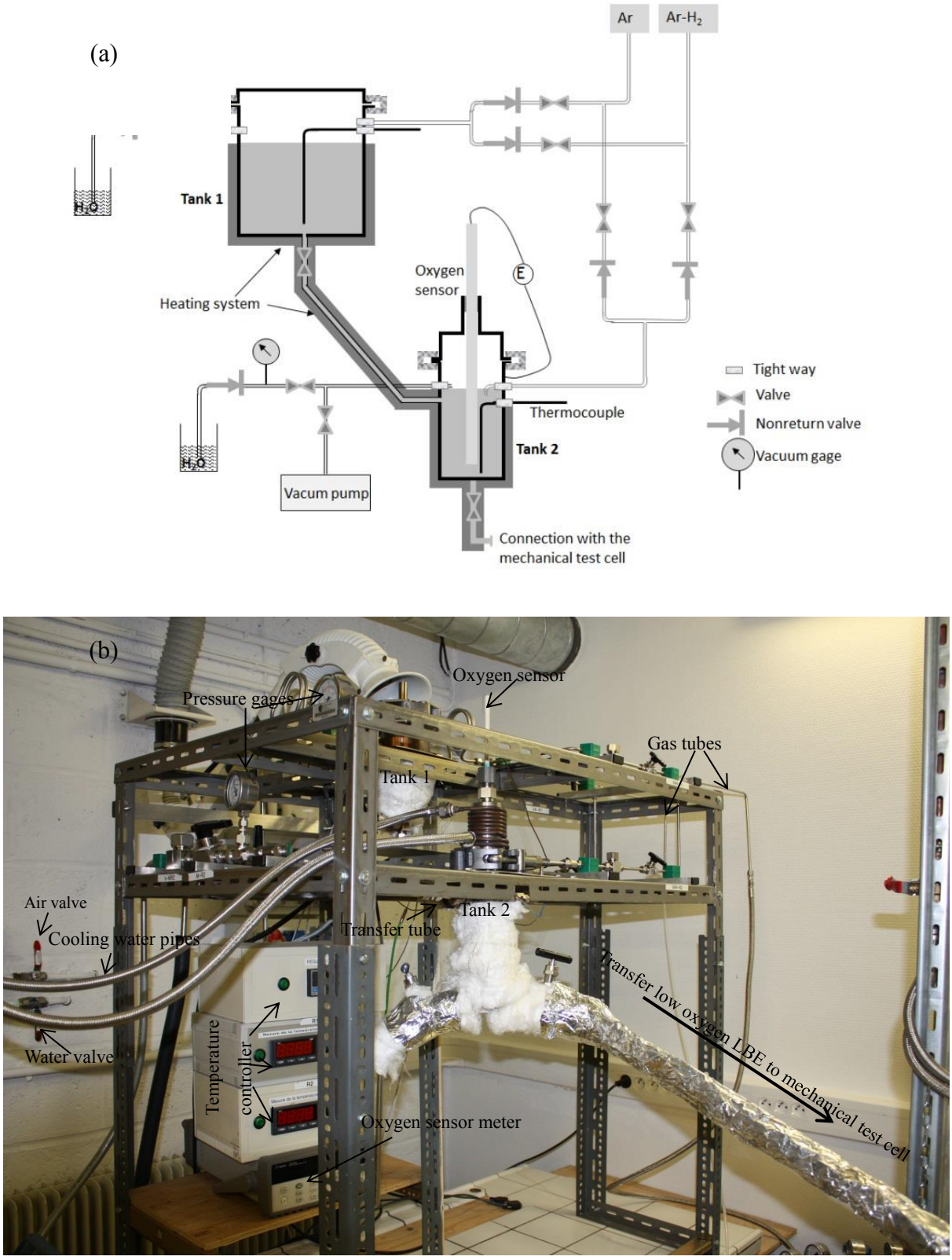

Figure 2.14: Setup of LBE purification unit and oxygen measure control system: (a) is the original design drawing, and (b) is the real photo of the purification system.

The purification unit used two kinds of gasses. One is the pure argon and the other one is the argon/hydrogen gas mixture (96.5% and 3.5% respectively, i.e. Ar-3.5%H_2 in volume ratio).

The latter is the effective agent for the purification of LBE through the chemical reaction at high temperature (between 500°C and 550°C) given by equation 2.11.

This LBE purification unit consisted in flowing the Ar-3.5%H_2 gas mixture through the LBE bath. This is preceded by a pre-purification step. The LBE ingot was molten in an external furnace and transferred in the liquid state to the tank 1 (preheated at 170°C) in which argon prevails. The argon worked as the protective and the preliminary purification atmosphere. The superficial floating oxide layer (PbO) was removed from the LBE surface and argon avoided contamination of the system. Then, the flow of argon is changed for Ar-3.5%H_2 gas mixture flow to start the pre-purification process. The atmosphere flow rate should be not too severe but be controlled at the stable speed of bubbling indicated at the outlet sink. Then tank 1 is heated slowly up to 550°C and maintained for one hour for chemical reaction of oxygen in LBE with the Ar-3.5%H_2 gas mixture. Then the temperature of tank 1 is decreased to 250°C, and while at the same time tank 2 is heated to the same temperature of 250°C. Tank 2 is cleaned, and oxygen is removed with argon sweeping, and purified and vacuuming cycles (turned off argon and pumped the atmosphere ten seconds and repeated this process three times with ten minutes interval). Before the transfer of LBE from tank 1 to tank 2, the tank 2 was prewashed with Ar-3.5%H_2 gas mixture after argon. Once the temperature of the three parts (tank 1 and tank 2, and the connected tube) reached the same (250°C), the pre-purified liquid LBE was transferred from tank 1 to tank 2. Tank 2 was then slowly heated to 510°C for the advanced purification step under Ar-3.5%H_2 gas mixture. The reaction temperature has been chosen taking into account the protection of the oxygen sensor, too high temperature may induce fracture of the sensor. The liquid LBE can rest several hours (2-4 hours) in tank 2 at 510°C until the data of oxygen sensor meter was stable. Then the oxygen content in liquid LBE in tank 2 was measured at 450°C by a BiO/Bi sensor [COU-2004] which is considered as the suitable temperature for oxygen sensor to get an accurate value. Normally, this purification unit can get very low oxygen content in liquid LBE around 10^{-8} wt%. After the second purification process, the qualified liquid LBE can be transferred at 220°C to the controlled atmosphere mechanical tests cell by a tilted heated tube which connects the tank 2 and the mechanical tests cell.

Two pressure gauges are installed in the gas outlet portion connected with the two tanks respectively to indicate the pressure as the safety instructions during the process of purification operation. A sink was put at the end of the gas outlet and the gas tubes were submerged into the water, which can help to observe roughly the atmosphere flow rate. The

atmosphere flow rate should not be too severe but has to be controlled at the stable speed of bubbling indicated at the outlet sink. Each heated part was temperature controlled. Furthermore, in order to measure the liquid metal LBE temperature inside the tanks, there are two additional thermocouples inside the tanks to indicate the actual temperatures of the chemical purification reaction.

Oxygen in LBE was estimated with a sensor plunged in the liquid LBE in tank 2. The oxygen sensor was developed by the CEA (Commissariat à l'énergie atomique et aux energies alternatives), particularly by J-L. Courouau. A collaboration between CEA-Saclay and UMET-Université Lille1 allowed the use of the sensor and a transfer concerning its manufacturing. The next section, which is supported by the Chapter 4 of the handbook on Lead-Bismuth Eutectic Alloy and Lead Properties, Materials Compatibility, Thermal-hydraulics and Technologies, OECD/NEA, 2007 [HAN-2007], explains the working of the sensor. As to the specific shape of the oxygen sensor after operation, it is shown by Fig. 2.15 and is similar to that employed in my PhD thesis.

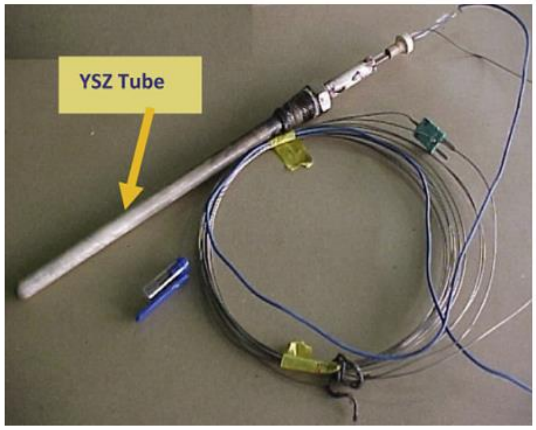

Figure 2.15: Oxygen sensor removed from the loop after operation [BOR-2011].

According to the dimension in the original design drawings (Fig. 2.14a), the maximum volume of the liquid LBE used inside the tanks is about 77 cm^3. Considering the security applications and the volumes of thermocouple and oxygen sensor inside the vessels which are used to measure the liquid metal LBE temperature and the oxygen concentration, it was decided to use 70 cm^3 as the final volume of liquid LBE for the purification system.

2.3.1.2 Oxygen measurement

The oxygen content in liquid LBE has been measured by an oxygen sensor (Fig. 2.16) which consists of a one-end closed Yttria Stabilised Zirconia (YSZ) tube as solid electrolyte with Bi/Bi_2O_3 mixture as reference electrode. The molten LBE alloy, in which the tube is immersed, serves as the other electrode.

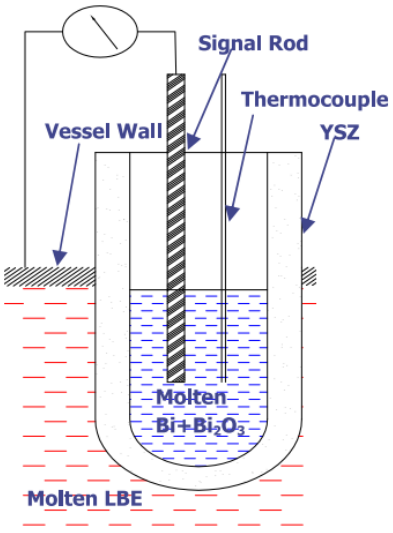

Figure 2.16: YSZ Oxygen sensor [BOR-2011].

The sensor concept is based on the potential measurement method at null current for this galvanic cell built with (1) a solid electrolyte: zirconia doped with yttria, (2) the reference electrode (Bi/Bi_2O_3), (3) the working electrode (LBE/PbO). The yttria-stabilised zirconia (YSZ) ceramic, which conducts specifically oxygen ions, separates two medias showing different oxygen activities: an electromotive force (emf) is then formed across the solid electrolyte. If one of the media is defined to act as a reference (in our case Bi/Bi_2O_3), so as to maintain constant the oxygen partial pressure to a defined value, then the emf is a function of the oxygen activity in the other medium.

Assuming pure ionic conduction in the solid electrolyte, and assuming that all transfers at the various interfaces developed in the electrochemical cell are reversible, the Nernst relation giving the theoretical emf, noted E_{th}, can be written in the form of equation 2.12, with E_{th} in Volts, R the perfect gas constant (8.31441 J/mol/K), F the Faraday constant (96484.6 C/mol), T the temperature (Kelvin), and P_{O_2} the oxygen partial pressure in the lead alloy.

$$E_{\text{th}} = \frac{RT}{4F}\, In\, \frac{P_{\text{O}_2(\text{reference})}}{P_{\text{O}_2}} \qquad 2.12$$

The oxygen partial pressure of the reference, $P_{O_2(\text{reference})}$, is defined by the following reaction:

$$\frac{4}{3}\, Bi + O_2 \rightleftarrows \frac{2}{3}\, Bi_2O_{3\,(\text{solid})} \qquad 2.13$$

Note that all reactions are written so that it corresponds to the consumption of one mole of oxygen. The units of the free enthalpies of formation are then expressed in J/mol of oxygen O_2.

As, the reference is built so as to present a constant oxygen partial pressure, both the metal (Bi) and its oxide (Bi_2O_3) are present in excess to ensure the thermodynamic equilibrium of the reaction. In addition, the liquid solution corresponds to the pure metal (Bi), so that the activities of the reference and its oxide are equal to one and then get the equation 2.14.

$$\text{In}\, P_{O_2\, Bi/Bi_2O_3} = \frac{\Delta_r G^0_{Bi/Bi_2O_3}}{RT} \qquad 2.14$$

In another part, the oxygen partial pressure in the lead alloy melt is given by the thermodynamic equilibrium of lead monoxide, considering that it is the most stable oxide in lead-bismuth eutectic (LBE).

$$2Pb_{(liquid)} + O_{2(gas)} \rightleftarrows\ 2PbO_{(dissolved)} \qquad 2.15$$

In order to calculate the dissolved oxygen concentration, the hypothesis of an ideal solution is often made, and the Henry's law is applied to the dissolved oxygen. Assuming solid lead monoxide as the standard state for the oxygen in lead alloy, the oxygen activity, a_0, shall be equal to unity when saturated is reached [HAN-2007]:

$$a_0 = \frac{C_0}{C_0^*} \qquad 2.16$$

where C_0 is the dissolved oxygen concentration and C_0^* is the saturated oxygen concentration.

Note that the operating specification to avoid any oxide precipitation in the liquid LBE is:

$$a_0 \leq 1 \text{ or } C_0 \leq\ C_0^* \qquad 2.17$$

Concerning the formation of PbO, we can write the equation 2.18:

$$\Delta_r G^0_{PbO} = -\mathrm{RT\ In}\ \frac{a^2_{PbO}}{a^2_{Pb} P_{O_2}} \qquad 2.18$$

and then

$$\mathrm{In}\ P_{O_2} = \frac{\Delta_r G^0_{PbO}}{RT} + 2\ \mathrm{In} \frac{a_0}{a_{Pb}} \qquad 2.19$$

In the case of saturated oxygen concentrations in liquid LBE, the link between the temperature and the oxygen concentration is given for 400°C < *T* < 700°C by [HAN-2007]:

$$\text{LBE: } \mathrm{In}\ C^*_{0(wt\%)} = A - \frac{B}{T_{(K)}} \qquad with\ A = 2.7631\ \ and\ B = 7828.789 \qquad 2.20$$

Lead activity is equal to unity in pure lead solution, and is given by the following Russian relation in LBE solution shown by equation 2.21.

$$\text{LBE: } \mathrm{In}\ a_{Pb} = -\alpha - \frac{\beta}{T_{(K)}} \qquad with\ \alpha = 0.8598\ \ and\ \beta = 135.21 \qquad 2.21$$

The free enthalpies of formation for the various oxides are expressed by the following relation, assuming that all relations are given for the consumption of one mole O_2.

$$\Delta G^0_{(J/mol)} = \Delta H^0 - \Delta S^0 T_{(K)} \qquad 2.22$$

Calculations were made with the help of the HSC database software, which represents a compilation of some of the latest thermodynamic data available. The free energies of formation are linearly regressed on a limited temperature range, 400K-1000K, so as to determine the standards enthalpy and entropy by the least mean squares method. The latter data, standard enthalpy and entropy, are constant over the temperature range (Table 2.4) [HAN-2007].

Table 2.4: Main oxides free enthalpies coefficients for the 400-1000 Kelvin temperature range per mole of oxygen O_2 consumed [HAN-2007].

$\Delta G^0_{(J/mol)} = \Delta H^0 - \Delta S^0 T_{(K)}$	ΔH^0 (J/mol)	ΔS^0 (J/mol)
$4/3\ \mathrm{Bi} + \mathrm{O_2} = 2/3\ \mathrm{Bi_2O_3}$	-389140	-192.6
$2\ \mathrm{Pb} + \mathrm{O_2} = 2\ \mathrm{PbO}$	-437608	-199.1

The relationship for a metal-metal oxide reference (Bi/Bi_2O_3) could then be derived from previous equations (2.12, 2.14 and 2.19), assuming a pure ionic conduction in the solid electrolyte:

$$E_{th} = \frac{\Delta G^0_{Bi/Bi_2O_3} - \Delta G^0_{PbO}}{4F} - \frac{RT}{2F} \ln \frac{a_0}{a_{Pb}} \quad 2.23$$

We define the following constants:

$$a = \frac{\Delta H^0_{Bi/Bi_2O_3} - \Delta H^0_{PbO}}{4F} \quad 2.24$$

$$b = \frac{\Delta S^0_{Bi/Bi_2O_3} - \Delta S^0_{PbO}}{4F} \quad 2.25$$

$$c = -\frac{R}{2F} \quad 2.26$$

These constants allow simplifying the equation 2.23 concerning the LBE as the equation 2.27.

$$E_{th(V)} = (\mathrm{a} + \mathrm{c}\beta) + (\mathrm{b} + \mathrm{c}\alpha) \cdot T_{(K)} + \mathrm{c} \cdot T_{(K)} \cdot \ln a_0 \quad 2.27$$

Hence for saturated oxygen solution, a_0=1, the previous relations depend only on the temperature. The potential is done by the equation 2.28.

$$E^{SAT}_{th(V)} = (\mathrm{a} + \mathrm{c}\beta) + (\mathrm{b} + \mathrm{c}\alpha) \cdot T_{(K)} \quad 2.28$$

We used the concentration of oxygen expressed in wt% to explain the potential by the followed equation:

$$E_{th(V)} = (\mathrm{a} + \mathrm{c}\beta + cB) + (\mathrm{b} + \mathrm{c}\alpha - cA) \cdot T_{(K)} + \mathrm{c} \cdot T_{(K)} \cdot \ln C_{0(wt\%)} \quad 2.29$$

The constants of the Nernst relations can then be calculated, and are reported in Table 2.5 for Bi/Bi_2O_3 reference electrode which is used in my PhD subject for a cell immersed into a lead alloy melt according to the following emf (E) vs temperature (T) and oxygen concentration (C_0) relationships.

$$E_{(mV)} = K_1 + K_2 \cdot T_{(K)} + K_3 \cdot T_{(K)} \cdot \ln C_{0(ppm\,weight)} \qquad \text{for E} > E_{sat} \quad 2.30$$

$$E_{(mV)}^{SAT} = K + K' \cdot T_{(K)} \qquad \text{for E} = \text{E}_{\text{sat}} \qquad 2.31$$

Table 2.5: Theoretical relations for Bi/Bi_2O_3 reference for LBE - *E in mV, P in bar, T in Kelvin, C in ppm (10^{-6} g/g) [HAN-2007].*

LBE	Bi/Bi_2O_3 reference (melting point 271°C)
$E_{sat}(T)$	$E_{(mV)}^{SAT} = 119.8 - 0.0539 \cdot T$
E (T, a_0), E> E_{sat}	$E_{(mV)} = 119.8 - 0.0539 \cdot T - 0.0431 \cdot T \cdot \ln a_0$
E (T, C_0), E> E_{sat}	$E_{(mV)} = -218 + 0.0652 \cdot T - 0.0431 \cdot T \cdot \ln C_{0\,(wt\%)}$ $E_{(mV)} = -218 + 0.462 \cdot T - 0.0431 \cdot T \cdot \ln C_{0\,(ppm)}$
ln a_0 (T, E), E> E_{sat}	$\ln a_0 = -23209 \cdot \frac{E_{(mV)}}{T} + \frac{2780}{T} - 1.251$
ln C_0 (T, E), E> E_{sat}	$\ln C_{0\,(wt\%)} = -23.21 \cdot \frac{E_{(mV)}}{T} - \frac{5049}{T} + 1.512$ $\ln C_{0\,(ppm)} = -23.21 \cdot \frac{E_{(mV)}}{T} - \frac{5049}{T} + 10.723$
ln P_{sat} (T), E= E_{sat}	$\ln P_{O_2}^{SAT} = -\frac{52362}{T} + 25.67$
ln P (T, E), E= E_{sat}	$\ln P_{O_2} = -\frac{46803}{T} - 46.418\frac{E}{T} + 23.16$

These relations enable to plot E vs T (C_0 as parameter) diagram as illustrated in Fig. 2.17, which are most useful for reading sensor output as well as for calibration of sensor. At Fig. 2.17, the oxygen iso-concentration lines are indicated, as well as the PbO saturation and the Fe_3O_4 stability lines for an iron activity of one, the iron oxide being stable below the line. It allows plotting the reading easily and comparing the relative position of the oxygen when compared to the PbO saturation line, defining the lower potential value achievable, which must be avoided to keep clear from the contamination by PbO precipitation. Similarly, other oxide stability threshold can be plotted for direct information on the position of the oxygen potential when compared to the stability of some oxides.

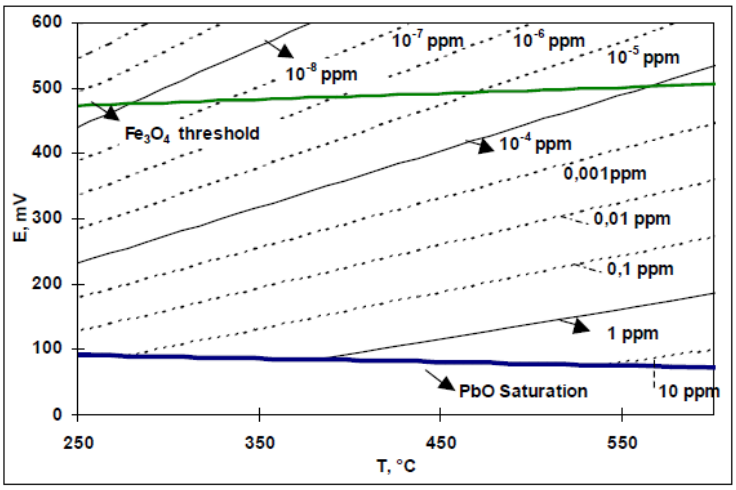

Figure 2.17: Diagram *E* vs. *T* for the oxygen sensor reading in LBE [HAN-2007].

Fig. 2.17 shows the predicted variation of electromotive force (emf) in Volts (V) generated in the oxygen sensor with different temperatures at different oxygen concentrations (wt%) in liquid LBE. If the EMF value of the sensor goes below 0.1 V, then PbO oxide layer formation starts. If EMF goes above 0.45V, the protective oxide layer on the metal surface becomes unstable which may lead to corrosion. For normal operation range (i.e. 300°C-500°C) the concentration of oxygen, 10^{-7} to 10^{-5} wt% is assumed as a safe zone of operation. In terms of emf, it is 0.2-0.4 V which is the safe value for all temperatures.

Because of the electrolyte conduction properties (the ceramic), the influence of the reaction electrode / electrolyte interface (LBE / Zirconia), the cell irreversibility at low oxygen, the theoretical equation can be only considered and it is necessary to calibrate and verify the value done by the oxygen sensor.

The oxygen sensors used in this thesis were calibrated by the CEA. The used equations 2.32, 2.33 were done by the CEA-Saclay (J-L. Courouau) and give the measured tension E (in mV) versus the temperature (in K) according to the oxygen content in LBE: in the case of the saturation (2.32) and if the oxygen content is inferior to the oxygen saturation content (2.33).

$$E_{saturation} = 1000 \times (0.11975905 - 5.389 \times 10^{-5} \times T) \qquad 2.32$$

$$E = 1000 \times (-0.3229 + 2.287 \times 10^{-4} \times T - 4.309 \times 10^{-5} \times TIn(O\%)) \qquad 2.33$$

The tension E corresponds to the difference of potential between the Bi_2O_3 reference electrode and the liquid metal. In practice, we measured the difference between the tank 2 and a conductor cord in contact with the reference electrode.

We verified the oxygen sensor by determination of the values for different temperatures in the case of the oxygen saturation. The result of the verification tested in liquid oxygen saturated is shown in Fig. 2.18, which is similar to that in literature (Fig. 2.17).

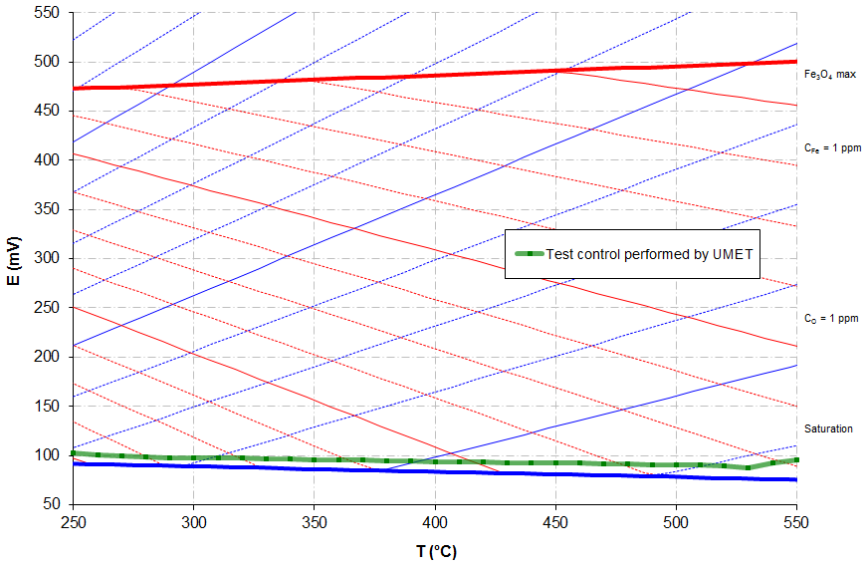

Figure 2.18: Variation of electromotive force E(mV) of the oxygen sensor with temperature in LBE.

2.3.2 Controlled atmosphere of mechanical tests cell

The mechanical tests (SPT, three-point bending tests, and tensile tests) in liquid low oxygen LBE were performed using a tensile electro-mechanical INSTRON which can control the experimental cross-head displacement velocities of 0.5, 0.05, 0.005, 0.0005 mm/min. Furthermore, the mechanical tests setup is installed in the controlled atmosphere cell made of stainless steel to insure the possibility to do tests in the range of temperature 200°C to 450°C under Ar-3.5%H_2 gas mixture. In addition, to protect the purified LBE from oxidation, the cell interior atmosphere was controlled thanks to a purification unit (JACOMEX) in order to remove water vapor and oxygen, which was based on flux sweeping by input Ar-3.5%H_2 gas mixture, and output through on use of reactive filters. The oxygen and the water contents in the cell interior are lowered as low as 0.1 ppm and 5~20 ppm respectively indicated by the atmosphere controller monitor, elimination/purification O_2/H_2O JACOMEX module. Therefore, the increase of the oxygen content in LBE is limited by the very little oxygen content in the mechanical test cell.

2.3.2.1 Setup of purification system and mechanical tests cell

The entire setup of purification system and mechanical experiment test machine included the controlled atmosphere cell is shown by Fig. 2.19. There are three main parts in this setup: the LBE purification unit described in chapter II 2.3.1.1, the atmosphere controller for oxygen and water vapor contents with the help of Ar-3.5%H_2 gas mixture simply described above, and the controlled atmosphere cell for mechanical tests. About the unit of controlled atmosphere mechanical tests cell, the unit is mounted on the tensile electro-mechanical INSTRON machine and it comprises two areas, the compartment part and the mechanical tests zone (Fig. 2.19).

- The compartment part (Fig. 2.19b): it allows us to enter or exit the specimens and various tools for handling the mechanical test in the controlled atmosphere environment without polluting the atmosphere for preparing the mechanical tests in liquid low oxygen LBE or in Ar-3.5%H_2 gas mixture;
- The mechanical tests zone (Figs. 2.19b, 2.19c): This zone is used to mount the specimens and assemble all the fixtures for doing the mechanical tests in the controlled atmosphere environment, including a beaker for storing and heating LBE transferred from the LBE purification unit. The setup with the specimen is installed at the exact loading axis of the INSTRON machine. It comprises a platform and a base plate for laying assembly prepared specimens and for carrying out the mechanical tests (Fig. 2.19c). The upper part of the tests zone is physical linked to the cross-head of the INSTRON machine through a flexible stainless steel which provides a very good sealing between the mechanical machine and the controlled atmosphere cell. The mechanical tests zone is continuously purified by the Ar-3.5%H_2 gas mixture and the atmosphere is controlled. The atmosphere of the mechanical tests zone is connected with the input Ar-3.5%H_2 gas mixture bottle and the output of the oxygen and moisture uptake through a reactor filter which can further help to purify the controlled atmosphere. Normally, in order to do mechanical tests at high temperature, there is a heating ring surround the setup with the specimen and the liquid LBE. The temperature was controlled by a heating thermo controller and a thermocouple. The exact temperature of the mechanical test is given by another thermocouple plunged in the liquid LBE environment. The range of temperature for mechanical tests in this thesis is from room temperature to 450°C.

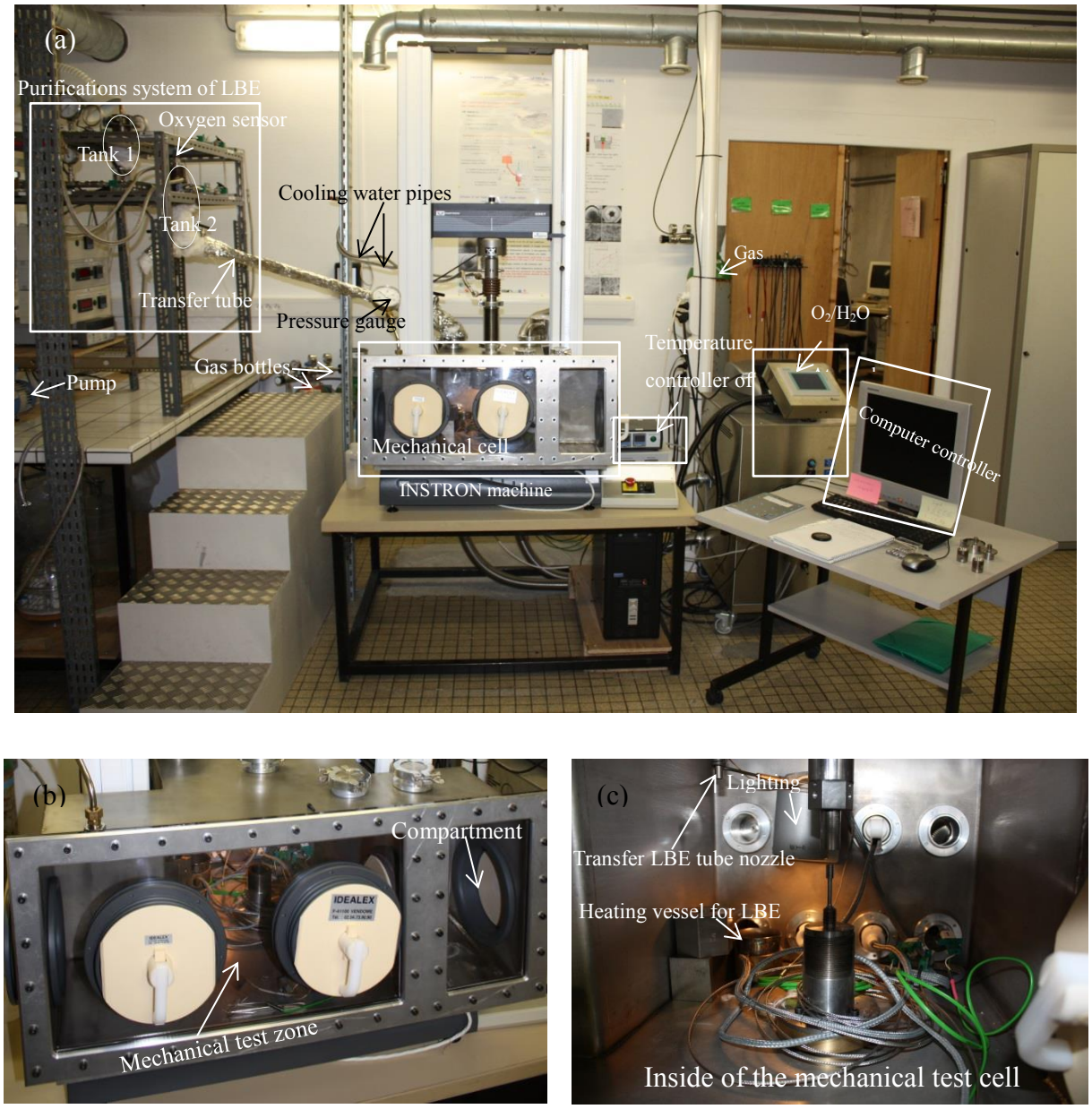

Figure 2.19: Purification system and mechanical experiment test machine.

The manipulation procedures for mechanical tests (SPT, three-point bending tests, and tensile tests) in liquid low oxygen LBE environment depend on the kinds of mechanical tests methods which have been presented in chapter II 2.2. Furthermore, the general procedures to operate the mechanical tests in liquid low oxygen LBE environment with rubber gloves in the controlled atmosphere cell are, firstly, installing the specimen at the very position with its fixtures, secondly, putting the liquid low oxygen LBE (heat LBE to liquid state in the beaker at 170°C) to the special location to create a liquid metal experimental environment, thirdly, heating the specimen to the experimental temperature and keeping the stable test temperature ten minutes then to start the mechanical tests, and finally, once the experiment is finished, stop the heating and cooling in the nature state.

2.3.2.2 Pressure of oxygen and protection of the low oxygen LBE

The session proposed to show that the liquid low oxygen LBE (purified in the purification unit), which has been transferred into the mechanical tests cell, is not oxidized by the residual oxygen, even in weak quantities, present in the environment inside the test cell. For that, it is necessary to calculate the pressure of oxygen in the controlled atmosphere cell to understand the specific purification and protection status to avoid the low oxygen LBE purified is secondary polluted.

The main oxide formed in liquid LBE is lead monoxide (PbO), as it is the most stable oxide when compared to other lead oxides and bismuth oxides [HAN-2007]. The oxygen pressure at the equilibrium Pb-PbO is lower than the oxygen pressure at the equilibrium Bi-Bi_2O_3. Then, under an oxygen pressure, an alloy Pb-Bi is oxidized into PbO. Only the alloys very rich in Bi may be oxidized into Bi_2O_3. Therefore, the reactions between oxygen and the liquid lead-bismuth eutectic (LBE) are shown by equation 2.34.

$$2(Pb)_{liquid} + O_2 \rightarrow 2 < PbO >_{solid}$$
$$\Delta_r G^0(T) = -454456 + 347.27T - 19.031\ T\ \mathrm{In}\ T \qquad 2.34$$

The above expression 2.34 is valid between 600 K (temperature of melting of the lead) and 1145 K (temperature of the monotectic Pb-PbO). In this temperature range, Pb is liquid and PbO is solid. From the phase diagram of the literature, the system Pb-Bi presents an eutectic for 45% lead-55% bismuth with a melting temperature of 125.5°C. Although the equilibrium (Pb)/<PbO> is valid only for a temperature range above 600 K, it is necessary to extrapolate the above expression towards the lower temperature down to 400 K, because the LBE is liquid above that temperature. The oxygen pressure at equilibrium Pb-PbO is given by equation 2.35 for the equilibrium of pure liquid Pb-solid PbO.

$$P_{O_2} = \exp[\Delta_r G^0(T)/RT] \qquad 2.35$$

In the case of LBE, we must take into account the lead activity into the LBE. In first approximation, we can suppose that the liquid solution which is made of very similar metals, as an ideal solution. We keep the hypothesis $a_{Pb} = 0.45$, and work at 200°C-500°C.

So, for the equilibrium of LBE-solid PbO, we consider:

$$P_{O_2} = (1/a_{Pb})\exp[\Delta_r G^0(T)/RT] \quad \text{with } a_{Pb} = 0.45 \qquad 2.36$$

We can evaluate the data of P_{O_2} at different temperatures (200°C-500°C) for the equilibrium Pb/PbO (Table 2.6).

Table 2.6: Data of P_{O_2} at different temperatures at equilibrium Pb/PbO.

T (°C)	200	300	400	500
$P_{O_2}(bar) = (1/a_{Pb})\exp[\Delta_r G^0(T)/RT]$	1.506×10^{-38}	5.567×10^{-30}	5.512×10^{-24}	1.467×10^{-19}

Now, to evaluate the P_{O_2} in the atmosphere of the cell, we make the hypothesis that there is 1 ppm of O_2 (the range of the oxygen content in the controlled atmosphere closed box is inferior to 0.1 ppm in the Ar-3.5%H_2 gas mixture). H_2 with O_2 gives H_2O following the reaction equation 2.37.

$$2H_2 + O_2 \rightarrow 2H_2O \text{ (gas)} \qquad 2.37$$

$\Delta_r G$ of the reaction 2.37 is given by equation 2.38.

$$\Delta_r G(T) = -489486 + 56.79T - 6.875\,T \ln T = -RT \ln K \qquad 2.38$$

The oxygen pressure in the atmosphere is given by equations 2.39 with $P_{H_2} = 0.035$ (bar) and P_{H_2O}=2×10^{-6} (bar).

$$P_{O_2} = \frac{P_{H_2O}^2}{P_{H_2}^2 \cdot K} \qquad 2.39$$

In fact, if we accept that the initial concentration of oxygen in the initial atmosphere (Ar-3.5%H_2) is 1×10^{-6} bar (1 ppm) and is fully transformed in H_2O, the equilibrium concentration of H_2O into the atmosphere will be 2×10^{-6} bar. So we can calculate the O_2 pressure in the atmosphere (Table 2.7).

Table 2.7: Data of P_{O_2} at different temperatures in the atmosphere.

T (°C)	400	500
K	2.303×10^{37}	3.144×10^{32}
$P_{O_2}(bar) = (P_{H_2O}/P_{H_2})^2/K$	1.476×10^{-46}	1.039×10^{-41}

The oxygen pressure in the atmosphere is less important than the oxygen pressure at equilibrium PbO/Pb-Bi eutectic (indicated by Table 2.6 and Table 2.7). Thus, the atmosphere (Ar-3.5%H_2) of our mechanical cell does not oxidize the Pb-Bi eutectic alloy.

In conclusion, the liquid low oxygen LBE, obtained with the purification unit is not oxidized by the residual atmosphere of the mechanical cell. Therefore, we validated the mechanical cell to perform mechanical tests in low oxygen LBE.

CHAPTER III : INVESTIGATION OF THE SENSITIVITY TO LBE EMBRITTLEMENT OF T91 STEEL BY SPT

This chapter aims at investigating the factors that influence the mechanical behaviour and the fracture mechanism of T91 steel in liquid LBE. For that, Small Punch Tests (SPT) technology is employed not only in liquid oxygen saturated LBE but also in liquid low oxygen LBE. Tests were performed at 130°C, 200°C, 250°C, 300°C, 400°C and at cross-head velocities of 0.5, 0.05, 0.005 and 0.0005 mm/min. Since the mechanical behaviour of T91 steel is strongly influenced by the tempering temperature, the fracture resistance in LBE of the T91 steel after the standard heat treatment (tempering temperature T=750°C) and after tempering at 500°C which considerably hardened the steel has been investigated.

3.1 Small Punch Tests (SPT) performed in LBE to investigate the sensitivity to embrittlement of T91 steel

In this chapter, the factors which can promote the sensitivity to LBE embrittlement of T91 steel are investigated by Small Punch Tests (SPT). The small punch test was repeated at least three times in the same condition. The research will take into account the displacement velocity, the test temperature, the heat treatment of the steel and will be guided through the role of oxygen in liquid LBE. The results will be discussed on the bases of the SPT curves and on SEM observations.

For this part of the study, SPT were carried out in liquid LBE (oxygen saturated / low oxygen) bath at five different temperatures (130°C, 200°C, 250°C, 300°C, 400°C) with different cross-head displacement velocities (0.5, 0.05, 0.005, 0.0005 mm/min). Tests were also done in air at room temperature (RT) and at 200°C, 250°C, 300°C and 400°C for comparison. In addition, since the factors considered in this thesis on the liquid LBE embrittlement sensitivity of T91 steel are relatively complex, a reference standard is selected in order to better compare the experimental results for analysis. This reference standard is the response of TR750 steel (after standard heat treatment) tested in liquid oxygen saturated LBE at 300°C with a cross-head velocity of 0.5 mm/min.

3.1.1 Small Punch Tests in liquid oxygen saturated LBE

Small punch tests were carried out in oxygen saturated LBE. The characterization of the standard reference, the effects of the test temperature and the displacement velocity will be presented in this section.

3.1.1.1 Characterization of the standard reference

The preliminary small punch tests were performed on material TR750 steel in air at room temperature and in air at 300°C with the velocity of 0.5 mm/min to clearly identify the reference standard.

Normally, according to previous research (see chapter I) the material TR750 steel is expected to exhibit the ductile performance with SPT at a conventional velocity of 0.5 mm/min in air at

room temperature or in air at high temperature (for example at 300°C), and even at 300°C in liquid oxygen saturated LBE.

In the present investigation in air, at RT and at 300°C, the fractured specimen presents a dome with large plastic deformation marks and a lot of small circular cracks. Furthermore, fractographic observation indicates that lots of dimples, typical of ductile fracture cover the fracture surface, as shown in Fig. 3.1a. However, at the same conventional velocity (0.5 mm/min) but in liquid oxygen saturated LBE environment at 300°C, the SPT specimen has the main crack also circular but cracking occurred at the entire circumference as shown in Fig. 3.1b which is not the case of the material TR750 SPT tested in air. It is interesting to note that around the circular crack there are several radial cracks extended outside (Fig. 3.1b).

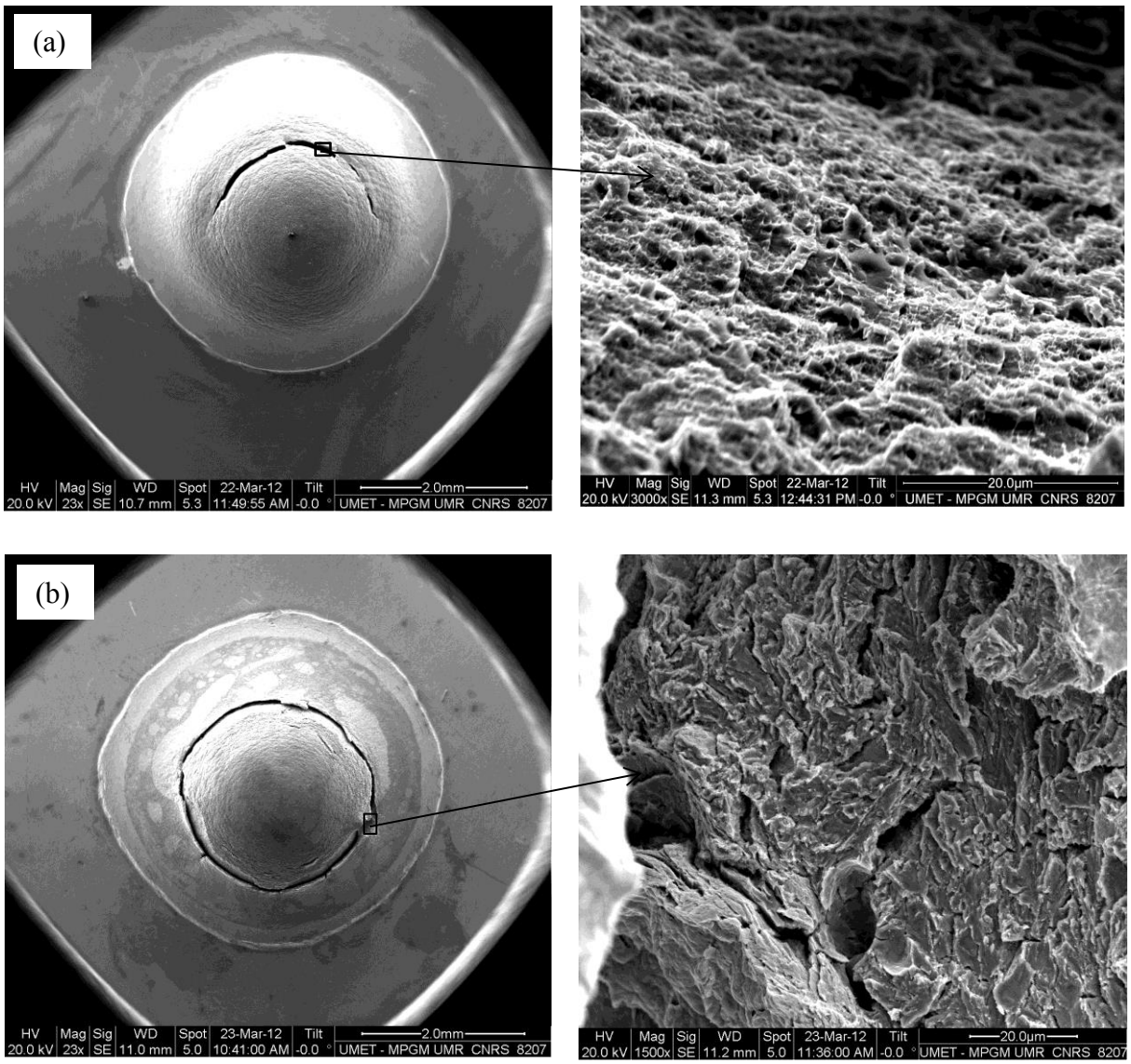

Figure 3.1: SEM images of TR750 SPT specimens tested at a velocity of 0.5 mm/min: (a) in air at room temperature, (b) in liquid oxygen saturated LBE at 300°C.

The fracture characteristic of the crack is complicated and it is not easy to define if this kind of fracture is completely brittle or completely ductile. It is mixed and it changed with the place of the crack. The brittle crack characteristic was found at the outside edge of the circle crack, a brittle cleavage type fracture was in a dominant position at this condition (Fig. 3.1b). The results obtained in the present thesis differ from the literature (see chapter I). Indeed, though T91 steel was investigated in its standard heat treatment, the observed morphology of the SPT specimen did not consist of a semi-circular crack as it was the case in previous investigation. Moreover, the fracture surface was not fully ductile.

Anyway, the SPT curves of TR750 steel exhibited all the same shape with the typical SPT four stages associated with a ductile behaviour as presented in chapter II whether tested in air or in liquid oxygen saturated LBE at the conventional velocity of 0.5 mm/min recorded for the different conditions (see Fig. 3.2). However, both the maximum load F_{max} and the displacement value at the maximum load d_{Fmax} are reduced by increasing the test temperature from RT to 300°C. At 300°C, the same remark holds when the SPT is performed in liquid oxygen saturated LBE instead of in air. However, no significant change in the SPT yield load can be noticed (Fig. 3.2 and Table 3.1).

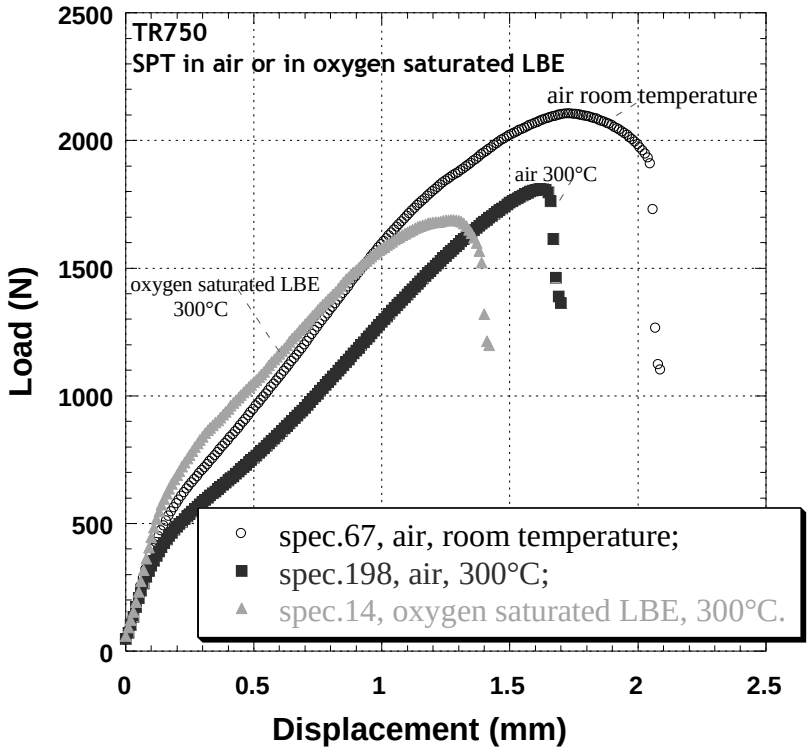

Figure 3.2: SPT curves of TR750 tested in air at room temperature, in air at 300°C, and in liquid oxygen saturated LBE at 300°C (0.5 mm/min).

Table 3.1: Values of key points measured in the SPT of TR750 tested at room temperature and at 300°C in air, and at 300°C in oxygen saturated LBE, and the test velocity employed is 0.5 mm/min.

SPT conditions	Air/RT (spec.67)	Air/300°C (spec.198)	Oxygen saturated LBE/300°C (spec.14)
F_e (N)	425	423	446
d_{Fe} (mm)	0.12	0.17	0.11
F_{max} (N)	2103	1810	1689
d_{Fmax} (mm)	1.73	1.64	1.29

3.1.1.2 Effect of test temperature

The effect of test temperature was investigated in a temperature range from 200°C to 400°C at a velocity of 0.5 mm/min in air and in oxygen saturated LBE.

The SPT curves of TR750 specimens tested at high temperature (200°C, 250°C, 300°C, 400°C) in air exhibit the large ductile plastic deformation with the typical SPT four stages characteristics shown in Fig. 3.3a. The change in the mechanical properties of TR750 tested in air, such as the maximum load (F_{max}), is not obvious at the test temperature higher than 250°C (250°C, 300°C, 400°C), while F_{max} reaches the maximum value at 200°C. Furthermore, at this test condition, the value of the displacement at the maximum load, d_{Fmax}, is not sensitive to the test temperature, and all the specimens exhibit the similar value of d_{Fmax} (Fig. 3.3a, Table 3.2). The fractured specimen presents a semi-circular fracture with a dome accompanied by large plastic deformation marks, and furthermore, this typical ductile fracture is confirmed by the fractographic observation, that is the presence of lots of big dimples on the fracture surface as shown in Fig. 3.4a.

In addition, the SPT curves of TR750 tested in oxygen saturated LBE also exhibited the typical SPT four stages associated with a ductile behaviour. However, the effect of the test temperature on TR750 in oxygen saturated LBE differs from that in air as shown in Fig. 3.3. There is an obvious temperature sensitivity for TR750 specimens tested at a velocity of 0.5 mm/min in oxygen saturated LBE indicated by the information of SPT curves (Fig. 3.3b). Both the values of the maximum load (F_{max}) and the displacement at the maximum load (d_{Fmax}) are decreased gradually when the test temperature increases from 200°C to 400°C, and F_{max} reaches the minimum value at 400°C (Fig. 3.3b, Table 3.2).

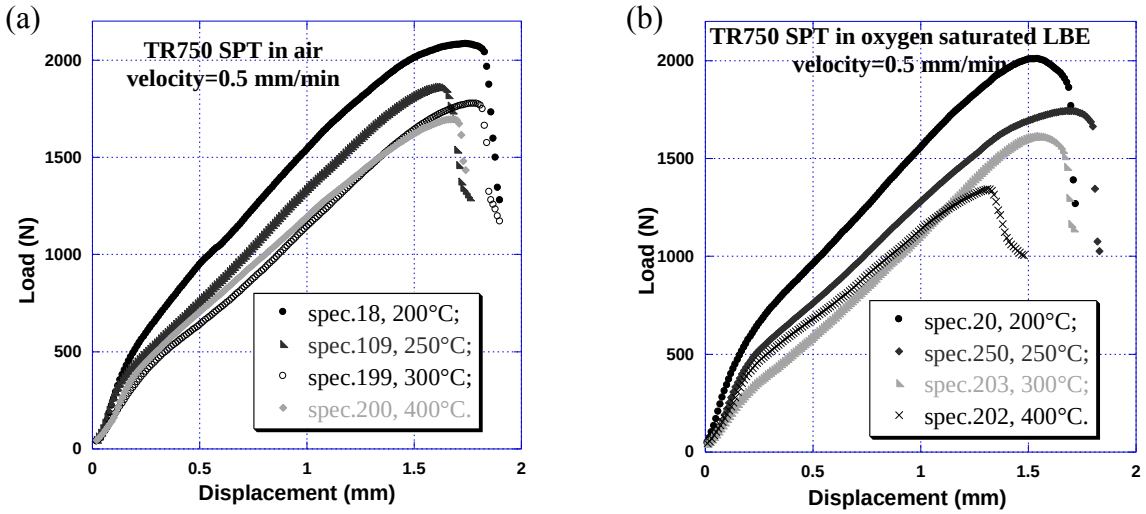

Figure 3.3: SPT curves of TR750 tested with a velocity of 0.5 mm/min at four different temperatures (200°C, 250°C, 300°C, 400°C): (a) in air, and (b) in liquid oxygen saturated LBE.

Table 3.2: Values of key points measured in the SPT of TR750 tested in air and in oxygen saturated LBE at four different temperatures (200°C, 250°C, 300°C, 400°C) and the test velocity employed is 0.5 mm/min.

SPT conditions		F_e (N)	d_{Fe} (mm)	F_{max} (N)	d_{Fmax} (mm)
Air	200°C (spec.18)	428	0.16	2083	1.74
	250°C (spec.109)	353	0.13	1864	1.61
	300°C (spec.199)	328	0.19	1777	1.76
	400°C (spec.200)	383	0.19	1696	1.67
Oxygen saturated LBE	200°C (spec.20)	448	0.13	2008	1.53
	250°C (spec.250)	398	0.17	1743	1.68
	300°C (spec.203)	285	0.18	1614	1.55
	400°C (spec.202)	371	0.19	1344	1.32

The reduction in mechanical properties of TR750 is obvious when the test temperature is higher than 300°C (300°C, 400°C) in comparison with air experimental condition. Indeed, this kind of temperature sensitivity for TR750 tested in oxygen saturated LBE with a velocity of 0.5 mm/min even starts at 200°C. However, no significant change in the SPT yield load for TR750 can be noticed at both experimental conditions in air and in oxygen saturated LBE with a velocity of 0.5 mm/min (Table 3.2). At 200°C, the fractured specimen tested in oxygen saturated LBE presents a rough circular fracture but not the ductile semi-circular one. Furthermore, the fractographic observation indicates that the fracture surface is the not

classical ductile feature instead of the big dimples shown in Fig. 3.4b.

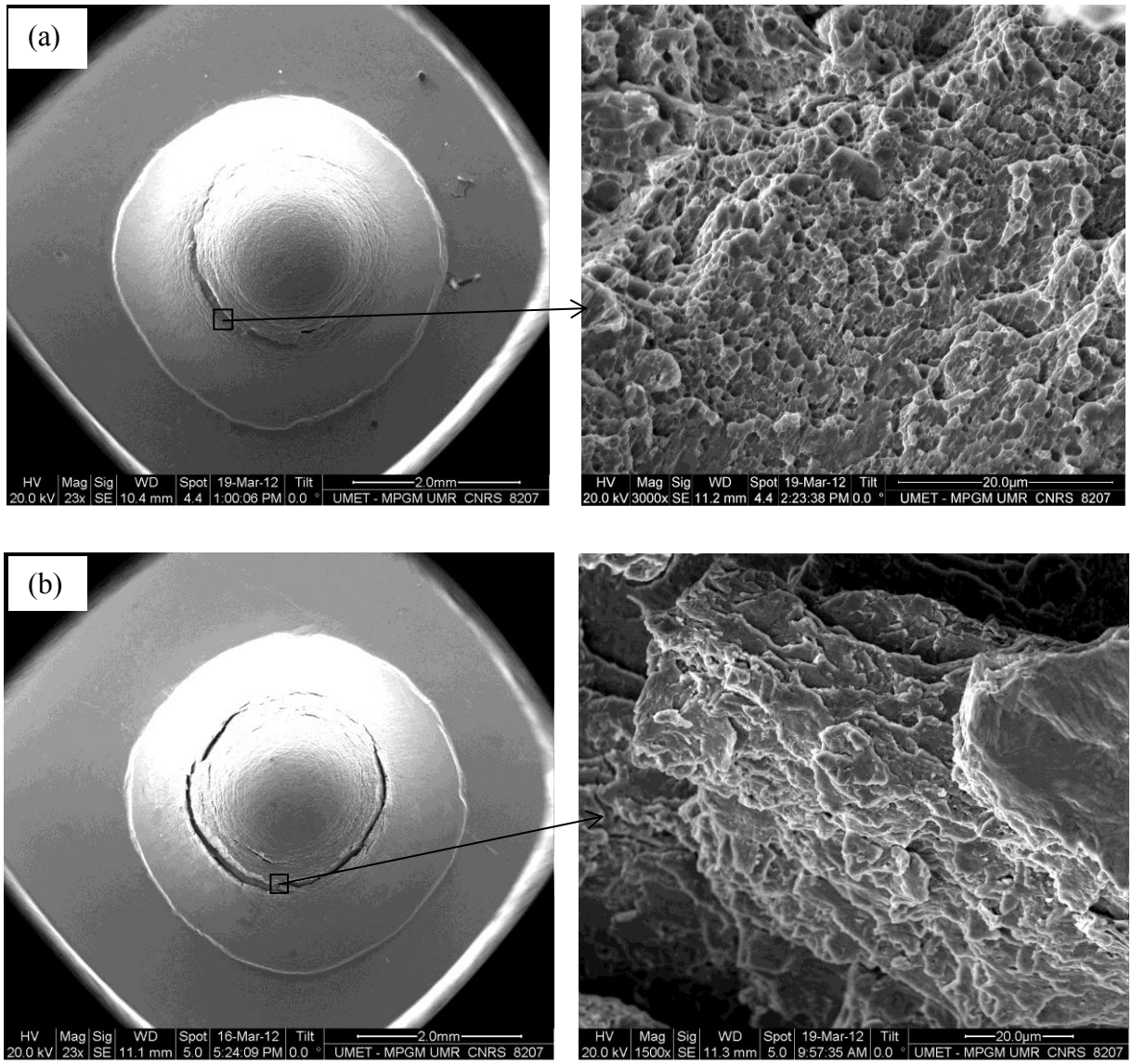

Figure 3.4: SEM images of TR750 SPT specimens tested at a velocity of 0.5 mm/min: (a) in air at 200°C, (b) in liquid oxygen saturated LBE at 200°C.

The failure features of the specimens tested in oxygen saturated LBE with a velocity of 0.5 mm/min at 250°C and 200°C are similar. But at 300°C and 400°C, the presence of the brittle characteristic was discovered at the edge of the circular fracture described prior in 3.1.1.1.

3.1.1.3 Effect of displacement velocity

The SPT behaviour in liquid oxygen saturated LBE of the material TR750 steel has been investigated first by decreasing the cross-head velocity by a factor of 10, i.e. at 0.05, 0.005, 0.0005 mm/min at three different temperatures (250°C, 300°C, 400°C) in liquid oxygen

saturated LBE.

Figs. 3.5a to 3.5c present the punched specimens of TR750 respectively at 250°C, 300°C and 400°C, all at a cross-head speed of 0.05 mm/min. In Figs. 3.5a, 3.5b, 3.5c, the shapes of the cracks are circular and cracking occurred at the entire circumference except at 400°C where the specimen contained a small ligament. Several radial cracks extended outside from the main circular crack. They were more obviously visible at 300°C and 400°C than at 250°C. For all the specimens tested in liquid oxygen saturated LBE at the temperature range from 250°C to 400°C, the fracture surfaces contain ductile and brittle zones depending on the location. The ductile characteristic fracture locates normally at the inside of the circular fracture, toward the centre of the fractured specimen. Brittle fracture is found normally at the outside edge of the circular crack especially a brittle cleavage type of fracture was in a dominant position.

The load-displacement SPT curves of TR750 steel show that all the specimens' curves shown in Fig. 3.6 comprise the four stages typical of a ductile response. But for the specimen tested at 300°C the load is higher than the other two curves (250°C, 400°C) until fracture failure. The SPT performed at 400°C strongly differs from the two other ones. The mechanical properties were changed as indicated by the reduction in the values of both the maximum load and the displacement value at the maximum load, while its stretching of the membrane in the third stage remained coincident state with 250°C until separation at the fourth stage. In addition, there is still no significant change in the SPT yield load tested in liquid oxygen saturated LBE with a slow velocity of 0.05 mm/min at three temperatures 250°C, 300°C, 400°C. From the comparative analysis of the specimens SPT at 300°C in liquid oxygen saturated LBE but with different velocities (0.5, 0.05 mm/min) shown in Fig. 3.1b and Fig. 3.5b, it is found that the material TR750 steel seems much more sensitive to LBE embrittlement at the slow velocity of 0.05 mm/min experimental condition indicated by the much longer of the radial crack than that of rapid conventional velocity of 0.5 mm/min.

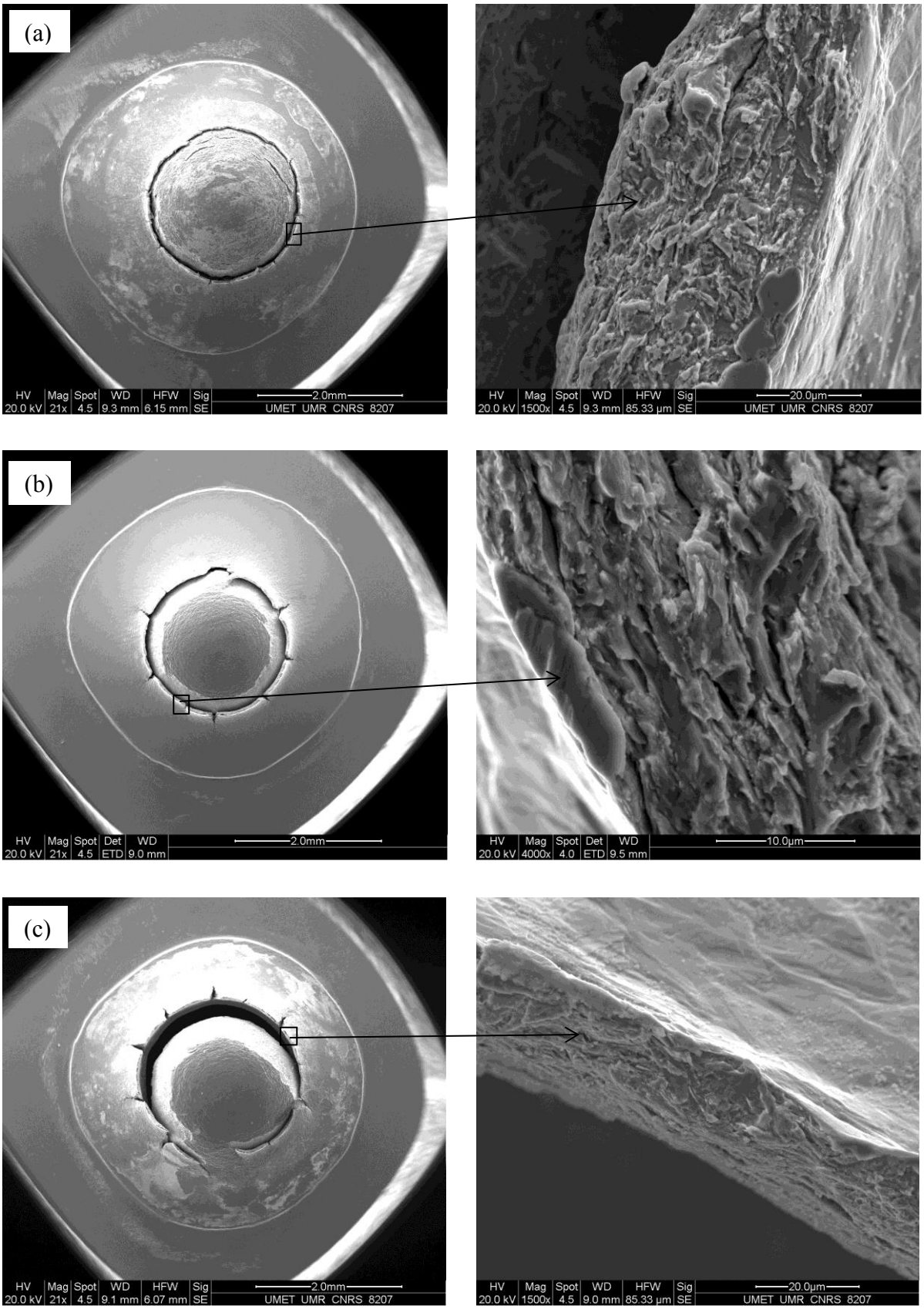

Figure 3.5: SEM images of TR750 tested in liquid oxygen saturated LBE specimens with a velocity of 0.05 mm/min: (a) 250°C, (b) 300°C, (c) 400°C.

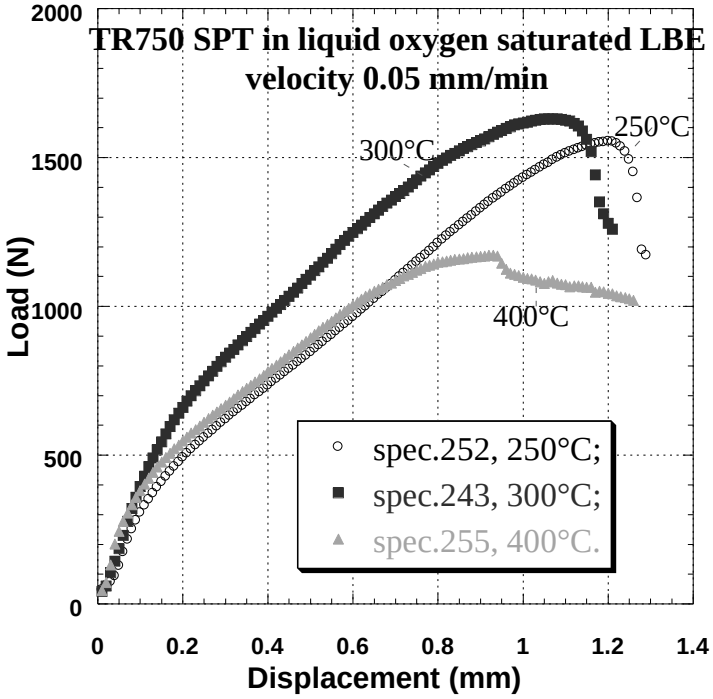

Figure 3.6: SPT curves of TR750 corresponding to the three different temperature conditions.

Therefore, the role of the velocity was realized as an important factor on the LBE embrittlement sensitivity of TR750 steel. It was therefore decided to decrease the cross-head velocity, i.e. to perform SPT at 0.005 and 0.0005 mm/min at three different temperatures 250°C, 300°C, 400°C. The results are shown in Figs. 3.7, 3.8, 3.9, 3.10 for the tests performed at a velocity of 0.005 mm/min and 0.0005 mm/min respectively.

An entire circular crack accompanied with radial cracks is observed on the fractured specimen for the SPT performed in liquid oxygen saturated LBE with a velocity of 0.005 mm/min at 250°C and 300°C. At 400°C, the circular crack is not entire and contains a small ligament. The SPT curves are similar and in total coincidence when SPT were done at 250°C and 300°C. The curve of the SPT performed at 400°C coincides with the two other ones for a large part of the test but both the maximum load and the displacement at the maximum load were reduced. At 250°C and 300°C, the brittle cleavage crack characteristic was found at the edge of the circular crack but not for 400°C as shown in Figs. 3.7a, 3.7b, and 3.7c. At 400°C, the edge of crack has the ductile characteristic but not brittle cleavage.

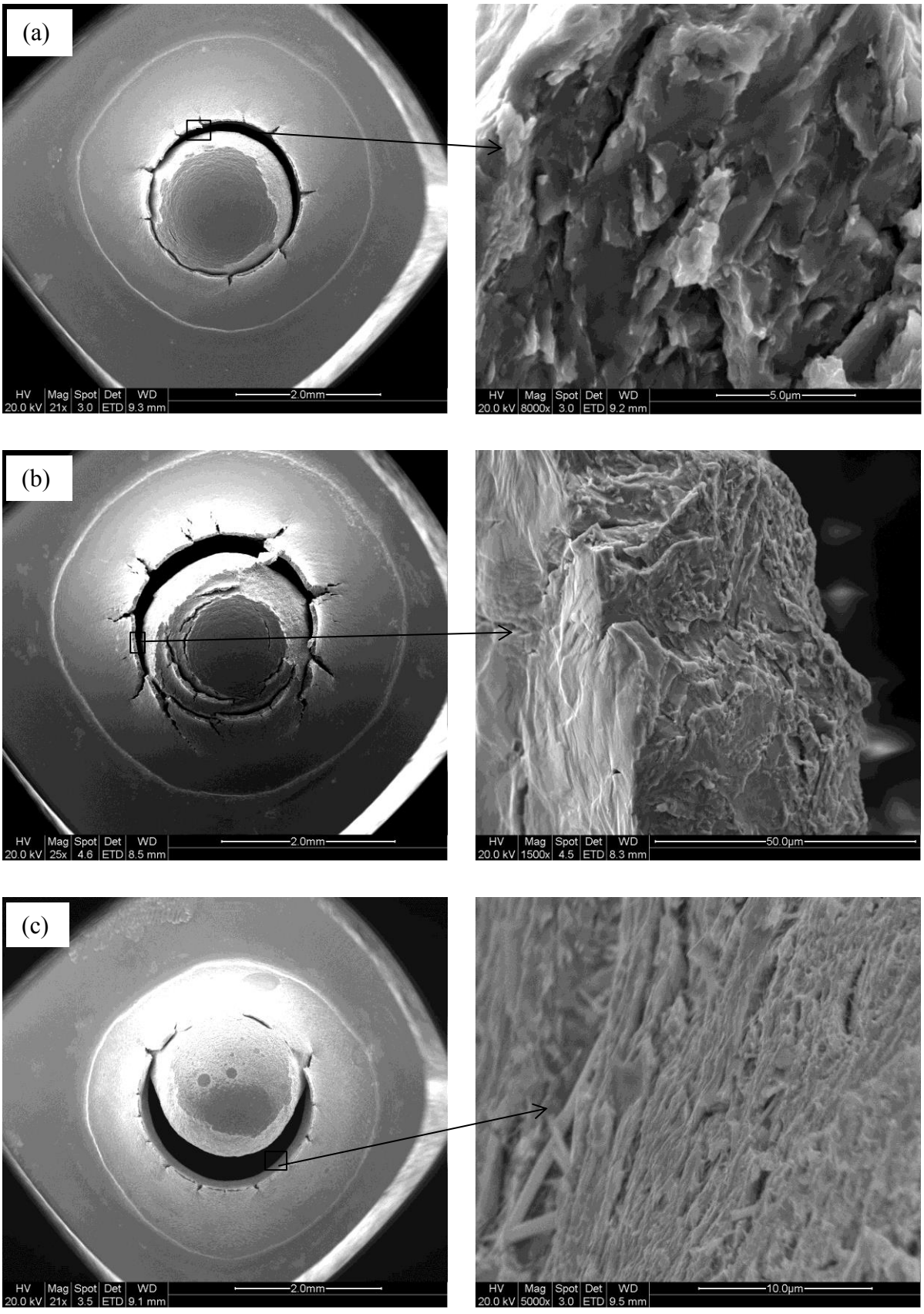

(d)

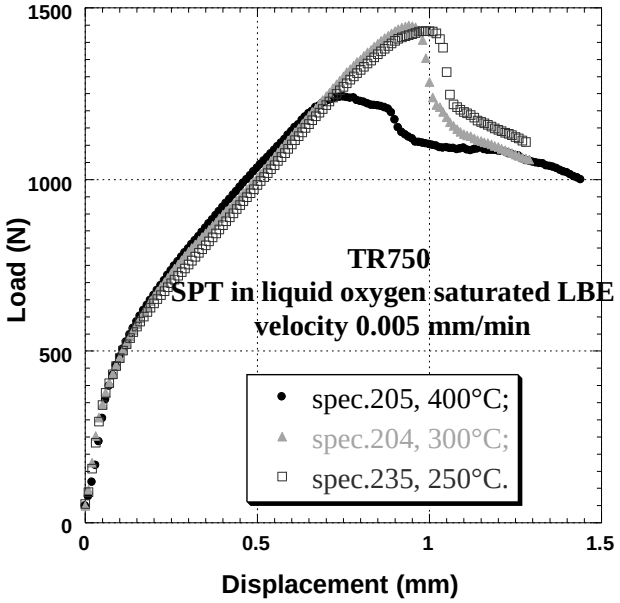

Figure 3.7: SEM images of TR750 tested in liquid oxygen saturated LBE specimens with a velocity of 0.005 mm/min: (a) 250°C, (b) 300°C, (c) 400°C, and (d) SPT curves of TR750 corresponding to the three different temperature conditions.

The results from the lowest velocity test (0.0005 mm/min) are similar to that of the velocity of 0.005 mm/min tests in liquid oxygen saturated LBE at 250°C and 400°C (Figs. 3.10a, 3.10b), including the morphology of the specimens and its SPT curves. However, at 300°C, TR750 deformed in liquid oxygen saturated LBE at 0.0005 mm/min exhibited an odd behaviour (Fig. 3.8). Not only the values of the maximum load and the displacement at maximum load are decreased with the velocity reduction but also the yield load is changed obviously. The yield loads of three lower velocities curves (0.05, 0.005, 0.0005 mm/min) are higher than that of rapid conventional velocity curve (0.5 mm/min). Moreover, the two lower velocities (0.05, 0.005 mm/min) curves share the same yield load values. But the curve related to the test carried out at 0.0005 mm/min is featuring two peculiar points. The first one is that the difference between the yield load and the maximum load value is very small for the test conducted at the lowest velocity (0.0005 mm/min) in comparison with the tests performed at the other three velocities (0.5, 0.05, 0.005 mm/min). The second point is the presence of a sudden drop at a displacement of about 0.25 mm but this is not very pronounced.

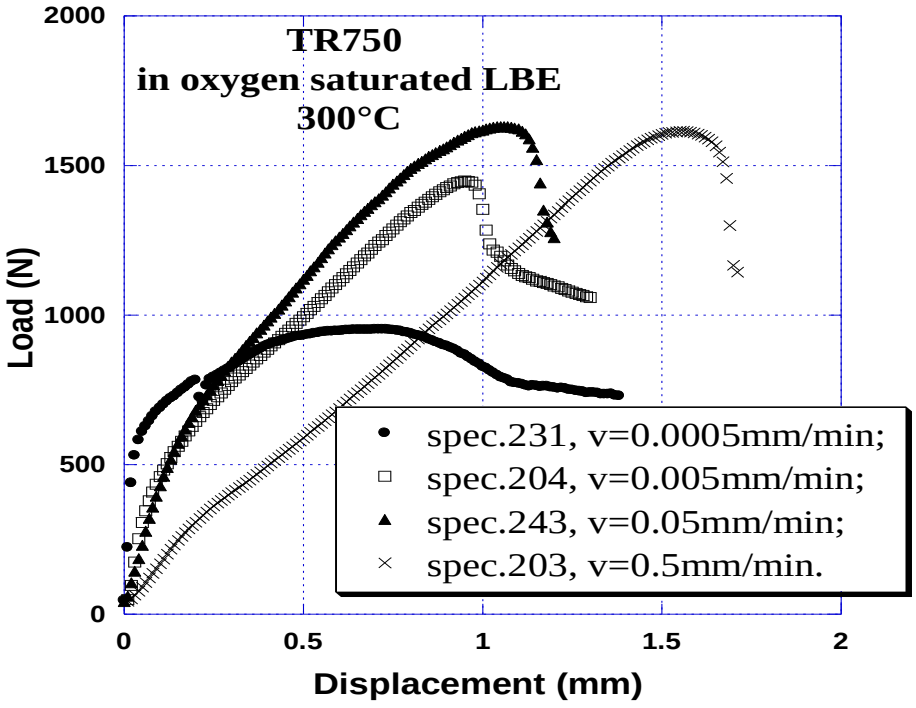

Figure 3.8: TR750 specimens tested in liquid oxygen saturated LBE at 300°C: SPT curves at four different velocities (0.5, 0.05, 0.005, 0.0005 mm/min).

Furthermore, for this test, the material TR750 steel presented several signs of very brittleness. Indeed, for the SPT carried out at 0.0005 mm/min in liquid oxygen saturated LBE condition at 300°C, the number of the radial cracks initiated from the main circular crack is smaller, six radial cracks, but much longer, than that at the same temperature tested with the relatively rapid velocities as shown in Figs. 3.1b, 3.5b, 3.7b, 3.9. In addition, cleavage was observed on the fracture surface of the circular crack (Fig. 3.9). At 300°C, SPT in liquid oxygen saturated LBE environment at 0.0005 mm/min resulted in an abrupt change in the morphology of the cracked specimen. Moreover, the thickness of the brittle surface of the specimen was maximum for the lowest velocity of 0.0005 mm/min.

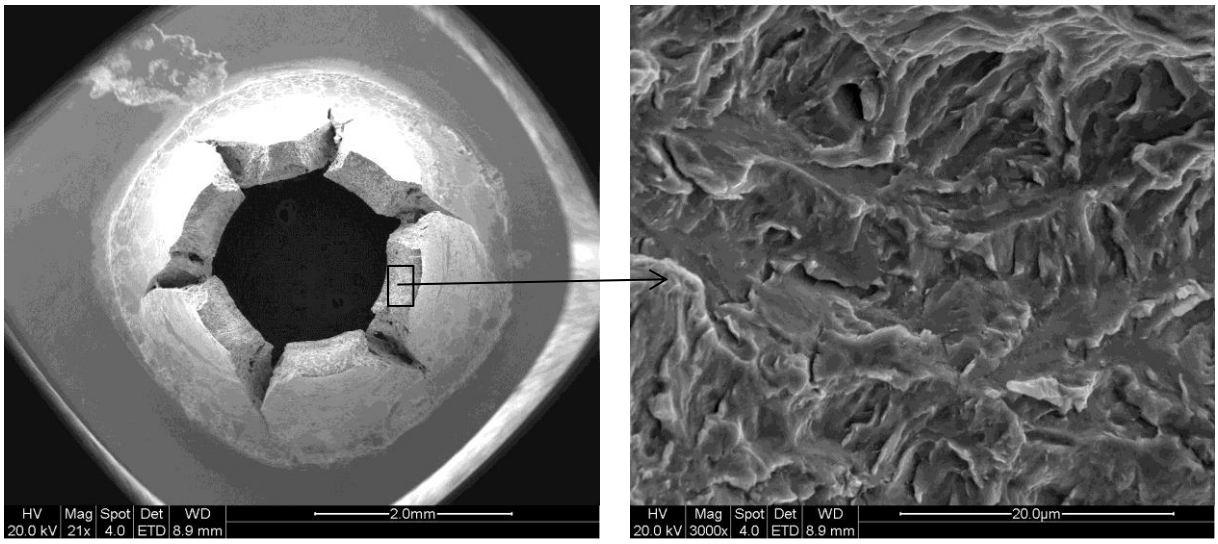

Figure 3.9: TR750 specimens tested in liquid oxygen saturated LBE at 300°C: SEM images of the specimen tested at the lowest velocity of 0.0005 mm/min.

This analysis concluded that the characteristic of the totally ductile material TR750 was changed by liquid oxygen saturated LBE tested at 300°C with the lowest velocity of 0.0005 mm/min, the failure was accelerated (indicated by the reduction in the values of both the maximum load and the displacement at maximum load) and presence of the brittle cleavage with a large area on the fracture surface.

However, the sensitivity to liquid oxygen saturated LBE embrittlement through the velocity parameter was not pointed out at 250°C and 400°C. The SPT curves are not significantly modified by changing the velocity experimental conditions (0.05, 0.005, 0.0005 mm/min) shown in Figs. 3.10a and 3.10b. Moreover at 400°C in liquid oxygen saturated LBE, the mechanical property can be recovered at the lowest velocity of 0.0005 mm/min. The values of both the maximum load and the displacement at the maximum load back approach to those for the initial state tested at the conventional velocity of 0.5 mm/min and its crack surface is the ductile characteristic.

According to the investigation above, the conclusion is that the velocity plays an important role in the fracture mechanism of the material TR750 steel fractured by small punch tests. The temperature 300°C is the sensitive liquid LBE embrittlement experimental temperature, which is helpful for planning next step experiments.

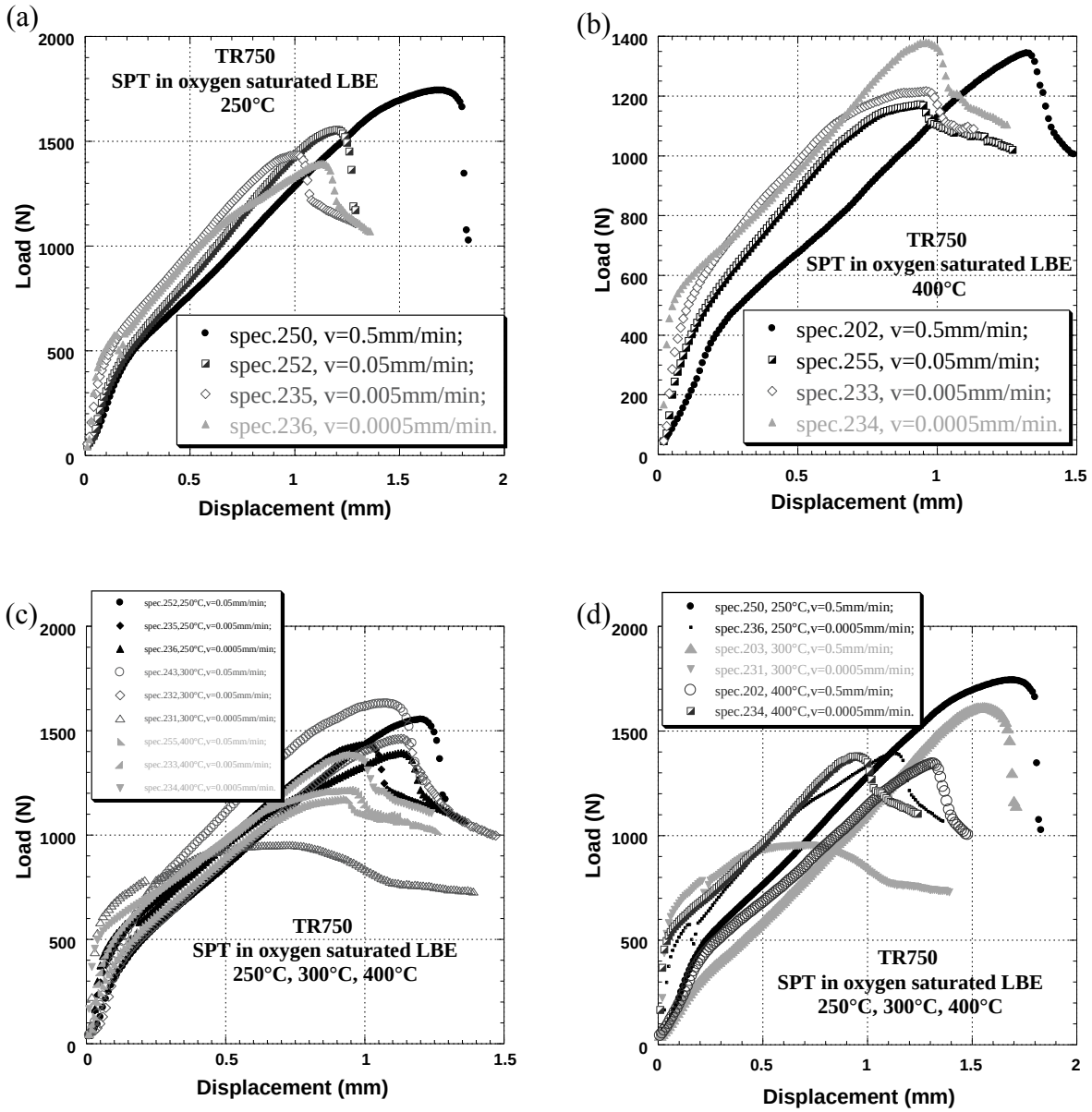

Figure 3.10: SPT curves of TR750 steel tested in liquid oxygen saturated LBE at different temperatures and different velocities: (a) at 250°C with four velocities (0.5, 0.05, 0.005, 0.0005 mm/min); (b) at 400°C with four velocities (0.5, 0.05, 0.005, 0.0005 mm/min); (c) at 250°C, 300°C, 400°C with three velocities (0.05, 0.005, 0.0005 mm/min); (d) at 250°C, 300°C, 400°C with two velocities (0.05, 0.0005 mm/min).

3.1.2 Mechanical response in air and in Ar-3.5%H_2 gas mixture of TR750 material evidenced by SPT

Because the oxygen removed from LBE and the cleaning of the test cell was achieved by using a mixture of argon and hydrogen, it was decided to confirm that the gas mixture did not play any effect on the mechanical response of the T91 steel. Therefore, SPT at 300°C and at

400°C in air and in Ar-3.5%H_2 gas mixture (Fig. 3.11) were performed.

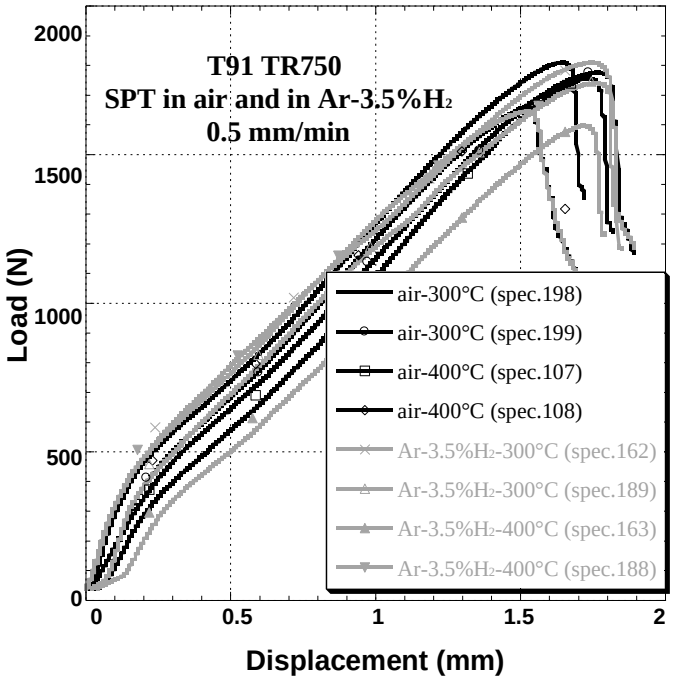

Figure 3.11: Load-displacement SPT curves of the TR750 material tested in air and in Ar-3.5%H_2 gas mixture, at 300 °C and 400°C, at 0.5 mm/min.

In the two environments, the SPT curves show the ductile behaviour of the TR750 material which was confirmed by the observation of a dome with a large plastic deformation traces of the specimen, of a circular crack, and of the presence of dimples only on the fracture surfaces. The curves for tests in air and in Ar-3.5%H_2 differ slightly, for instance in the maximum load value or in the value of displacement at maximum load but the deviation are within the classical scattering of the SPT technique. So, no effect of Ar-3.5%H_2 gas mixture was observed. This result also showed that the presence of hydrogen in the protective gas mixture in the testing cell had no effect on the mechanical response of the TR750 material.

3.1.3 Small Punch Tests in low oxygen LBE

The aim of this thesis part is to point out the role of the oxygen content in liquid LBE on the LBE embrittlement sensitivity of the material TR750. In addition, the other factors likely to promote the embrittlement sensitivity of the material TR750 steel in liquid low oxygen LBE were also studied. Again, we started the SPT in liquid low oxygen LBE with the standard velocity (0.5 mm/min) in a temperature range from 200°C to 400°C (Fig. 3.12).

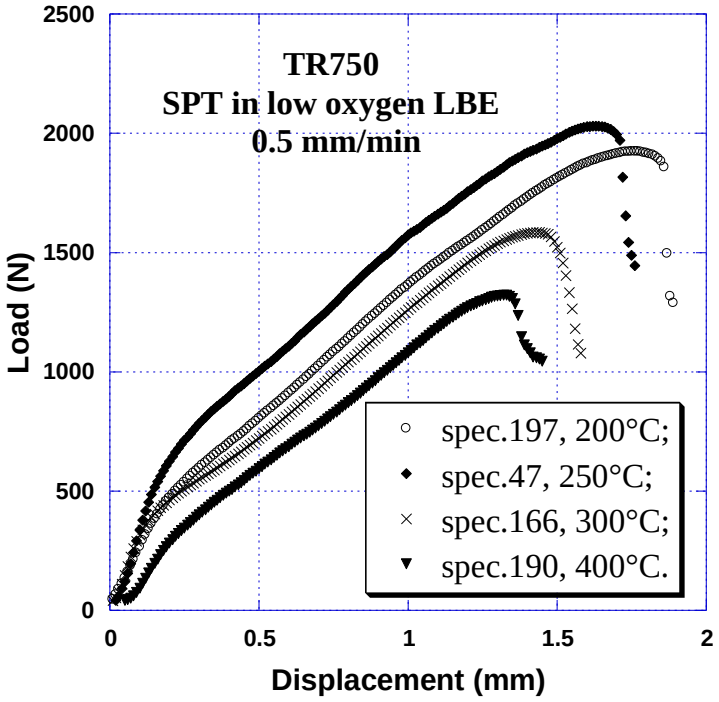

Figure 3.12: SPT curves of TR750 specimens tested in liquid low oxygen LBE with a velocity of 0.5 mm/min at four test temperatures (200℃, 250℃, 300℃, and 400℃).

The analysis of the curves indicates that the temperature effect is visible from the loss of mechanical properties of the material TR750 steel, including the reduction in the values of both the maximum load and the displacement at the maximum load, especially when the temperature is higher than 250°C. For all the studied temperatures (200°C, 250°C, 300°C, 400°C) SPT in low oxygen LBE and with a rapid conventional velocity of 0.5 mm/min, the curves suggest a typical ductile behaviour of the material TR750 with the presence of 4 primary stages as it occurred for tests in oxygen saturated LBE.

When the present results are compared with those obtained in liquid oxygen saturated LBE (Fig. 3.13), it seems that the oxygen content in LBE does not play an obvious influence on the characteristics of the SPT curves at the rapid conventional velocity condition (0.5 mm/min).

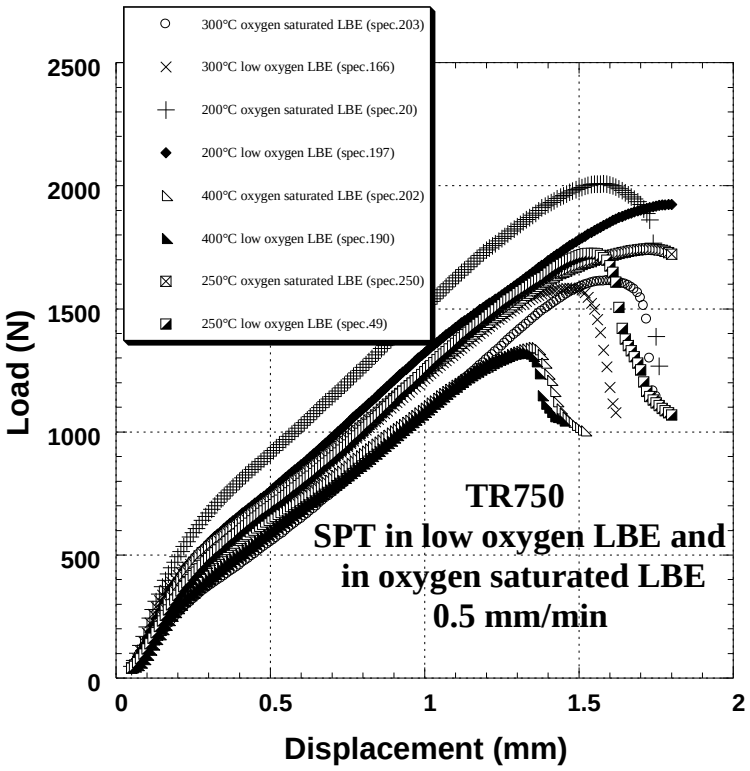

Figure 3.13: SPT curves of TR750 specimens tested at 200℃, 250°C, 300℃, and 400℃ in low oxygen LBE and in oxygen saturated LBE tested with a velocity of 0.5 mm/min.

A main circular crack with radial cracks has been found as after test in low oxygen LBE, but unlike the reference standard (SPT at 300°C in oxygen saturated LBE of TR750), the circular crack was entire without any ligament (Fig. 3.14a). Moreover the brittle cleavage crack characteristic also appeared at the outside edge of the circular crack shown in Fig. 3.14b.

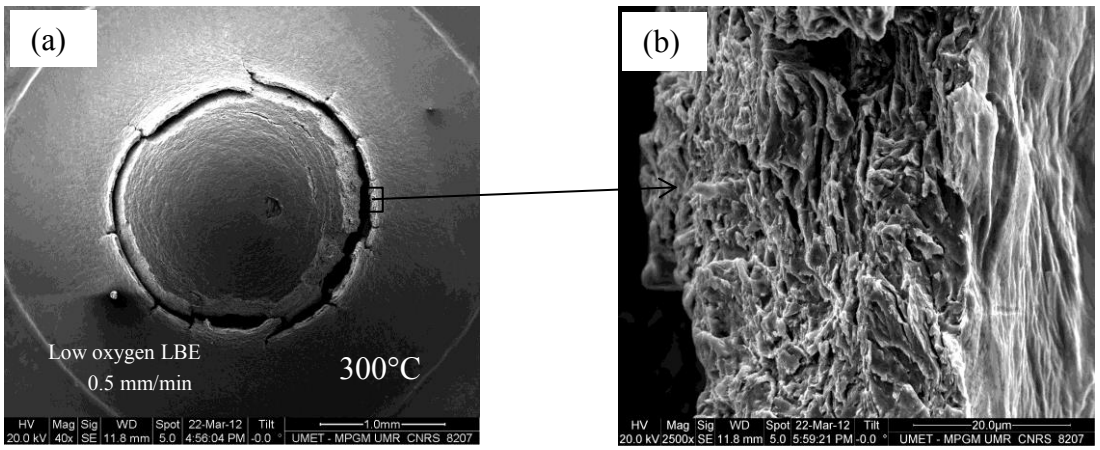

Figure 3.14: SEM images of TR750 SPT specimen tested in liquid low oxygen LBE with a velocity of 0.5 mm/min at 300°C: (a) overview of the specimen, and (b) partial enlarged SEM image corresponding to (a).

For a standard velocity, 0.5 mm/min, the effect of environment and temperature is

summarized in Table 3.3 and Fig. 3.15 by using the normalized fracture energy parameter.

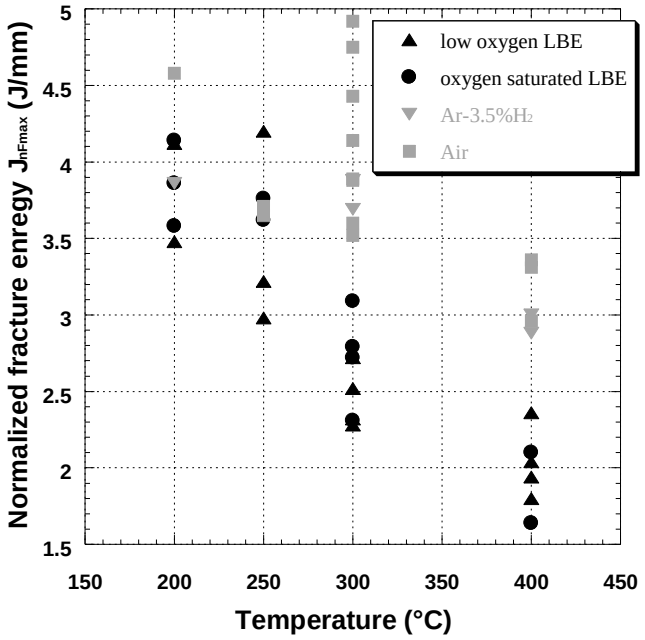

Figure 3.15: Normalized fracture energy J_{nFmax} of TR750 at F_{max} according to the temperature and to the environment (SPT with velocity 0.5 mm/min).

Table 3.3: Normalized fracture energy J_{nFmax} (J/mm) of TR750 at F_{max} with velocity 0.5 mm/min.

Experimental conditions	Air	Ar-3.5%H_2	oxygen saturated LBE	low oxygen LBE
200°C	4.58	3.86	3.86±0.28	3.80±0.32
250°C	3.68±0.03	/	3.69±0.07	3.47±0.73
300°C	4.14±0.56	3.79±0.13	2.73±0.32	2.46±0.2
400°C	3.21±0.22	2.94±0.08	1.87±0.33	2.04±0.24

At low temperature (200°C and 250°C), taking into account the scattering, the environment did not affect the fracture energy. But at 300°C and at 400°C, the normalized fracture energy is reduced in LBE whatever the oxygen content in comparison with tests in Ar-3.5%H_2 gas mixture or in air by about a factor of 0.66 (Table 3.3). This result suggests an effect of the liquid metal on the behaviour of the T91 steel at these temperatures.

So, as a whole, no clear effect of oxygen content in LBE appeared during the SPT at a velocity of 0.5 mm/min except a higher degree of ductility in the SPT in oxygen saturated LBE indicated by the presence of a ligament.

Thus, the small decrease of the fracture energy in presence of the LBE is in good connection

with the formation of radial cracks and the very localized brittle fracture which are the sign of earlier damage by LBE. This effect depends on the temperature at the considered cross-head velocity of 0.5 mm/min but does not depend on the oxygen content in LBE.

Therefore, for the same reason presented in the investigation for oxygen saturated LBE embrittlement effects on the material TR750 steel and based on the experimental results inspiration, another slightly slow velocity of 0.05 mm/min was chosen to do SPT in low oxygen LBE at three different temperatures (250°C, 300°C, 400°C).

The results are shown in Fig. 3.16.

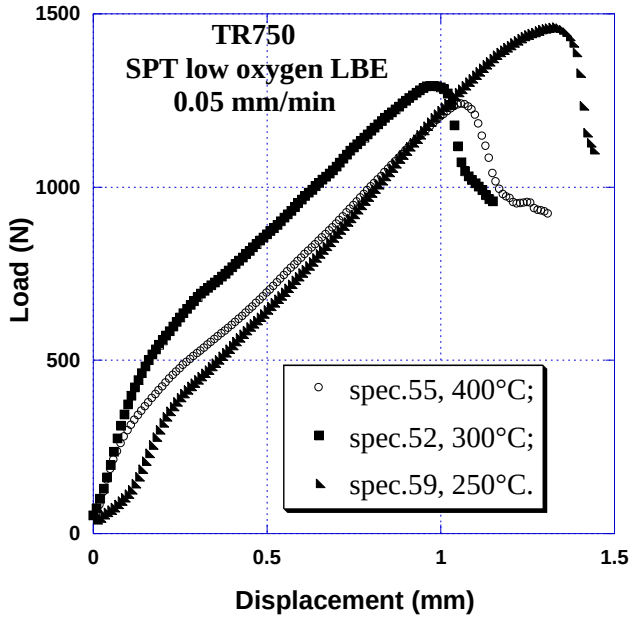

Figure 3.16: SPT curves of TR750 tested in liquid low oxygen LBE with velocity 0.05 mm/min at three different temperature experimental conditions (250°C, 300°C and 400°C).

The load-displacement curves of TR750 steel tested in low oxygen LBE still experience the typical SPT four stages ductile deformation at the slow velocity of 0.05 mm/min. According to the experimental environment, only a weak evolution of the mechanical behaviour can be noted which differs by some typical values measured from the curves such as the maximum load F_{max} and the normalized fracture energy at the maximum load J_{nFmax}. The curve of the specimen tested with the velocity of 0.05 mm/min at 250°C has much higher maximum load value than that at 300°C and 400°C. As compared with tests in oxygen saturated LBE condition, the collapse of mechanical resistance occurred at lowest test temperature in low oxygen LBE. But as a whole, no obvious effect of oxygen content on the mechanical

properties of TR750 steel SPT is really pointed out with the velocity of 0.05 mm/min.

The effect of velocity was carefully investigated at 300°C in liquid low oxygen LBE by reducing the velocity step by step until the brittle failure effect clearly appeared.

The SPT curves of Fig. 3.17 also show that the values of maximum load and the displacement at maximum load decreased step by step when the velocity was decreased gradually, while the yield loads increased a little bit but not enough to be considered as an efficient indicator. However, the curve related to the test performed at a velocity of 0.0005 mm/min exhibits two sudden drops (at 0.2 mm and 0.8 mm).

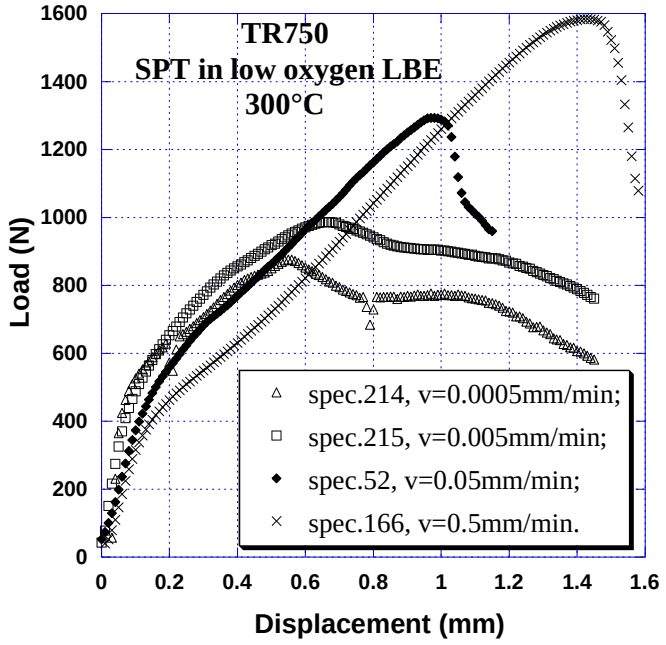

Figure 3.17: SPT curves of TR750 small punch tests in liquid low oxygen LBE at 300°C with four different velocities (0.5, 0.05, 0.005, 0.0005 mm/min).

SEM observations on the fractured surface characteristic of TR750 SPT specimens tested in low oxygen LBE at 300°C at different velocities (0.5, 0.05, 0.005, 0.0005 mm/min) show a ductile to brittle transition. The mixed ductile and brittle fracture was found for the TR750 specimens tested in low oxygen LBE with a velocity of 0.5, and of 0.05 mm/min. The ductile area normally appeared inside the circular fracture toward the center of the specimen, while the brittle fracture preferred located at the outside edge of the circular fracture as shown in Figs. 3.18a, 3.18b.

Furthermore, an interesting thing found is that the brittle intergranular fractures and

transgranular fractures have appeared clearly on the fractured specimens' surfaces tested at 300℃ with the lower velocity (0.005, 0.0005 mm/min) (Figs. 3.18c, 3.18d), and the flower star shape brittle feature becomes much more prominent with the decreasing of the velocity based on the observation of SEM images shown by Figs. 3.18abcd.

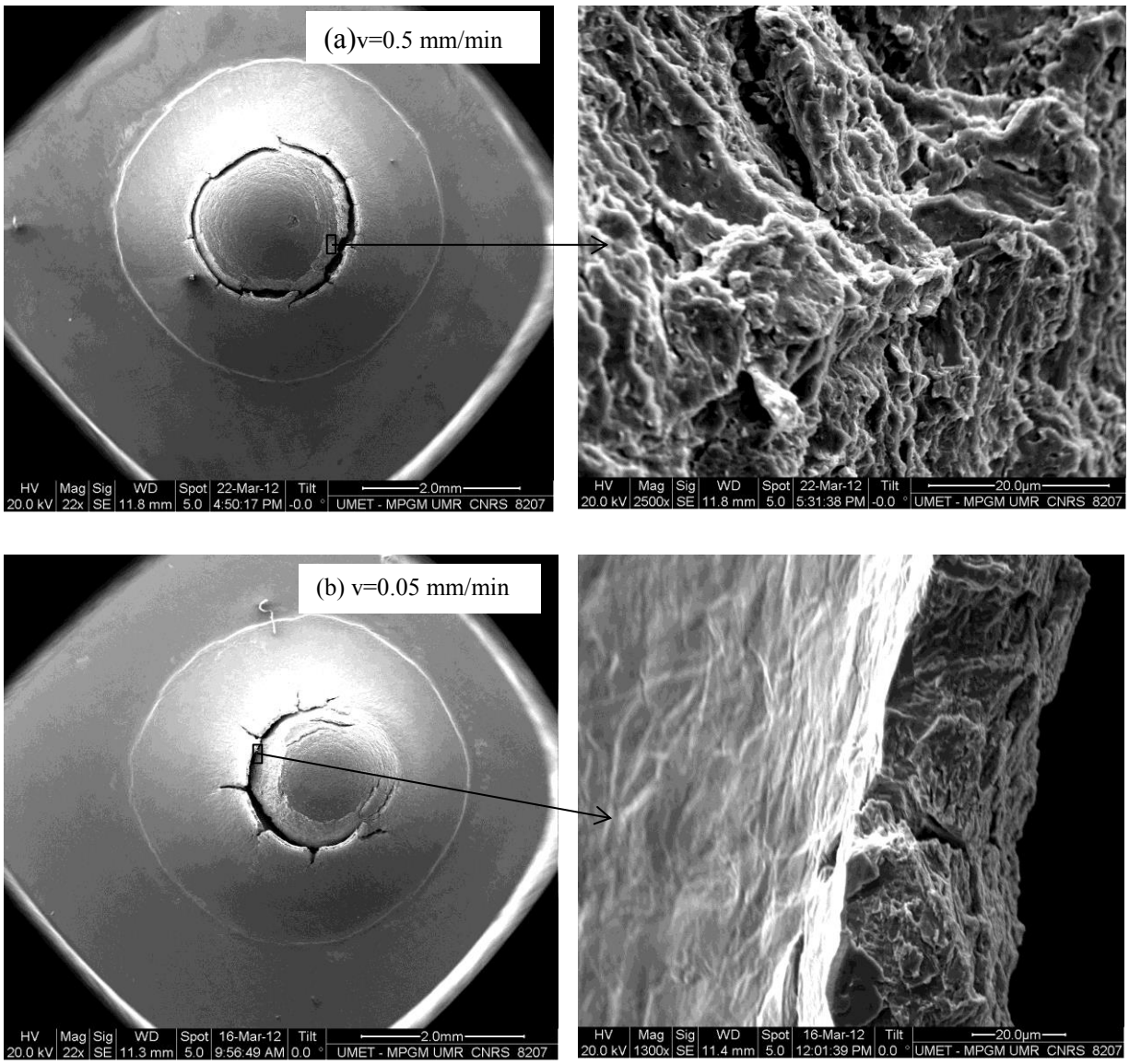

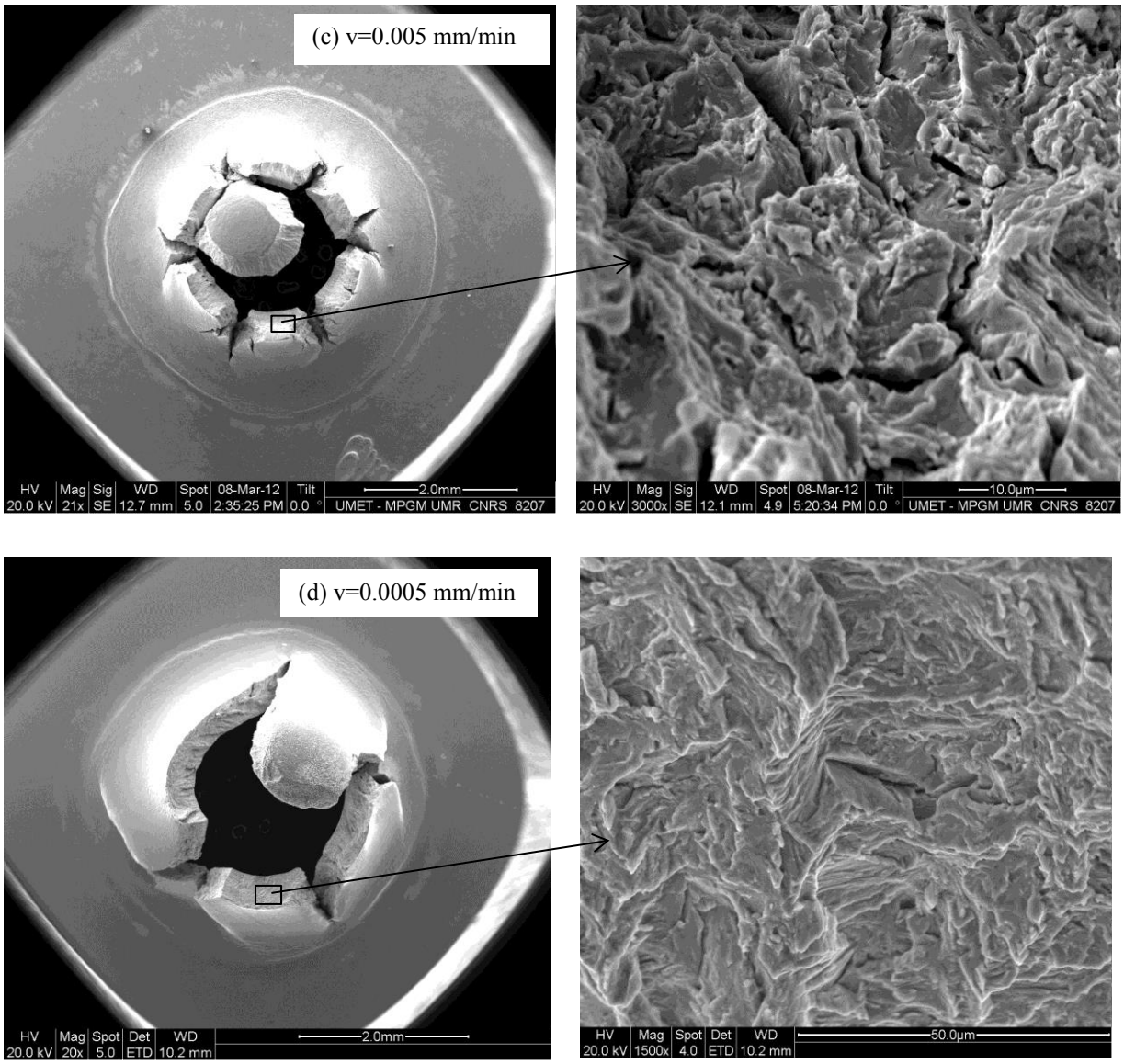

Figure 3.18: SEM images of TR750 SPT specimens at 300°C with different velocities in liquid low oxygen LBE.

In comparison with tests in oxygen saturated LBE at 300°C, the fully brittle fracture occurred for a higher velocity, here 0.005 mm/min. Therefore, this incited us to investigate this velocity conditions by scanning a temperature range from 130°C to 400°C. In addition, in order to understand the influence of the velocity on the fracture characteristics, four different velocities are used (0.5, 0.05, 0.005, 0.0005 mm/min) during the experiments and the other conditions are controlled the same.

Fig. 3.19 shows the SPT curves, which indicate that the yield load values are not discernible according to test temperature. Furthermore, the temperature effect is obvious, both the values of the maximum load and the displacement of the maximum load decrease along with the increasing of the test temperature range from 130°C to 300°C, expect 400°C. At 400°C, the accelerated failure effect is recovered because both values of maximum load and of

displacement at the maximum load are higher than that of 300°C, and which approach to 250°C. Also let us keep in mind the peculiar shape of the curve of the test at 300°C.

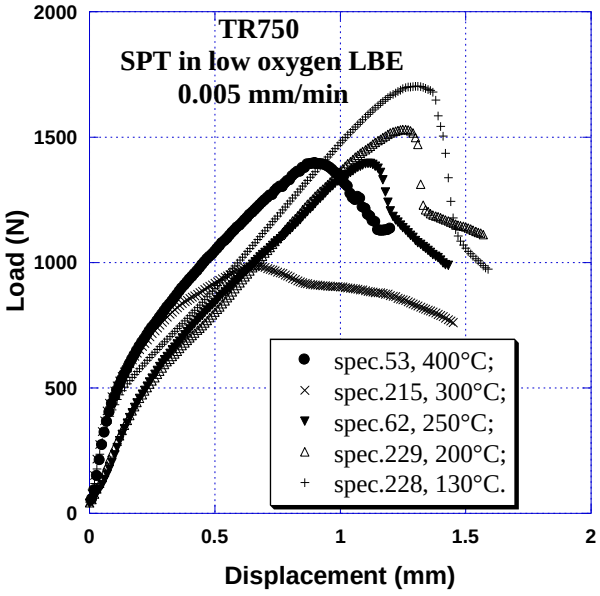

Figure 3.19: Curves of TR750 small punch tests in liquid low oxygen LBE with velocity 0.005 mm/min at five different temperature experimental conditions (130°C, 200°C, 250°C, 300°C and 400°C).

SEM was used to analyze the fracture characteristics of TR750 SPT specimens tested in liquid low oxygen LBE in order to know whether the crack is brittle or ductile or something mixed.

At the velocity of 0.005 mm/min and in low oxygen LBE condition, the TR750 specimen tested at 130°C shown a semi-circular fracture with a dome that experienced a large deformation. There were lots of small radial cracks around the outside edge of the crack. Even though the presence of the small radial cracks around the semi-circular fracture opened, the fractured surface of TR750 specimen still exhibits the ductile characteristic shown in Fig. 3.20a. In other words, TR750 experienced ductile failure tested in low oxygen LBE with a velocity of 0.005 mm/min at the approximate melting point (130°C) experimental condition. But at 200°C, the mixed ductile and brittle fracture characteristics were discovered for TR750 tested in low oxygen LBE with a velocity of 0.005 mm/min. Furthermore, the shape of the fractured specimen is circular with deep radial cracks obviously shown in Fig. 3.20b. The result of micrographic observation pointed out that the ductile fracture normally appeared inside the circular fracture toward the center of the specimen, while the brittle fracture preferred located at the outside edge of the circular fracture (Fig. 3.20b).

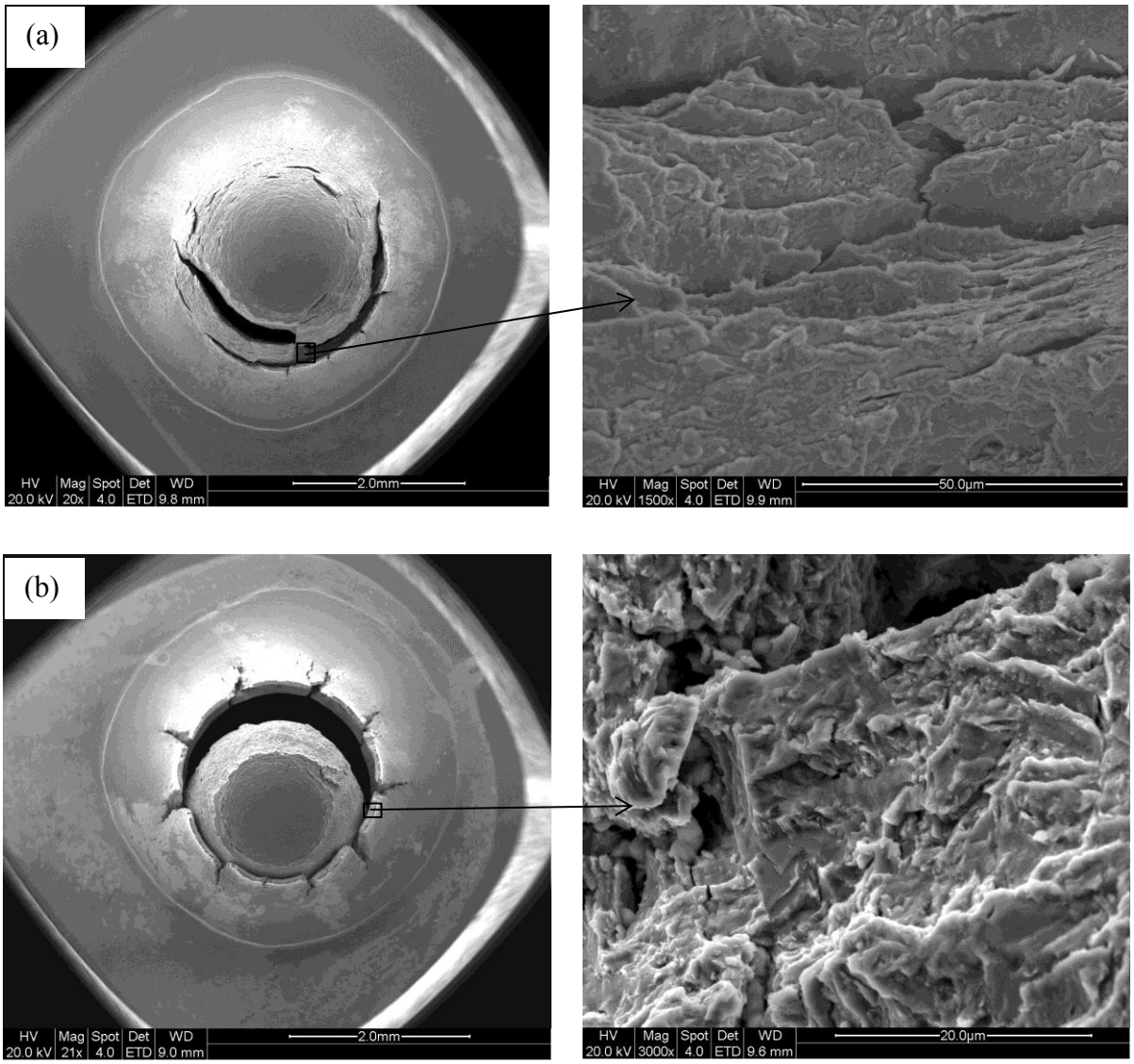

Figure 3.20: SEM images of TR750 SPT specimens tested in low oxygen LBE with a velocity of 0.005 mm/min: (a) at 130°C, and (b) at 200°C.

At 250°C, three velocities were utilized for the experimental tests. Fig. 3.21a, Fig. 3.21b, and Fig. 3.21c show the images of TR750 SPT specimens at 250°C with the velocities of 0.5 mm/min, 0.05 mm/min, and 0.005 mm/min respectively in liquid low oxygen LBE. The SEM observation indicates that the fracture characteristic changed from ductile to brittle. The failure fractograph confirmed that the mixed brittle-ductile fracture existed in some area of the crack. Furthermore, this kind of brittle fracture is more obvious with the decrease of the velocity. Actually, it seems that the much more clearly brittle characteristic of the specimen can be seen to the naked eyes by the star shape of the cracks which is also very obvious with the decrease of the velocity. Normally, when the brittleness characteristic is much more conspicuous, the number of the cracks around the star shape fracture will become scarce. In addition, at the velocity of 0.005 mm/min, the brittle area proportion of the fractured

specimens tested in low oxygen LBE at 250°C is larger than 200°C (Figs. 3.20b, 3.21c).

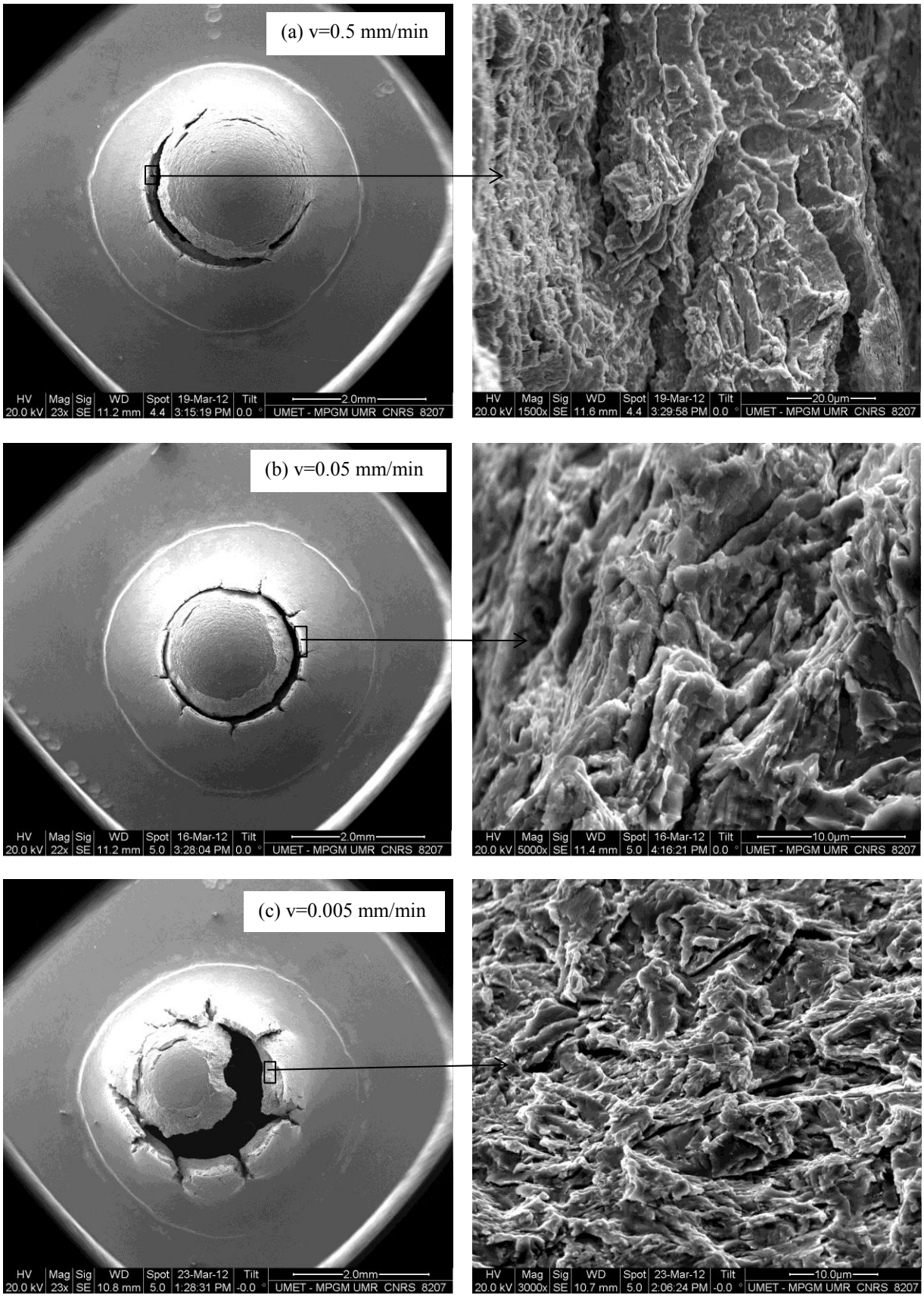

Figure 3.21: SEM images of TR750 SPT specimens at 250°C with different velocities in liquid low oxygen LBE.

With the increase of the experimental temperature, at 400°C, the fracture characteristics of TR750 SPT specimens are not very similar with that at 250°C and 300°C, although the transgranular brittle fracture is particularly very clearly observed at the slow velocities of 0.05 and of 0.005 mm/min shown by Figs. 3.22b and 3.22c. The occurrence of the brittle star shape in SPT specimens of TR750, at 250°C and 300°C experimental conditions suggests coupled effects between the velocity and the temperature in liquid low oxygen LBE. That is to say, with the increasing of the temperature (from 250°C to 300°C) or decreasing of the velocity (from 0.5 to 0.0005 mm/min) TR750 material will increase the sensitivity to the liquid LBE embrittlement. However, this phenomenon is not adapted to the test at 400°C. At 400°C, TR750 SPT specimen seems to more or less recover a little the ductility from the brittleness in liquid low oxygen LBE, especially at the lowest velocity 0.0005 mm/min condition the ductile 'dimple' characteristic is much more prominent as shown by Fig. 3.22d. However, at 400°C with the velocities of 0.5, 0.05, 0.005 mm/min experimental conditions, the fracture characteristics are complicated, which exhibited mixed ductile and brittle crack surface, and furthermore, the brittle characteristics of the specimen usually located at the outer edge of the cracks.

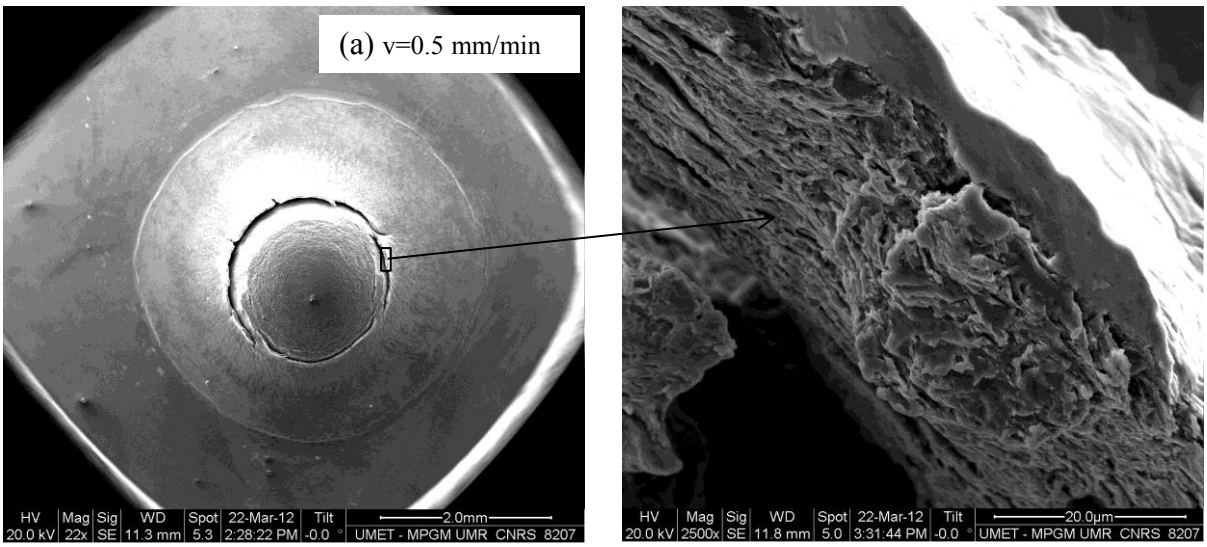

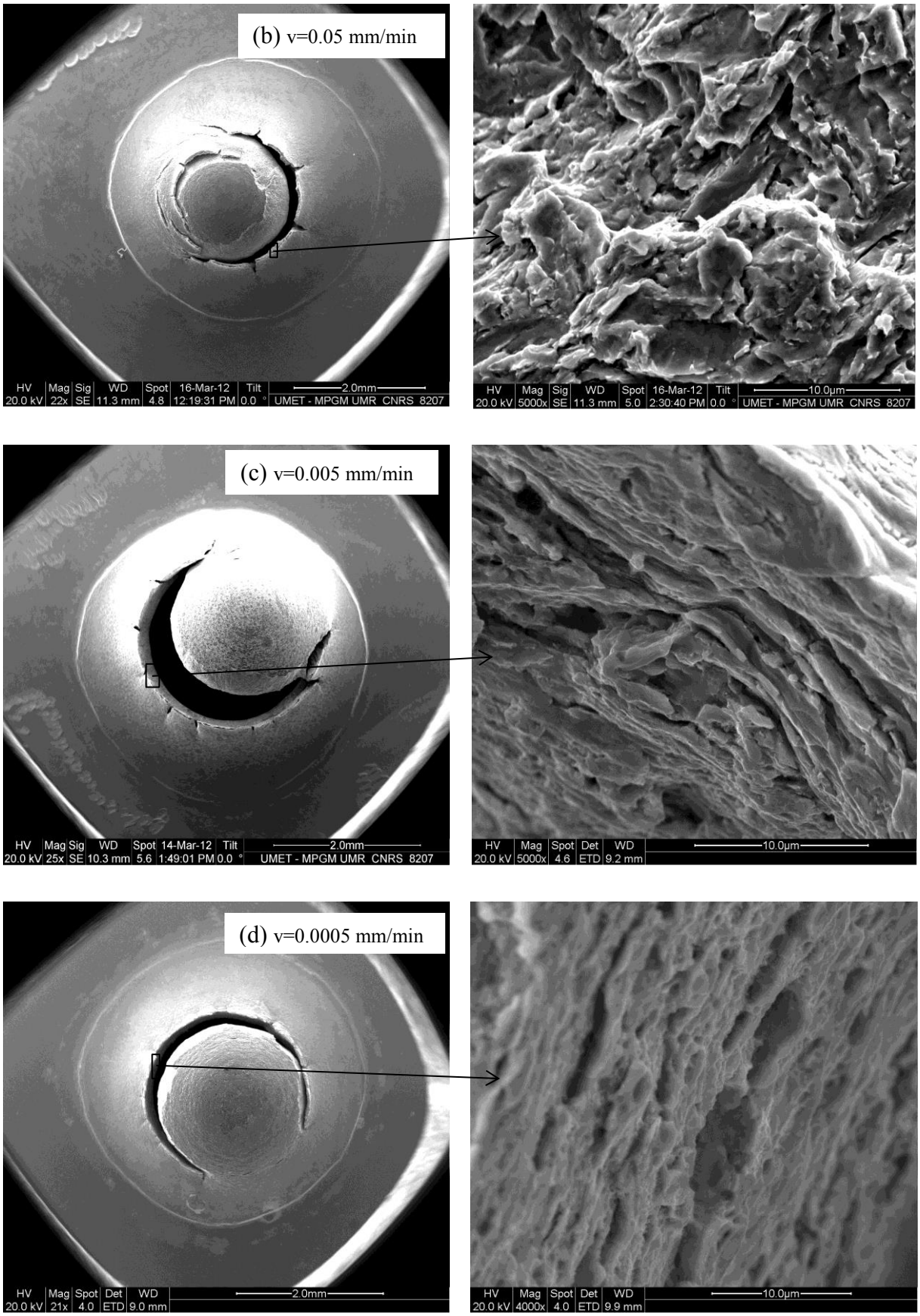

Figure 3.22: SEM images of TR750 SPT specimens at 400°C with different velocities in liquid low oxygen LBE.

3.1.4 Effect of microstructure on LBE embrittlement sensitivity of T91 steel

To study the LBE embrittlement sensitivity according to the microstructure of the steel, SPT were carried out on the material T91 steel according to the two heat treatments (TR750 and TR500) in both low oxygen and oxygen saturated LBE at 300°C and in air at RT and 300°C with a velocity from 0.5 to 0.0005 mm/min. Indeed, the LME of material TR500 in LBE has been reported in the literature presented in chapter I, but nevertheless we still study the LBE embrittlement sensitivity of TR500 to verify the results of the literature and try to conduct a comparative study with TR750.

Large changes in mechanical properties of TR500 were found with the conversion of the test condition. In air, with the increase of the test temperature from RT to 300°C, the mechanical resistance of TR500 is reduced to a large extent indicated by the SPT curves at a velocity of 0.5 mm/min (Fig. 3.23a). For example, the maximum load, F_{max}, reduced from 3442 N to 2261 N, and the normalized fracture energy, J_{nFmax}, dropped by more than the half (from 6.86 J/mm to 3.16 J/mm) due to the rise of the test temperature in air shown in Table 3.4. In addition, despite the decrease in the mechanical properties, the fractured specimens of TR500 show a large deformation and the micrographic surface is the ductile characteristic ‘dimples’ tested in air at both RT and 300°C as shown in Fig. 3.24a.

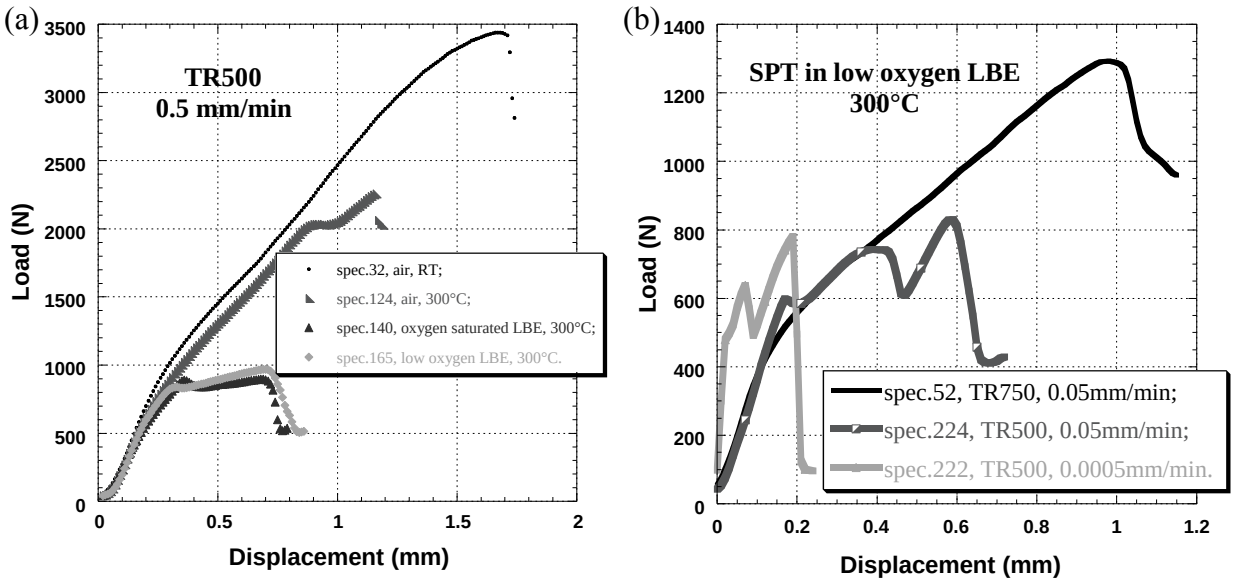

Figure 3.23: Load-displacement SPT curves of the materials TR750 and TR500 tested at RT and at 300°C in LBE (low oxygen LBE / oxygen saturated LBE) with three different velocities (0.5, 0.05, 0.0005 mm/min).

Table 3.4: Values of key points measured in the SPT of TR750 and TR500 materials tested in air and in LBE (oxygen saturated/low oxygen).

Materials	TR500						TR750
Velocity (mm/min)	0.5				0.05	0.0005	0.05
Medium	air		Oxygen saturated LBE	Low oxygen LBE			
Temperature	RT	300°C					
Specimen No.	(32)	(124)	(140)	(165)	(224)	(222)	(52)
F_{max} (N)	3442	2261	898	968	833	788	1293
d_{Fmax} (mm)	1.67	1.17	0.69	0.74	0.61	0.20	0.98
J_{nFmax} (J/mm)	6.86	3.16	0.92	0.92	0.68	0.22	1.62

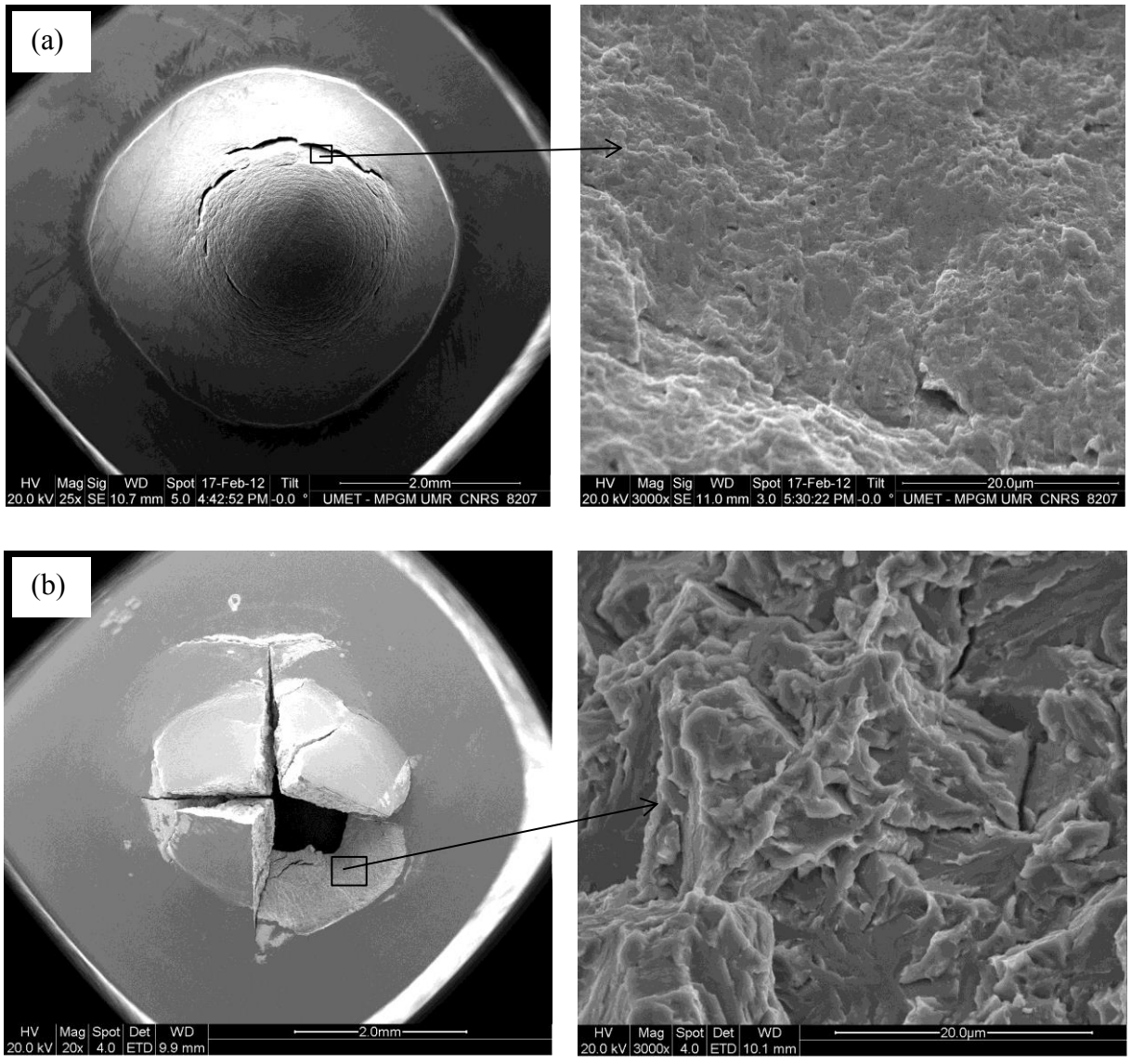

Figure 3.24: SEM images of TR500 specimens SPT: (a) in air at room temperature with a velocity of 0.5 mm/min and the fractured surface is the ductile characteristic 'dimples'; (b) in low oxygen LBE at 300°C with a velocity of 0.05 mm/min and the fractured surface is the brittle cleavage.

However, the mechanical response of TR500 SPT in LBE is completely different with that in air. The load-displacement SPT curves of TR500 tested at 300°C in both oxygen saturated LBE and low oxygen LBE are similar. They showed a linear increase at the beginning until the yield load, and then experienced instabilities which were more marked as the velocity was decreased (Fig. 3.23). Furthermore, this particular failure entire process stage of TR500 tested in LBE was not affected by the changes of the velocity. The load-displacement curves are in coincidence, which indicated that the effect of oxygen content in LBE on TR500 was negligible (Fig. 3.23a). SPT on TR500 in low oxygen LBE at 300°C showed that the velocity (in a range of 0.5 to 0.0005 mm/min) had no significant effect on the value of the maximum load (the average of F_{max} is 872 N), but affected the displacement at the maximum load (d_{Fmax}: from 0.74 to 0.20 mm) and the normalized fracture energy (J_{nFmax}: from 0.92 to 0.22 J/mm).

A strong difference can be seen between the SPT curves of the materials TR500 and TR750 steels. Let us remember that the TR750 curve recorded during test at 300°C in liquid low oxygen LBE with the velocity of 0.05 mm/min comprises four SPT stages (Fig. 3.23b). The shape of the specimen presented a main circular crack with several radial cracks. Furthermore, fractographic observation indicates that the brittle crack characteristic was found at the outside edge of the circular fracture (Fig. 3.18b). For the same experimental conditions, the load-displacement curve of the material TR500 starts in quasi linear manner and then contains instabilities. The first drop is associated to a primary fracture, although thereafter the load continues to rise until a second drop occurs, which is considered as the other second crack occurrence. This is repeated three times before the final fracture. For the material TR500, no circular crack was observed and the number of radial cracks was reduced down to four cracks. In addition, we found that so long as SPT was carried out on the material TR500 in liquid LBE, the fractured surfaces of the TR500 specimens tested in low oxygen LBE and in oxygen saturated LBE were always brittle with no traces of ductile fracture characteristics, essentially transgranular with some occasional intergranular decohesion (Fig. 3.24b).

From this study, it can be concluded that T91 steel in its standard heat treatment is possible to experience ductile deformation at 300°C as well in air as in low oxygen LBE under moderate loading rate 0.05 mm/min, and the brittle characteristic can just be discovered at the edge of the circular crack. However, LBE embrittlement is possible if unsuitable tempering treatment has been performed.

3.2 Synthesis and discussion of the transition from ductile to brittle in liquid LBE of T91 steel observed by Small Punch Test

Small punch tests have been conducted on TR750/TR500 specimens in oxygen saturated LBE and in low oxygen LBE. The mechanical behaviour of the T91 steel has been studied by taking into account various parameters in order to identify the most effective ones that promote liquid LBE embrittlement sensitivity. Based on the above experimental investigation, the small punch tests demonstrate that the factors which affect the ductile to brittle transition in liquid LBE of T91 steel are very complicated. T91 steel exhibits a certain degree of sensitivity to LBE embrittlement according to the oxygen content in LBE, the displacement velocity, the test temperature and the microstructure of the steel. In this section, the results are synthesised and commented.

From the load-displacement curves of SPT, different mechanical characteristics of the material could be determined (Chapter II, section 2.2.1.3). The Table 3.5 summarizes these values for the standard reference temperature (300°C) in the LBE (saturated oxygen LBE and low oxygen LBE) and for the four studied displacement velocities.

Table 3.5: Values of key points measured in SPT of TR750 tested at 300°C in LBE (oxygen saturated/low oxygen) with four different velocities (0.5, 0.05, 0.005, 0.0005 mm/min).

Medium	Oxygen saturated LBE				Low oxygen LBE			
Velocity (mm/min)	0.5	0.05	0.005	0.0005	0.5	0.05	0.005	0.0005
Fe (N)	426±166	422±10	390±10	653±24	374±79	379±80	529±62	556±47
d_{Fe} (mm)	0.14±0.02	0.12±0.04	0.11±0.04	0.05±0.01	0.20±0.09	0.17±0.07	0.17±0.16	0.07±0.02
F_{max} (N)	1720±134	1575±130	1458±6	1116±158	1525±61	1277±80	910±121	860±18
d_{Fmax} (mm)	1.38±0.17	1.06±0.04	1.05±0.10	0.69±0.02	1.47±0.16	1.09±0.11	0.66±0.05	0.48±0.09
J_{nFmax} (J/mm)	2.87±0.2	2.18±0.16	1.93±0.13	1.24±0.08	2.60±0.28	1.66±0.20	0.82±0.2	0.61±0.09
σ_{YS} (MPa)	513±169	557±36	515±13	844±14	493±105	514±117	637±83	678±57
σ_{UTS} (MPa)	556±21	533±32	493±2	373±49	516±21	439±26	292±42	278±6

We noted a good agreement at 0.5 mm/min of F_e and calculated σ_{YS} with the value obtained by Serre and Vogt [SER-2007]. The determination of σ_{UTS} from the SPT curves appears to be not pertinent. Indeed σ_{UTS} is classically determined from tensile curves obtained with standard specimens, with a specific ratio length/width. In the case of SPT, the strain condition is not the same, which induces some difficulties of correlation. The normalized energy J_{nFmax} decreases when the displacement velocity decreases. This effect is more important in low oxygen LBE.

To evaluate the effect of LME, we compared this value with those obtained in air or in Ar-3.5%H_2. So, the evolution of the ductility in liquid LBE in comparison with in inert atmosphere is represented by the ductility factor F_D given by equation 3.1:

$$F_D(\%) = \frac{J_{nFmax}(LBE)}{J_{nFmax}(Ar\text{-}3.5\%H_2)} x100 \quad 3.1$$

The factor of fragility F_{LMIE} is defined from F_D shown by equation 3.2:

$$F_{LMIE}(\%) = 100 - F_D(\%) \quad 3.2$$

The Table 3.6 summarizes the key values for the TR750 material and TR500 material at 300°C and 400°C for the standard reference velocity (0.5 mm/min) in low oxygen LBE.

Table 3.6: Variation of the rupture energy, and fragility factor F_{LMIE} of T91-TR750 and T91-TR500 steels (velocity=0.5 mm/min).

Materials	T91-TR750				T91-TR500			
Medium	Ar-3.5%H_2		Low oxygen LBE		Ar-3.5%H_2		Low oxygen LBE	
Temperature (°C)	300	400	300	400	300	400	300	400
J_{nFmax} *(J/mm)*	3.76±0.07	2.94±0.06	2.60±0.28	2.04±0.32	2.86	3.10	0.92	0.31
F_{max} (N)	1776±35	1624±25	1525±61	1358±106	2002	2282	968	568
d_{Fmax} (mm)	1.76±0.01	1.62±0.09	1.47±0.16	1.31±0.15	1.12	1.17	0.74	0.45
F_{LMIE}%	/	/	*31*	*31*	/	/	*68*	*90*

As observed by different authors after SPT [SER-2007, SER-2008], tensile tests with notched specimens [NIC-2001-A, NIC-2001-B], bending tests [LON-2008-B], point out a sensitivity of the TR500 steel in presence of LBE. This embrittlement is observed by a change in the fracture mode and by a very large factor of fragility. Therefore, the factor of fragility (F_{LMIE}) for TR500 appears much higher than that of TR750 as shown in Table 3.6. Furthermore, with the increase of the test temperature from 300°C to 400°C, the factor of fragility (F_{LMIE}) for TR500 reached 90% at 400°C for test in low oxygen LBE with a velocity of 0.5 mm/min, while it did not change obviously for TR750 steel and its factor of fragility kept at about 31% (Table 3.6).

At lower displacement velocities (Table 3.7), in LBE, the normalized energy at F_{max}, J_{nFmax} is small which is coherent with the observation of brittle fracture. Thus, whatever the reasons (heat treatment, irradiation et al.) that can harden and change the material microstructure and lead to brittle fracture, they are believed very dangerous for industry application, which

should be considered in evaluation carefully before real use.

Table 3.7: Variation of the rupture energy, of T91-TR750 and T91-TR500 steels tested in low oxygen LBE (velocity=0.05, 0.0005 mm/min).

Velocity	0.05 mm/min				0.0005 mm/min			
Materials	TR750		TR500		TR750		TR500	
Temperature(°C)	300	400	300	400	300	400	300	400
J_{nFmax} *(J/mm)*	*1.66±0.20*	*1.73±0.33*	*0.56±0.06*	*0.24±0.00*	*0.61±0.09*	*1.96*	*0.22*	*0.67*
F_{max} (N)	1277±80	1347±179	824±9	729±14	860±18	1507	788	950
d_{Fmax} (mm)	1.09±0.11	1.11±0.05	0.53±0.09	0.31±0.03	0.48±0.09	1.08	0.20	0.70

Concerning the TR750 steel, we note an effect of LBE at 0.5 mm/min and at 300°C and at 400°C (Table 3.8).

Table 3.8: Factor of fragility F_{LMIE} of TR750 steel tested at 0.5 mm/min in LBE.

Experimental conditions	200°C	250°C	300°C	400°C
oxygen saturated LBE	0	0	34	41
low oxygen LBE	0	0.06	31	31

In previous SPT studies [SER-2007, SER-2008], for the T91 steel in its standard heat treatment (TR750 steel), no effect of LBE has been observed in liquid oxygen saturated LBE, at 300°C with quick velocity 0.5 mm/min experimental condition. But, in the present investigation, an effect of oxygen saturated LBE is observed at 300°C and at 0.5 mm/min. Indeed, in these conditions a decrease of the fracture energy at F_{max} in comparison with air was noted (Table 3.8). Furthermore, a change in the cracking was observed. LBE promotes the formation of radial cracks and of localised brittle fractures. This apparent contradiction could be explained by the difference in the supply of the material T91 steel which occurs of two batches with different hardness. Though both T91 investigated in the present study and in the previous one fulfilled the chemical composition requirement, some minor differences in the composition however exist. Especially, the phosphorus content was 0.014 wt% in the previous against 0.021 wt% in the present one. The other difference between the two delivered steels concerns the forming process, a billet for the previous study and a rolled plate for the present one. Admitting the rule that the harder an alloy is, the more sensitive to LMIE it is, the T91 steel of present study appeared to be harder (HV=278±11) and should therefore appear more sensitive than the softer T91 steel (HV=256±5) investigated in the past.

Moreover, the transition from ductile to brittle behaviour as a function of hardness has been also carried out [SER-2007, SER-2008]. It was found that when the hardness exceeded a value of 285±1, a value close to that measured in the present investigation, the ductile to brittle transition starts to occur.

Furthermore, at 0.5 mm/min, the LBE effect of TR750 steel is more and more obvious with the temperature increase (Table 3.8). 300°C appears as a transition temperature between two regimes: (a) a LME sensitivity as more important temperature, (b) no effect of the LBE at lower temperature. The dependence of LME sensitivity of the T91 steel by LBE or lead with the temperature was already observed [NIC-2001-A, NIC-2001-B, BOS-2006, DAI-2006-A]. In air, increasing the test temperature in the studied range increases the ductility of the T91 steel. Therefore, the ductile to brittle transition resulting from increasing the temperature for the tests conducted at a displacement velocity of 0.5 mm/min reflects probably an effect of the chemical properties of the liquid LBE. Indeed, the surface tension of LBE decreases with increasing temperature [HAN-2007]. A low surface tension could promote the wetting at the tip of the microcracks or in the asperities of the roughness due to the plastic deformation. Accepting the fact that wetting is a prerequisite for LMIE, LBE embrittlement occurs for the highest test temperatures, as observed by Dai et al. [DAI-2006-A], even if the material is softer.

Changing the oxygen saturated LBE bath for the low oxygen LBE purified one did not modify the behaviour of the T91 steel in a temperature range between 200°C and 400°C when it was deformed at 0.5 mm/min. Indeed, when the T91 steel is in contact with the liquid low oxygen LBE, the native oxide is not affected because, no corrosion effect such as dissolution could take place in our present study.

According to the experimental results obtained in chapter III, the displacement velocity plays an important role in the investigation of the ductile to brittle transition for material TR750 tested in liquid LBE. Table 3.9 and Fig. 3.25 present the evolution of the normalized fracture energy J_{nFmax} at F_{max} according to the displacement velocity and the oxygen content in LBE at 300°C. The lower displacement velocity, more sensitive is the TR750 material to the liquid metal. Furthermore, the low oxygen content in LBE promotes all the more LME when the velocity is lower than 0.05 mm/min (0.05, 0.005, 0.0005 mm/min). Indeed, at 0.005 mm/min, the TR750 material is more sensitive to LBE if the oxygen content of the liquid metal is low. Whereas the T91 steel is essentially ductile in presence of liquid oxygen saturated LBE with

rapid test velocity, the fracture surface is almost completely brittle in presence of liquid LBE at the low test velocity condition.

Table 3.9: Normalized fracture energy J_{nFmax} at F_{max} (J/mm) of TR750 steel tested at 300°C in LBE.

Experimental conditions	0.5 mm/min	0.05 mm/min	0.005 mm/min	0.0005 mm/min
oxygen saturated LBE	2.73±0.32	2.18±0.16	2.10±0.28	1.2±0.11
low oxygen LBE	2.46±0.2	1.67±0.19	0.82±0.17	0.61±1.12

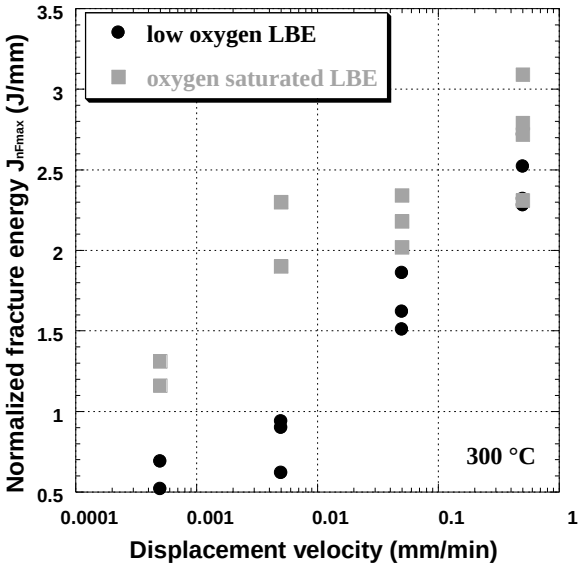

Figure 3.25: Normalized fracture energy J_{nFmax} at F_{max} of TR750 SPT steel specimens tested at 300°C according to the temperature and the environment.

The Tables 3.10, 3.11 and 3.12, and the Fig. 3.26 have summarized the normalized fracture energy J_{nFmax} at F_{max} according the temperature and the displacement velocity.

Table 3.10: Normalized fracture energy J_{nFmax} at F_{max} (J/mm) of TR750 steel tested at 200°C in LBE.

Experimental conditions	0.5 mm/min	0.05 mm/min	0.005 mm/min	0.0005 mm/min
oxygen saturated LBE	3.86±0.28	2.67±0.14	2.45	/
low oxygen LBE	3.8±0.4	/	1.55±0.33	/

Table 3.11: Normalized fracture energy J_{nFmax} at F_{max} (J/mm) of TR750 steel tested at 250°C in LBE.

Experimental conditions	0.5 mm/min	0.05 mm/min	0.005 mm/min	0.0005 mm/min
oxygen saturated LBE	3.69±0.09	2.14±0.2	3.58±0.14	2.16
low oxygen LBE	3.47±0.64	2.38±0.33	1.57±0.48	/

Table 3.12: Normalized fracture energy J_{nFmax} at F_{max} (J/mm) of TR750 steel tested at 400°C in LBE.

Experimental conditions	0.5 mm/min	0.05 mm/min	0.005 mm/min	0.0005 mm/min
oxygen saturated LBE	1.87±0.35	1.46±0.02	1.47±0.33	1.8
low oxygen LBE	2.04±0.32	1.73±0.33	1.7±0.06	1.96

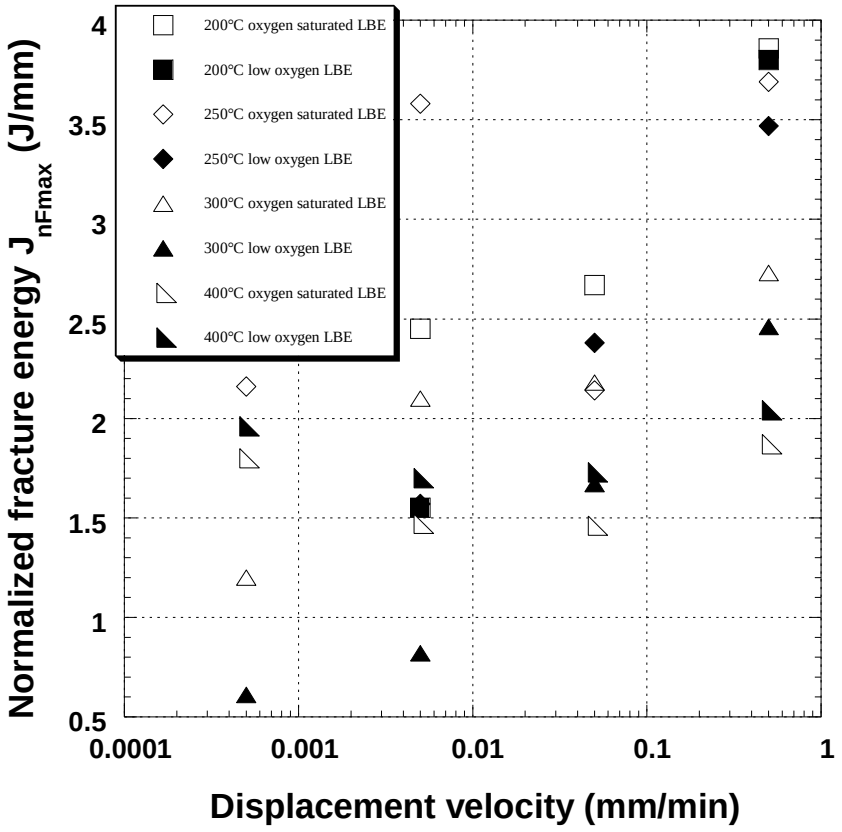

Figure 3.26: Normalized fracture energy J_{nFmax} at F_{max} of TR750 steel tested in LBE (oxygen saturated/ low oxygen) according to the temperature and displacement velocity.

Whatever the displacement velocity, the temperature 300°C appears as critical temperature concerning the LME sensibility. At 250°C, the LME sensibility is less important than at 300°C. The effect of displacement velocity is critical at these two temperatures (250°C, 300°C). However, at 400°C the LME sensitivity is different with that of 250°C and 300°C. Indeed, at 400°C, the TR750 steel is sensitive in presence of LBE at higher displacement velocities (0.05 mm/min, 0.5 mm/min) and not at the lower velocity (0.0005 mm/min).

3.3 Conclusion

Small punch tests have been conducted on T91 steel in atmosphere (air or Ar-3.5%H_2) and in LBE. The mechanical behaviour of the T91 steel has been studied by taking into account various parameters in order to identify the most effective ones that promote liquid LBE embrittlement sensitivity: the oxygen content in LBE, the temperature, the displacement velocity and the microstructure of the T91 steel.

Based on the above experimental investigation, the main conclusions are:

(a) T91 steel in its standard heat treatment (TR750) or after hardening heat treatment (TR500) exhibits high ductility in air;
(b) T91 steel in its standard heat treatment (TR750) exhibits a certain degree of sensitivity to LBE embrittlement;
(c) The key factor of the LME sensitivity of the TR750 steel is the displacement velocity;
(d) The LME sensitivity of the TR750 steel depends on the temperature: at 300°C the most important sensitivity to LME is observed;
(e) The decrease in the oxygen content in LBE promotes the LME sensitivity of the TR750 steel;
(f) The TR500 steel is brittle in presence of the LBE.

CHAPTER IV : THE EFFECT OF NOTCH ON LBE EMBRITTLEMENT OF T91 STEEL

In this chapter, the experimental investigation of the surface defects on the mechanical properties embrittlement sensitivity of material TR750 T91 steel in liquid LBE are described in detail, which include: (i) Vickers hardness treatment surface (VHTS) defect specimens in different small punch tests conditions (in air, Ar-3.5%H_2, oxygen saturated LBE, low oxygen LBE); (ii) the linear notched surface (LNS) defect specimens in different small punch tests conditions (in air, Ar-3.5%H_2, oxygen saturated LBE, low oxygen LBE); (iii) tensile tests performed on the smooth and V-notched surfaces cylindrical specimens at 300°C in LBE (oxygen saturated, low oxygen); (iv) three-point bending tests in air and in oxygen saturated LBE to quantitative investigation of LBE embrittlement sensitivity. The comparative analysis of the results between the defect surface specimens and the smooth ones is present. Then, some comments on the ultimate defect surface effect of material TR750 T91 steel at different experimental conditions are discussed.

4.1 Effect of a Vickers defect

Normally, surface defects can cause varying degrees of influence on the mechanical properties of structural materials. In order to study the surface defects effect on T91 steel, we have taken one form of surface defects in the center of the specimen, Vickers hardness treatment surface (VHTS), to investigate the embrittlement sensitivity of T91 in liquid LBE.

4.1.1 Vickers defect method

To achieve this VHTS defect on the center surface of SPT T91 steel specimens, the indenter of the Vickers micro hardness tester was employed to get seven hardness points with a load of 10 kg. Before performing VHTS defect, the surfaces of specimens were well polished to 1 μm. The shape and the dimensions of the Vickers hardness impressions on the specimen are shown in Fig. 4.1. After VHTS, the specimens were cleaned with ethanol with the ultrasonic machine, and then dried.

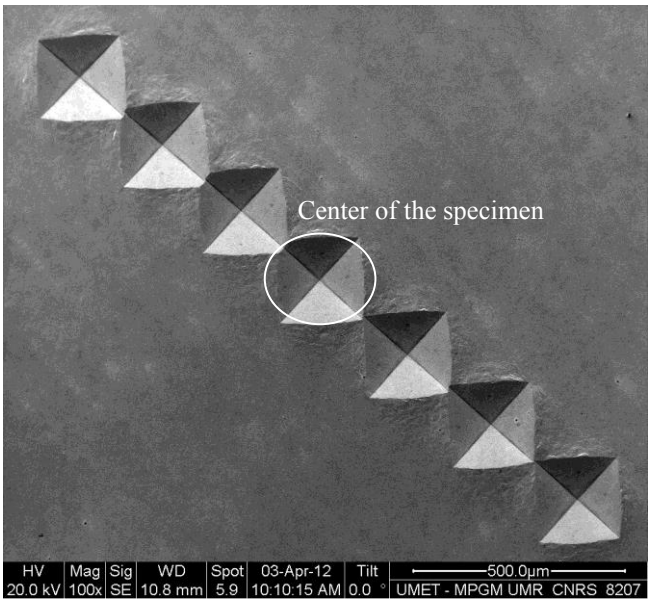

Figure 4.1: Dimension of the seven hardness surface defects points after Vickers hardness treatment.

4.1.2 SPT in Ar-3.5%H_2 gas mixture and in air

Small punch tests were performed on TR750-VHTS specimens at room temperature (RT) and at 300°C in air, and at 300°C and at 400°C in Ar-3.5%H_2 gas mixture at velocity of 0.5

mm/min. The load-displacement SPT curves are shown in Fig. 4.2.

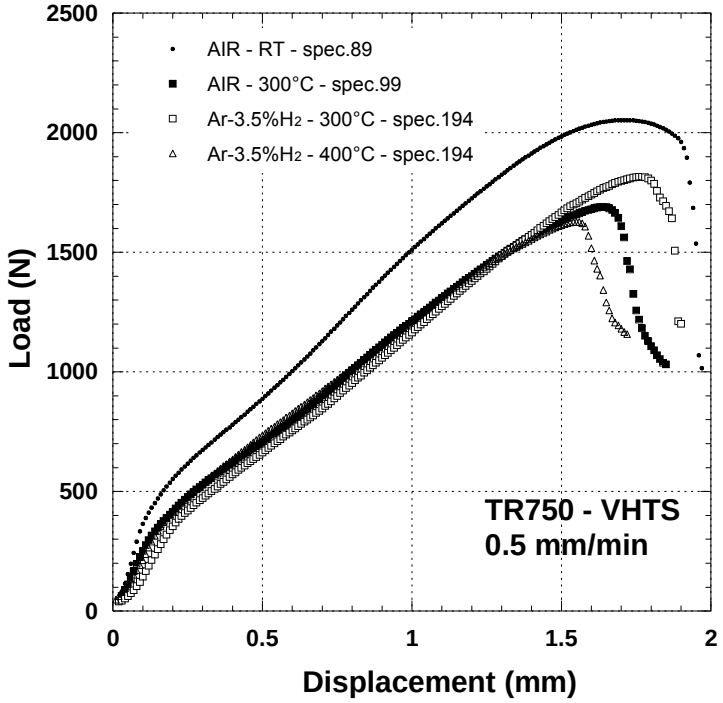

Figure 4.2: SPT curves of TR750 specimens with HVTS defect surface state tested in air at room temperature (RT) and at 300°C, and in Ar-3.5%H_2 at 300°C and 400°C.

All the curves exhibit the four deformation stages suggesting a ductile SPT response of the material. They do not differ from the SPT curves of TR750 on smooth specimen. The tests at different temperatures and environments lead to the same conclusions:

- at 300°C and 400°C, the curves performed in air and in Ar-3.5%H_2 gas mixture are nearly similar,
- increasing test temperature from RT requires less force to deform the material,
- the maximum load and the displacement at the maximum load are reduced with the increase in test temperature.

In addition, the SEM investigations show that all the specimens exhibit a main semi-circular fracture and large plastic deformation marks on the dome (e.g. Fig. 4.3). Short circular cracks can be found in the Vickers impression for those located near the necked part of the specimen. The fracture mode is ductile.

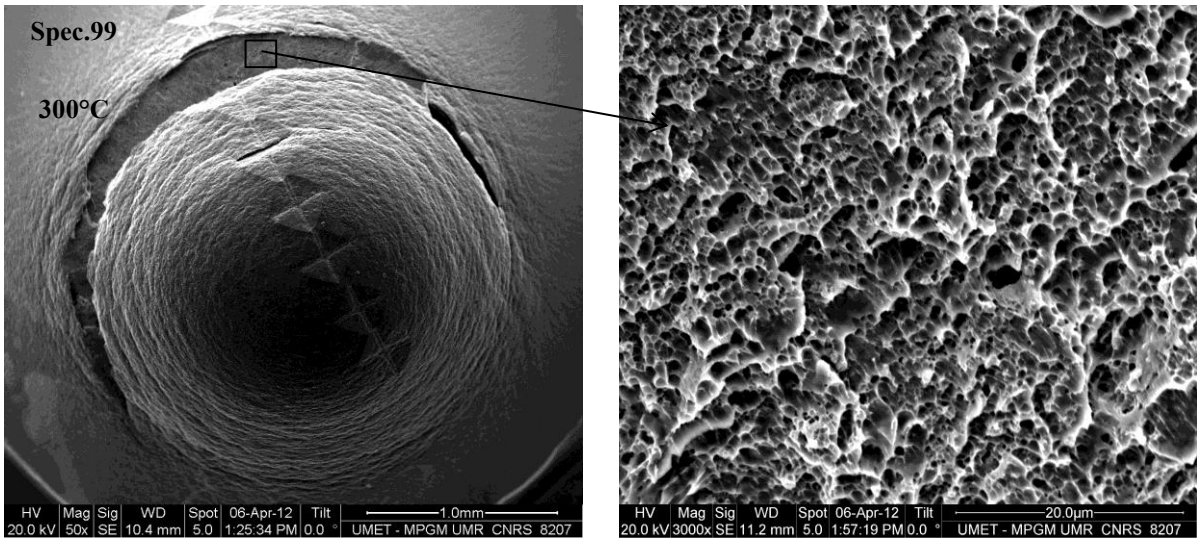

Figure 4.3: SEM images of TR750-VHTS specimen SPT at 300°C in air with a velocity of 0.5 mm/min.

So as to conclude, the presence of Vickers hardness impressions does not modify the behaviour of TR750 material when tests are performed in neutral environments at high temperatures.

4.1.3 SPT on TR750-VHTS specimen in low oxygen LBE

TR750-VHTS specimens were tested at a velocity of 0.5 mm/min in low oxygen LBE at 300°C and at 400°C. The SPT curves are shown in Fig. 4.4. For comparative study, the curves of SPT performed on TR750-VHTS in Ar-3.5%H_2 gas mixture with the same velocity (0.5 mm/min) and the same temperature (300°C and 400°C) are included.

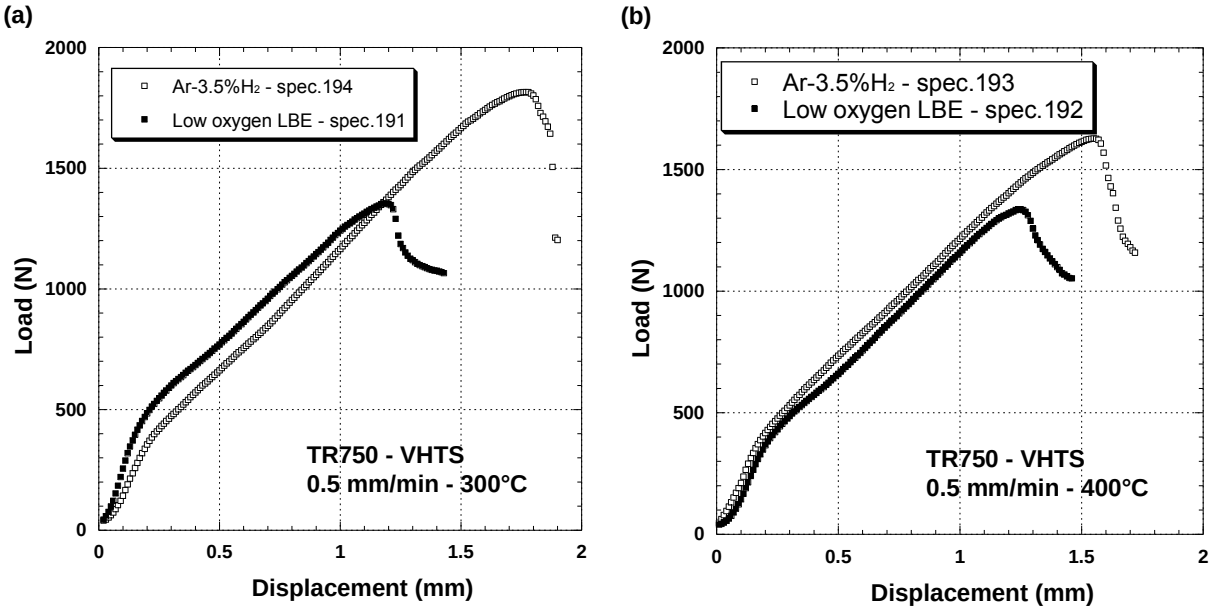

Figure 4.4: SPT curves of TR750-HVTS specimens tested at a velocity of 0.5 mm/min in Ar-3.5%H_2 atmosphere and in low oxygen LBE: (a) 300°C and (b) 400°C.

Testing the TR750-VHTS specimens in the low oxygen LBE instead of Ar-3.5%H_2 had an impact on the mechanical resistance. The curves still exhibit four stages. But both the values of the maximum load (F_{max}) and displacement at the maximum load (d_{Fmax}) are significantly reduced in comparison with those obtained in Ar-3.5%H_2 gas mixture.

TR750-VHTS specimens fractured in low oxygen LBE (300°C and 400°C) at a velocity of 0.5 mm/min has exhibit nearly the same feature as those fractured in Ar-3.5%H_2 gas mixture: a main semi-circular crack, large plastic deformation mark on the dome and presence of dimples on the fracture surface (Fig. 4.5).

Some differences can however be pointed out. For tests in low oxygen LBE (300°C and 400°C), firstly, the circular crack is accompanied by radial cracks which is typical for test performed in LBE as mentioned earlier (chapter III). Secondly, cracks are present at the diagonals of Vickers hardness impression. For the joining diagonals, crack coalesce was observed leading to a longer crack (Fig. 4.5cd). Furthermore, the fractured surfaces SEM observations confirm that the ductile fracture surface contains occasionally brittle zones at the outside edge representative of a test performed in low oxygen LBE.

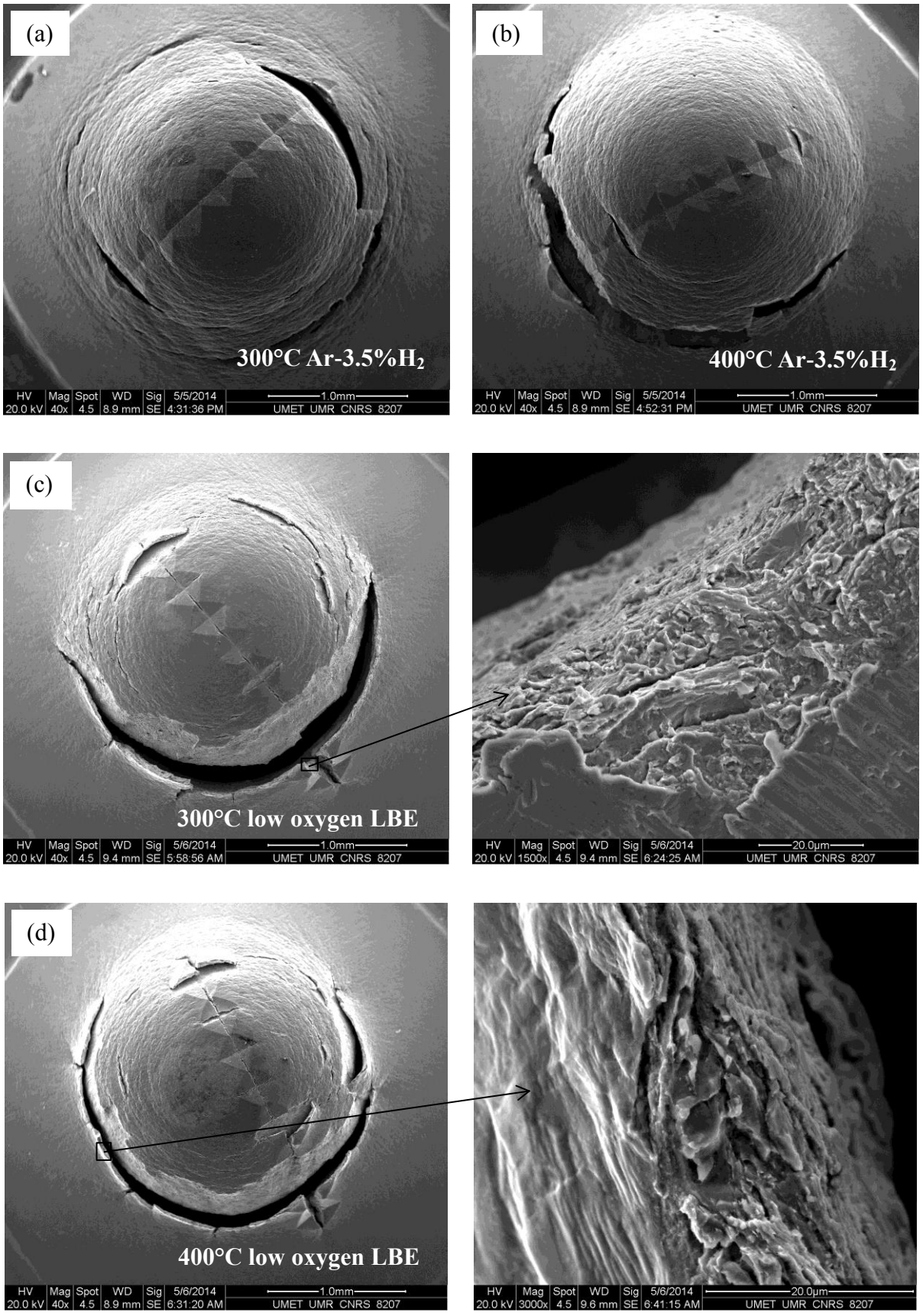

Figure 4.5: SEM images of TR750-VHTS specimens SPT at a velocity of 0.5 mm/min: (a) spec. 194 tested at 300°C in Ar-3.5%H_2; (b) spec. 193 tested at 400°C in Ar-3.5%H_2; (c) spec. 191 tested at 300°C in low oxygen LBE; (d) spec. 192 tested at 400°C in low oxygen LBE.

4.1.4 SPT in oxygen saturated LBE

TR750-VHTS specimens were tested at a velocity of 0.5 mm/min in oxygen saturated LBE at 250°C, 300°C and 400°C. The SPT curves are shown in Fig. 4.6. For comparative study, the curves of SPT performed on TR750-VHTS in air with the same velocity (0.5 mm/min) and the same temperatures (250°C, 300°C and 400°C) are included.

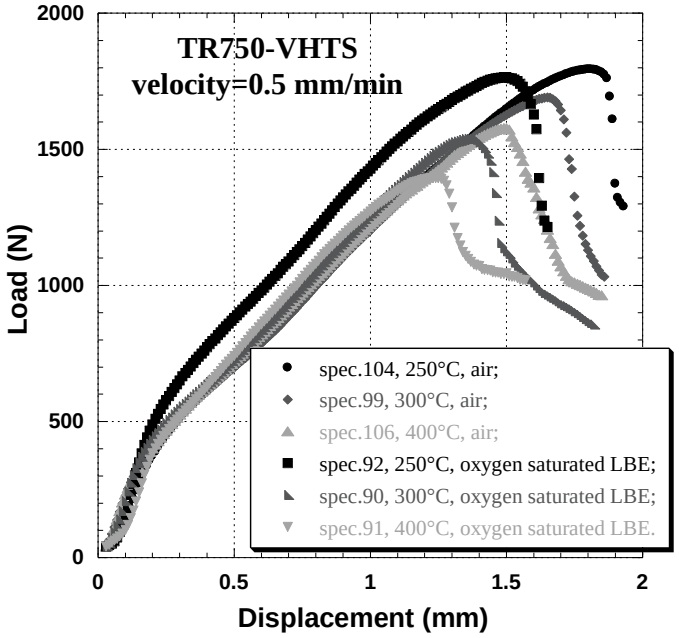

Figure 4.6: SPT curves of TR750 specimens with HVTS defect surface state tested in air and in liquid oxygen saturated LBE with a velocity of 0.5 mm/min at 250°C, 300°C, and 400°C.

The SPT behaviour of micro-notched specimens in air and in oxygen saturated LBE for the tested temperature range is similar to that of smooth specimens for a same experimental condition set: same curve shape, same mechanical values. As well, no difference in terms of fracture feature between smooth and micro-notched Vickers specimens was pointed out.

To study more deeply the role of Vickers defect, SPT on TR750-VHTS specimens were performed in oxygen saturated LBE at different cross-head velocities (0.5, 0.05, 0.005 mm/min) in the same range of temperatures (Fig. 4.7).

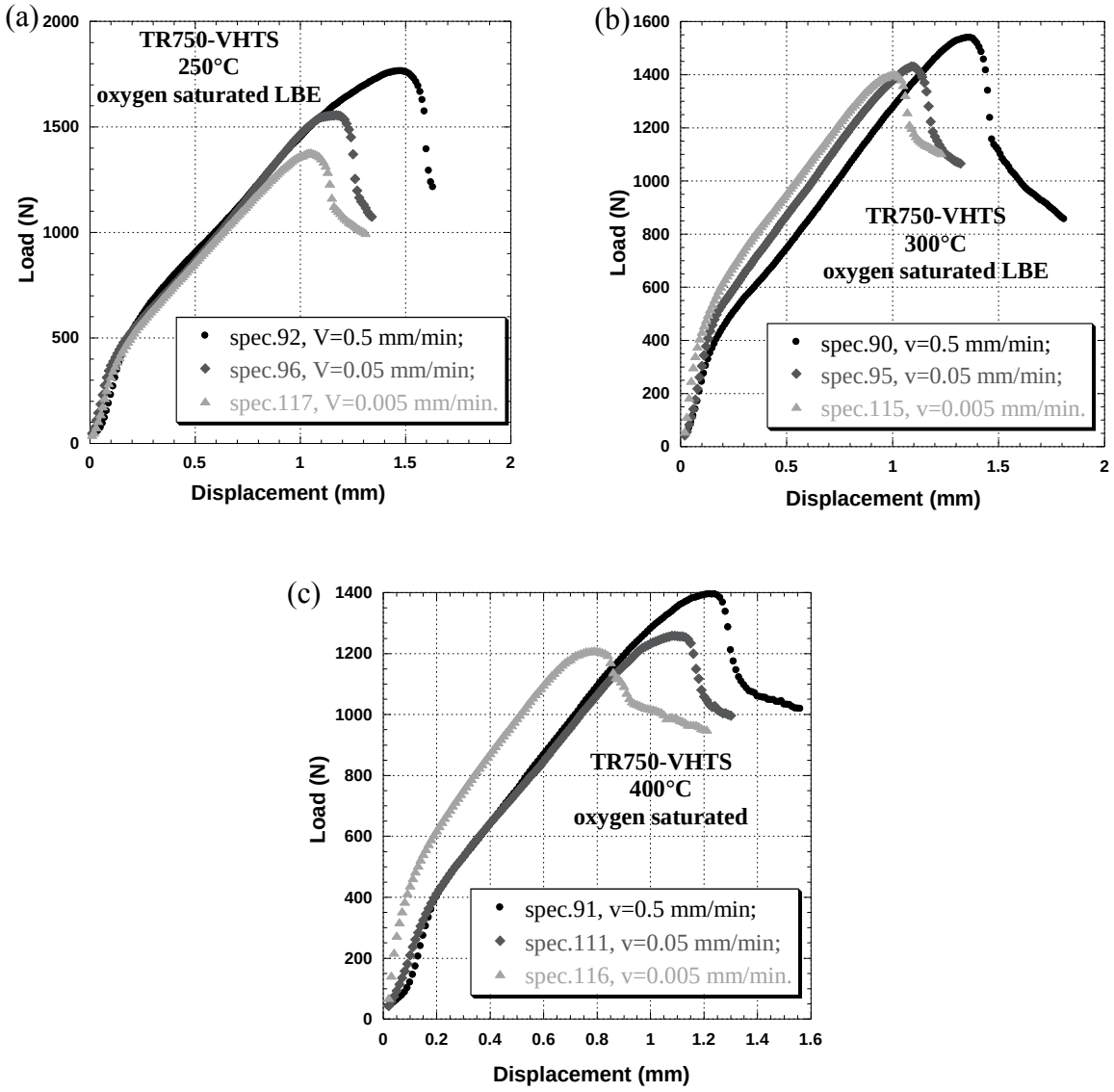

Figure 4.7: SPT curves of TR750 specimens with HVTS defect surface state tested in liquid oxygen saturated LBE with three different velocities of 0.5, 0.05, 0.005 mm/min at (a) 250°C, (b) 300°C, and (c) 400°C.

The reduction in the velocity from 0.5 to 0.005 mm/min resulted essentially in a decrease of the maximum load F_{max} and a decrease in the displacement at the maximum load d_{Fmax}. As for TR750-VHTS specimens, the decrease of F_{max} and d_{Fmax} with the decrease in velocity occurred very progressively for the test performed at 250°C (Fig. 4.7a). For the SPT performed at 300°C and 400°C, the decrease is noted when the velocity was decreased from 0.5 to 0.05 mm/min but not from 0.05 to 0.005 mm/min (Fig. 4.7b and Fig. 4.7c). Otherwise, all the SPT curves exhibit the typical SPT four stages characteristic of a ductile material.

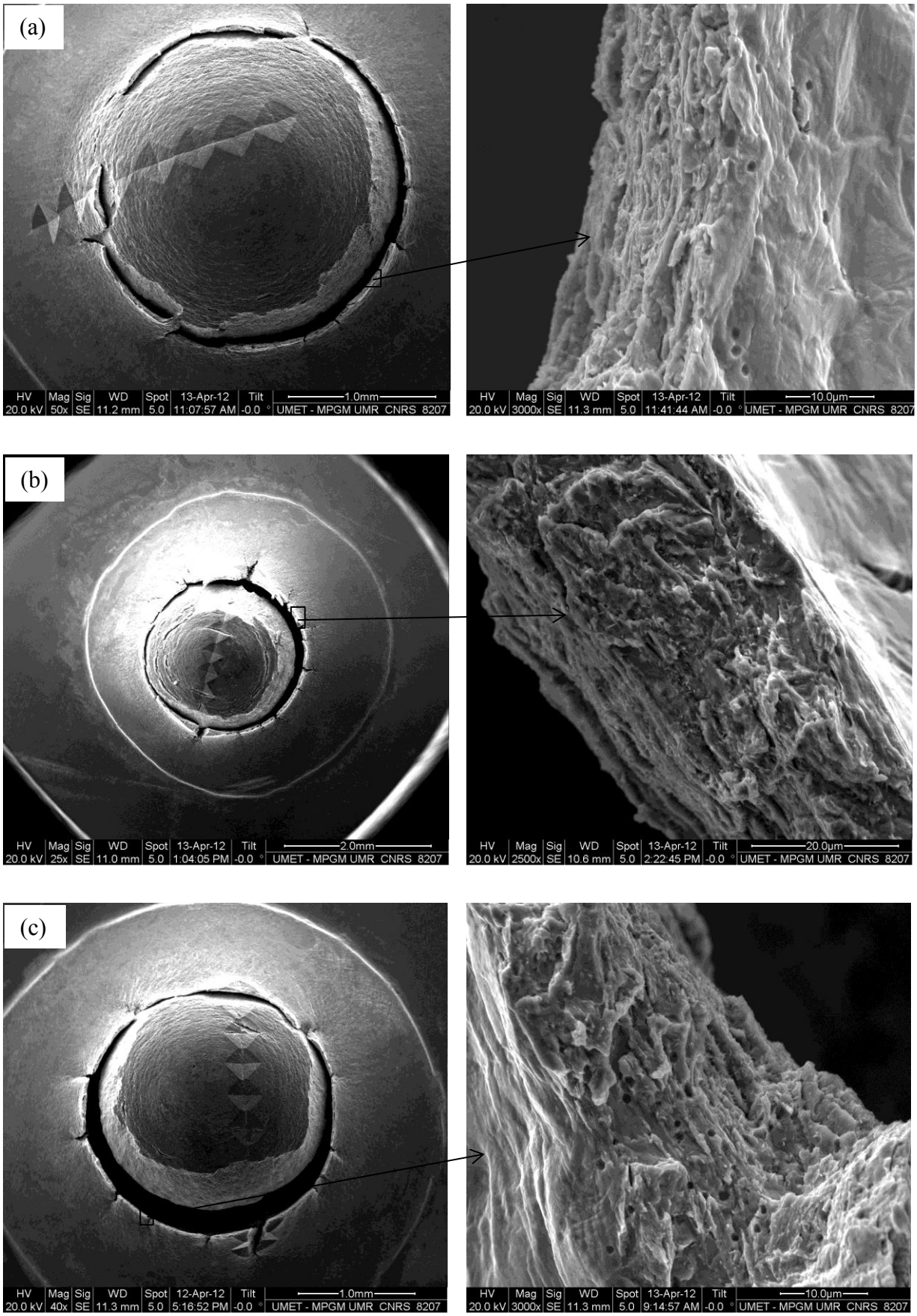

Figure 4.8: SEM images of TR750-VHTS specimens SPT in liquid oxygen saturated LBE with a velocity of 0.05 mm/min: (a) 250°C, (b) 300°C and (c) 400°C.

The SEM observation (Fig. 4.8) on the fractured TR750-VHTS specimens tested in oxygen saturated LBE shows a main circular crack accompanied by radial cracks. Short cracks were also observed in the diagonal of the Vickers impression but the length was only limited to the length of the diagonal and no coalescence was observed. Most of the fractured surfaces contain dimples and occasionally brittle zones at the outside of the circular fracture.

4.1.5 Conclusion

The presence of a 'Vickers' defect of TR750-VHTS specimen does not modify the global SPT response in neutral atmospheres (air and Ar-H_2 gas mixture) nor in LBE (oxygen saturated or low oxygen). The response in these environments can be considered as similar whatever the presence of a Vickers defect (Fig.4.9). The variations of mechanical values are determined from the load-displacement curves in the normal range of data scattering.

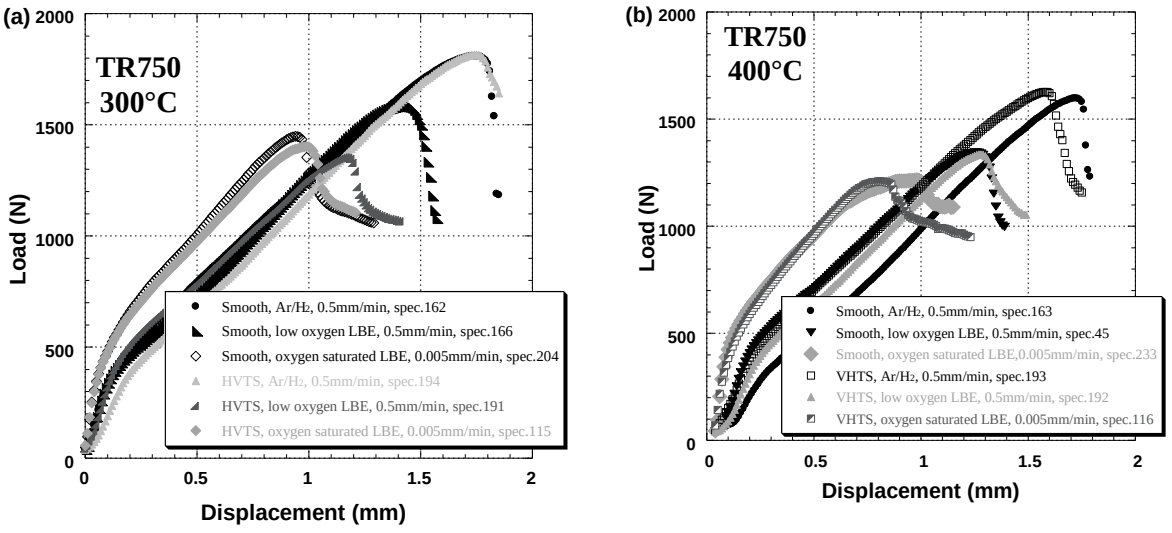

Figure 4.9: SPT curves of TR750 with different surface states (smooth/HVTS) at three different experimental conditions (tested in Ar-3.5%H_2, low oxygen LBE, oxygen saturated LBE) with two different velocities 0.5, 0.05 mm/min: (a) at 300°C, and (b) at 400°C.

There is no combined effect between notch and displacement velocity visible on the SPT curves for the three test temperatures (250°C, 300°C and 400°C).

The macroscopic aspect of the fracture specimen is a dome with marked traces of plasticity, a main circular crack and short radial cracks for test in LBE. The interesting point is that low oxygen LBE promotes cracking in the joined diagonals but this is not enough to deteriorate

the mechanical resistance of TR750 T91 steel.

4.2 Effect of linear notch

The objective of the present investigation is to take into account the geometry and dimensions of a defect on the response of the TR750 material. The kind of defect considered in this part is a linear notch. In the following, these specimens will be labeled as LNS (for Linear Notched Specimen) SPT.

4.2.1 Characterization of the linear notch

After standard heat treatment, a linear notch has been processed by electro spark machine in the middle of the specimen and parallel to the side. Fig. 4.10 shows the geometry and the dimensions of the notch produced on the TR750 SPT specimen. The depth is about 200±20µm and the radius is about 100 µm. 3D images give the profile of the notch for different samples.

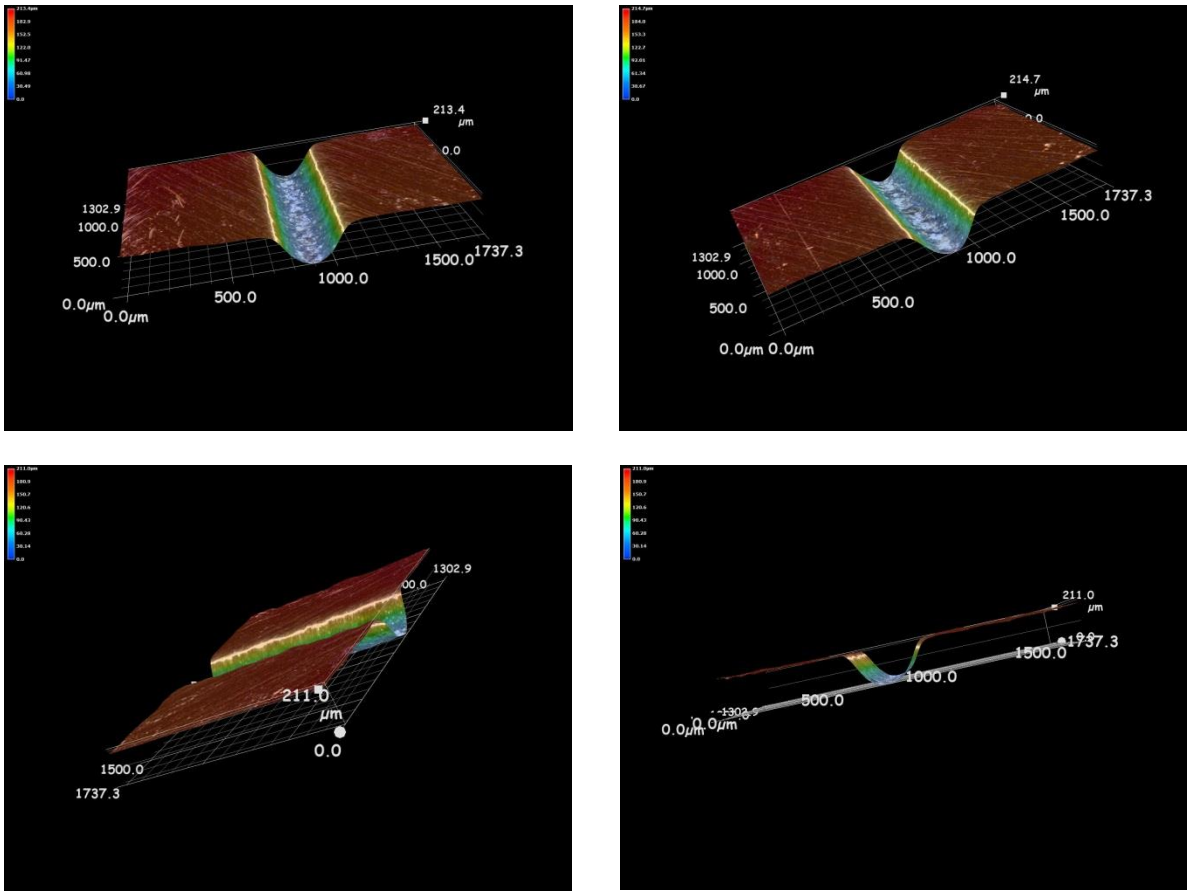

Figure 4.10: 3D photos of TR750-LNS SPT linear notched surface specimens.

4.2.2 SPT in Ar-3.5%H_2 gas mixture and in air

Fig. 4.11 shows the SPT load-displacement curves of TR750-LNS tested at 300°C in air and in Ar-3.5%H_2 with a velocity of 0.5 mm/min. With these conditions, no obvious effect of the linear notch on the mechanical properties is visible. Therefore, the SPT curves of TR750-LNS specimens do not differ from that recorded on smooth specimens or VHTS specimens. Furthermore, even at higher temperature, 400°C, there was also no large distinct difference between the two atmospheres on the mechanical property of TR750-LNS.

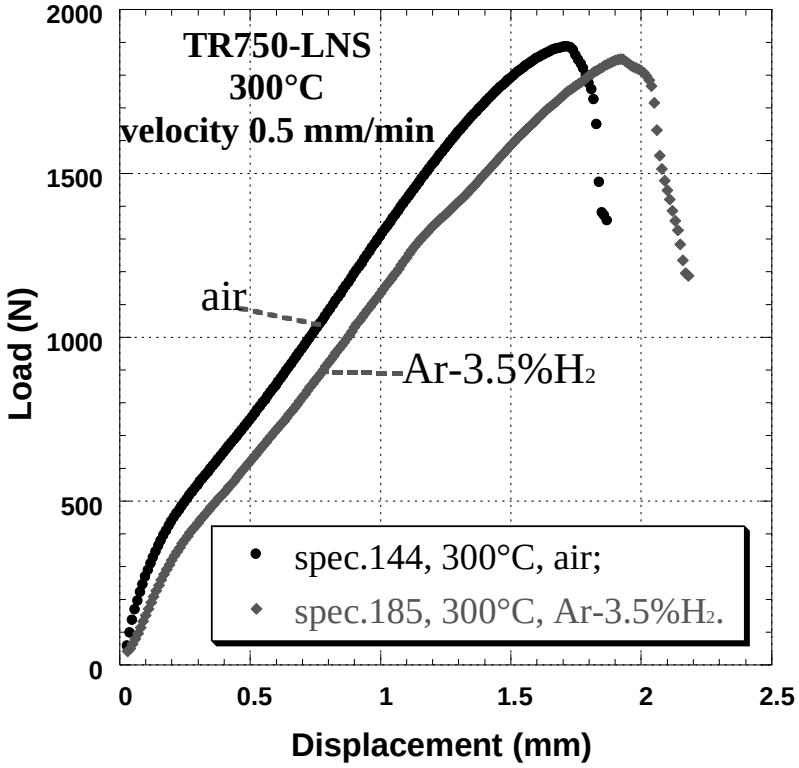

Figure 4.11: SPT curves of TR750-LNS specimens tested at 300°C in air and in Ar-3.5%H_2 with a velocity of 0.5 mm/min.

With this geometry, strain localized inside the notch and sprayed out on the dome. Crack initiated first at the root of the notch, extended along the notch and then turned off to join a circular crack (Fig. 4.12). SEM investigation on the fractured TR750-LNS tested in air or in Ar-3.5%H_2 indicates that the fracture is ductile in the temperature range of room temperature to 400°C.

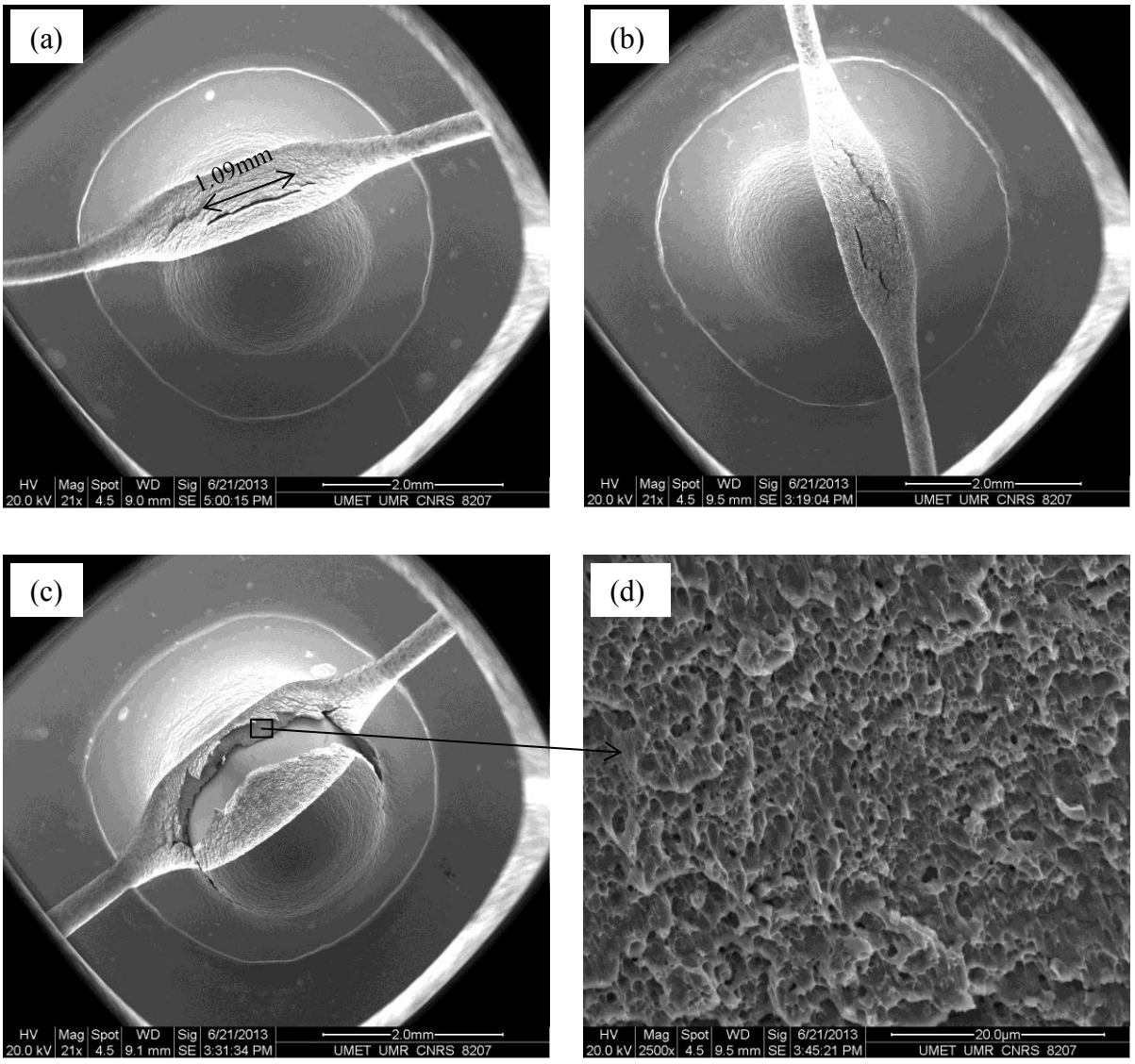

Figure 4.12: SEM images of TR750-LNS specimens tested at a velocity of 0.5 mm/min: (a) 300°C in Ar-3.5%H_2 (spec.161); (b) RT in air (spec.143); (c) 400°C in Ar-3.5%H_2; (d) is the ductile fractured surface of specimen corresponding to (c) with 'dimples'.

4.2.3 SPT in low oxygen LBE

Fig. 4.13 and Fig. 4.14 represent the SPT curves for tests performed at 300°C and 400°C respectively in low oxygen LBE at two displacement velocities 0.5 and 0.05 mm/min. Both diagrams contain curves related to tests in Ar-3.5%H_2 gas mixture on smooth and notched specimens. This allows appreciating the difference in load as a consequence of smaller volume of material in the notched specimen.

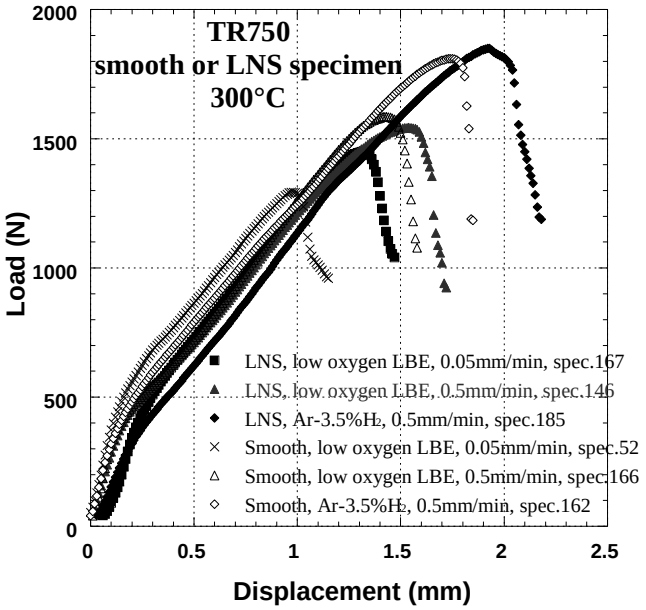

Figure 4.13: SPT curves of linear notched/smooth surfaces TR750 specimens tested at 300°C in Ar-3.5%H_2 and in low oxygen LBE with two different velocities (0.5, 0.05 mm/min).

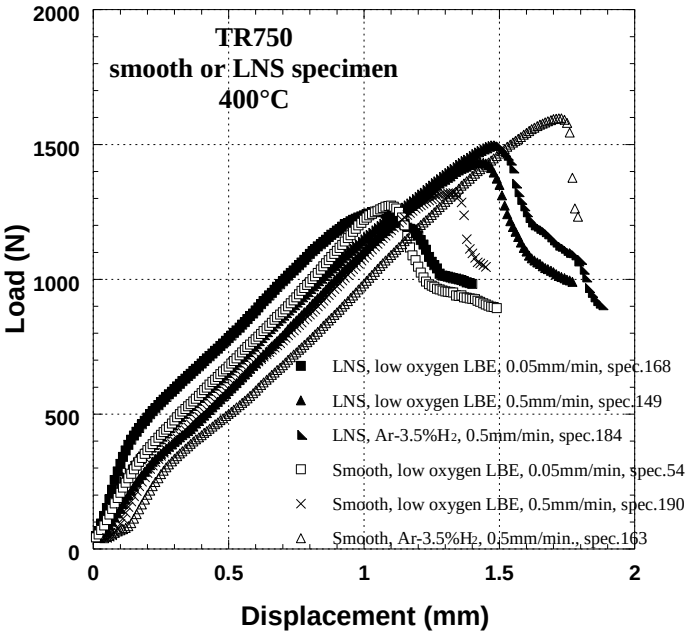

Figure 4.14: SPT curves of linear notched/smooth surfaces TR750 specimens tested at 400°C in Ar-3.5%H_2 and in low oxygen LBE with two different velocities (0.5, 0.05 mm/min).

It is found that the presence of the linear notch did not lead to a deleterious effect on the behaviour as well at 300°C as at 400°C. Even more, the loss of mechanical strength resulting from the reduction in displacement velocity for tests in low oxygen LBE on smooth specimen

tends to be reduced for notched specimens. That is, the difference in the behaviour between smooth and notched specimen is in fact only visible for the slowest test (0.05 mm/min) at 300°C. At 400°C, the recovery of properties again appears and the difference between notched and smooth specimen are in the range of scattering.

The SEM observations of the linear notched specimens punched in low oxygen LBE at 300°C and 400°C show that the linear notch does not influence the fracture feature (Fig. 4.15). Indeed, a main circular crack accompanied with short radial brittle cracks is present and seems to have been formed independently of the notch. No crack is observed in the groove of the notch. The fractured surface of the main crack is ductile and contains a cleavage zone at the outside edge as it occurred for smooth specimen.

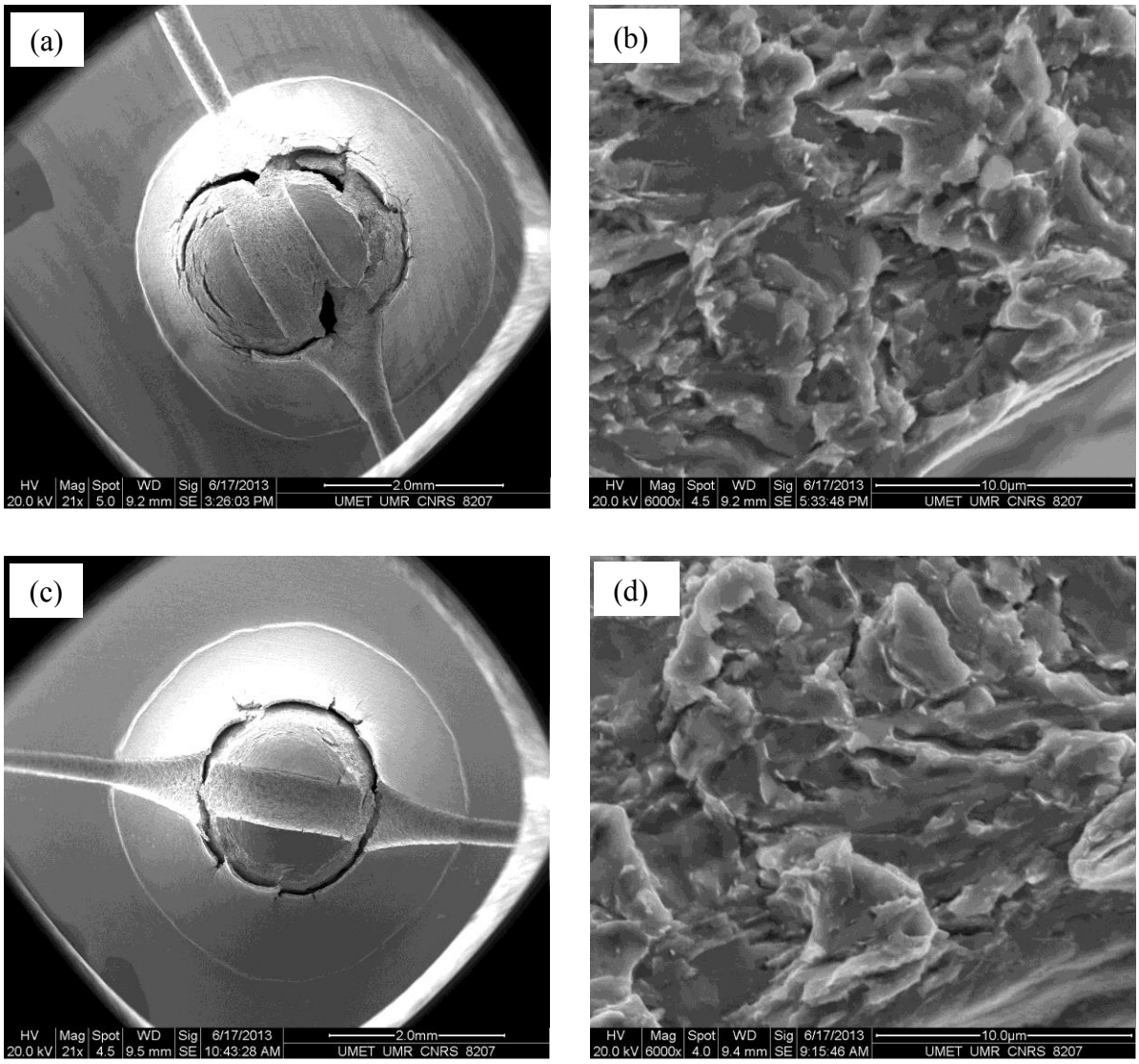

Figure 4.15: SEM images of TR750 steel SPT LNS with displacement velocity=0.5 mm/min in low oxygen LBE: (a) at 300°C (spec. 147), (b) fracture surface near outside of the star radiation brittle crack at 300°C (spec. 148), (c) at 400°C (spec. 150), (d) fracture surface near outside of the star radiation crack at 400°C with cleavage (spec. 151).

4.2.4 Conclusion

The effects of linear notches on the surfaces of TR750 SPT specimens have been investigated in neutral environment (air or Ar-3.5%H_2) and in liquid low oxygen LBE. The result indicates that the linear notch did not obviously modify the mechanical behaviour of TR750 steel in LBE since the variations in the mechanical values are within the scattering range (Fig. 4.16). In terms of fracture, no basic change has been noticed.

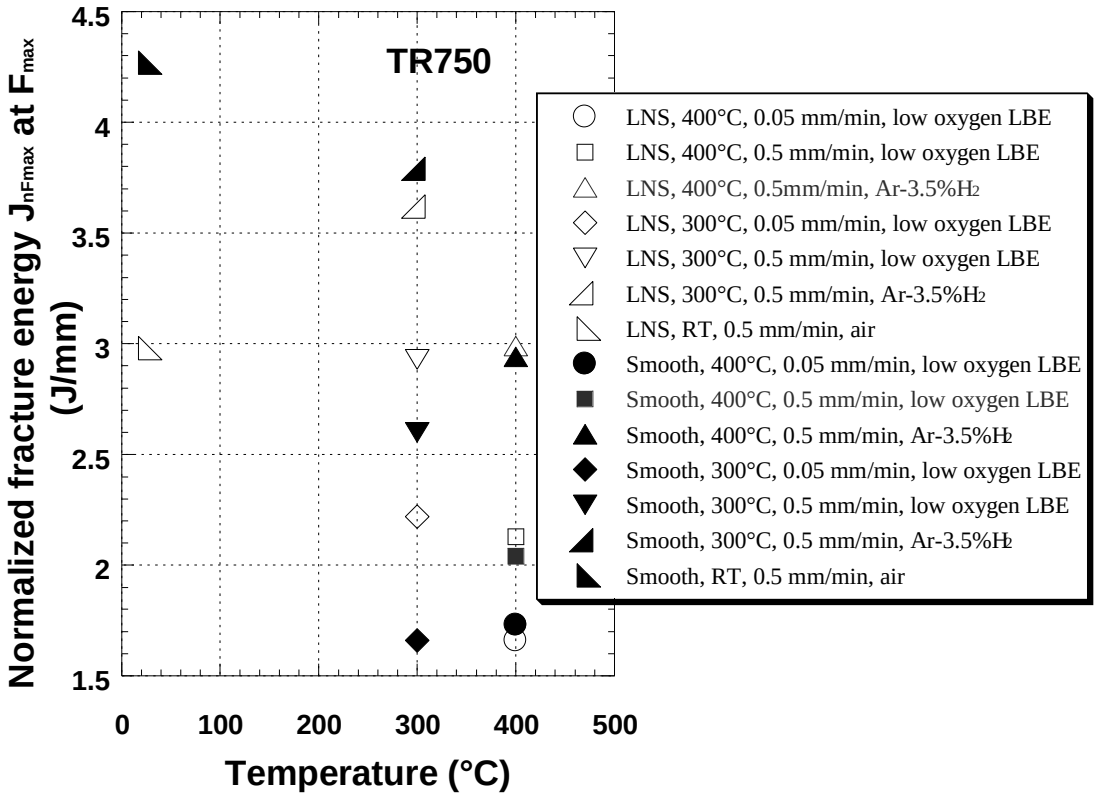

Figure 4.16: Normalized fracture energy J_{nFmax} at F_{max} according to the temperature and the experimental condition (the points are the average value).

4.3 Tensile tests performed on the smooth and notched surfaces cylindrical TR750 specimens in LBE

As mentioned in chapter I, when a metal specimen is tested under conditions of biaxial or triaxial tension, a high level of tensile stress can be attained and brittle fracture by cleavage

can be promoted. Nevertheless, Nicaise et al. [NIC-2001-B] showed that the presence of a notch in a tensile specimen of TR750 steel did not change the fracture, the material being deformed in air or in saturated oxygen LBE at 200°C and a displacement velocity of 0.12 mm/min.

In light of the results presented in the previous chapter, especially considering that the displacement velocity and the oxygen content are first order and second order respectively key factors, it was decided to run tests on smooth and notched cylindrical TR750 specimens at 300°C in oxygen saturated LBE and in low oxygen LBE at low displacement velocities. Therefore, a circular V-notch around the gage of a cylindrical tensile test TR750 specimen as described in chapter II is employed. In addition, in this thesis, the process for preparing the tensile tests TR750 specimens (smooth and V-notch) is after standard heat treatment.

4.3.1 The mechanical response of tensile tests on TR750 in oxygen saturated LBE and in low oxygen LBE

Tests were performed at cross-head velocity of 0.12, 0.005, 0.0005 mm/min to obtain a deformation of 10^{-4} s^{-1}, 4×10^{-6} s^{-1}, 4×10^{-7} s^{-1} respectively. Only the experimental load-displacement curves are drawn in order to appreciate the effect of notch on the values of the load. To calculate the mechanical tensile characteristics of smooth specimens (Table 4.1), the stress was calculated by dividing the measured force by the initial section (S_0=12.56 mm^2) and the strain was obtained by dividing the measured displacement by the initial length of the tensile test specimen (L_0=20 mm).

Fig. 4.17a and Fig. 4.17b show the experimental curves of tensile tests performed at 300°C in both oxygen saturated LBE and low oxygen LBE on cylindrical TR750 smooth and notched specimens respectively. The tensile tests conditions and the values of key points measured in the tensile tests of TR750 at 300°C in LBE (oxygen saturated/low oxygen) are summarized in Table 4.1.

All the curves in Fig. 4.17a exhibit the same shape whatever the test condition. No sudden load drop as it can be observed on TR500 is noticed (see the results of section 1.4 in chapter I).

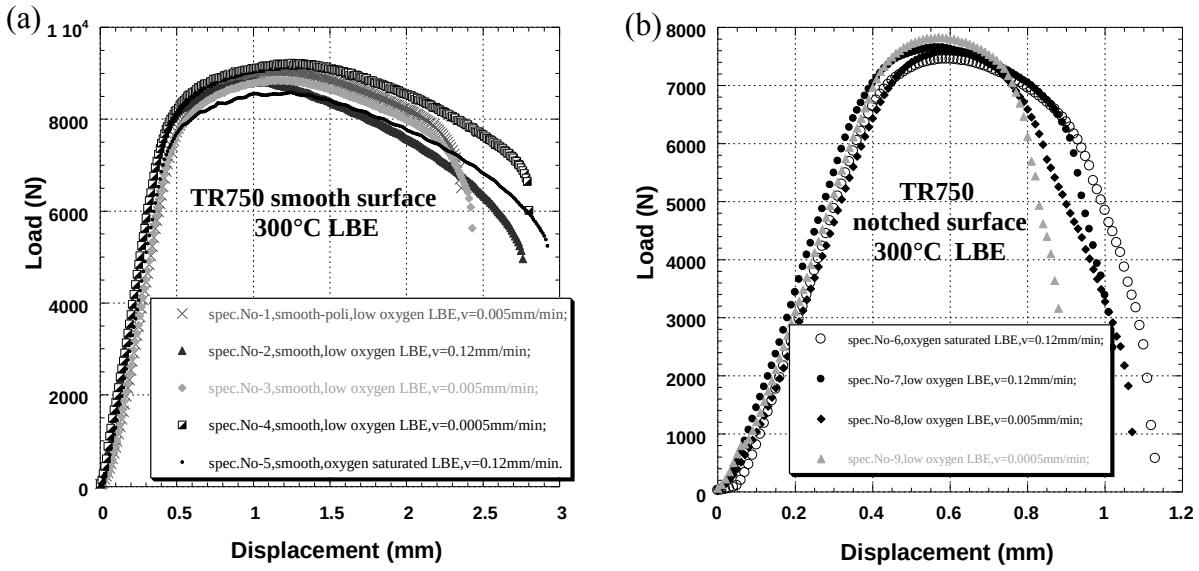

Figure 4.17: Tensile tests performed on cylindrical TR750 specimens at 300°C in LBE (oxygen saturated/low oxygen) using the constant cross-head speed of 0.12, 0.005, 0.0005 mm/min: (a) Load-displacement curves tested on the smooth surface specimens; (b) Load-displacement curves tested on the notched surface specimens.

Table 4.1: Values of key points measured in the tensile tests of TR750 in LBE (oxygen saturated (noted SO)/low oxygen (noted LO)) at 300°C.

Specimen No.	1	2	3	4	5	6	7	8	9
Surface state	Smooth-poli	Smooth	Smooth	Smooth	Smooth	Notch	Notch	Notch	Notch
LBE [O] state	LO	LO	LO	LO	SO	SO	LO	LO	LO
Velocity (mm/min)	0.005	0.12	0.005	0.0005	0.12	0.12	0.12	0.005	0.0005
F_e (N)	7943	7903	7935	7939	7577	6853	6829	7046	7329
d_{Fe} (mm)	0.53	0.42	0.55	0.45	0.48	0.40	0.37	0.44	0.43
F_{max} (N)	9024	8828	8852	9224	8584	7456	7688	7596	7832
d_{Fmax} (mm)	1.19	1.00	1.16	1.25	1.25	0.57	0.56	0.58	0.57
d_{max} (mm)	2.36	2.76	2.44	2.80	2.95	1.11	1.02	1.06	0.9
σ_{YS} (MPa)	648	648	635	651	648	/	/	/	/
σ_{UTS} (MPa)	722	703	705	734	699	/	/	/	/
Brittle area proportion (%)	28	17	25	23	16	ductile	ductile	ductile	ductile

The result clearly indicates that the oxygen content in LBE (oxygen saturated/low oxygen) does not have the obvious effect on the mechanical response of smooth surfaces TR750 specimens (spec.2 and spec.5) tested at 300°C with a velocity of 0.12 mm/min.

Surprisingly, the SEM observation indicates that the fractured surfaces of specimen fractured in LBE (oxygen saturated LBE and low oxygen LBE, spec.2 and spec.5 respectively) exhibit a mixture of ductile and brittle areas, the latter being located at the outside edge of the round fractured surfaces. The proportions of brittle area are 17% and 16% respectively for the low oxygen LBE and the saturated oxygen LBE (Fig 4.18). Decreasing the velocity from 0.12 to 0.0005 mm/min for tests on smooth surface TR750 specimens (spec.2 and spec.4) at 300°C did not result in clear variation of mechanical properties. The variation of the yield stress and the ultimate tensile strength are in the range of scattering. Let us note that the electro polished and the non-polished specimen tested at a velocity of 0.005 mm/min (spec.1 and spec.3) have similar mechanical properties leading to the conclusion that the surface state is not of prime importance for these test conditions (Figs. 4.18, 4.19).

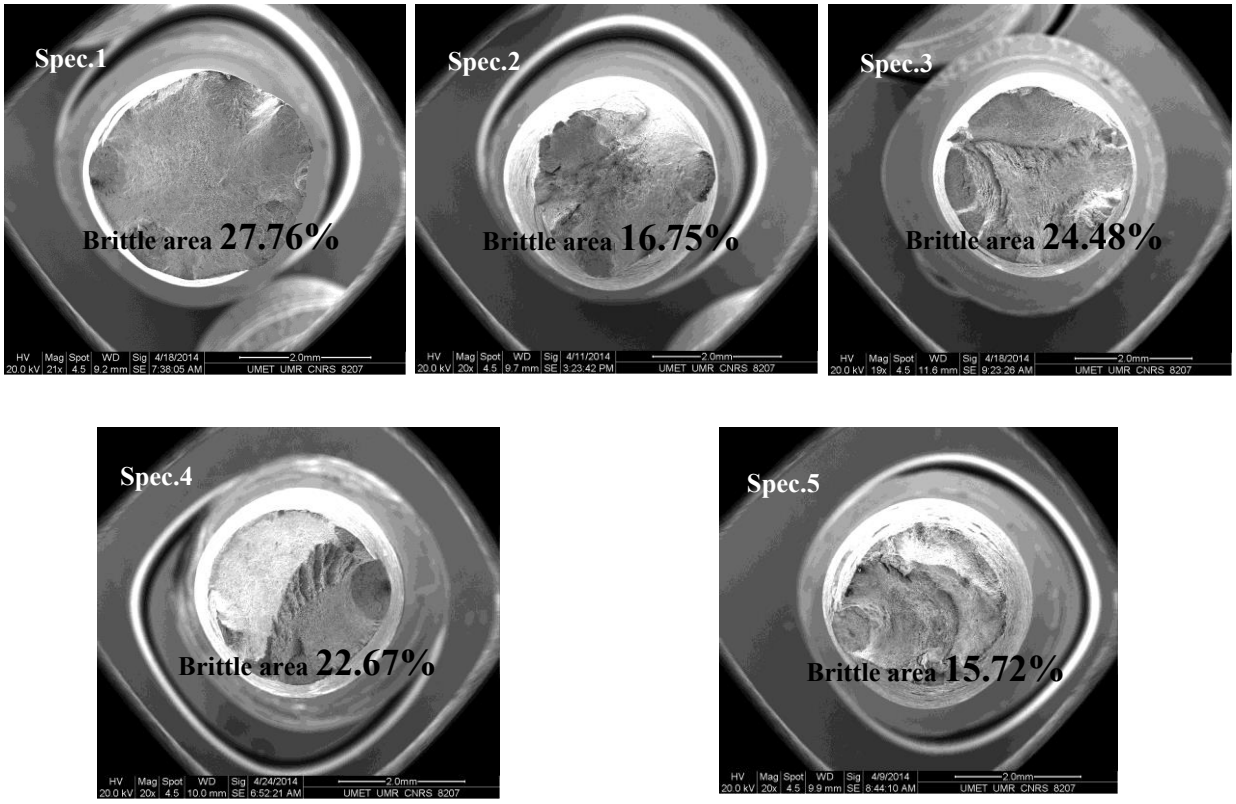

Figure 4.18: SEM images of smooth surfaces TR750 tensile specimens tested in LBE (oxygen saturated/low oxygen) at 300°C with three different velocities (0.12, 0.005, 0.0005 mm/min).

The main effect of the velocity is to modify the proportion of brittle and ductile areas. It increases with decreasing the velocity, about 16% for the test at 0.5 mm/min and 23% for the test at 0.005 mm/min. For specimen 4, tested at 0.0005 mm/min, the brittle cleavage was located not only at the outside edge of the round fractured surface but also propagated into the center of round fractured surface and intertwined with the ductile dimples.

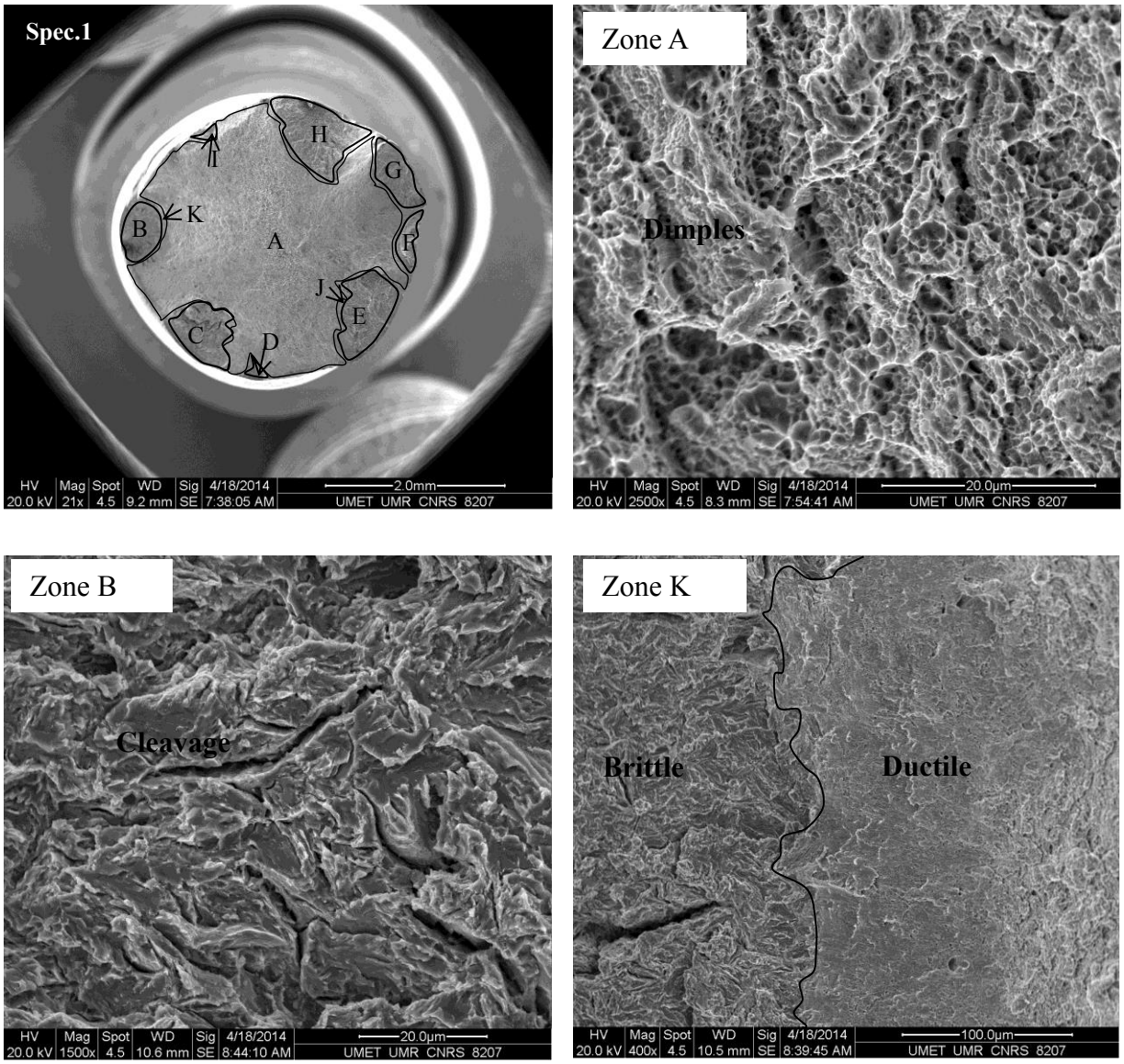

Figure 4.19: SEM images of TR750 tensile specimen (spec.1) with the smooth surface experienced electro-polish tested at 300°C with a velocity of 0.005 mm/min in low oxygen LBE.

For the notched specimens of TR750 tested at 300°C in LBE (oxygen saturated/low oxygen) at test velocities ranging from 0.12 to 0.0005 mm/min, the tensile curves (Fig. 4.17b) are also similar and the typical mechanical values are nearly the same. Again, no effect of oxygen is noticed (compare spec.6 and spec.7). Let us remark that the design of the notch did not produce very high load values as compared to the smooth specimen though it produced a strain localization as the displacement to fracture or the displacement at maximum load indicated. Furthermore, all the fractured surfaces present the ductile characteristics with large 'dimples', and there is no traces of brittle (Figs. 4.20, 4.21). For example, the notched surface tensile test specimen 6 shown in Fig. 4.21, both the center zone A and the edge zone B exhibit the ductile characteristics 'dimples' on the fractured round surface.

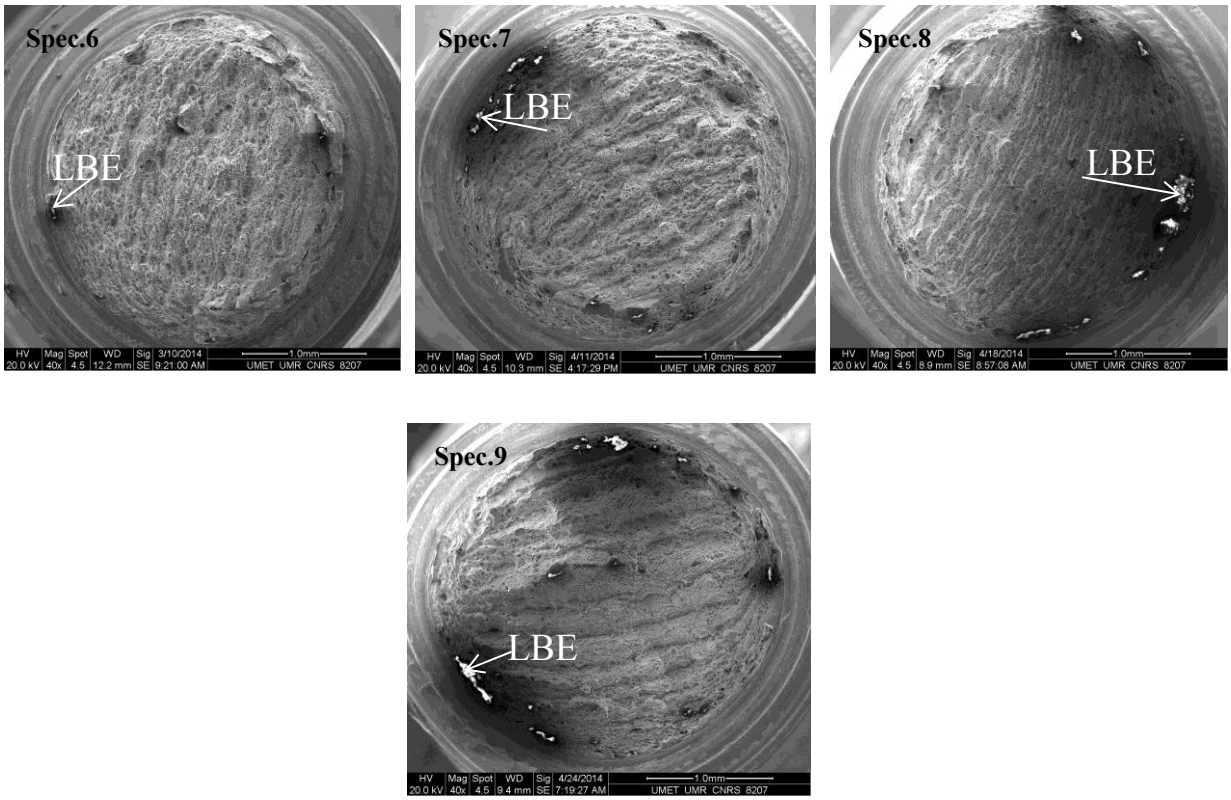

Figure 4.20: SEM images of notched surfaces TR750 tensile specimens tested in LBE (oxygen saturated/low oxygen) at 300°C with three different velocities (0.12, 0.005, 0.0005 mm/min).

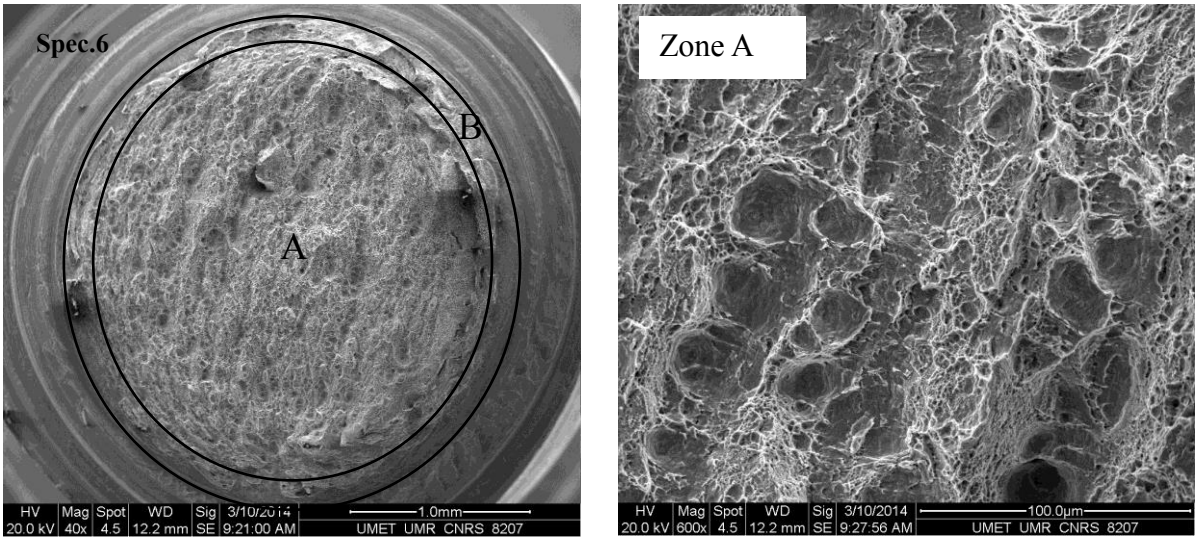

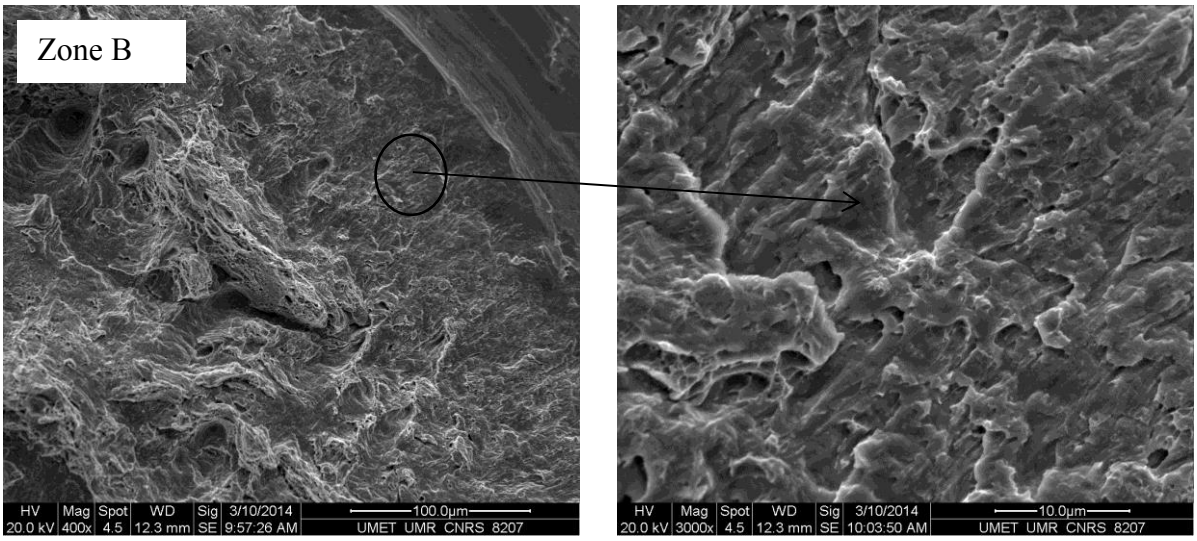

Figure 4.21: SEM images of notched surface TR750 tensile specimen (spec.6) tested at 300°C in oxygen saturated LBE with a velocity of 0.12 mm/min.

4.3.2 Conclusion

Tensile tests have been performed on smooth and notched specimen of TR750 in LBE (oxygen saturated/low oxygen) at 300°C by changing the test velocity (0.12, 0.005, 0.0005 mm/min). The mechanical behaviour and the fracture characteristics of TR750 have been studied with the help of SEM observation. The main conclusions are presented as follow:

(1) The effect of the notch is essentially visible by the decrease of displacement but not by the load values;

(2) All the smooth surface TR750 tensile specimens exhibit the mixed ductile and brittle characteristics fractured surfaces tested at 300°C in LBE (oxygen saturated/low oxygen). The brittle cleavage is normally placed at some zones near the outside edge of the round fractured surfaces and the large area ductile dimples locate mainly at the center of the round fractured surfaces. In addition, it is possible that the brittle fracture propagates into the center of the round fractured surface when conducted the tensile test at the lowest velocity of 0.0005 mm/min;

(3) All the notched surface TR750 tensile specimens have similar tensile curves and all the fractured surfaces exhibit the ductile characteristics with large ‘dimples’ without brittle traces;

(4) The estimate values of yield stress and ultimate tensile stress by tensile tests and the small punch tests (Table 4.1 and Table 3.5) are in good agreement for the yield stress (678±57

MPa by SPT, 646 MPa by tensile test at 0.0005 mm/min). For ultimate tensile strength, disagreement has been found. However, the ultimate tensile stress is 278±6 MPa by SPT and 713 MPa by tensile test.

4.4 Three-point bending tests in air and in LBE for quantitative investigation of LME effect on the mechanical properties of T91 steel

In this section, the quantitative assessment of the effect of liquid LBE on the crack propagation of material TR750 is attempted. Three-point bending tests with standard specimens (according to the ASTM-E1820) were done in liquid oxygen saturated LBE environment. The number of experiments and of data is limited due to the difficulty in handling so small specimens, especially when placing the specimen between rolls. Three-point bending tests were therefore performed only in liquid oxygen saturated LBE at 300°C with velocity 0.005 mm/min and in air at room temperature with two different velocities (0.5, 0.05 mm/min) for comparative study. Nevertheless, at least two specimens were tested per condition. In total, eight tests have been performed.

4.4.1 Mechanical response of three-point bending tests on material TR750 in air or in oxygen saturated LBE

The dimensions of the three-point bending test notched specimen fulfil the ASTM-E1820 standard described in Chapter II. The notch of the specimen was achieved by the micro-fine diamond disc. SEM observations confirmed the compliance with standard (Fig. 4.22).

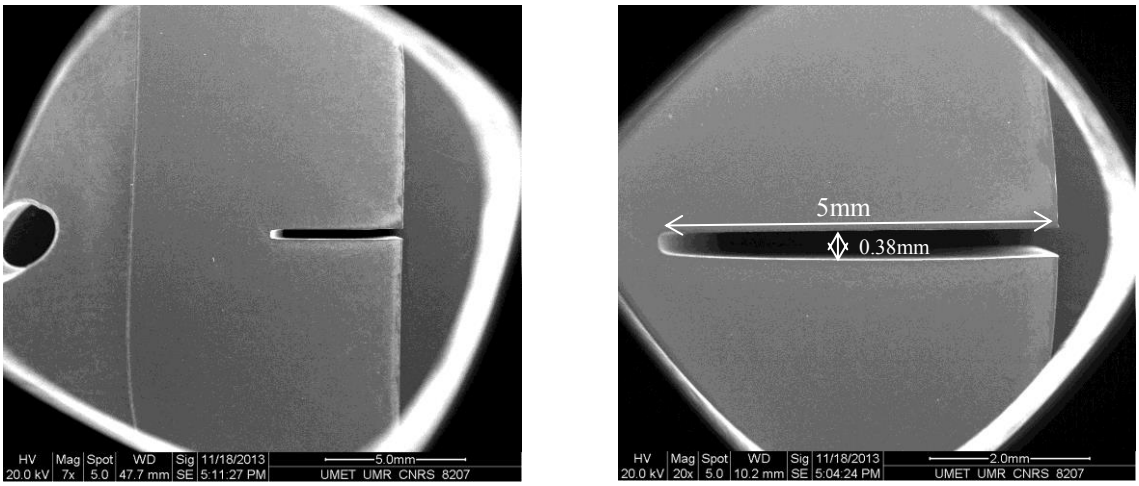

Figure 4.22: Notch dimensions of the three-point bending test specimen measured by SEM.

Fig. 4.23 presents the load-displacement curves of the TR750 specimens tested either in air or in liquid oxygen saturated LBE.

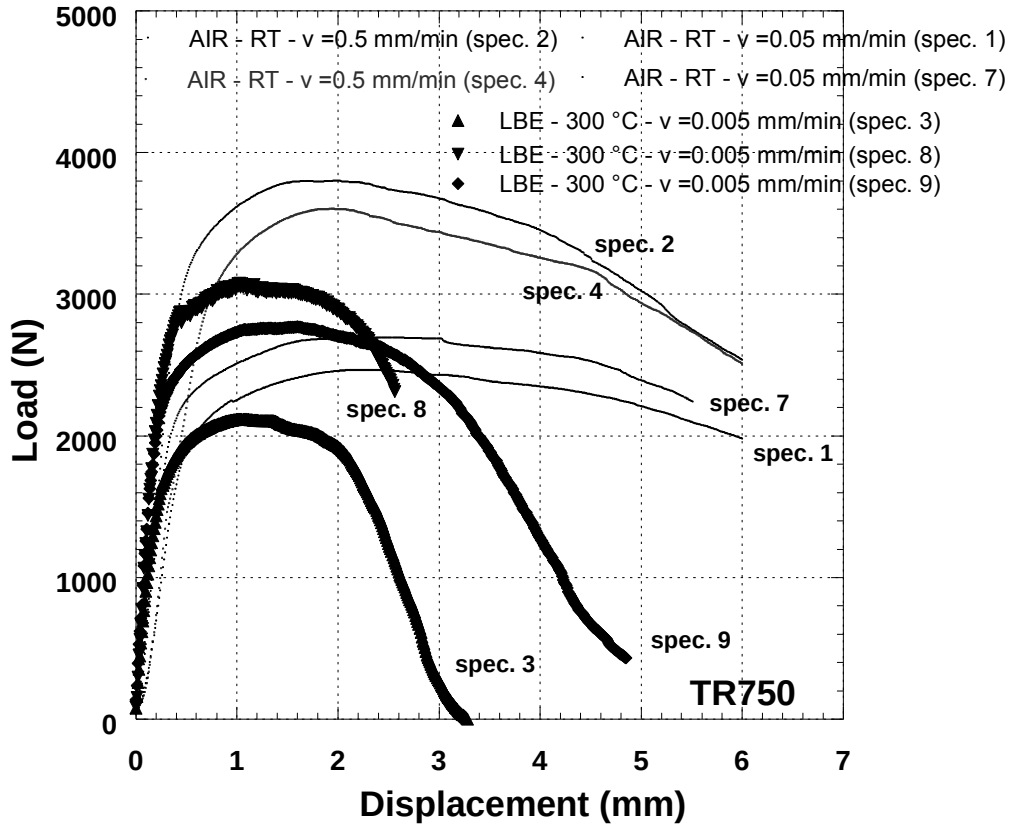

Figure 4.23: Three-point bending tests load-displacement curves of the material TR750 tested in air at room temperature with two different velocities (0.5, 0.05 mm/min) and or in oxygen saturated LBE at 300°C with a velocity of 0.005 mm/min.

All the curves start with a linear increase of the load and then, from a yielding point, tend to curve up to a maximum load. Then a decrease of the load, first moderate and then abrupt is recorded. The curves can be classified into two groups according the instability point between the moderate and abrupt decrease of the load. For tests at 300°C in LBE, the displacement corresponding to this stability point is ranging between 2 mm and 3 mm while at RT in air it is at least 4 mm and much over. SEM investigations are needed to explain the difference between these two groups of curves.

In air and at room temperature, the decrease of the velocity was reflected by a decrease of the yielding point and of the maximum load P_{max} and an increase of the instability point displacement.

4.4.2 SEM failure analysis of three-point bending tests

It can be seen from Fig. 4.24 that the specimen tested at RT in air exhibit very good plasticity and a very large bending deformation before rupture. SEM observation showed that all the specimens tested at this condition failed in a ductile fracture mode.

The crack length after test arrests at a displacement of 6 mm was depending on the velocity: average 0.87 mm for the rapid velocity condition (0.5 mm/min) against average 0.26 mm for the low velocity condition (0.05 mm/min).

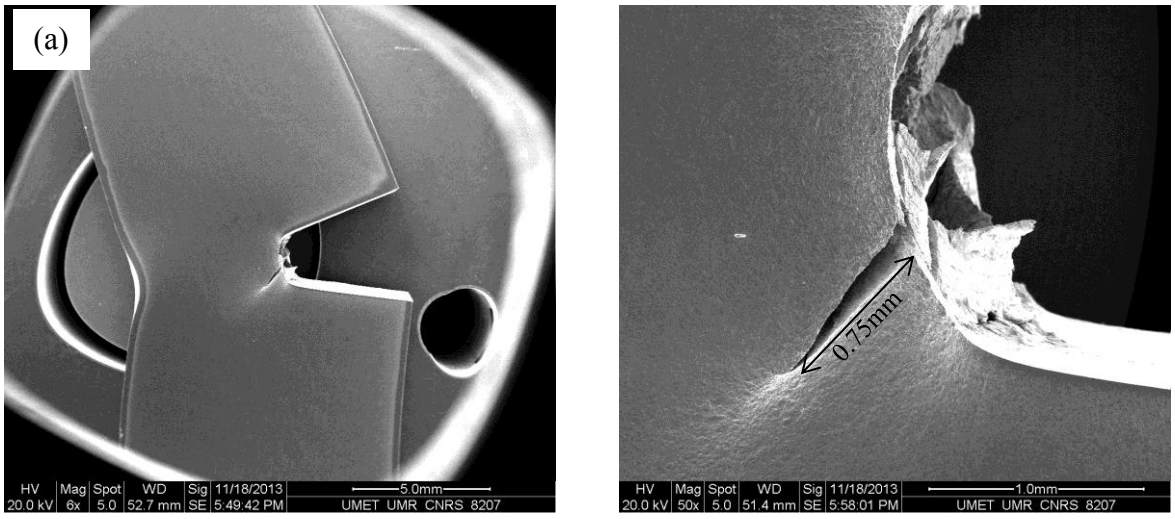

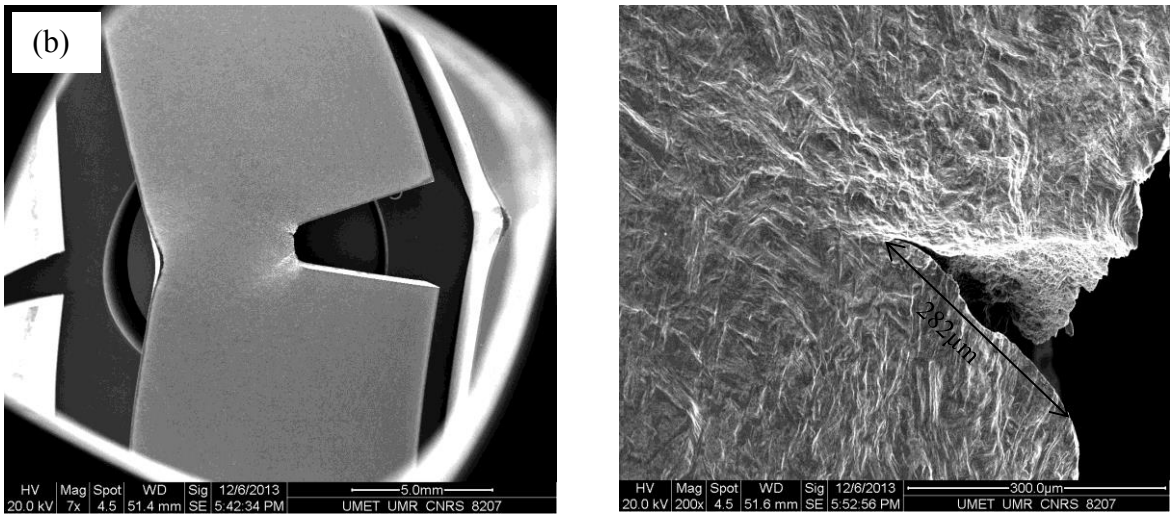

Figure 4.24: SEM images of three-point bending tests specimens in air at room temperature with different velocities: (a) 0.5 mm/min; and (b) 0.05 mm/min.

However, the morphology of three-point bending specimens of material TR750 tested at 300°C with velocity 0.005 mm/min in liquid oxygen saturated LBE is completely different from that in air. SEM observation shown by Fig. 4.25 indicates that material TR750 can fail without large plastic deformation.

Fig. 4.25a shows a specimen loaded up to the instability point and it is possible to see very short cracks at the corner of the notch which can be considered as the initial stage of the instable brittle crack. Indeed, when the test is completed, an entire crack propagated the specimen and the load fell to zero. Fig. 4.25b is the micrograph of a specimen containing a 4.33 mm long crack without large plastic deformation.

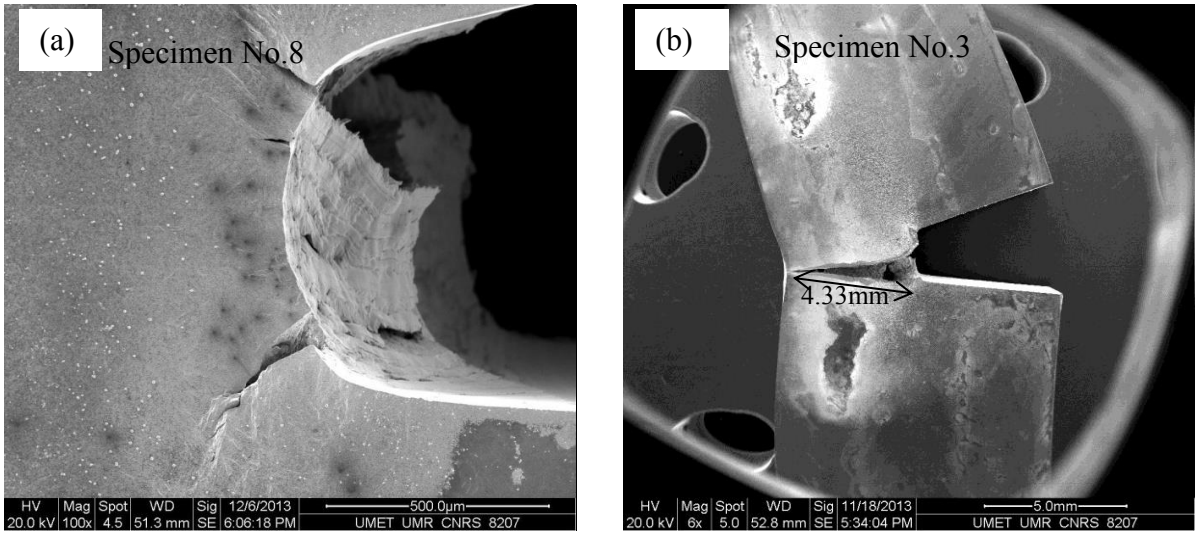

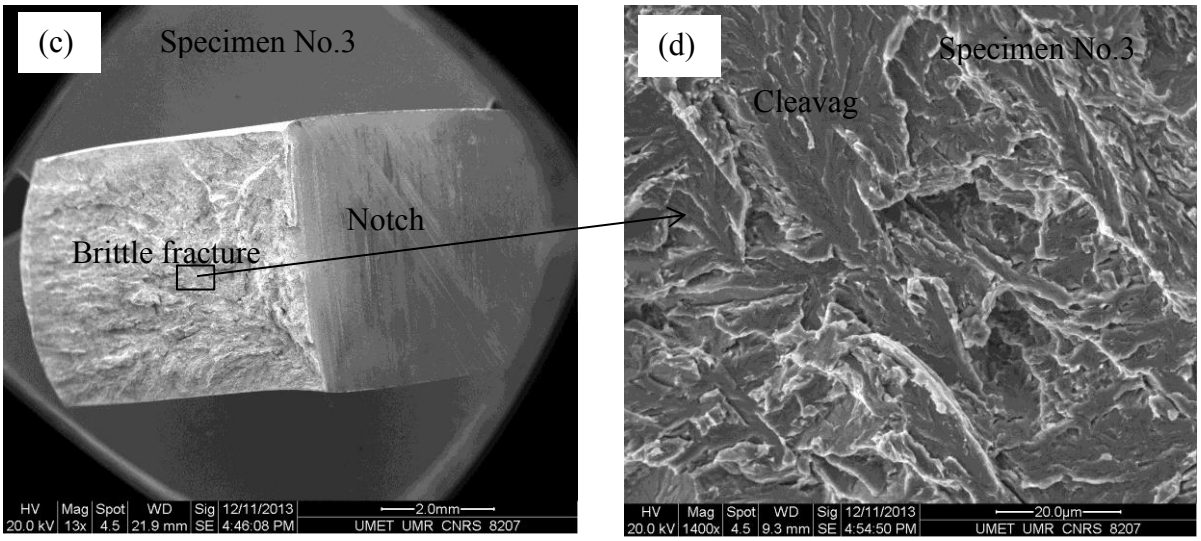

Figure 4.25: SEM images of three-point bending tests specimens in liquid oxygen saturated LBE at 300°C with velocity 0.005 mm/min: (a) specimen No.8, stop when failed happened (a_Q=0.33mm); and (b), (c), (d) specimen No.3, stop until the bend distance limit (a_Q=4.33mm).

The brittle fracture was confirmed from fracture surface analyses which unambiguously show mainly cleavage fracture and occasionally intergranular fracture without any trace of ductile fracture (Fig. 4.25 c, d).

4.4.3 Calculation of J-integral

The J-integral was calculated from three-point bending tests (as explain in chapter 2) in air at room temperature with two different velocities (0.5, 0.05 mm/min) or in liquid oxygen saturated LBE at 300°C with velocity 0.005 mm/min (Table 4.2). The verification of the final length of un-ruptured ligament was performed by SEM on all specimens to determine a_Q and b_Q=W-a_Q.

The standard ASME-E1820 [AST-2001] requires to calculate first an hypothetical stress intensity factor K_Q (stress intensity factor calculated from P_Q). All the three-point bending tests load-displacement curves are the type I (Fig. 2.10) and the ratios P_{max}/P_Q of all the specimens do not exceed or approximate to 1.10 (Table 4.2). Therefore, the equations 2.7 and 2.8 can be used to calculate K_Q corresponding to the load P_Q and to the crack length a_Q. Then, the quantity of $2.5(K_Q/\sigma_{YS})^2$ need to be calculated. The yield stress σ_{YS} of material TR750 is determined by the tensile tests and is equal to 646 MPa in liquid oxygen saturated LBE at 300°C with velocity 0.005 mm/min (chapter IV). In air at room temperature and for the velocities 0.5, 0.05 mm/min, the yield stress was calculated from the SPT curves. The used α

parameter for the equation 2.1 (chapter 2) is 0.33, verified for the T91 steel in air by Serre and Vogt [SER-2007]. Then we used this parameter to calculate the σ_{YS} in air and at room temperature. It is equal to 518 MPa for 0.5 mm/min and 586 MPa for 0.05 mm/min. After calculation, we verified that the quantity of $2.5(K_Q/\sigma_{YS})^2$ is significantly less than both the specimen thickness, B, and the length of the initial uncracked ligament, b_0, which confirms the good choice of dimensions according the ASME-E1820 standard.

Table 4.2: Dimensions of three-point bending tests specimens and calculation results of the J-integral for TR750.

Medium	V (mm/min)	T (°C)	a_Q (mm)	b_Q (mm)	P_{max} (N)	P_Q(N)	J_{el} (KJ/m^2)$^{j)}$	J_{pl}~J_Q (kJ/m^2)
Air	0.5	RT	0.75	9.25	3803	3239	**2.00**	**1574**
Air	0.5		0.99	9.01	3605	2858	**1.98**	**1458**
Air	0.5		0.86	9.14	2825	2597	**1.45**	**1223**
Air	0.05		0.23	9.77	2466	2233	**0.33**	**1053**
Air	0.05		0.28	9.72	2698	2388	**0.45**	**1088**
LBE	0.005	300	4.33	5.67	2120	1621	**4.73**	**380**
LBE	0.005		0.33	9.67	3080	2776	**0.79**	**561**
LBE	0.005		2.30	7.70	2771	2358	**3.43**	**810**

Based on the results of J_Q integral calculation (Table 4.2), the elastic component of J_Q (J_{el}) is really small and which can be ignored relative to the plastic component energy J_{pl} both in air and in liquid oxygen saturated LBE, even though the proportion of J_{el} seems to increase in presence of liquid oxygen saturated LBE.

In air and at room temperature, we note an influence of the displacement velocity. The J-integral and so the energy to the elastically and plastically deformation of the specimen and to initiate crack until the material final failure is more important for the higher velocity. In liquid oxygen saturated LBE at 300°C with velocity 0.005 mm/min, we note the lower values for the J-integral. Despite the no-similar conditions of tests in air and in LBE, the results indicate that the liquid oxygen saturated LBE plays an essential role in the propagation phase of brittle cracks of material TR750, in addition, the fracture toughness of TR750 in terms of the J-integral falls in the presence of liquid oxygen saturated LBE. So it is possible to conclude that the toughness decreases in presence of oxygen saturated LBE at low velocity (0.005 mm/min) and at 300°C.

4.4.4 Conclusion

Due to the difficulty of the experiments in LBE, bending tests were performed only in air at room temperature and in oxygen saturated LBE at 300°C. The fractured specimens were observed by SEM and the fracture toughness to quantitatively estimate the effect of liquid oxygen saturated LBE on the mechanical properties of material TR750 was calculated.

The main conclusions are:

(a) The embrittlement effect of liquid LBE on TR750 is very obvious based on the calculation of J_Q integral, and the presence of LBE promotes the decreasing of the J_Q value and so of the fracture toughness;

(b) The specimens tested in air exhibit very good plasticity and a very large bending deformation before rupture, and the fracture is ductile;

(c) At 300°C in oxygen saturated LBE and at velocity of 0.005 mm/min, the material can fail without large plastic deformation. The fracture is brittle with cleavage fracture and occasionally intergranular fracture without any trace of ductile fracture.

4.5. Conclusion

The effect of surface defects on the liquid LBE embrittlement sensitivity of TR750 steel was investigated by SPT performed on VHTS specimens, SPT performed on LNS specimens, tensile tests performed on smooth and V-notched surface cylindrical specimens, and three-point bending tests performed with the notched single edge specimens.

The main conclusions are:

(a) The surface defects of both the VHTS and the LNS on TR750 steel do not modify the global SPT response in liquid LBE. But in the case of the smaller defect (VHTS), we observed the fracture in the joined diagonals as an effect of LBE;

(b) The V-notched effect of the cylindrical tensile test specimen is essentially visible by the decrease of the displacement. In addition, all the V-notched surface TR750 tensile specimens fractured in ductile feature while the smooth surface TR750 tensile specimens fractured in the mixed ductile and brittle characteristics tested at 300°C in LBE (oxygen saturated/low oxygen);

(c) The notched single edge TR750 specimens tested in oxygen saturated LBE at 300°C by bending tests exhibited obvious LBE embrittlement sensitivity. The presence of the LBE assists the decreasing of the J_Q value and so of the fracture toughness.

CHAPTER V : AN EXPLANATION OF LIQUID LBE EMBRITTLEMENT OF T91 MARTENSITIC STEEL

As described in the previous chapters, liquid LBE embrittlement effect on martensitic T91 steel has been confirmed and investigated qualitatively and quantitatively. This chapter focuses on an interpretation of the experimental phenomena and opens a discussion on the mechanism of LBE embrittlement of T91 martensitic steel. In addition, the role of surface coating as a solution to prevent from LBE embrittlement is also presented in this chapter.

5.1 Interpretation and discussion on LBE induced embrittlement phenomena of T91 steel

Concerning the LBE induced embrittlement of T91 steel, there exists a model that represents qualitatively the phenomenon but the starting hypotheses of this model are rather restrictive. Based on the abundant experimental results obtained in this PhD thesis, it is possible to propose an enhanced explanation of the phenomenon and the related mechanism can be applied for much numerous situations. This is the objective of the present section.

5.1.1 Identification of the key parameters promoting LBE embrittlement of T91 steel

The present investigations conducted in this PhD thesis confirm the need to take into account properly the loading parameters (temperature, strain rate, notch effect) susceptible to affect LME. Having taken into account, one of the specificities of LME which states that no material can be considered as immune against LME is borne out. The LBE embrittlement of T91 steel is actually a tough and complex problem. Anyway, we have obtained some qualitative and quantitative results of the fracture characteristics (ductile or brittle) of T91 steel after standard heat treatment (TR750) tested in a temperature range from RT to 400°C, in different mediums (air, Ar-3.5%H_2 gas mixture, oxygen saturated LBE, low oxygen LBE), at different strain rates and with the influence of notch size.

Table 5.1 summarizes the experimental conditions where brittle or ductile (or a mixture of both) fracture was observed in T91-TR750 material after tests in a temperature range from RT to 400°C in different mediums (air, Ar-3.5%H_2 gas mixture, oxygen saturated LBE and low oxygen LBE) by three different mechanical test methods (Small punch test, three-point bending test, tensile test) with five different velocities (0.12, 0.5, 0.05, 0.005, 0.0005 mm/min). The determination of brittle or ductile feature is made from the fracture analysis and with the mechanical response.

Table 5.1: Fracture mode (ductile/brittle) of T91-TR750 specimens tested according loading parameters.

Mechanical test method	Surface state	Medium	Temperature (°C)	Velocity (mm/min)	Ductile	Brittle	Very marked brittle
Small Punch Test	Smooth surface	AIR	RT	0.5	Fully	No	/
				0.05	Fully	No	/
			200	0.5	Fully	No	/
			250		Fully	No	/
			300		Fully	No	/
			400		Fully	No	/
		Ar-3.5%H_2	200		Fully	No	/
			300		Fully	No	/
			400		Fully	No	/
		Oxygen saturated LBE	200	0.5	Fully	unobvious	/
			250	0.5	Fully	unobvious	/
				0.05	Mainly	Little	/
				0.005	Mainly	Little	/
				0.0005	Mainly	Little	/
			300	0.5	Mainly	Little	/
				0.05	Mainly	Little	/
				0.005	Mainly	Large	/
				0.0005	Little	Yes	Yes
			400	0.5	Mainly	Little	/
				0.05	Mainly	Little	/
				0.005	Fully	unobvious	/
				0.0005	Fully	unobvious	/
		Low oxygen LBE	130	0.005	Fully	unobvious	/
			200	0.5	Fully	unobvious	/
				0.005	Mainly	Little	/
			250	0.5	Fully	unobvious	/
				0.05	Mainly	Little	/
				0.005	Mainly	Large	/
			300	0.5	Mainly	Little	/
				0.05	Mainly	Little	/
				0.005	Little	Yes	Yes
				0.0005	Little	Yes	Yes
			400	0.5	Mainly	Little	/
				0.05	Mainly	Little	/
				0.005	Mainly	Large	/
				0.0005	Fully	unobvious	/
	VHTS surface	AIR	RT	0.5	Fully	No	/
			300	0.5	Fully	No	/

See following table

		Ar-3.5%H_2	300	0.5	Fully	No	/
			400	0.5	Fully	No	/
		Oxygen saturated LBE	250	0.5	Fully	unobvious	/
				0.05	Mainly	Little	/
				0.005	Mainly	Little	/
			300	0.5	Mainly	Little	/
				0.05	Mainly	Little	/
				0.005	Mainly	Large	/
			400	0.5	Mainly	Little	/
				0.05	Mainly	Little	/
				0.005	Fully	unobvious	/
		Low oxygen LBE	300	0.5	Mainly	Little	/
			400	0.5	Mainly	Little	/
	LNS surface	AIR	RT	0.5	Fully	No	/
			300	0.5	Fully	No	/
		Ar-3.5%H_2	300	0.5	Fully	No	/
			400	0.5	Fully	No	/
		Low oxygen LBE	300	0.5	Mainly	Little	/
				0.05	Mainly	Little	/
			400	0.5	Mainly	Little	/
				0.05	Mainly	Little	/
Three point bending tests	Notched single edge specimens	AIR	RT	0.5	Fully	No	/
				0.05	Fully	No	/
		Oxygen saturated LBE	300	0.005	No	Yes	Yes
Tensile tests	Smooth surface	Oxygen saturated LBE	300	0.12	Mainly	Large brittle area <30%	/
		Low oxygen LBE		0.12			/
				0.005			/
				0.0005			/
	Smooth surface polish			0.005			/
	V-notched surface	Oxygen saturated LBE	300	0.12	Fully	No	/
		Low oxygen LBE		0.12	Fully	No	/
				0.005	Fully	No	/
				0.0005	Fully	No	/

From the present results obtained in this PhD thesis, there are at least three main points to be mentioned which clarify the sensitivity to liquid LBE embrittlement of T91 steel:

1) T91 steel in its standard heat treatment (here referred as TR750 steel) can be embrittled in liquid oxygen saturated LBE if a slow strain rate is applied and even without any initial defect present on the surface;

2) LBE with low oxygen content is not a necessary and sufficient condition to evoke LME;

3) There is an effect of notch but it can be present or in the process of forming before loading. The effect of notch depends on its size, and a critical size of the order of few grains seems to appear critical.

According to the reports in literature, several researchers have studied the liquid LBE embrittlement effect of T91 steel from the aspects of surface defects effects, including the microcracks and the macroscopic large notch, from the aspect of chemistry of LBE and from the aspect of heat treatments. Basically, our results do not contradict the literature though some differences can be noted which can help to more precisely assess the risk of liquid LBE embrittlement with physical arguments.

Let us remember that, in 2000, our laboratory (Unité Matériaux Et Transformations, Lille) was the first who claimed that T91 could be embrittled by liquid metals including Pb, LBE and Sn [NIC-2001-A] [VOG-2002] [VOG-2004]. Nevertheless, the effect was only observed on the hardened heat treatment material TR500 steel loaded at a strain rate of 10^{-4} s^{-1} in oxygen saturated LBE at 260°C or in liquid lead in a temperature range of 350°C to 425°C using the notched cylindrical surface specimen. At that time, if any of these conditions was not respected, then the fracture was ductile. Moreover, it was really believed that liquid LBE embrittlement could not be observed on TR750 with the explored experimental conditions.

Dai et al. [DAI-2006-A] found that liquid LBE embrittlement effect of T91 steel in the standard heat treatment (TR750) was possible. During this research period, emphasis was put on the role of LBE chemistry. And indeed, some (but not all) of the dog-bone shaped flat specimens deformed at a slow strain rate (1×10^{-5} s^{-1}) in low oxygen LBE (1 wppm oxygen) in a temperature range of 250°C to 425°C exhibited the LME. Nevertheless, they admitted that the brittle fracture was observed on specimen that contained microcracks on the lateral surfaces indicated while it was not observed for those without microcracks. On the other hand, LBE embrittlement effect was indicated by some variation in the tensile curve after necking, that is to say the yield and ultimate tensile strengths and uniform elongation were not affected by LBE. The propagations of the microcracks on the lateral surfaces of the specimens filled with LBE at tips are much deeper than those without LBE.

Van den Bosch et al. [BOS-2006], [BOS-2008] also noticed the importance of notch at the surface of specimen to trigger liquid LBE embrittlement. Their tensile test results on smooth

specimen surface of T91 steel (standard heat treatment) in liquid low oxygen LBE at strain rate varying from 1×10^{-3} to 1×10^{-6} s^{-1} in a temperature range from 150°C to 450°C did not lead to brittle fracture. Only their notched samples showed LME. The notched specimens (60° opening angle; notch radius <0.025 mm) were tested at 200°C using a strain rate of 5×10^{-5} s^{-1} and had partly brittle fracture at the rim of the specimen or disc-shaped in tension (DCT) T91 steel (approximate standard heat treatment) specimens were tested at 200°C and a displacement rate of 0.25 mm/min [BOS-2009]. They mentioned an important role of the sharpness of the crack.

Besides, in addition to the role of defect or crack, all the above mentioned researches insist on the necessity to wet the crack tip. Therefore, the mechanism of LBE induced embrittlement of T91 based on the surface energy reduction by atoms of the liquid metal, here Pb or Bi, proposed and confirmed by numerical simulation by Unité Matériaux Et Transformations [NIC-2001-A] [VOG-2002] [VOG-2004] is strengthened and accepted by most researchers. Note that the adsorption induced reduction in cohesion model (SJWK model) could also fit our experimental evidence since it predicts weakening of the interatomic bonds at region of high stress concentrations, and then cleavage crack growth by breaking bonds at the crack tip. Ahead an existing crack tip, the interatomic bonds are stressed by the both tensile stress σ and shear stress τ components (Fig. 5.1).

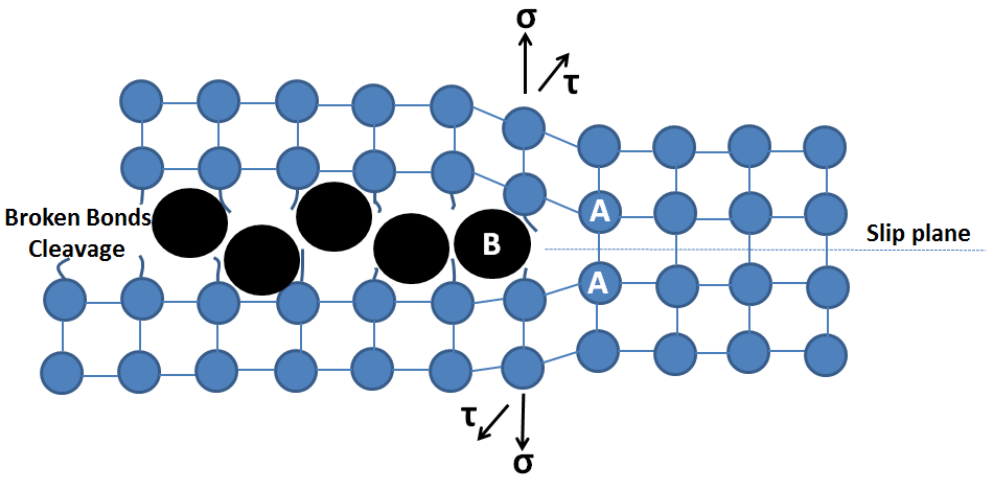

Figure 5.1: Schematic illustration of LBE embrittlement effect on TR750 steel. The bond A-A constitutes the crack tip of the material TR750 steel. B is a surface active liquid LBE atom.

If the shear stress is promoted, then dislocations sources are activated and either ductile fracture or liquid metal assisted damage occurs depending on the efficient presence of atoms

of a liquid metal. If not, then the fracture mode will depend on the resistance to tensile stress of the interatomic bonds, and finally the brittle fracture occurs when the local stress intensity factor K_I approaches the toughness of the material (K_{IC} or J_{IC}). This means that locally, ahead the crack, the real critical stress intensity factor in case where foreign atoms have adsorbed the crack tip, is not K_{IC} (the bulk toughness) but K_{ICloc}.

The question is how to reach first K_{ICloc} before K_{IC}. Since the Griffith criterion for the expansion of a crack is a function of E (Young modulus), γ_s (surface energy) and the crack length, any evolution of one (or more) of these term will affect the toughness of the material. From the present investigation, it turns out that the strain rate helps the initiation and growth of short crack wetted by LBE, and this event occurs more rapidly than nucleation and growth of micro void in the bulk.

5.1.2 The mechanism of liquid LBE embrittlement of T91 steel

The following explanation is proposed:

- For TR500, K_{IC}, the bulk critical stress intensity factor (toughness) is rather low. It will be easy to have a low value of K_{ICloc}.
    - Nevertheless, in air, a surface short crack under tensile loading has a local stress intensity factor K_{Iloc}, which increases very slowly during increasing loading and remains inferior to K_{ICloc}, here equal to K_{IC} the bulk critical stress intensity factor, allowing damage initiation in the bulk of the material. The fracture is ductile.
    - However, in LBE, the same value of K_{Iloc} is encountered but due to adsorption of Pb or Bi atoms, K_{ICloc} is decreased and K_{Iloc} exceeds the value of K_{ICloc}. LME occurs and propagation of brittle crack is triggered before damage initiation in the bulk of the material.

- For TR750, K_{IC}, the bulk critical stress intensity factor (toughness) is rather high. It will be less likely to have a low value of K_{ICloc}. In LBE, even with the adsorption of Pb or Bi atoms, K_{ICloc} is not enough affected so that K_{Iloc} reaches the value of K_{ICloc}. LME is not triggered and damage by void nucleation and growth occurs in the bulk of the material. The fracture is ductile. This mechanism is valid for high strain rate.

What is the contribution of the strain rate in LME of TR750?

When TR750 is deformed, slip bands emergence and misorientation between martensitic laths and between grain boundaries fracture the protective native oxide layer. Slip band/matrix interfaces, lath boundaries and grain boundaries constitute a microstructural defect nucleation site. SEM (Figs. 5.2a, 5.2b) and 3D optical surface profiler (Figs. 5.2c, 5.2d) techniques were employed to appreciate the roughness resulting from deformation by SPT.

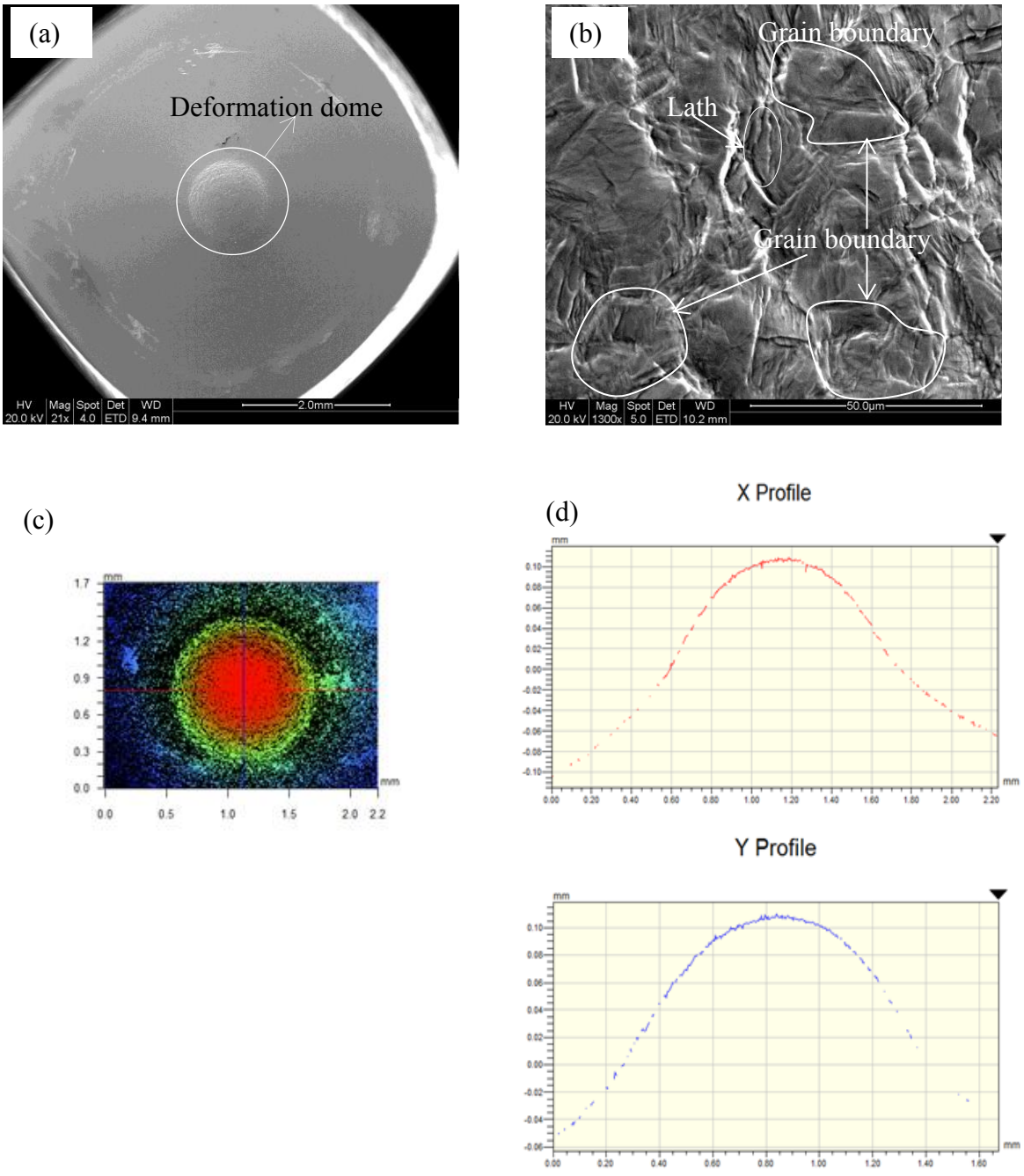

Figure 5.2: SEM and 3D optical surface profiler photos for analyzing the elastic or plastic deformation of material TR750 tested at 300℃ in air with a velocity of 0.005 mm/min (SPT 0.20mm-832N, No.246, deformation value=110µm).

The interesting phenomenon is that the grain boundary and the martensitic laths are clearly revealed in accordance with the degree of deformation, and the stress concentration and the early crack initiate position may be considered to occur at this place.

Fresh material is exposed to LBE, Pb or Bi atoms which can adsorb and an environmental effect is possible. Besides, the nucleation and growth of micro void in the bulk is still valid and is a pure mechanical effect, see Fig. 5.3.

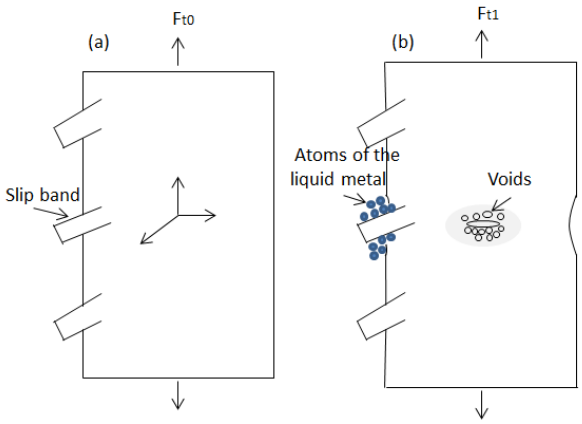

Figure 5.3: Schematic illustration of brittle atoms (LBE or lead) adsorption at slip band of T91 steel during deformation from the original state (a) F_{t0} to (b) F_{t1}.

- If the strain rate is high, static emerging slip bands or roughness at grain boundaries or martensite lath boundaries are formed. Pb or Bi may adsorb but oxidation of fresh material occurs. Pb or Bi atoms have no effect and bulk damage resulting from triaxiality effect governs the fracture mode. A fully ductile fracture is observed.
- If the strain rate is low, emergence of slip bands or roughness at grain boundaries or martensite lath boundaries are expected as a more continuous event. At the beginning of deformation, Pb or Bi atoms adsorb and oxidation of the fresh metal surface also occurs but the oxide layer is continuously destroyed. Penetration of Pb or Bi atoms at the slip band/matrix interface or martensite lath interface is possible. This leads to have much larger surface to be wetted by Pb or Bi atoms resulting in breaking a large number of atomic bonds. Therefore, the local toughness K_{ICloc} can be reached because a synergic effect between strain rate and of Pb or Bi atoms allows an increase of the crack length together with a decrease of the surface energy. LME occurs before the bulk damage.

- If the strain rate is medium, both phenomena described above occur competitively resulting in a mixed ductile-brittle fracture. The brittle fracture is located near the out part of the specimen and the ductile fracture is located in the center of specimen.

The present explanation clearly shows the LME occurrence will depend as well on the ease to grow a brittle crack as the ease to initiate and growth a bulk defect. And this is confirmed by the macro notch specimen (tensile or linear notch specimen). In these specimens, strong stress triaxiality develops very rapidly in the bulk of the specimen and controls the damaging process (Fig. 5.4).

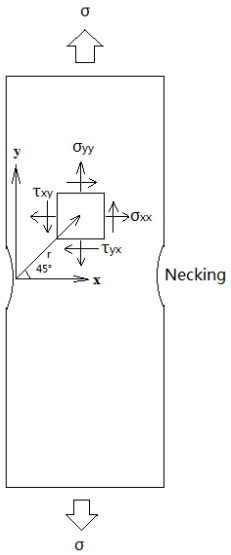

Figure 5.4: Tensile test stresses near the necking zone of the smooth surface TR750 specimen.

- **Role of oxygen content**. Loading the material in oxygen saturated LBE or in low oxygen LBE does not modify the mechanism. The less oxygen atoms in LBE accelerate the initiation of brittle crack at the interface between slip band and matrix. The purity of LBE plays a role but not as strong as it was expected at the beginning of the work. Indeed, a fully oxygen free LBE would be necessary for that.
- **Role of temperature**. A ductility trough has been pointed out. The effect of temperature is obvious but complex. It modifies as well the properties of the solid material (the T91 steel) such as yield strength and toughness as of the liquid metal (LBE) such as viscosity and wettability.
- **Highlight of the synergic effect between plastic deformation and environment.**
  To check the synergic effect between plastic deformation and environment, a series of SPT were done at 300°C and 400°C by maintaining the specimen in LBE under load

(0N, 500 N, 800 N, 1000N) for a given duration (0 h or 4 h) before doing the SPT. Then the SPT were done at 300°C or 400°C in low oxygen LBE at a velocity of 0.5 mm/min. No effect of maintaining period was observed. The curves exhibit the same shape (Figs. 5.5 and 5.6) and the fracture was the same that the specimen were directly punched or punched after maintaining period.

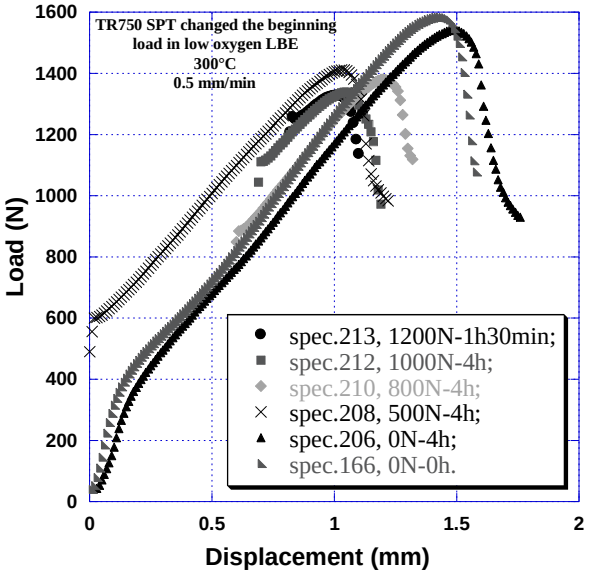

Figure 5.5: SPT curves of TR750 tested at 300°C in low oxygen LBE with a velocity of 0.5 mm/min changed the beginning load (0N-0h, 0N-4h, 500N-4h, 800N-4h, 1000N-4h and 1200N-1h30min).

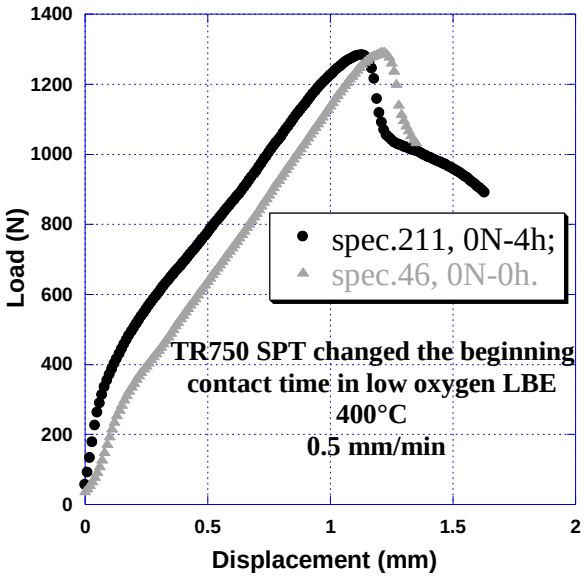

Figure 5.6: SPT curves of TR750 tested at 400°C in low oxygen LBE with a velocity of 0.5 mm/min changed the beginning contact time (0N-0h, 0N-4h).

In the same way, secondary ion mass spectrometry (SIMS) analyses were carried out on TR750 specimen deformed in low oxygen LBE at 300°C at a velocity of 0.005 mm/min by SPT up to the entrance of the plastic deformation. The first sample was loaded up to 500 N and immediately unloaded for SIMS investigation. The second specimen was loaded up to 450 N and maintained for two days in LBE before unloading.

After removing the LBE layer, the SIMS analysis did not point out a homogenous partition of Pb or Bi atoms in surface and no presence of Pb or Bi was measured in the sub-surface (100 nm in depth). The Pb or Bi atoms did not diffuse inside of the specimens at the early elastic or plastic stage. We must admit that it was difficult to find traces of Pb or Bi at the grain boundaries even though the signals of Pb and Bi were a little bit more pronounced at the stress concentration points (Fig. 5.7) which could comfort LBE embrittlement at these places.

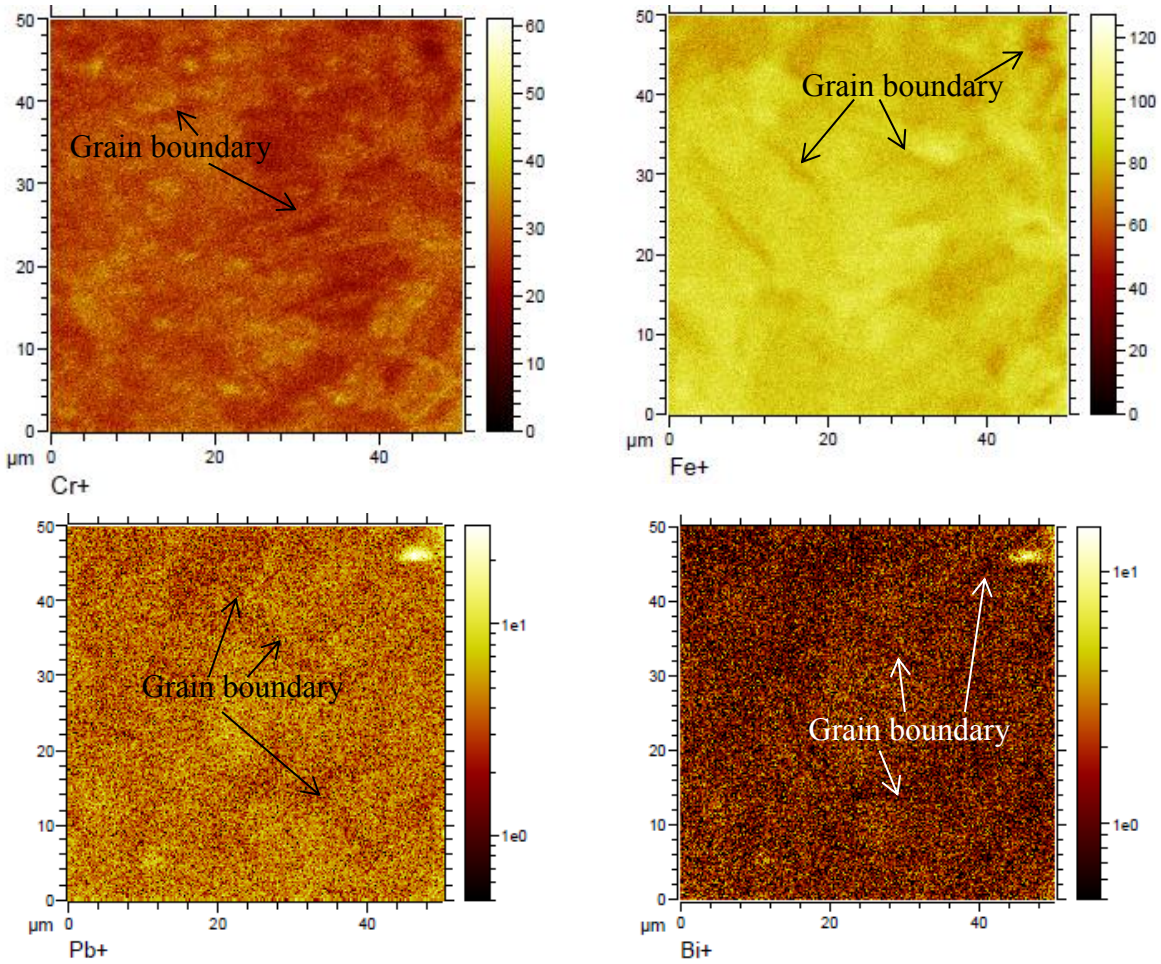

Figure 5.7: SIMS analysis of TR750 SPT specimen No.267 tested at 300°C in low oxygen LBE with a velocity of 0.005 mm/min and stopped early at 500N.

For the specimen kept in liquid low oxygen LBE two days with 450N, the trace of bismuth was found around the grain boundary but not clearly the lead (Fig. 5.8).

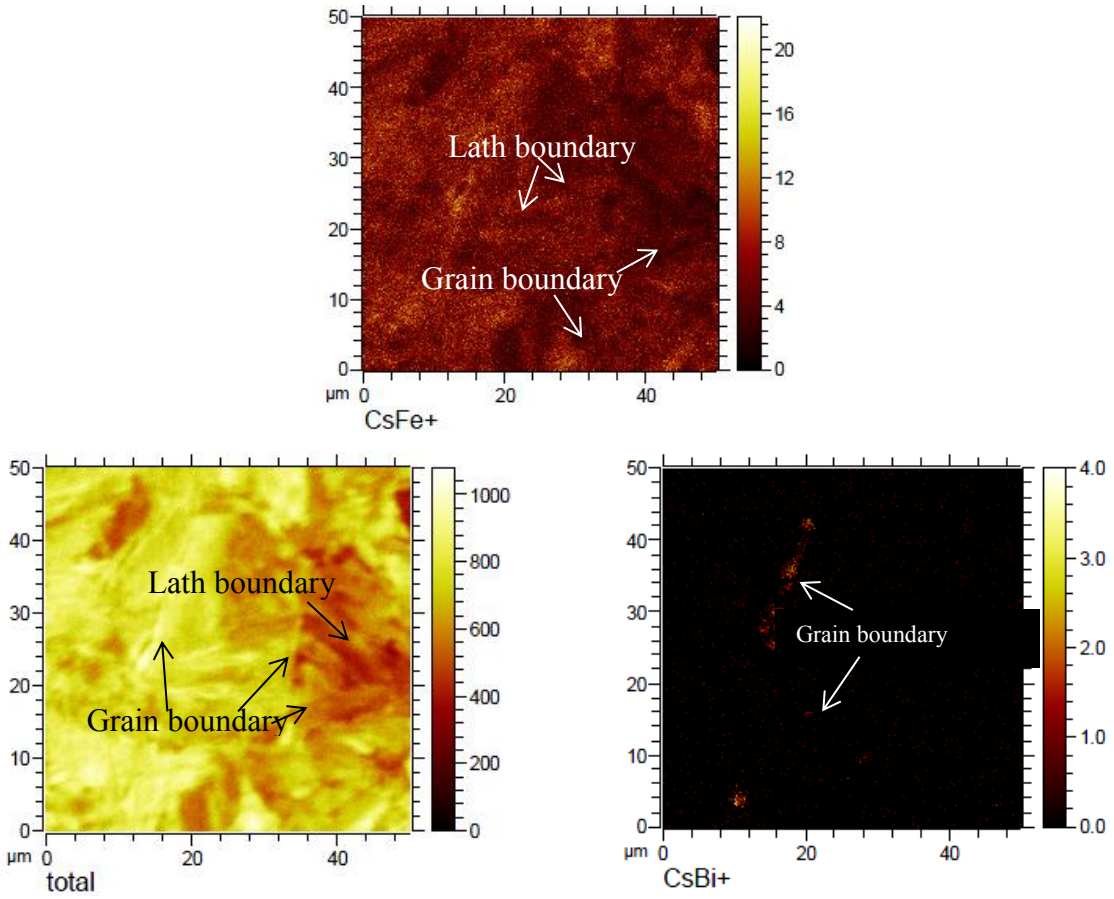

Figure 5.8: SIMS analysis of TR750 SPT specimen No.272 tested at 300°C in low oxygen LBE with a velocity of 0.005 mm/min and kept at 450N for two days then stopped.

These analyses are the preliminary exploratory study for confirming the proposed mechanism of liquid LBE embrittlement sensitivity of T91 steel. We are aware of the too few amounts of SIMS investigations and it is necessary to continue in this way.

5.2 Tentative solution to overcome LBE embrittlement on T91 steel

Since liquid LBE embrittlement is possible even for T91 in its standard heat treatment, and taking into account that it results from the synergic effect between plastic strain kinetics and adsorption effects, it appears that the surface of T91 must avoid the contact with LBE and must remained protected even when plasticity induced roughness develops. During the PhD thesis, we had the opportunity to work with the Center of Nano Science and Technology of the Italian Institute of Technology (ITT), Torino, Italy. ITT Torino is developing advanced coatings ($FeCrAlY/Al_2O_3$) which appeared to be very protective against LBE corrosion (see

chapter I) [GAR-2013]. Therefore the behaviour of T91 steel covered with such coatings has been tested by SPT in LBE.

Different surface coating structures have been processed on the T91 SPT specimens and are described hereafter in four groups:

- Group I: 5µm Al_2O_3 deposited on a 250nm bonding layer FeCrAlY
  Specimens n°.274-3 and n°.282-4
- Group II: 5µm Al_2O_3
  Specimens n°.275-5, n°.280-9
- Group III: 1µm Al_2O_3
  Specimens n°.276-6, n°.279-7, n°.283-10
- Group IV: 1µm Al_2O_3 deposited on a 250nm bonding layer FeCrAlY
  Specimens n°.278-1, n°.281-2, n°.284-8 (the surface treatment technique is not stable for these specimens)

All the surface treatment specimens were tested in liquid oxygen saturated LBE with very low velocity 0.0005 mm/min, the most deleterious situation for T91 in its standard heat treatment. The SPT curves were compared with those obtained on uncoated specimen tested in the same environment (Fig. 5.9).

The SPT curves indicate that all the surface coatings have a positive effect on the mechanical response of material TR750 in liquid oxygen saturated LBE, because both the values of maximum load (F_{max}) and the displacement at the maximum load (d_{Fmax}) are improved compared to the uncoated specimen. However, there is a scattering in the responses. For instance, the specimen No.276-6 (1µm Al_2O_3) and No.284-8 (250nm bonding layer FeCrAlY and 1µm Al_2O_3) of the groups III and IV have very high load values and displacement values in comparison with other specimens of the same group. These specimens have very good results for protecting TR750 in liquid oxygen saturated LBE environment with obvious ductile curves characteristics, both the values of maximum load and displacement at the maximum load are approaching the values of T91 tested in air and in liquid oxygen saturated LBE at a rapid velocity (0.5 mm/min), see Fig. 5.10.

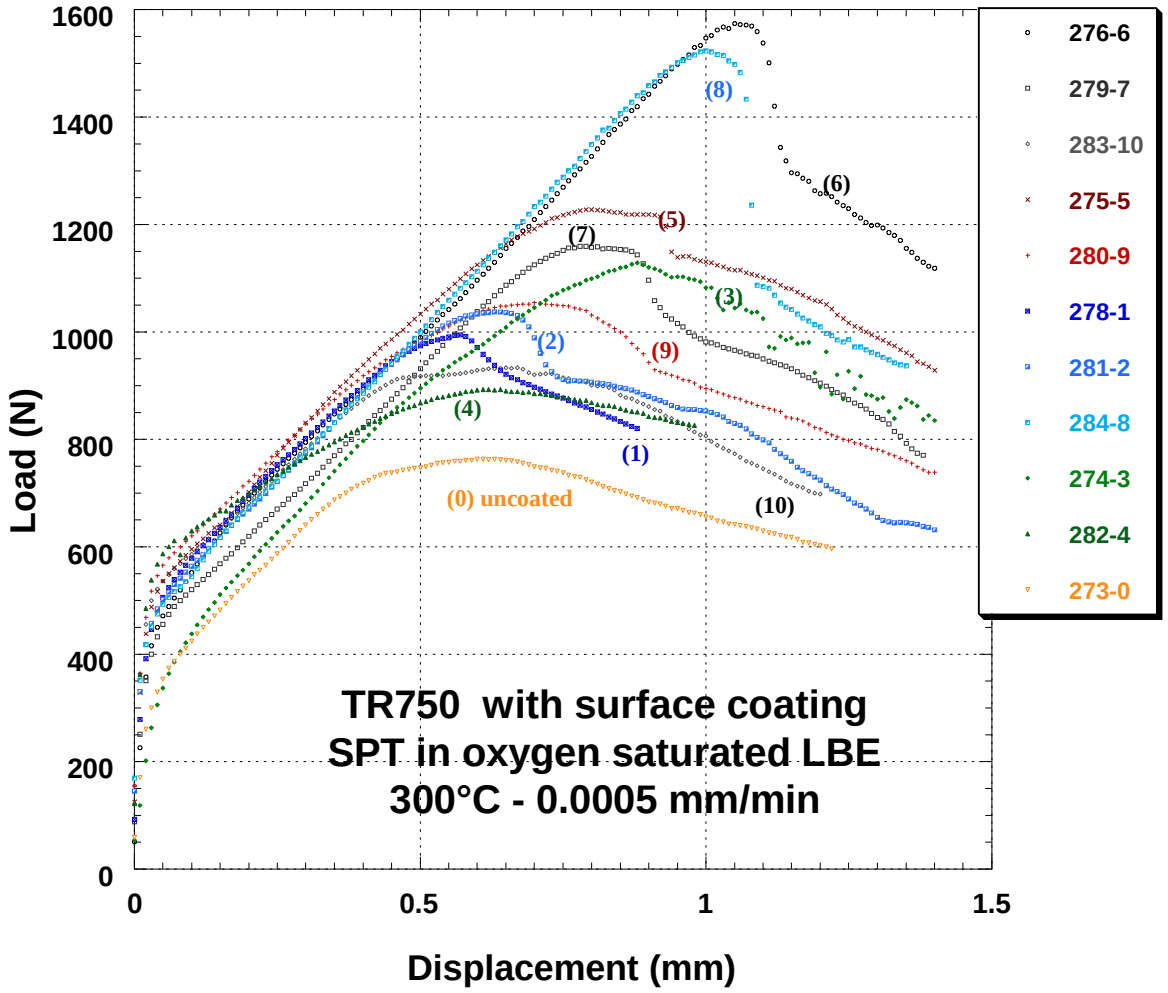

Figure 5.9: SPT curves of material TR750 after different surface treatment techniques tested at 300°C in liquid oxygen saturated LBE with lowest velocity 0.0005 mm/min, contrast curve is employed without surface coating.

Specimens n°.274-3, n°.282-4: 5µm Al_2O_3 deposited on a 250nm bonding layer FeCrAlY;
Specimens n°.275-5, n°.280-9: 5µm Al_2O_3 ;
Specimens n°.276-6, n°.279-7, n°.283-10: 1µm Al_2O_3 ;
Specimens n°.278-1, n°.281-2, n°.284-8: 1µm Al_2O_3 deposited on a 250nm bonding layer FeCrAlY.

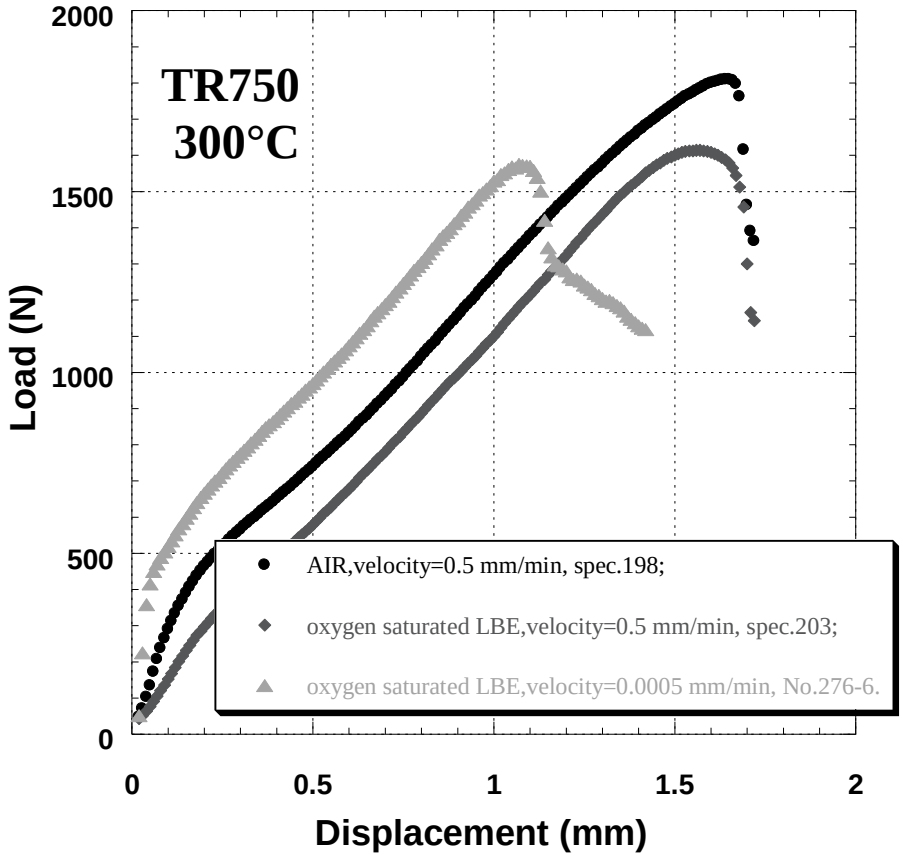

Figure 5.10: SPT curves of material TR750 tested at 300°C in liquid oxygen saturated LBE with surface coating at lowest velocity 0.0005 mm/min, contrast curves tested in air and in liquid oxygen saturated LBE with rapid velocity 0.5 mm/min are employed.

The observations of the fractured specimens will state on the effect of the coating. Fig. 5.11 is macroscopic views of some of the specimens fractured by SPT.

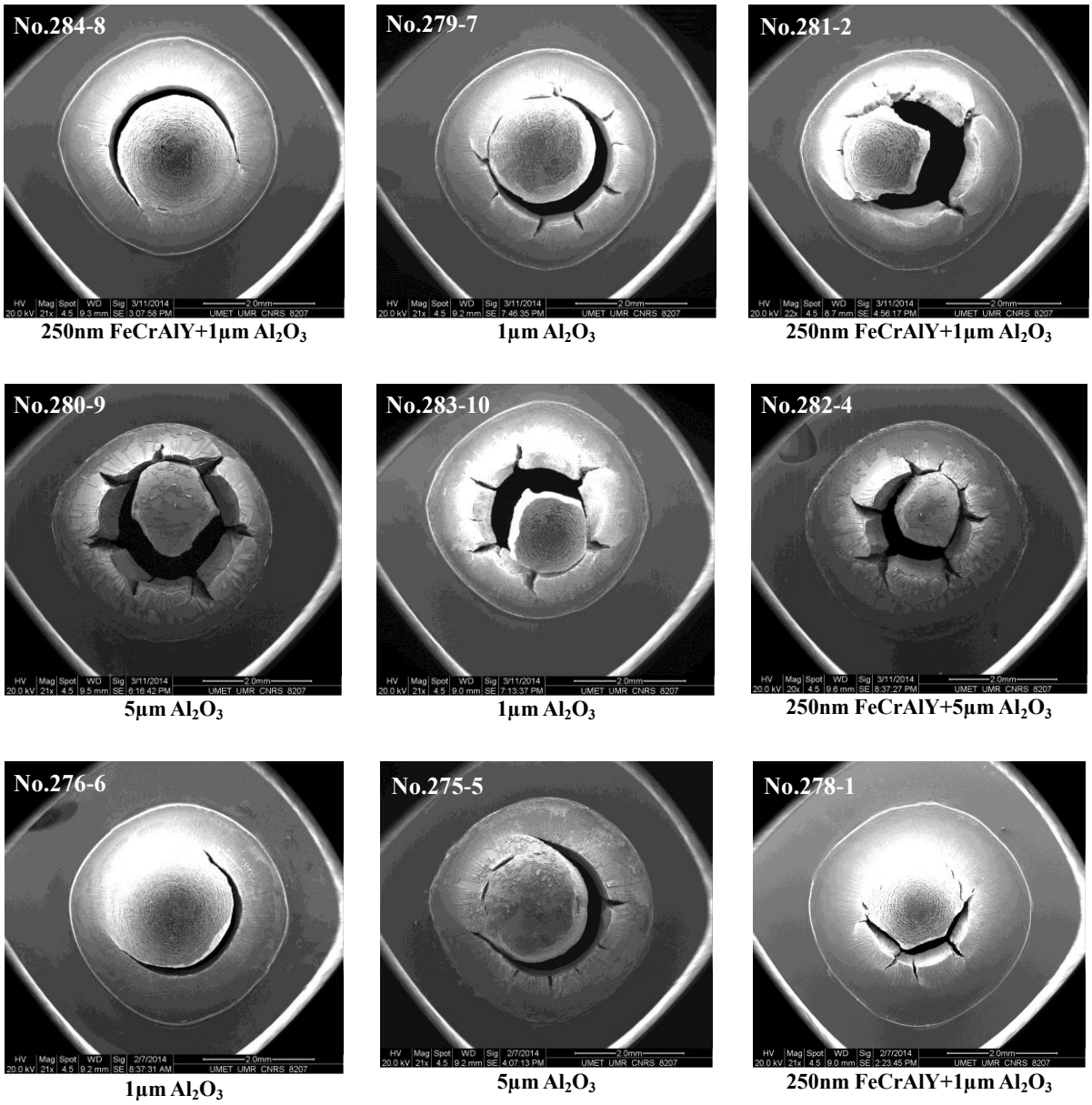

Figure 5.11: SEM images of material TR750 steel surface coating (FeCrAlY/Al_2O_3) specimens SPT at 300°C in liquid oxygen saturated LBE with velocity 0.0005 mm/min.

It can be seen that some specimens contain the main circular crack accompanied sometimes by radials cracks and a ligament suggesting a ductile behaviour. For the other ones, the radial cracks are well developed. However, both situations can be found for a same coating process. Nevertheless, it seems that the 1 µm Al_2O_3 coating gives the best protection. Specimen No.276-6 was observed more in details (Fig 5.12).

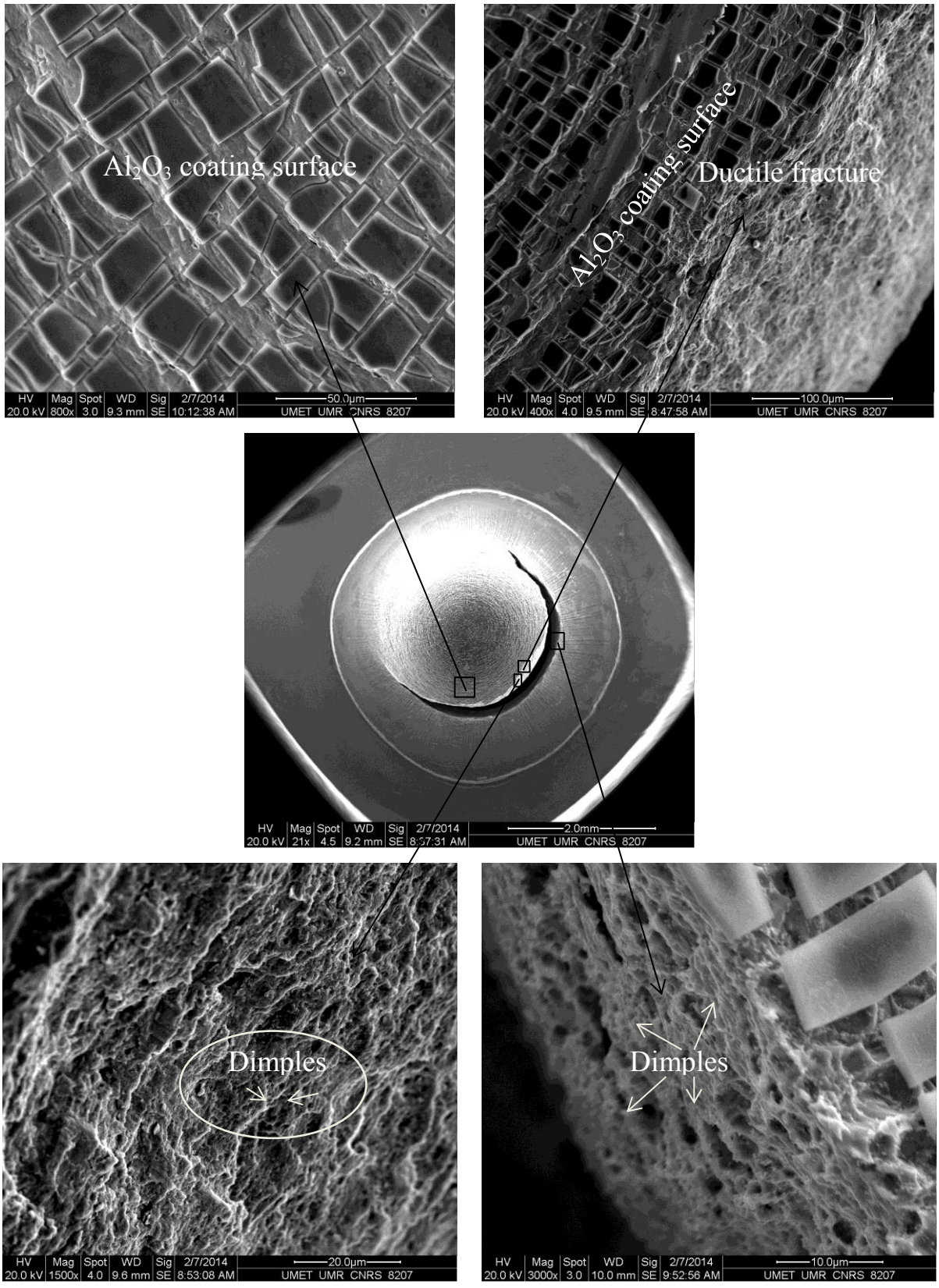

Figure 5.12: SEM images of TR750 surface coating (1µm Al_2O_3) specimen No.276-6 SPT at 300°C in liquid oxygen saturated LBE with a velocity of 0.0005 mm/min.

Due to large deformation, a well-developed crack network is in the Al_2O_3 coating but the fracture surface of T91 is ductile with dimples. This let suppose that for a large part of the test, the integrity of the coating was real. The same observation holds for the specimen No.284-8. Compared to the uncoated specimen SPT at the same conditions (at 300°C in liquid oxygen saturated LBE with lowest velocity 0.0005 mm/min), specimens No.276-6 and No.284-8 have semi-circular crack shape rather than star shape radial cracks and the fractures thicknesses are relatively thin (Fig. 5.11, Fig. 5.12, Fig. 3.9).

However, the final analysis results indicate that the benefit of the surface coating FeCrAlY/Al_2O_3, specifically 1μm Al_2O_3 coating cannot be absent.

In addition, SEM observation also confirmed that the decrease in the mechanical properties is accompanied by an increase of amount of brittle fracture surface. A rough estimation of the ratios of brittle area ratio for specimens No.276-6, No.275-5, No.274-3, No.278-1, No.273-0 are 0%, 20%, 50%, 70%, 95% respectively (Figs. 5.11, 5.13).

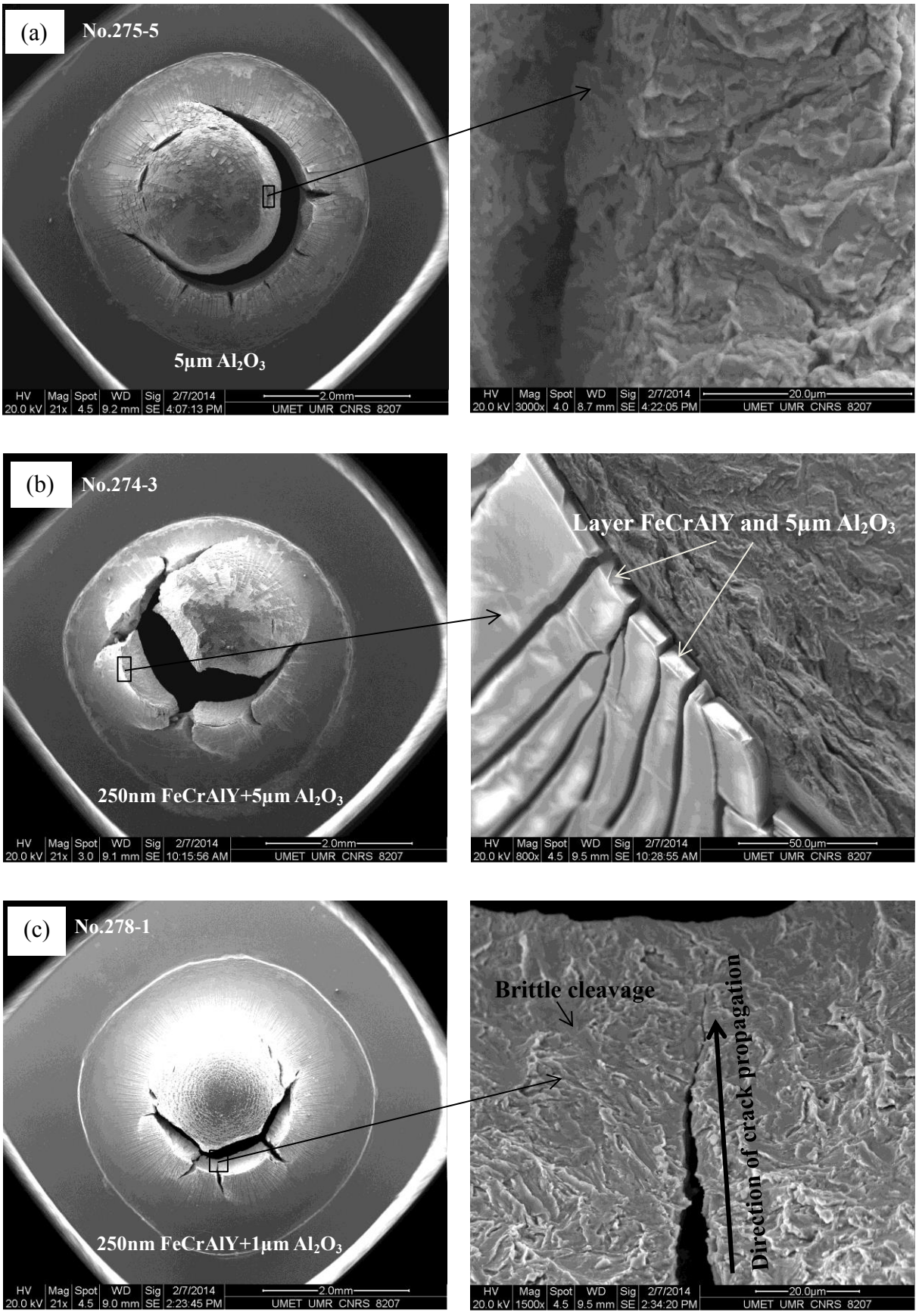

Figure 5.13: SEM images of TR750 surface coating specimens SPT at 300°C in liquid oxygen saturated LBE with a velocity of 0.0005 mm/min.

This research result is undoubtedly good news for enhancing the properties of material TR750 steel and expanding its application scope. However, scattering is observed for a considered coating process and one has to find the origin of this scattering to make more reliable the coating. In addition, in order to conduct a comprehensive analysis, it would be very necessary to repeat these results above through a lot of other experiments.

CONCLUSION AND PERSPECTIVE

The aim of this PhD thesis was to investigate the liquid LBE embrittlement of ferritic/martensitic T91 steel, to examine firstly the role of oxygen in LBE and secondly the role of mechanical loading parameters. The strategy of the research program started with the design and the manufacturing of a LBE purification unit and of a controlled atmosphere test cell. Then different mechanical tests (Small Punch Test, three-point bending test, tensile test) in different environments (air, Ar-3.5%H_2 gas mixture, oxygen saturated LBE, low oxygen LBE) have been performed and the results were analyzed with the point of view of the fractography. This allowed us proposing an enhanced mechanism of liquid LBE embrittlement.

The main progress resulting and the important conclusions are the following.

A purification unit aims at removing oxygen from LBE by Ar-H_2 bubbling in the liquid metal, has been designed and manufactured. It has been operating with success and can decrease the oxygen content in LBE as low as 10^{-8} wt%.

The results of SPT shows that the original ductile T91 steel in its standard heat treatment (TR750) experiences ductile deformation in a temperature range from 250°C to 400°C as well in air as in liquid LBE (oxygen saturated/low oxygen) under moderate loading rate (0.5, 0.05 mm/min). The presence of a circular crack is an indication of a ductile behavior and the presence of dimples confirms it. For the T91 steel considered in this thesis, some brittle zones have been discovered at the edge of the circular crack tested in LBE, which was not encountered for other similar grades of T91 steel studied in the past. However, T91 steel is very sensitive to liquid LBE embrittlement when tested at 300°C with a slow load velocity as well in oxygen saturated LBE (at 0.0005 mm/min) as in low oxygen LBE (at 0.005, 0.0005 mm/min). Therefore, it has been clearly established that the load velocity plays a key role in the fracture mechanism. The fracture can be fully brittle which is marked by the total absence of a circular crack and only by the presence of radial cracks. These can be very limited in number, the smaller number expressing a high degree of brittleness. The brittle fracture is mostly transgranular. Moreover, at 300°C, testing the T91 steel at a velocity of 0.0005 mm/min in oxygen saturated LBE is similar to testing at a velocity of 0.005 mm/min in low

oxygen LBE. A second important conclusion is that a low oxygen content in LBE plays a catalytic role in the liquid LBE embrittlement of T91 steel. In addition, the brittle fracture mechanism of TR750 at the temperature from 250°C to 300°C is different with that of 400°C where a little ductility is recovered.

LBE embrittlement sensitivity of T91 steel is strongly enhanced by hardening temper treatment at 500°C (TR500). All the fractured TR500 specimens consumed very little fracture resistance energy tested in LBE and the fracture surface is always brittle, especially transgranular cleavage with some occasional intergranular brittle feature. Furthermore, the oxygen content in liquid LBE (oxygen saturated/low oxygen) does not have obvious effect on the mechanical response and fracture mechanism of TR500.

LBE plays a role on the propagation of defects and with the considered conditions does not act on crack initiation in that sense that no dissolution corrosion occurs and no defect are initiated from that. The size of a defect or of a notch is a critical parameter. It has been noted that when macro notches are at the specimen surface, they do not interact with LBE. For instance, V-notched surface cylindrical tensile test specimen tested at 300°C in LBE (oxygen saturated/low oxygen) fractured in a ductile manner. The stress triaxiality in the centre of the specimen governs the damage process independently of LBE. When short cracks of the dimension of a few grain sizes are present or initiated during the first moment of the plastic deformation, then a brittle crack propagation assisted by LBE is possible. A dual brittle - ductile fracture surface is then observed and the proportion of brittle and ductile varies depends on the experimental conditions. The brittle area proportion has been found to be less than 30%. However, the ductile zone is always in the center of the specimen and the brittle areas at the outer part of the fracture surface.

The quantitative results of three-point bending tests indicate that the embrittlement effect of liquid LBE on TR750 is obvious based on the calculation of J_Q integral. The proportion of fracture toughness for TR750 steel in liquid LBE is just half of that in air.

One new proper hypothetical mechanism is proposed to interpret LBE embrittlement of T91 steel in its standard heat treatment based on the abundant experimental results obtained in this PhD thesis work. When a short crack is present or when a plasticity induced roughness is in the process of occurring, LBE atoms (Pb, Bi) adsorb at the crack tip or at the groove tip which result in the reduction of both the values of interatomic bonds cohesive strength and surface

energy of T91 steel. When the strain rate is high, the crack tip is re-oxidized very quickly and remained in this state during deformation so that stress triaxiality in the bulk controls the damage process. No LME is observed. When the strain rate is low, oxidation-oxide film rupture sequences can occur consecutively and periodically due to continuous displacement of matter at crack tip. Adsorption is really promoted and allows breaking of the interatomic bonds. A brittle crack can propagate into the bulk.

An advanced coating ($FeCrAlY/Al_2O_3$) on the surface of material TR750 has been envisaged as a mean to overcome liquid LBE embrittlement of TR750 steel. The beneficial role of this coating has not been fully pointed out since some scattering was observed. Nevertheless, better response has been sometime observed with the coated specimen, especially when a 1μm Al_2O_3 has been deposited, as compared with the uncoated ones. In addition, no deleterious effect of the coating has been observed. So, this route appears as promising but additional experiments are necessary.

Without a doubt, the present result obtained in this PhD thesis is meaningful for promoting the scientific research on the LBE embrittlement effect on T91 steel. However, in order to achieve realistic prediction and guidance in the future, there is still a lot of work to do in depth theoretical study on LBE embrittlement phenomena acting on T91 steel as well as other metals. Especially, the plasticity process in T91 steel is not well documented. The effect of strain rate on the growth speed of emerging slip bands is unknown. This should be documented to strengthen the proposed liquid LBE embrittlement mechanism.

REFERENCES

[AIE-2004-A] A. Aiello, M. Azzati, G. Benamati, A. Gessi, B. Long, G. Scaddozzo, Corrosion behaviour of stainless steels in flowing LBE at low and high oxygen concentration, *Journal of Nuclear Materials*, Volume 335, 169-173, 2004.

[AIE-2004-B] A. Aiello, M. Agostini, G. Benamati, B. Long, G. Scaddozzo, Mechanical properties of martensitic steels after exposure to flowing liquid metals, *Journal of Nuclear Materials*, Volume 335, 217-221, 2004.

[AST-2001] ASTM international, E1820-01, Standard test method for measurement of fracture toughness, Volume 3, 8-22, 2001.

[AUG-2004] T. Auger, G. Lorang, S. Guérin, J.-L. Pastol, D. Gorse, Effect of contact conditions on embrittlement of T91 steel by lead-bismuth, *Journal of Nuclear Materials*, Volume 335, 227-231, 2004.

[AUG-2005] T. Auger, G. Lorang, Liquid metal embrittlement susceptibility of T91 steel by lead-bismuth, *Scripta Materialia*, Volume 52, 1323-1328, 2005.

[AUG-2008-A] T. Auger, I. Serre, G. Lorang, Z. Hamouch, D. Gorse, J-B. Vogt, Role of oxidation on LME of T91 steel studied by small punch test, *Journal of Nuclear Materials*, Volume 376, 336-340, 2008.

[AUG-2008-B] T. Auger, Z. Hamouche, L. Medina-Almazàn, D. Gorse, Liquid metal embrittlement of T91 and 316L steels by heavy liquid metals: A fracture mechanics assessment, *Journal of Nuclear Materials*, Volume 377, 253-260, 2008.

[AUG-2011] T. Auger, D. Gorse, Z. Hamouche-Hadjem, J. Van den Bosch, G. Coen, A. Almazouzi, A. Hojna, K. Dalikova, F. Di Gabriele, M. Serrano, A. Gessi, P. Agostini, J-B. Vogt, I. Serre, Fracture mechanics behavior of the T91 martensitic steel in contact with liquid lead-bismuth eutectic for application in an accelerator driven system, *Journal of Nuclear Materials*, Volume 415, 293-301, 2011.

[BAR-2001] F. Barbier, G. Benamati, C. Fazio, A. Rusanov, Compatibility tests of steels in

flowing liquid lead-bismuth, *Journal of Nuclear Materials*, Volume 295, 149-156, 2001.

[BOR-2011] A. Borgohain, B.K. Jaiswal, N.K. Maheshwari, P.K. Vijayan, D. Saha, R.K. Sinha, Natural circulation studies in a lead bismuth eutectic loop, *Progress in Nuclear Energy*, Volume 53, 308-319, 2011.

[BOS-2006] J. Van den Bosch, D. Sapundjiev, A. Almazouzi, Effects of temperature and strain rate on the mechanical properties of T91 material tested in liquid lead bismuth eutectic, *Journal of Nuclear Materials*, Volume 356, 237-246, 2006.

[BOS-2008] J. Van den Bosch, R.W. Bosch, D. Sapundjiev, A. Almazouzi, Liquid metal embrittlement susceptibility of ferritic-martensitic steel in liquid lead alloys, *Journal of Nuclear Materials*, Volume 376, 322-329, 2008.

[BOS-2009] J. Van den Bosch, G. Coen, A. Almazouzi, J. Degrieck, Fracture toughness assessment of ferritic-martensitic steel in liquid lead-bismuth eutectic, *Journal of Nuclear Materials*, Volume 385, 250-257, 2009.

[BOS-2010-A] J. Van den Bosch, G. Coen, W. Van Renterghem, A. Almazouzi, Compatibility of ferritic-martensitic steel T91 welds with liquid lead-bismuth eutectic: Comparison between TIG and EB welds, *Journal of Nuclear materials*, Volume 396, 57-64, 2010.

[BOS-2010-B] J. Van den Bosch, G. Coen, R.W. Bosch, A. Almazouzi, TWIN ASTIR: First tensile results of T91 and 316L steel after neutron irradiation in contact with liquid lead-bismuth eutectic, *Journal of Nuclear Materials*, Volume 398, 68-72, 2010.

[BUL-2002] J.H. Bulloch, A review of the ESB small punch test data on various plant components with special emphasis on fractographic details, *Engineering Failure Analysis*, Volume 9, 511-534, 2002.

[CAR-2012] E. Cárdenas, F.J. Belzunce, C. Rodríguez, I. Peñuelas, C. Betegón, Application of the small punch test to determine the fracture toughness of metallic materials, *Fatigue and Fracture of Engineering Materials and Structures*, Volume, 1-10, 2012.

[COE-2010] G. Coen, J. Van den Bosch, A. Almazouzi, J. Degrieck, Investigation of the effect of lead-bismuth eutectic on the fracture properties of T91 and 316L, *Journal of Nuclear Materials*, Volume 398, 122-128, 2010.

[CON-2008] M.A. Contreras, C. Rodriguez, F.J. Belzunce, C. Betegon, Use of the small punch test to determine the ductile-to-brittle transition temperature of structural steels, *Fatigue and Fracture Engineering Materials and Structures*, Volume 31, 727-737, 2008.

[COU-2004] J-L. Courouau, Electrochemical oxygen sensors for on-line monitoring in lead-bismuth alloys: status of development, *Journal of Nuclear Materials*, Volume 335, 254-259, 2004.

[DAI-2006-A] Y. Dai, B. Long, F. Gröeschel, Slow strain rate tensile tests on T91 in static lead-bismuth eutectic, *Journal of Nuclear Materials*, Volume 356, 222-228, 2006.

[DAI-2006-B] Y. Dai, B. Long, X. Jia, H. Glasbrenner, K. Samec, F. Groeschel, Tensile tests and TEM investigations on LiSoR-2 to -4, *Journal of Nuclear Materials*, Volume 356, 256-263, 2006.

[DAI-2006-C] Y. Dai, C. Fazio, D. Gorse, F. Gröschel, J. Henry, A. Terlain, J.-B. Vogt, T. Auger, A. Gessi, Summary on the preliminary assessment of the T91 window performance in the MEGAPIE conditions, *Nuclear Instruments and Methods in Physics Research A*, Volume 562, 698-701, 2006.

[DAI-2008] Y. Dai, B. Long, Z.F. Tong, Tensile properties of ferritic/martensitic steels irradiated in STIP-I, *Journal of Nuclear Materials*, Volume 377, 115-121, 2008.

[DAI-2009] Y. Dai, W. Wagner, The Status of Studies on Structural Materials under High Energy Proton and Neutron Mixed Spectrum, PSI, Switzerland, AP/INT-01, 2009.

[DEL-2004] Ph. Deloffre, F. Balbaud-Célérier, A. Terlain, Corrosion behaviour of aluminized martensitic and austenitic steels in liquid Pb-Bi, *Journal of Nuclear Materials*, Volume 335, 180-184, 2004.

[DIE-1976] G.E. Dieter, Mechanical metallurgy, International student edition, second edition, 1976.

[DOU-2011] P. Dou, R. Kasada, Preliminary study on nano- and micro-composite sol-gel based alumina coatings on structural components of lead-bismuth eutectic cooled fast breeder reactors, *Journal of Nuclear Materials*, Volume 409, 177-182, 2011.

[FAZ-2003] C. Fazio, I. Ricapito, G. Scaddozzo, G. Benamati, Corrosion behaviour of steels

and refractory metals and tensile features of steels exposed to flowing PbBi in the LECOR loop, *Journal of Nuclear Materials*, Volume 318, 325-332, 2003.

[FAZ-2008] C. Fazio, F. Gröschel, W. Wagner, K. Thomsen, B.L. Smith, R. Stieglitz, L. Zanini, A. Guertin, A. Cadiou, J. Henry, P. Agostini, Y. Dai, H. Heyck, S. Dementjev, S. Panebianco, A. Almazouzi, J. Eikenberg, A. Letourneau, J.C. Toussaint, A. Janett, Ch. Perret, S. Joray, J. Patorski, W. Leung, P. Meloni, P. Turroni, A. Zucchini, G. Benamati, J. Konys, T. Auger, A. Gessi, D. Gorse, I. Serre, A. Terlain, J.-B. Vogt, A. Batta, A. Class, X. Cheng, F. Fellmoser, M. Daubner, S. Gnieser, G. Grötzbach, R. Milenkovic, C. Latgé, J.U. Knebel, The MEGAPIE-TEST project: Supporting research and lessons learned in first-of-a-kind spallation target technology, *Nuclear Engineering and Design*, Volume 238, 1471-1495, 2008.

[FER-1994] P.J.L. Fernandes, R.E. Clegg, D.R.H. Jones, Failure by Liquid Metal Induced Embrittlement, *Engineering Failure Analysis*, Volume 1-1, 51-63, 1994.

[FER-1996] P.J.L. Fernandes, D.R.H. Jones, Specificity in Liquid Metal Induced Embrittlement, *Engineering Failure Analysis*, Volume 3, 299-302, 1996.

[FER-1997] P. J. L. Fernandes, D. R. H. Jones, Mechanisms of liquid metal induced embrittlement, *International Materials Reviews*, Volume 42-6, 251-261, 1997.

[FET-2012] R. Fetzer, A. Weisenburger, A. Jianu, G. Müller, Oxide scale formation of modified FeCrAl coatings exposed to liquid lead, *Corrosion Science*, Volume 55, 213-218, 2012.

[FIN-2004] D. Finarelli, M. Roedig, F. Carsughi, Small punch tests on austenitic and martensitic steels irradiated in a spallation environment with 530 MeV protons, *Journal of Nuclear Materials*, Volume 328, 146-150, 2004.

[GAB-2008] F. Di Gabriele, A. Doubková, A. Hojná, Investigation of the sensitivity to EAC of steel T91 in contact with liquid LBE, *Journal of Nuclear Materials*, Volume 376, 307-311, 2008.

[GAN-2008] R. Ganesan, T. Gnanasekaran, Raman S. Srinivasa, Standard molar Gibbs energy of formation of $Pb_5Bi_8O_{17}$ and $PbBi_{12}O_{19}$ and phase diagram of the Pb-Bi-O system, *Journal of Nuclear Materials*, Volume 375, 229-242, 2008.

[GAR-2013-A] F. García Ferré, E. Bertarelli, A. Chiodoni, D. Carnelli, D. Gastaldi, P. Vena, M.G. Beghi, F. Di Fonzo, The mechanical properties of a nanocrystalline Al_2O_3/a-Al_2O_3 composite coating measured by nanoindentation and Brillouin spectroscopy, *Acta Materialia*, Volume 61, 2662-2670, 2013.

[GAR-2013-B] F. García Ferré, M. Ormellese, F. Di Fonzo, M.G. Beghi, Advanced Al_2O_3 coatings for high temperature operation of steels in heavy liquid metals: a preliminary study, *Corrosion Science*, Volume 77, 375-378, 2013.

[GLA-2003] H. Glasbrenner, F. Gröschel, T. Kirchner, Tensile tests on MANET II steel in circulating Pb-Bi eutectic, *Journal of Nuclear Materials*, Volume 318, 333-338, 2003.

[GLA-2004] H. Glasbrenner, F. Gröschel, Bending tests on T91 steel in Pb-Bi eutectic, Bi and Pb-Li eutectic, *Journal of Nuclear Materials*, Volume 335, 239-243, 2004.

[GLI-2000] E.E. Glickman, Mechanism of Liquid Metal Embrittlement by simple Experiments: from Atomistics to Life-time, in Multiscale Phenomena in Plasticity, J. Lepinoux, et al. (Eds.) Kluwer Academic Publishers (Dordrecht, The Netherlands), 383-401, 2000.

[GOR-1982] P. Gordon, H.H. An, The mechanisms of crack initiation and crack propagation in metal-induced embrittlement of metals, *Metallurgical Transactions A*, 13, 457, 1982.

[GOR-2007] D. Gorse-Pomonti, V. Russier, Liquid metal for nuclear applications, *Journal of Non-Crystalline Solids*, Volume 353, 3600-3614, 2007.

[GOR-2011] D. Gorse, T. Auger, J-B. Vogt, I. Serre, A. Weisenburger, A. Gessi, P. Agostini, C. Fazio, A. Hojna, F. Di Gabriele, J. Van Den Bosch, G. Coen, A. Almazouzi, M. Serrano, Influence of liquid lead and lead-bismuth eutectic on tensile, fatigue and creep properties of ferritic/martensitic and austenitic steels for transmutation systems, *Journal of Nuclear Materials*, Volume 415, 284-292, 2001.

[HAM-2008] Z. Hamouche-Hadjem, T. Auger, I. Guillot, D. Gorse, Susceptibility to LME of 316L and T91 steels by LBE: Effect of strain rate, *Journal of Nuclear Materials*, Volume 376, 317-321, 2008.

[HAN-2007] Handbook on lead-bismuth Eutectic Alloy and Lead Properties, Materials

Compatibility, Thermal-hydraulics and Technologies, OECD/NEA, 2007.

[JIA-2003] X. Jia, Y. Dai, Small punch tests on martensitic/ferritic steels F82H, T91 and Optimax-A irradiated in SINQ Target-3, *Journal of Nuclear Materials*, Volume 323, 360–367, 2003.

[JIA-2009] A. Jianu, G. Müller, A. Weisenburger, A. Heinzel, C. Fazio, V.G. Markov, A.D. Kashtanov, Creep-to-rupture tests of T91 steel in flowing Pb-Bi eutectic melt at 550°C, *Journal of Nuclear Materials*, Volume 394, 102-108, 2009.

[JON-1991] W.B. Jones, C.R. Hills, D.H. Polonis, Microstructural evolution of modified 9Cr - 1Mo steel*, Metallurgical and Materials Transactions A,* Volume 22, 1049-1058, 1991.

[JOS-1999] B. Joseph, M. Picat, F. Barbier, Liquid Metal Embrittlement: A state-of-the-art appraisal, *The European Physical Journal Applied Physics*, Volume 5, 19-31, 1999.

[JU-2003] J-B. Ju, J-I. Jang, D. Kwon, Evaluation of fracture toughness by small-punch testing techniques using sharp notched specimens, *International Journal of Pressure Vessels and piping*, Volume 80, 221-228, 2003.

[KAL-2003] D. Kalkhof, M. Grosse, Influence of PbBi environment on the low-cycle fatigue behavior of SNS target container materials, *Journal of Nuclear Materials*, Volume 318, 143-150, 2003.

[KAM-1973] M.H. Kamdar, Embrittlement by Liquid Metals, *Progress in Materials Science*, Volume 15, 289-372, 1973.

[KAM-1986] J. Kameda, O. Buck, Evaluation of the ductile-to-brittle transition temperature shift due to temper embrittlement and neutron irradiation by means of a small-punch test, *Material Science and Engineering*, Volume 83, 29-38, 1986.

[KEL-1975] M.J. Kelley, N.S. Stoloff, Analysis of liquid metal embrittlement from a bond energy viewpoint, *Metallurgical Transactions A*, Volume 6, 159-166, 1975.

[KIM-2005] M-C. Kim, Y.J Oh, B.S. Lee, Evaluation of ductile-brittle transition temperature before and after neutron irradiation for RPV steels using small punch tests, *Nuclear Engineering and Design*, Volume 235, 1799-1805, 2005.

[LON-2008-A] B. Long, Y. Dai, Investigation of LBE embrittlement effects on the fracture properties of T91, *Journal of Nuclear Materials*, Volume 376, 341-345, 2008.

[LON-2008-B] B. Long, Z. Tong, F. Gröschel, Y. Dai, Liquid Pb-Bi embrittlement effects on the T91 steel after different heat treatments, *Journal of Nuclear Materials*, Volume 377, 219-224, 2008.

[LON-2009] B. Long, Liquid Lead-Bismuth Embrittlement Effects on Unirradiated and Irradiated Ferritic/martensitic Steels for Nuclear Applications, PhD thesis, École polytechnique fédérale de Lausanne (EPFL), 2009.

[LON-2011] B. Long, Y. Dai, N. Baluc, Investigation of liquid LBE embrittlement effects on irradiated ferritic/martensitic steels by slow-strain-rate tensile tests, *Journal of Nuclear Materials*, Volume 434, 85-90, 2012.

[LYN-1981] S. P. Lynch, Liquid-metal embrittlement in an Al 6% Zn 3% Mg alloy, *Acta Metallurgica*, Volume 29, 325-340, 1981.

[MAL-2006] S.A. Maloy, T. Romero, M. R. James, Y. Dai, Tensile testing of EP-823 and HT-9 after irradiation in STIP II, *Journal of Nuclear Materials*, Volume 356, 56-61, 2006.

[MAN-2001] L.K. Mansur, T.A. Gabriel, J.R. Haines, D.C. Lousteau, R&D for the Spallation Neutron Source mercury target, *Journal of Nuclear Materials*, Volume 296, 1-16, 2001.

[MAR-2004] F.J. Martín, L. Soler, F. Hernández, D. Gómez-Briceño, Oxide layer stability in lead-bismuth at high temperature, *Journal of Nuclear Materials*, Volume 335, 194-198, 2004.

[MAR-2008-A] L. Martinelli, F. Balbaud-Célérier, A. Terlain, S. Delpech, G. Santarini, J. Favergeon, G. Moulin, M. Tabarant, G. Picard, Oxidation mechanism of a Fe-9Cr-1Mo steel by liquid Pb-Bi eutectic alloy (Part I), *Corrosion Science*, Volume 50, 2523-2536, 2008.

[MAR-2008-B] L. Martinelli, F. Balbaud-Célérier, A. Terlain, S. Bosonnet, G. Picard, G. Santarini, Oxidation mechanism of an Fe-9Cr-1Mo steel by liquid Pb-Bi eutectic alloy at 470°C (Part II), *Corrosion Science*, Volume 50, 2537-2548, 2008.

[MAR-2008-C] L. Martinelli, F. Balbaud-Célérier, G. Picard, G. Santarini, Oxidation mechanism of a Fe-9Cr-1Mo steel by liquid Pb-Bi eutectic alloy (Part III), *Corrosion Science*, Volume 50, 2549-2559, 2008.

[MAR-2008-D] L. Martinelli, T. Dufrenoy, K. Jaakou, A. Rusanov, F. Balbaud-Célérier, High temperature oxidation of Fe-9Cr-1Mo steel in stagnant liquid lead-bismuth at several temperatures and for different lead contents in the liquid alloy, *Journal of Nuclear Materials*, Volume 376, 282-288, 2008.

[MAR-2011-A] F.J. Martín-Muñoz, L. Soler-Crespo, D. Gómez-Briceño, Assessment of the influence of surface finishing and weld joints on the corrosion/oxidation behaviour of stainless steels in lead bismuth eutectic, *Journal of Nuclear Materials*, Volume 416, 80-86, 2011.

[MAR-2011-B] F.J. Martín-Muñoz, L. Soler-Crespo, D. Gómez-Briceño, Corrosion behaviour of martensitic and austenitic steels in flowing lead-bismuth eutectic, *Journal of Nuclear Materials*, Volume 416, 87-93, 2011.

[MIL-2006] K. Milicka, F. Dobes, Small punch testing of P91 steel, *International Journal of Pressure Vessels and Piping*, Volume 83, 625-634, 2006.

[MIS-1987] T. Misawa, T. Adachi, M. Saito, Y. Hamaguchi, Small punch tests for evaluating ductile-brittle transition behavior of irradiated ferritic steels, *Journal of Nuclear Materials*, Volume 150, 194-202, 1987.

[MUL-2000] G. Müller, G. Schumacher, F. Zimmermann, Investigation on oxygen controlled liquid lead corrosion of surface treated steels, *Journal of Nuclear Materials*, Volume 278, 85-95, 2000.

[NIC-1979] M.G. Nicholas, C.F. Old, Review : Liquid metal embrittlement, *Journal of Materials Science*, Volume 14, 1-18, 1979.

[NIC-2001-A] G. Nicaise, A. Legris, J-B. Vogt, F. Foct, Embrittlement of the martensitic steel 91 tested in liquid lead, *Journal of Nuclear Materials*, Volume 296, 256-264, 2001.

[NIC-2001-B] G. Nicaise, Sensibilité de l'acier martensitique Z10CDNbV9-1, Thèse de l'université des sciences et technologies de Lille, 2001.

[PRO-2011] I. Proriol Serre, I. Diop, N. David, M. Vilasi, J-B. Vogt, Mechanical behavior of coated T91 steel in contact with lead-bismuth liquid alloy at 300°C, *Surface & Coatings Technology*, Volume 205, 4521-4527, 2011.

[REE-1973] R.E. Reed-Hill, Physical Metallurgy Principles Second Edition, D. Van Nostrand Company, New York, Copyright © 1973 by Litton Educational Publishing, Inc, 1973.

[RIV-2008] A.K. Rivai, M. Takahashi, Compatibility of surface-coated steels, refractory metals and ceramics to high temperature lead-bismuth eutectic, *Progress in Nuclear Energy*, Volume 50, 560-566, 2008.

[RIV-2010-A] A.K. Rivai, M. Takahashi, Corrosion characteristics of materials in Pb-Bi under transient temperature conditions, *Journal of Nuclear Materials*, Volume 398, 139-145, 2010.

[RIV-2010-B] A.K. Rivai, M. Takahashi, Corrosion investigations of Al-Fe-coated steels, high Cr steels, refractory metals and ceramics in lead alloys at 700°C, *Journal of Nuclear Materials*, Volume 398, 146-152, 2010.

[SAP-2006-A] D. Sapundjiev, A. Al Mazouzi, S. Van Dyck, A study of the neutron irradiation effects on the susceptibility to embrittlement of A316L and T91 steels in lead-bismuth eutectic, *Journal of Nuclear Materials*, Volume 356, 229-236, 2006.

[SAP-2006-B] D. Sapundjiev, S. Van Dyck, W. Bogaerts, Liquid metal corrosion of T91 and A316L materials in Pb-Bi eutectic at temperatures 400-600°C, *Corrosion Science*, Volume 48, 577-594, 2006.

[SCH-2012] C. Schroer, O. Wedemeyer, A. Skrypnik, J. Novotny, J. Konys, Corrosion kinetics of steel T91 in flowing oxygen-containing lead-bismuth eutectic at 450°C, *Journal of Nuclear Materials*, Volume 431, 105-112, 2012.

[SER-2007] I. Serre, J-B. Vogt, Liquid metal embrittlement of T91 martensitic steel evidenced by small punch test, *Nuclear Engineering and Design*, Volume 237, 677-685, 2007.

[SER-2008] I. Serre, J-B. Vogt, Heat treatment effect of T91 martensitic steel on liquid metal embrittlement, *Journal of Nuclear Materials*, Volume 376, 330-335, 2008.

[SHO-2013] M. P. Short, R.G. Ballinger, H.E. Hänninen, Corrosion resistance of alloys F91 and Fe-12Cr-2Si in lead-bismuth eutectic up to 715°C, *Journal of Nuclear Materials*, Volume 434, 259-281, 2013.

[SOL-2004] L. Soler, F.J. Martín, F. Hernández, D. Gómez-Briceño, Corrosion of stainless

steels in lead-bismuth eutectic up to 600°C, *Journal of Nuclear Materials*, Volume 335, 174-179, 2004.

[TAN-2009] T. Tan, Y. Chen, X. Tan, Buoyancy-Enhanced Oxygen Transport in the Experimental Liquid Lead Bismuth Eutectic Container, *Journal of nuclear Science and Technology*, Volume 46-2, 109-131, 2009.

[TAS-1988] H. Tas, S. Malang, F. Reiter, J. Sannier, Liquid breeder materials, *Journal of Nuclear Materials*, Volume 155-157, 178-187, 1988.

[TOT-2006] T.C. Totemeier, H. Tian, J.A. Simpson, Effect of normalization temperature on the creep strength of modified 9Cr-1Mo steel, *Metallurgical and Materials Transactions A*, Volume 37, 1519-1525, 2006.

[VER-2006] A. Verleene, J-B. Vogt, I. Serre, A. Legris, Low cycle fatigue behaviour of T91 martensitic steel at 300°C in air and in liquid lead bismuth eutectic, *International Journal of Fatigue*, Volume 28, 843-851, 2006.

[VOG-2002] J-B. Vogt, G. Nicaise, A. Legris, Embrittlement of a ductile Fe9Cr1Mo steel by liquid metals, Proc. European. Conference on Fracture ECF 14 Fracture Mechanics beyond 2000, A. Neimitz, I.V. Rokach, D. Kocanda and K. Golos (Edit.), Vol. III p. 511-519, EMAS Publications ISBN 83-88906-09-7 2002, KRAKOW (Pologne), 8-13, 2002.

[VOG-2004] J-B. Vogt, A. Verleene, I. Serre, A. Legris, Mechanical behaviour of the T91 martensitic steel under monotonic and cyclic loadings in liquid metals, *Journal of Nuclear Materials*, Volume 355, 222-226, 2004.

[VOG-2007] J-B. Vogt, A. Verleene, I. Serre, F. Balbaud-Célérier, L. Martinelli, A. Terlain, Understanding the liquid metal assisted damage sources in the T91 martensitic steel for safer use of ADS, *Engineering Failure Analysis*, Volume 14, 1185-1193, 2007.

[VOG-2011] J-B. Vogt, I. Proriol-Serre, L. Martinelli, N. David, M. Vilasi, Fatigue Resistance in Liquid Lead-Bismuth Eutectic Alloy of T91 Steel, Proceedings of ICAPP 2011, Nice, France, May 2-5, Paper 11328, 2011.

[WAN-2008] Z-X. Wang, H-J. Shi, J. Lu, P. Shi, X-F. Ma, Small punch testing of assessing the fracture properties of the reactor vessel steel with different thickness. *Nuclear Engineering*

and Design, Volume 238, 3186-3193, 2008.

[WEI-2008-A] A. Weisenburger, A. Heinzel, G. Müller, H. Muscher, A. Rousanov, T91 cladding tubes with and without modified FeCrAlY coatings exposed in LBE at different flow, stress and temperature conditions, *Journal of Nuclear Materials*, Volume 376, 274-281, 2008.

[WEI-2008-B] A. Weisenburger, A. Heinzel, C. Fazio, G. Müller, V.G. Markow, A.D. kastanov, Low cycle fatigue tests of surface modified T91 steel in 10^{-6} wt% oxygen containing $Pb_{45}Bi_{55}$ at 550°C, *Journal of Nuclear Materials*, Volume 377, 261-267, 2008.

[WEI-2011] A. Weisenburger, C. Schroer, A. Jianu, A. Heinzel, J. Konys, H. Steiner, G. Müller, C. Fazio, A. Gessi, S. Babayan, A. Kobzova, L. Martinelli, K. Ginestar, F. Balbaud-Célerier, F.J. Martín-Muñoz, L. Soler Crespo, Long term corrosion on T91 and AISI1 316L steel in flowing lead alloy and corrosion protection barrier development: Experiments and models, *Journal of Nuclear Materials*, Volume 415, 260-269, 2011.

[WEI-2012] A. Weisenburger, A. Jianu, W. An, R. Fetzer, M. Del Giacco, A. Heinzel, Creep, creep-rupture tests of Al-surface-alloyed T91 steel in liquid lead bismuth at 500 and 550 °C, *Journal of Nuclear Materials*, Volume 431, 77-84, 2012.

[YEL-2008] O. Yeliseyeva, V. Tsisar, G. Benamati, Influence of temperature on the interaction mode of T91 and AISI 316L steels with Pb-Bi melt saturated by oxygen, *Corrosion Science*, Volume 50, 1672-1683, 2008.

[YUR-2011] M. Yurechko, C. Schroer, O. Wedemeyer, A. Skrypnik, J. Konys, Creep-to-rupture of 9%Cr steel T91 in air and oxygen-controlled lead at 650°C, *Journal of Nuclear Materials*, Volume 419, 320-328, 2011.

[ZHA-2009] J. Zhang, A review of steel corrosion by liquid lead and lead-bismuth, *Corrosion Science*, Volume 51, 1207-1227, 2009.

ACKNOWLEDGEMENTS

This thesis was done at the group of Métallurgie Physique et Génie des Matériaux (MPGM) in Unité Matériaux Et Transformations (UMET) Laboratory.

First of all, I would like to express my deep gratitude to my two PhD directors, Prof. Jean-Bernard Vogt and Dr. Ingrid Proriol Serre, for giving me the opportunity to study and work in such a dynamic and open-minded research group. Thank you for the suggestions when I did research and wrote scientific articles during last four years. Without your support and encouragement, there would not be the realization of this thesis. I am glad I was able to spend four years in this research group which did and will greatly influence my career. Please allow me to thank you again for your patience, efficient guidance and lots of help for both research and French language learning, especially the French language, which already does and will benefit my life.

Secondly, I would like to thank Prof. Alexandre Legris also, the director of UMET, who accepted me to work as a doctoral student in the laboratory.

Meanwhile, I am thankful for the technical support and assistance from Ing. Jocelyn Golek and Damien Creton during my experimental work. It was their help that allowed me to finish my mechanical tests parts of my thesis. In addition, working together with them is amazing with a lot of French fun and I really cherish those unforgettable moments. I appreciate the assistance from Dr. Jérémie Bouquerel for helping me learning SEM analysis technique what is applied to my thesis work, especially for fluent discussions and suggestions.

I want to thank Mrs. Corinne Henry and Isabelle Samain for their support in administrative matters.

Specially, I would like to thank my family members and all my friends. Their love, support and encouragement give me enormous energy to overcome all the difficulties in my life abroad.

Finally, I must be very grateful to my husband, Xiao Fang. He married me during my pursuit of PhD, which makes me feel great happiness and joy. It is him, who stayed with me in my most lonely days, gives me a loving harbor. I love you, darling!

ABSTRACT

Ferritic/martensitic T91 steel is designated to constitute structural material for both Generation IV nuclear reactors and the high temperature components of future accelerator driven system (ADS) which employ liquid metals. The liquid LBE embrittlement of is one of the critical issues for the compatibility between the structural material T91 steel and the liquid metal. This thesis research has estimated the embrittlement sensitivity of T91 steel in liquid LBE qualitatively and quantitatively. A specific unit of LBE purification has been manufactured to remove oxygen from LBE. Special setup of Small Punch Test, three-point bending test and tensile test, have been developed in the laboratory to perform mechanical tests in low oxygen LBE inside an environmentally controlled atmosphere cell.

In general, T91 steel is a ductile material even when stressed in LBE but there exists a set of conditions which results in a ductile to brittle transition. T91 steel has appeared very sensitive to liquid LBE embrittlement at 300°C when it very slowly loaded as well in oxygen saturated LBE as in low oxygen LBE even in the standard heat treatment. In addition, a low oxygen content in LBE accelerates this brittle damage. Surface defects play a role when their size is of the order of a few grain sizes. The fracture toughness for T91 steel in liquid LBE can be just half of that in air. The mechanism of liquid LBE embrittlement of T91 is based on the reduction of both the values of interatomic bonds cohesive strength and of surface energy. Straining very slowly the material is supposed to favour oxidation-oxide film rupture sequences which allows real adsorption at crack tip and then propagation of brittle crack.

Keywords: liquid metal embrittlement (LME), liquid lead-bismuth eutectic (LBE), martensitic steel, ductile to brittle transition, Small Punch Test, three-point bending test, tensile test, *J* integral.

RESUME

Les aciers martensitiques Fe9Cr1MoNbV (acier T91) sont des bons candidats pour les composants des réacteurs nucléaires de Génération IV ou pour les réacteurs hybrides. Ces technologies employant des métaux liquides, la fragilisation par métal liquide est un problème pour l'intégrité des structures. Ce travail de thèse est une contribution à l'étude de la sensibilité de l'acier T91 en présence de l'eutectique Pb-Bi (LBE). L'approche, fortement expérimentale, a pour but de déterminer qualitativement et quantitativement les paramètres les plus pertinents pour déclencher la fragilisation. Une unité de purification de l'eutectique Pb-Bi a été conçue et construite au laboratoire pour retirer l'oxygène de l'eutectique Pb-Bi. Des essais mécaniques de type Small Punch Test, flexion 3 points et traction monotone ont pu être réalisés dans l'eutectique à faible teneur en oxygène dans une cellule d'essais à atmosphère contrôlée.

L'acier T91 présente en général un comportement ductile même lorsqu'il est sollicité en présence de LBE mais il existe un ensemble de conditions qui conduit à une transition ductile-fragile. L'acier T91, après avoir reçu son traitement thermique standard, s'est montré très sensible à la fragilisation par l'eutectique Pb-Bi à 300°C quand la vitesse de chargement était très faible aussi bien dans l'eutectique saturé ou appauvri en oxygène. Il s'avère que la vitesse de sollicitation est le facteur clé et la teneur en oxygène un facteur accélérateur de la fragilisation. Les défauts de surface et les entailles jouent également un rôle important quand leur taille est faible et de l'ordre de quelques tailles de grains. La ténacité de l'acier T91 est divisée par deux en présence de l'eutectique par comparaison à l'air. Le mécanisme de fragilisation par l'eutectique Pb-Bi repose sur une diminution de l'énergie de surface et une diminution des forces de cohésions suite à l'adsorption des atomes Pb et Bi en fond de fissure. Une vitesse de déformation lente favorise la séquence oxydation- rupture du film d'oxyde qui se produit périodiquement au cours de la déformation. Ceci permet une réelle adsorption des atomes Pb et Bi en fond d'entaille et leur rapide propagation.

Mots clés: fragilisation par métal liquide, eutectique plomb-bismuth, acier martensitique, transition ductile-fragile, essais mécaniques sous atmosphère contrôlée, fractographie au MEB.